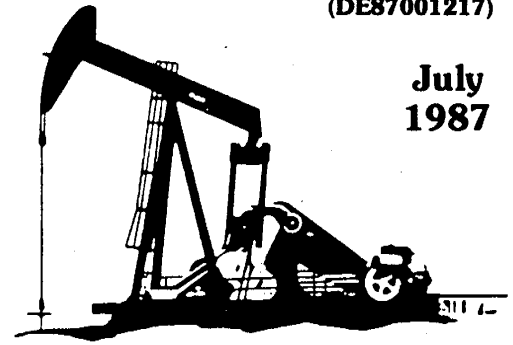
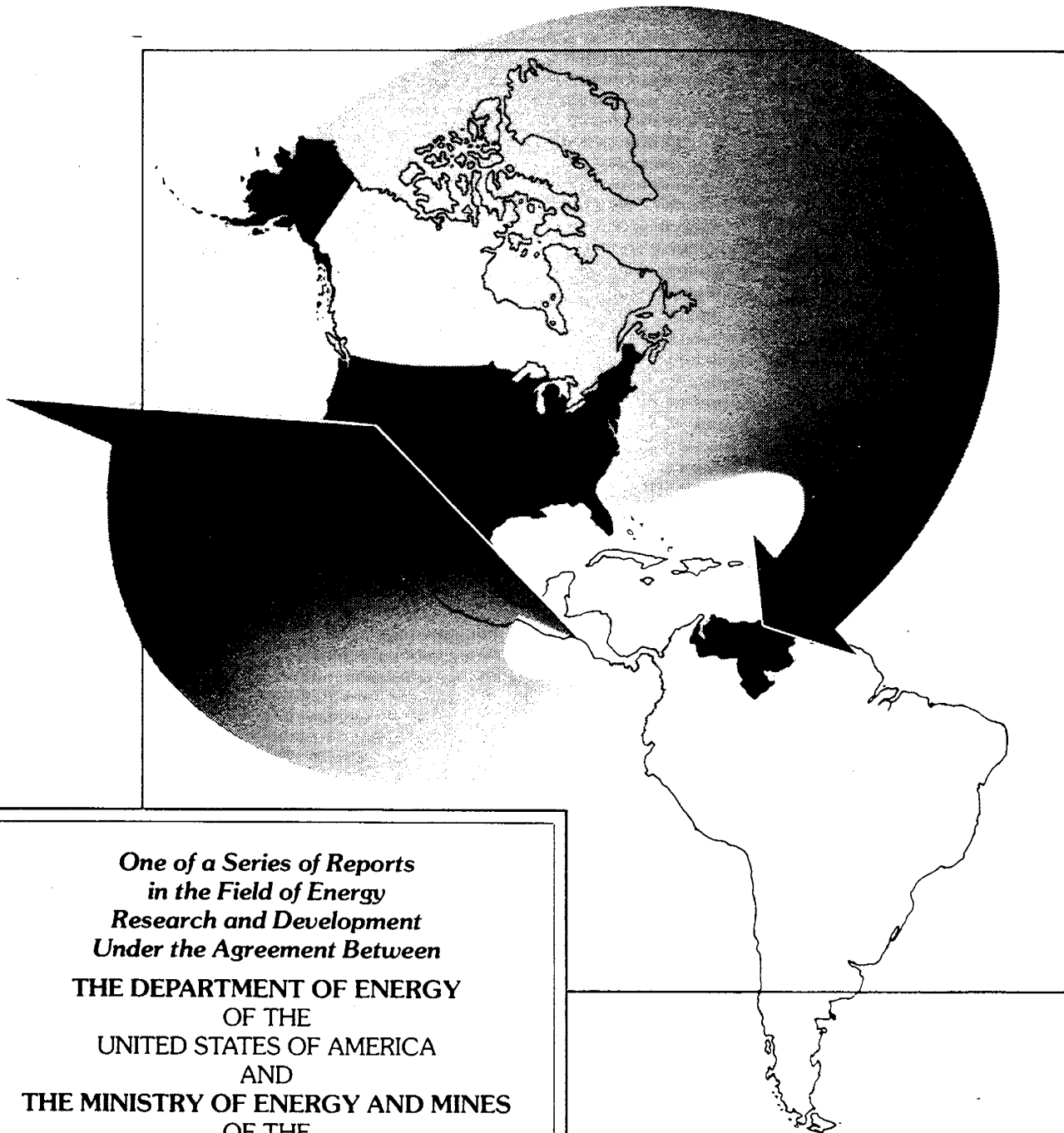


SUPPORTING TECHNOLOGY FOR ENHANCED OIL RECOVERY



July
1987

EOR THERMAL PROCESSES



*One of a Series of Reports
in the Field of Energy
Research and Development
Under the Agreement Between*
THE DEPARTMENT OF ENERGY
OF THE
UNITED STATES OF AMERICA
AND
THE MINISTRY OF ENERGY AND MINES
OF THE
REPUBLIC OF VENEZUELA

DISCLAIMER

This report was prepared as an account of work sponsored by an agency of the United States Government. Neither the United States Government nor any agency thereof, nor any of their employees, makes any warranty, express or implied, or assumes any legal liability or responsibility for the accuracy, completeness, or usefulness of any information, apparatus, product, or process disclosed, or represents that its use would not infringe privately owned rights. Reference herein to any specific commercial product, process, or service by trade name, trademark, manufacturer, or otherwise, does not necessarily constitute or imply its endorsement, recommendation, or favoring by the United States Government or any agency thereof. The views and opinions of authors expressed herein do not necessarily state or reflect those of the United States Government or any agency thereof.

Printed in the United States of America. Available from:
National Technical Information Service
U.S. Department of Commerce
5285 Port Royal Road
Springfield, VA 22161

NTIS price codes
Paper copy: **A13**
Microfiche copy: **A01**

**THIRD AMENDMENT AND EXTENSION TO
ANNEX IV ENHANCED OIL RECOVERY THERMAL PROCESSES**

Implementing Agreement Between

THE DEPARTMENT OF ENERGY OF THE UNITED STATES OF AMERICA

And

THE MINISTRY OF ENERGY AND MINES OF THE REPUBLIC OF VENEZUELA

Submitted by:

Gary Peterson, Fossil Energy
Program Manager
San Francisco Operations Office
U.S. Department of Energy

José Diaz Muñoz, Manager
Petroleum Engineering
INTEVEP, S.A.
Filial de Petroleos de Venezuela, S.A.



Approved by:



Robert L. Folstein, Director
Bartlesville Project Office
P.O. Box 1398
Bartlesville, OK 74005

Enrique Vasquez, Technology Coordinator
Petroleos de Venezuela, S.A.
Apartado Postal 169
Caracas 1010A, Venezuela



PREFACE

An Agreement between the Department of Energy of the United States of America and the Ministry of Energy and Mines of the Republic of Venezuela to cooperate in energy research and development was signed March 6, 1980. This Agreement supported the Agreement for Scientific and Technological Cooperation between the two countries which was signed on January 11, 1980. The general agreement was supplemented by six annexes to describe specifically the work to be done. Additional annexes have been signed, resulting in a total of ten annexes as of January 1, 1987. They are:

- I. Joint Characterization of Heavy Crude Oils
- II. Supporting Research at Universities, Government Energy Technology Centers, and Government Laboratories
- III. Evaluate Past and On-Going Enhanced Oil Recovery Projects in the United States and Venezuela
- IV. Enhanced Oil Recovery Thermal Processes
- V. Oil Drilling, Coring, and Telemetry
- VI. Residual Oil Saturation
- VII. Petroleum Products Utilization and Evaluation
- VIII. Coal Combustion Studies
- IX. Subsidence Due to Extraction of Fluids
- X. Training for Venezuelan Engineers

Each of these annexes has a document describing the work to be done as part of the cooperation. Amendments and Extensions to the Annexes are provided for in the Agreement.

Currently, Annexes I, II, III, IV, VIII, IX, X are active. Annexes V, VI, and VII have been completed.

CONTENTS

	<u>Page</u>
Preface	ii
Abstract	iv
TASK 25 DOE-Lawrence Livermore National Laboratory Thermal Front Tracking Tests	25-1
TASK 26 INTEVEP Thermal Front Tracking Test	26-1
TASK 27 DOE-Sandia CSAMT Surveys	27-1
TASK 28 DOE-Stanford University Petroleum Research Steam Additive Research	28-1
TASK 29 INTEVEP Steam Additive Research	29-1
TASK 30 DOE-Sandia Laboratories Steam and Combustion Gas Study	30-1
TASK 31 INTEVEP Carbon Dioxide Research	31-1
APPENDIX A. Full test of the "Third Amendment and Extension of Implementing Agreement IV Between the Department of Energy of the United States of America and the Ministry of Energy and Mines of the Republic of Venezuela in the Area of Enhanced Oil Recovery Thermal Processes."	

ABSTRACT

This report contains the results of efforts under the seven tasks of the Third Amendment and Extension of Annex IV, Enhanced Oil Recovery Thermal Processes of the Venezuela/USA Agreement. The report is presented in sections (for each of the 7 tasks) and each section contains one or more reports prepared by various individuals or groups describing the results of efforts under each of the tasks.

A statement of each task, taken from the agreement, is presented on the first page of each section. The tasks are numbered 25 through 31. The first, second, and third reports on Annex IV, [(Venezuela-MEM/USA-DOE Fossil Energy Report IV-1, IV-2, and IV-3 (DOE/BETC/SP-83/15, DOE/BC-84/6/SP, and DOE/BC-86/2/SP)] contain the results from the first 24 tasks. Those reports are dated April 1983, August 1984, and March 1986.

APPENDIX A

Full test of the "Third Amendment and Extension of Implementing Agreement IV Between the Department of Energy of the United States of America and the Ministry of Energy and Mines of the Republic of Venezuela in the Area of Enhanced Oil Recovery Thermal Processes."

THIRD AMENDMENT AND EXTENSION
OF THE
IMPLEMENTING AGREEMENT
BETWEEN
THE DEPARTMENT OF ENERGY OF THE UNITED STATES OF AMERICA
AND
THE MINISTRY OF ENERGY AND MINES OF THE REPUBLIC OF VENEZUELA
IN THE AREA OF
ENHANCED OIL RECOVERY THERMAL PROCESSES

WHEREAS, the United States Department of Energy (DOE) and the Ministry of Energy and Mines of Venezuela (MEMV) did on the 29th day of September 1980, enter into an Implementing Agreement for cooperation in the area of Enhanced Oil Recovery Thermal Processes (hereinafter referred to as the Implementing Agreement);

WHEREAS, DOE and MEMV have previously agreed to the First and Second Amendments and Extensions to the Implementing Agreement;

WHEREAS, DOE and MEMV have discharged their principal obligations and duties under the Implementing Agreement and the First and Second Amendments and Extensions to their mutual satisfaction and benefit;

WHEREAS, DOE and MEMV now desire to further extend ongoing cooperative efforts and further desire to initiate and pursue new and additional cooperative activities;

WHEREAS, the need exists to increase the recovery efficiency of steam injection methods for the recovery of heavy crude oil, and the use of additives is an attractive method of potentially increasing recovery efficiency;

WHEREAS, DOE and MEMV desire to cooperate in the application of additives to injection steam for the recovery of heavy oil crude;

WHEREAS, DOE and MEMV desire to further pursue cooperative efforts on the development of thermal front tracking methods, IT IS AGREED AS FOLLOWS:

ARTICLE 1

In accordance with Article 7 of the Implementing Agreement, and in accordance with Article V of the Energy Research and Development Agreement of March 6, 1980, DOE and MEMV hereby further amend and extend the Implementing Agreement as hereinafter provided.

ARTICLE 2

Article 1 of the Implementing Agreement and all other articles and provisions not herein amended are extended as written. The identification of Parties in Article 1 of the Implementing Agreement shall be used throughout this Amendment and Extension Agreement.

ARTICLE 3

Article 2 of the Implementing Agreement is amended by adding the following Tasks 25 through 31.

A. Thermal Front Tracking

Task 25 - DOE shall provide INTEVEP with information from the project and field tests conducted by the Lawrence Livermore National Laboratory on the use of seismic and electromagnetic methods for cross bore-hole probing to determine the location of steam zones and fronts within a petroleum reservoir.

Task 26 - INTEVEP shall provide DOE with final information from its thermal front tracking acoustic signal experiments in the M-6 field.

Task 27 - DOE shall provide INTEVEP with information from the project and field tests conducted by Sandia Laboratories on the use of Controlled Source AudioMagnetoTelluric (CSAMT) surveys to determine the location of steam zones and fronts within a petroleum reservoir.

B. Steam Additives

Task 28 - DOE shall provide INTEVEP with information from the foam diversion research and steam additive computational model development conducted by the Stanford University Petroleum Research Institute. The Project Managers will consult with one another on the foam diversion research and computational modeling being conducted at SUPRI and INTEVEP laboratories with a view to avoid duplication of effort and enhancing the respective research efforts.

Task 29 - INTEVEP shall provide DOE with information from research and screening tests performed by INTEVEP leading to a field test on steam with additives in Venezuela. The Project Managers shall consult with one another concerning screening tests and exchange information on screening tests previously obtained to avoid unnecessary duplication of research efforts.

C. Effects of Gases on Recovery

Task 30 - DOE shall provide INTEVEP with information from laboratory studies conducted by Sandia on the injection of combustion gases with steam as a thermal recovery method. The project will determine the possible effects of non-condensable gases, such as nitrogen, and potentially soluble carbon dioxide on oil recovery efficiency.

Task 31 - INTEVEP will provide DOE with information from laboratory studies on the injection of carbon dioxide as a potential oil viscosity reduction agent.

ARTICLE 4

The Implementing Agreement between DOE and INTEVEP shall hereafter consist of the Implementing Agreement as amended by the First, Second, and Third Amendments and Extensions.

ARTICLE 5

This Third Amendment and Extension shall become effective when signed by the members of the Joint Steering Committee or their designated representatives. The Implementing Agreement, as amended, shall remain in effect until September 30, 1986, or until terminated by written notice as provided in Article 8.

Done at Cancun in the English and Spanish Languages, each text being equally authentic, this 25th day of February, 1985.

THE JOINT STEERING COMMITTEE

On behalf of DOE

On behalf of MEMV

Keith N. Fryer
Member

[Signature]
Member

George J. Harkin
Member

[Signature]
Member

[Signature]
Member

Member

Feb 25, 1985
Member DATE

Feb. 25th, 1985
Date

Task 25 - DOE shall provide INTEVEP with information from the project and field tests conducted by the Lawrence Livermore National Laboratory on the use of seismic and electromagnetic methods for cross borehole probing to determine the location of steam zones and fronts within a petroleum reservoir.

Remote Monitoring of the Steamflood
Enhanced Oil Recovery Process

E. F. Laine

Electronics Engineering Department
Lawrence Livermore National Laboratory
Livermore, CA 94550

March 6, 1986

CONTENTS

Abstract.....	2
Introduction.....	3
Model.....	4
Kern River Test Site.....	5
Project Methods.....	6
Seismic Method.....	6
Electromagnetic Method.....	7
Velocity Tomograph.....	8
Electromagnetic Tomograph.....	9
Conclusion.....	10
Acknowledgements.....	11
References.....	11

Remote monitoring of the steam-flood
enhanced oil recovery process

E. F. Laine

Electronics Engineering Department
Lawrence Livermore National Laboratory
Livermore, California 94550

ABSTRACT

Cross-borehole seismic velocity and high frequency electromagnetic attenuation data were obtained to construct tomographic images of heavy oil sands in a steam flood environment. First arrival seismic data were used to construct a tomographic color image of a 10 meter by 8 meter vertical plane. Two high frequency (17 and 15 megahertz) electromagnetic transmission tomographs were constructed of a 20 by 8 meter vertical planes. The velocity tomograph clearly shows a shale layer with oil sands on both sides. The EM tomographs show a more complex geology of oil sands with shale inclusions. The deepest EM tomograph shows the upper part of an active steam zone and indicates steam channeling just below the shale layer. The results show detailed structure of the entire plane between boreholes and may provide a better means to understand the in-situ heavy oil recovery steam flood process.

INTRODUCTION

Remote sensing based on cross-borehole seismic and high frequency electromagnetic methods has recently received considerable attention. Electromagnetic (EM) wave propagation using high frequencies was reported (Lytle, et al., 1974) to image high explosive fracturing of coal seams. This work led to high frequency electromagnetic sensing of the in-situ coal gasification fire front and cavity growth (Davis, et al., 1979; Laine, et al., 1982). The simpler methods for remote sensing from boreholes of the cavity and fire front for in situ coal gasification led to the more sophisticated tomographic imaging of the in situ retorting of oil shale such as in the vertical rubblized retort at Logan Wash, Colorado (Daily, et al., 1981) and at Vernal, Utah (Daily, 1984). The evolution of geotomography as a method to assist scientists in evaluating the dynamics of in situ fossil fuel processing is being continuously refined and may soon be of commercial value to help understand the complex in situ processes due to the extraction or conversion of fossil fuels.

Two methods are discussed. The seismic tomograph and the high frequency electromagnetic tomograph. Both methods are field experimental programs in heavy oil sands that are in the process of steam recovery of the oil. The oil sands are shallow (245 meters) and the data were taken from wells dedicated to the experimental program. The wells are spaced 7.6 meters apart since the objective was to develop both seismic and EM tomographs without introducing complications due to extreme ranges.

The model used is shown in Fig. 1 where two vertical boreholes are shown with all possible ray paths between the source and receiver. The procedure used to reconstruct an image from the data is as shown in Fig. 2. The cells are of the same dimensions as the data increments (i.e., 0.25 m, 0.5 m, or 1.0 meter). We can use either the attenuation or velocity between the source and the receiver which is the sum of the differential attenuation or velocity along any of the individual paths linking the source and receiver. Only three paths are shown to illustrate the different combinations. Our model only has four cells as shown 11, 12, 21 and 22. The attenuation/velocity in cell ij is denoted as α_{ij} . The length of the kth ray path through ij is shown as D_{ijk} . The attenuation or velocity is shown in path 1 to be

$$\text{ATTEN}_1/\text{Vel}_1 = D_{11}\alpha_{11} + D_{12}\alpha_{12} + D_{21}\alpha_{21} + D_{22}\alpha_{22}$$

To reconstruct our image we assume straight line ray-optic equations. These may not hold strictly true for seismic velocity as for high frequency electromagnetic waves. At the Texaco site our boreholes are placed close together (7.6 meters) to attempt to minimize refraction, reflection and diffraction problems. From the above model and using an equation format similar to that of Fig. 2 a linear system of equations can be constructed to solve for the attenuation/velocity of each cell. A number of data-processing algorithms are available to solve for the system of equations (Dines and Lytle, 1978).

KERN RIVER TEST SITE

The experimental test site is located near Kern River and is on Texaco property identified as Section 33. Figure 3 is a sectional view and shows typical strata of the section and an LLNL test well. The oil-sand layers are identified as G, K, K₁, K₂, R, R₁, and R₂. Each layer is approximately 24 m thick and separated by an impermeable shale layer about 3 m thick. The average oil sand porosity is 30-32% with oil saturates of 45-55%. The oil viscosity ranges from 1000 to 20000 centipoise at 90°F. Injection steam quality is 50-60% with formation pressures of 70-200 psig. The formation water has an electrical conductivity of 1200 to 1700 micromohos/cm from well water samples.

The highest temperatures are at the R₁ level, the present steam layer and as shown in Fig. 4. Figure 5 shows the layout of the LLNL test wells and their relationship to each other and to the injection and production wells. A typical steam flood area is an inverted five-spot of approximately 2.5 acres. The steam-injection well is in the center of the field, and one production well is located in each of the four corners. Figure 6 shows a typical cased test well.

Before installing the casings, we were able to get caliper measurements, short- and long-spaced resistivity readings, self potential (SP) logs, and gamma logs of two boreholes. The area was under steam process and, even though the injection had been turned off, the oil sands were hot and under pressure. Therefore, we installed the casings quickly to prevent borehole damage or loss. We could log only the two boreholes, but presumed these data were representative of the immediate area.

From the time the boreholes were drilled, each had a temperature log made once each year. The temperature profiles are similar for all boreholes and had remained unchanged since 1981. In 1984, a pressure buildup began in Borehole No. 4, indicating a leak. We believe the fiberglass and high-temperature cement failed. The borehole can be reworked and made usable for seismic work. It is still usable for EM probing, since the noise and lack of water does not disturb EM measurements.

The seven experimental boreholes were each drilled to a depth of 243 m. The lower 121 m of the casing is 2000-psi fiberglass, which is transparent to high-frequency EM transmissions. The upper 122 m of casing is steel, a ball valve is installed at the surface. The entire 243-m length of the casing is surrounded by high-temperature cement to protect the fiberglass casing from the elevated temperatures in the active steam zone.

PROJECT METHODS

Seismic Method

Experimental seismic data obtained in this project was constrained to use of first p-wave arrival. No attempt was made to use shear wave or amplitude data. The p-wave velocity was used to construct a tomograph between two boreholes (2 and 4). The tomographic data was taken at one meter intervals over a vertical depth of 10 meters (100 ray paths). The tomograph pixels are one meter square. The color bar indicates the velocity range.

A seismic source was placed in a water-filled borehole. The seismic source was an underwater spark gap, connected, via coaxial cable, to an above

ground capacitive-discharge energy source. Figure 7 shows the frequency response spectrum of the spark gap, as recorded in a water tank. Three geophones (two horizontal and orthogonal to each other, one vertical) in a standard casing comprised the seismic receiver. The casing was modified to accommodate a simple wedge clamping mechanism that was operated by a separate cable (see Fig. 8).

The signal conditioning and monitoring apparatus consisted of a variable-gain differential amplifier and a sampling storage oscilloscope. All pertinent data (including the digitized output from the oscilloscope, date, time, depth of receiver, depth of source, received signals, and borehole identification) were stored on magnetic tape by a desk-top computer. A program, written for this application, controlled the cable reels, and read and stored the data. The complete system is diagrammed in Fig. 9.

Electromagnetic Method

The electromagnetic data obtained used the received signal amplitude variations to construct a tomograph of the transmission loss pattern in the plane between two boreholes (boreholes 1 and 2).

The transmitted frequency was 15 MHz. The EM data were taken with a short dipole for transmitter (1 meter) and a short active monopole probe (25 cm) for the receiver.

Data was taken at 0.25 meter increments over a total vertical distance of 20 meters (1600 ray paths). Each pixel of the tomograph is 0.25 meter square.

A desk-top computer controlled all equipment, including the cable reels. The computer program was menu driven, and allowed selection of start

and stop depths, number of data points to be collected, and frequencies to be scanned. All data are stored on magnetic tape.

A programmable frequency synthesizer generated the EM signal, and an aboveground amplifier amplified this signal to 100 watts. The amplified signal travelled through coaxial cable to the cable reel, and from there to an underground transmitting antenna in one of the boreholes. An underground receiving antenna, located in an adjacent borehole, received the transmitted signal. This receiving antenna was connected, through a cable reel and coaxial cable, to a programmable spectrum analyzer.

Velocity Tomograph

The velocity tomograph (Fig. 10) may be very useful because longer ranges are possible than the electromagnetic method and the seismic method can be used in steel cased boreholes. The electromagnetic method requires non-metallic casing. The velocity tomograph can discriminate between oil saturated sands, water saturated sands and gas sands at the shallow depths.

We installed the underwater spark gap in Borehole No. 4, and the three-axis geophone in Borehole No. 2. Borehole Nos. 4 and 2 are along the axis of and located between the steam injection well and one of the production wells. We took data at 1-m increments between depths of 80 and 90 m. The 7.62-m plane between the boreholes is divided into a matrix of 88 cells, 11 m by 8 m each.

Because of instrumentation problems, we were able to obtain data from only one horizontal geophone and the one vertical geophone. We used the seismic signal first-arrival to construct the color velocity tomograph (Fig. 10) using all of the ray paths intersecting the geophone and the source.

The velocity tomograph clearly shows a shale layer separating two oil sand layers. The shale layer corresponds to well log data taken in the same area.

The oil sand layers are shown to be relatively homogeneous as far as velocity changes.

The velocity tomograph obtained was not meant to be a stand-alone diagnostic tool, but to be used as a reference for a pre-steam zone and compared with later tomographs obtained after steam flood is initiated in this zone. The subsequent difference tomographs would show formation changes that would be related to the replacement of oil by water. The tomograph images the entire two-dimensional plane, and therefore, channeling can be observed if it occurs.

Electromagnetic Tomograph

The high frequency electromagnetic tomographs (Figs. 11 and 12) offer the complement to the seismic tomograph. The EM tomograph shows an attenuation image for signals transmitted from one borehole to another. The EM tomograph is more useful in areas of low conductivity media and can be made much faster than seismic methods. It is a non-contacting method, operates in dry or wet boreholes and is not bothered by seismic noise.

One drawback to the EM method is the requirement for non-metallic casing.

In the first tomograph (Fig. 11) we took cross-borehole data from 150 meters deep to 170 meters deep at 0.25 meter increments between boreholes 1 and 2. The bottom part of the tomograph is in the active steam zone with the upper part bound by a shale layer. The oil sand layer is denoted as R1 in

Fig. 3. The attenuation levels in the lowest quadrant are consistent with low loss such as a steam channel, the formation water is highly conductive and the signal loss would otherwise be high if this area were water saturated. The central portion of the tomograph shows much higher attenuation indicating the presence of a shale layer. Since this layer has been steamed and pumped for over four years a channel could easily have been formed. We expect to conduct more tests in the near future and examine the area below 170 meters with both amplitude and phase data.

A second set of tomographic data (Fig. 12) were taken in the same boreholes from 125 meters deep to 145 meters deep at 0.5 m increments and at 17 MHz. This data covered the area above the active steam zone. The bottom of the tomograph shows the shale layer again and above that oil sands with some shale inclusions. The upper left corner is caused by incomplete coverage of rays. This tomograph will serve as a reference for future steam activity in the R layer (Fig. 4).

CONCLUSION

The seismic velocity tomograph and the high frequency electromagnetic tomograph can serve as valuable diagnostic tools to observe the changes that occur in oil/water saturated sands during steam flood or other enhanced oil recovery methods. These changes are related to the seismic velocity and electromagnetic attenuation as the saturated oil sands are changed to steam or saturated hot water sands. The tomographs that were made in pre-steamed oil sands will serve as reference tomographs for later tomographs repeated after these zones are steamed. We can then difference the later tomographs with the reference tomographs to observe changes occurring in time.

As long as a seismic velocity or electrically anomalous condition is induced by the extraction process, the location and time history of the process can be monitored by using cross-borehole seismic or high frequency electromagnetic tomographic imaging of the entire plane between boreholes. By suitable arrangement of diagnostic boreholes, a three-dimensional tomographic image can be constructed. These tomographic images can provide operations with a method to help better understand the in-situ recovery process and to increase the efficiency of the oil recovery process.

ACKNOWLEDGEMENTS

I wish to thank George Stosur, DOE, Washington, D.C.; Gary Peterson, DOE, SAN; and Keith Westhusing, DOE, Bartlesville, OK, for their continued support and encouragement of this project. I would also like to thank my colleagues at LLNL, including the late Dr. R. Jeffrey Lytle for his continued efforts and support of this program, Dr. Robert Latorre for his experimental insight, Jane Beatty for the image reconstruction, and Ray Egbert for field support. I also want to thank W. Gordon Graves of Getty Oil Company and Pat Blough of Texaco Oil Company for the excellent cooperation and assistance given us at the Kern River test site.

REFERENCES

Daily, W. D., Lytle, R. J., Laine, E. F., Okada, J. T., Deadrick, F. J., 1981, Geotomography in oil shale: Lawrence Livermore National Laboratory, Livermore, CA, UCRL-85748.

Daily, W. D., 1984, Underground oil-shale retort monitoring using geotomography: Geophysics, 49, 1701-1707.

Davis, D. T., Laine, E. F., and Okada, J. T., 1979, Electromagnetic burn front mapping during ARCO's 1978 in situ coal gasification project: Lawrence Livermore National Laboratory, Livermore, CA, UCRL-52772.

Davis, D. T., Lytle, R. J., and Laine, E. F., 1979, Use of high frequency electromagnetic waves for mapping an in situ coal gasification burn front, In Situ 3, 95-119.

Dines, K. A. and Lytle, R. J., 1979, Computerized Geophysical Tomography, Proceeding of the IEEE, Vol. 67, No. 7.

Laine, E. F., and Lytle, R. J., 1981, In situ measurements of high frequency electrical conductivity and permittivity of oil shale: Society of Mining Engineers of AIM-E Transactions, 272, 1829-1830.

Laine, E. F., Chakakis, N. J., Daily, W. D., Deadrick, F. J., Holladay, G., Kishiyama, K. I., 1982, HFEM monitoring of coal gasification, Rawlins, Wyoming: Lawrence Livermore National Laboratory, Livermore, CA, UCID-19363.

Lytle, R. J., Laine, E. F., and Lager, D. L., 1974, Coal fracture measurements using in situ electrical methods: preliminary results: Lawrence Livermore National Laboratory, Livermore, CA, UCID-16639.

* This work performed under the auspices of the U.S. Department of Energy by the Lawrence Livermore National Laboratory, under contract W-7405-Eng-48 in cooperation with Texaco Oil Co.

LIST OF FIGURES

Fig. 1. Typical straight-line ray path configuration of all data used to construct tomograph.

LIST OF FIGURES

Fig. 2. Model for tomograph.

Fig. 3. Sectional view of LLNL test borehole area, Kern River Site.

Fig. 4. Typical temperature log of borehole.

Fig. 5. Plan view of LLNL test boreholes, Kern River Site.

Fig. 6. Plan view of LLNL test borehole construction.

Fig. 7. Frequency spectrum of underwater spark-gap pulse.

Fig. 8. Line drawing of geophone assembly with clamping mechanism.

Fig. 9. Block diagram of seismic instrumentation system.

Fig. 10. Seismic velocity tomograph. Data were taken from boreholes Nos. 2 and 4 at depths from 80 m to 90 m at 1-m increments. Borehole separation is 7.62 m. Straight-line ray path is assumed.

Fig. 11. Electromagnetic tomograph at 15 Megahertz, 0.25 m increments, showing possible steam channel.

Fig. 12. Electromagnetic tomograph at 17 Megahertz, 0.5 m increments.

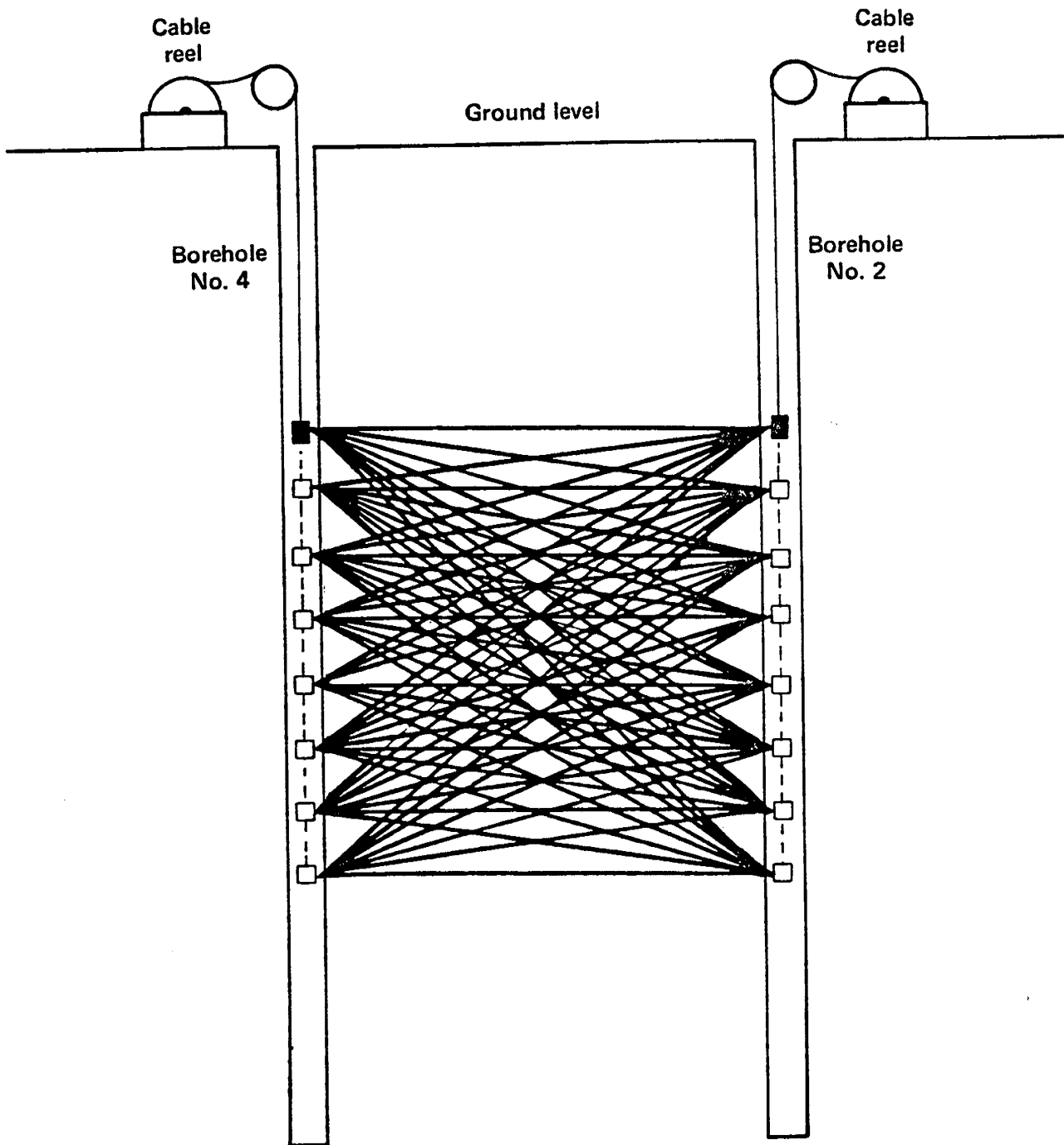
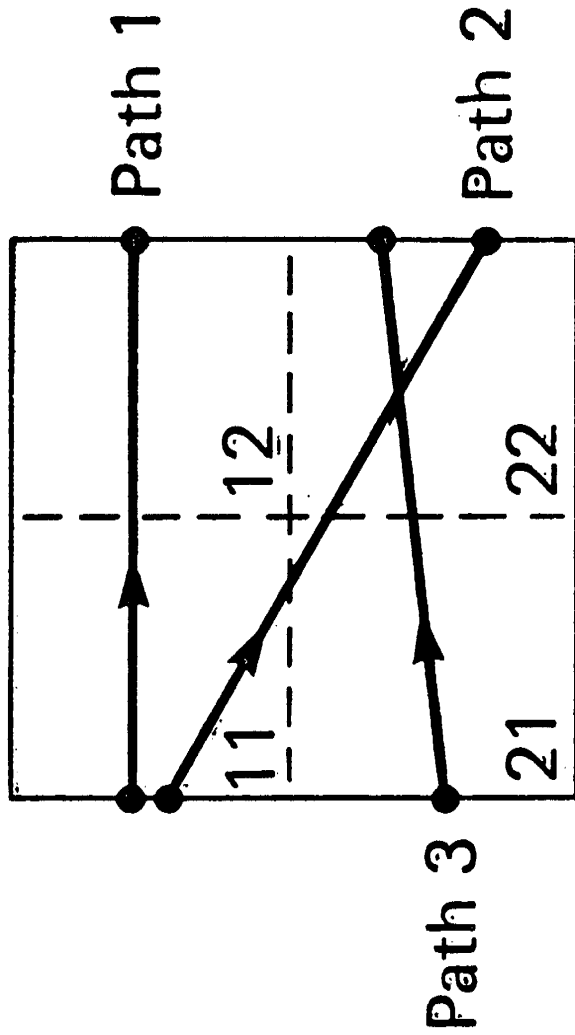


Fig. 1. Typical straight-line ray path configuration of all data used to construct tomograph.



$$\text{Atten}_1 = {}_1D_{11}\alpha_{11} + {}_1D_{12}\alpha_{12} + {}_1D_{21}\alpha_{21} + {}_1D_{22}\alpha_{22}$$

$$\text{Atten}_2 = {}_2D_{11}\alpha_{11} + {}_2D_{12}\alpha_{12} + {}_2D_{21}\alpha_{21} + {}_2D_{22}\alpha_{22}$$

$$\text{Atten}_3 = {}_3D_{11}\alpha_{11} + {}_3D_{12}\alpha_{12} + {}_3D_{21}\alpha_{21} + {}_3D_{22}\alpha_{22}$$

• • •

Fig. 2. Model for tomograph.

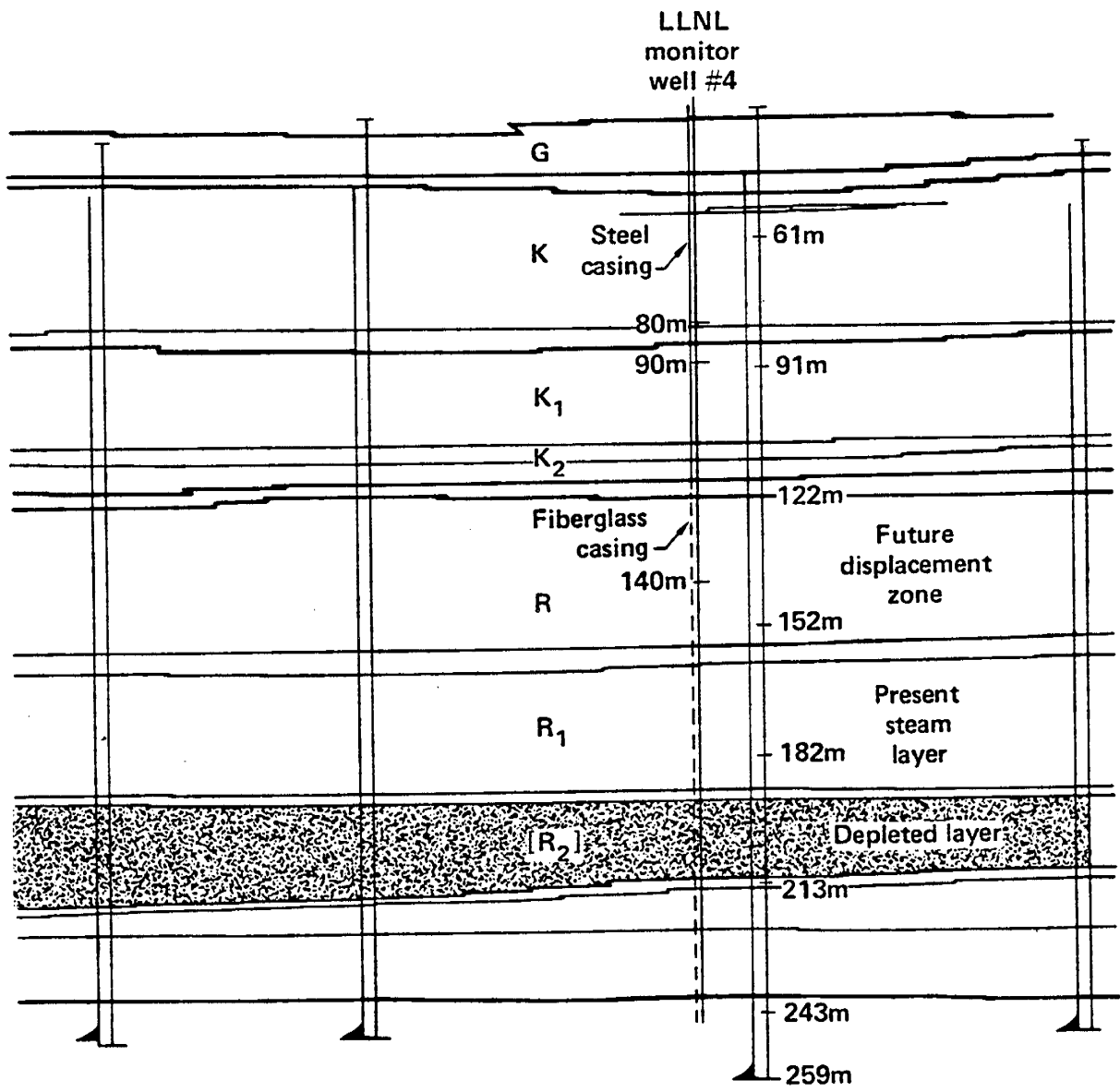


Fig. 3. Sectional view of the LLNL test borehole area, Kern River Site

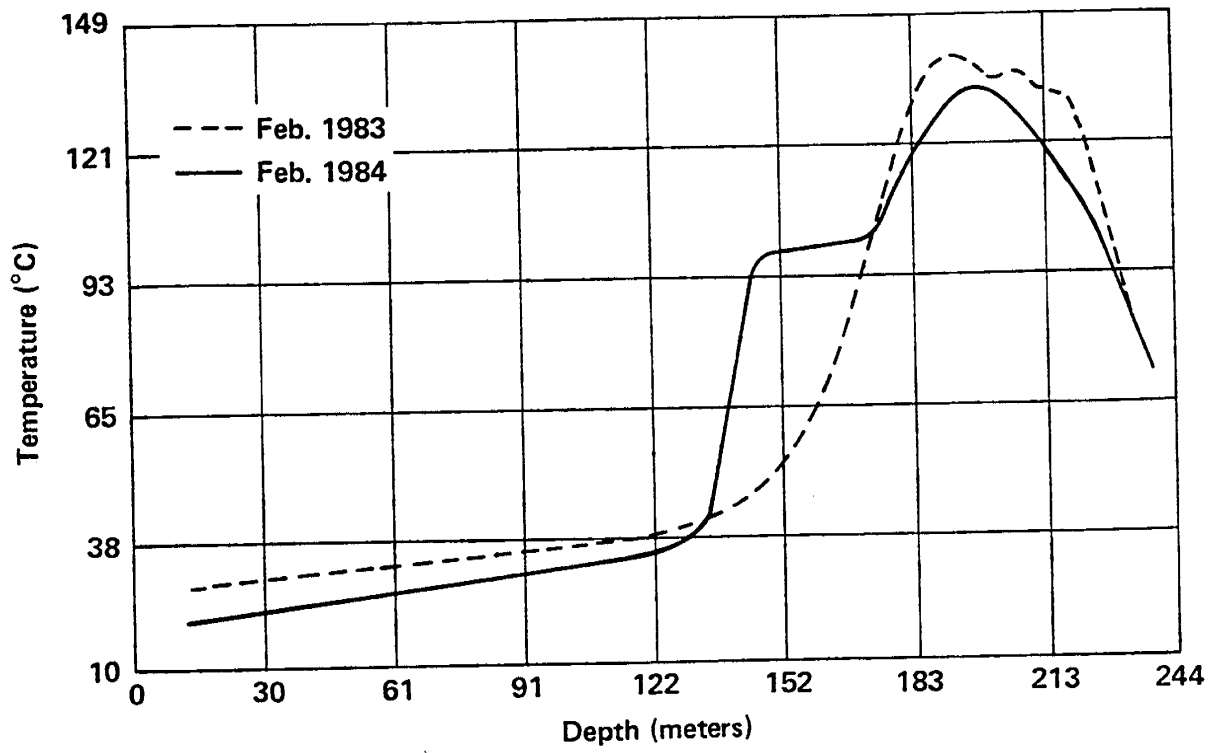


Fig. 4. Typical temperature log of borehole.

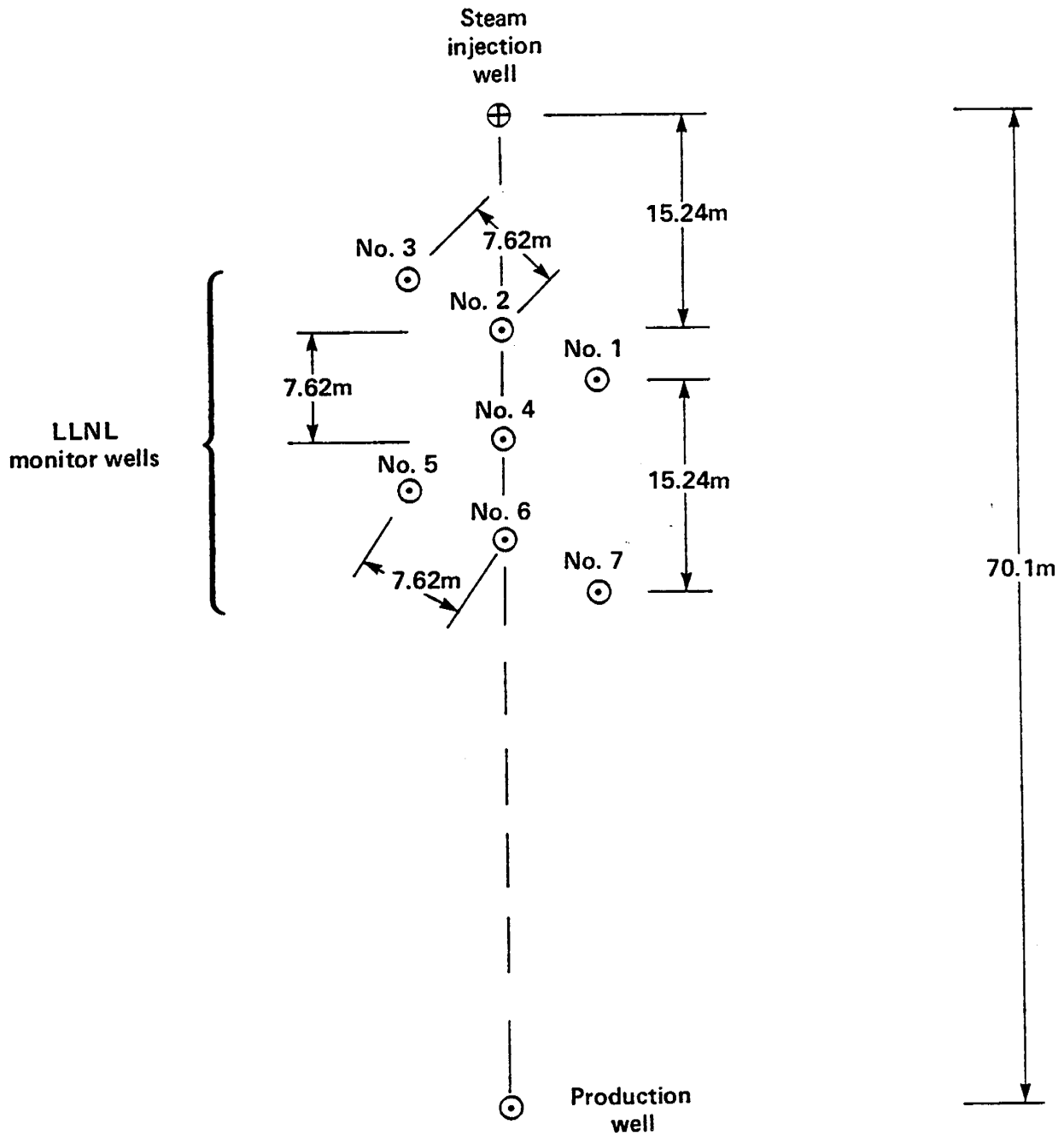


Fig. 5. Plan view of LLNL test boreholes, Kern River Site.

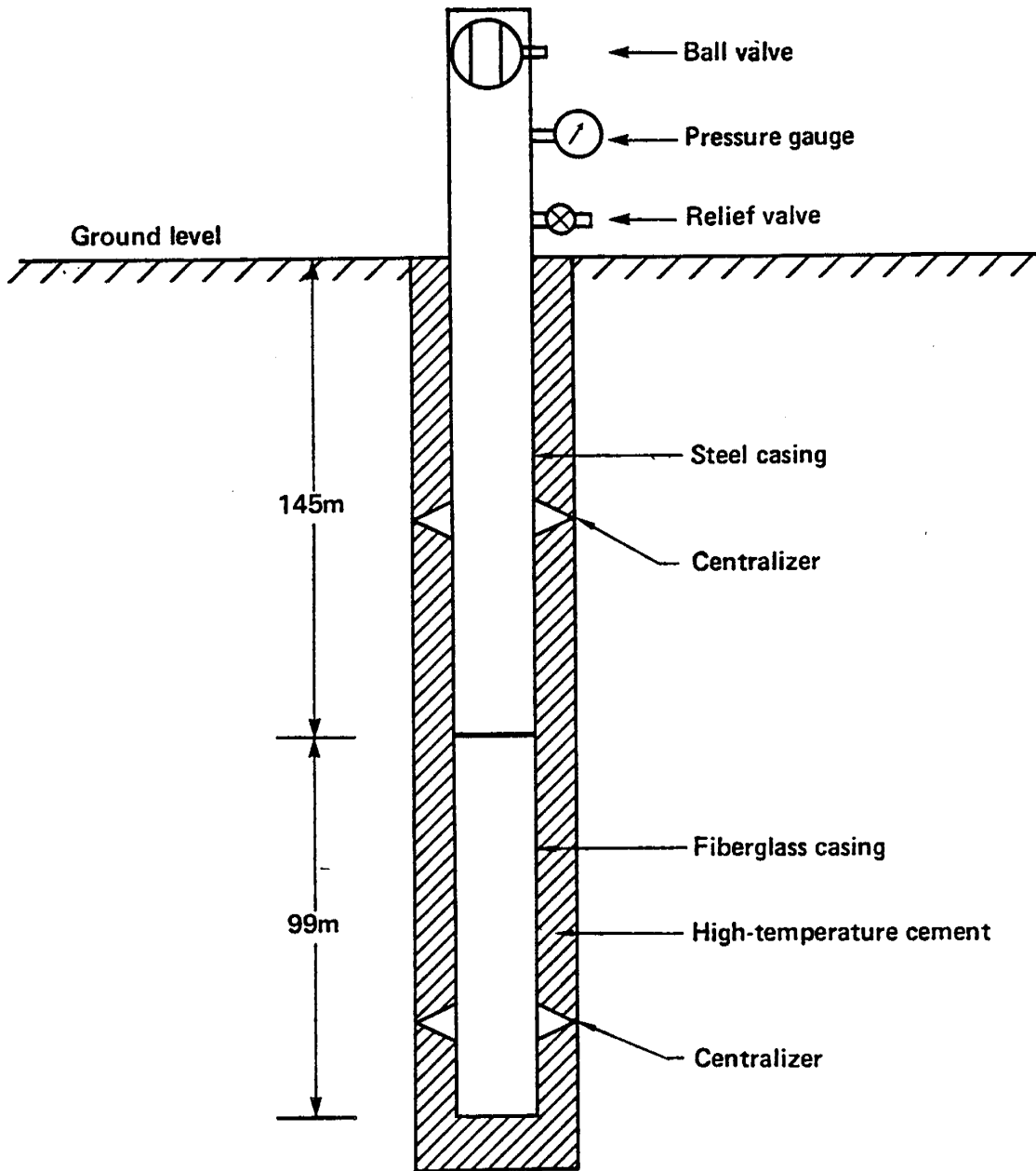


Fig. 6. Sectional view of LLNL test borehole construction.

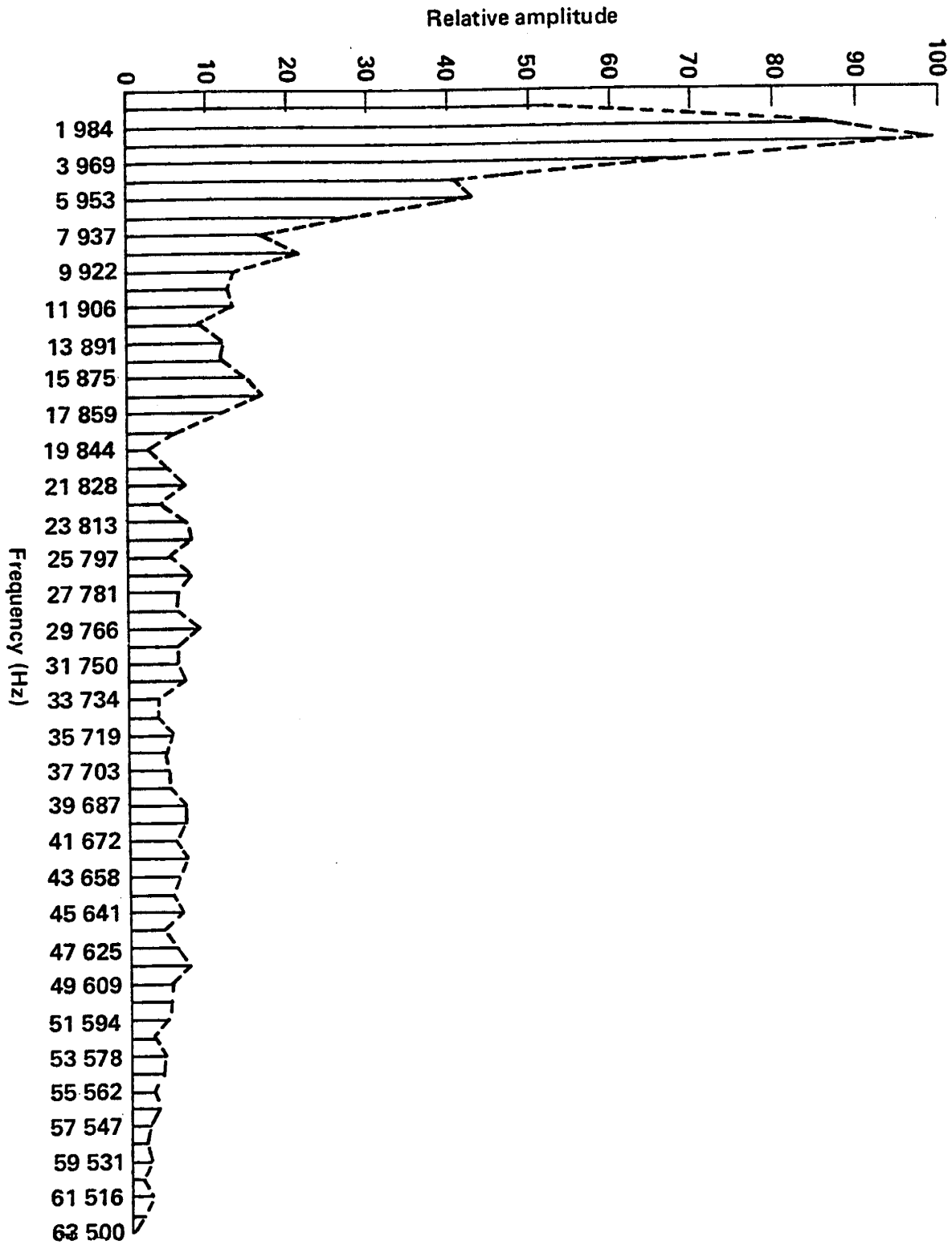


Fig. 7. Frequency spectrum of underwater spark-gap pulse.

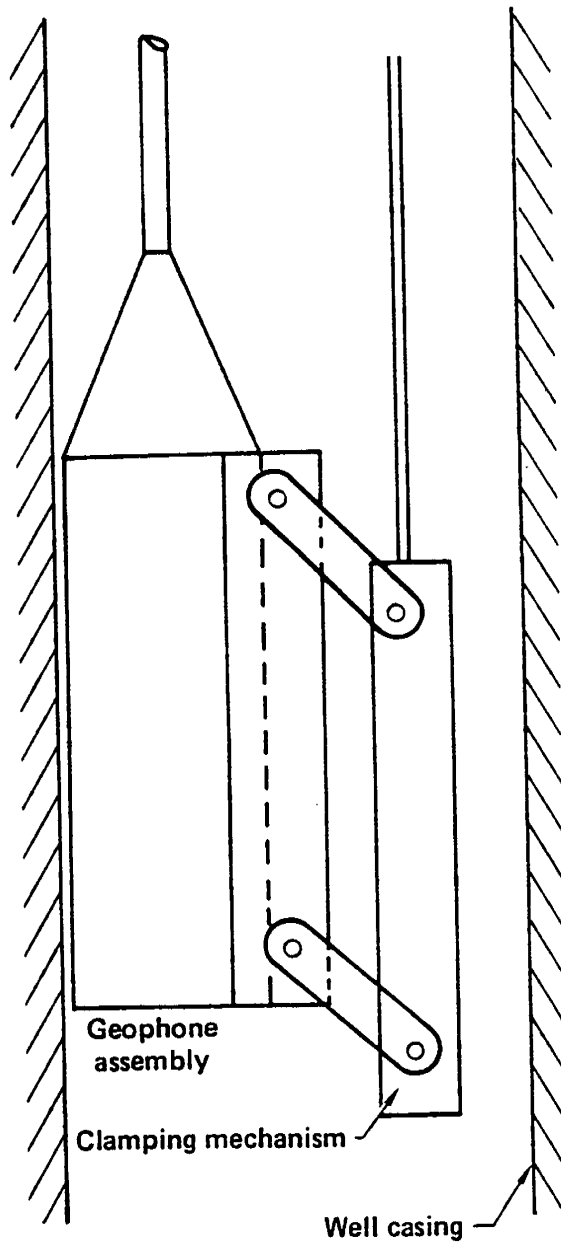


Fig. 8. Line drawing of geophone assembly with clamping mechanism.

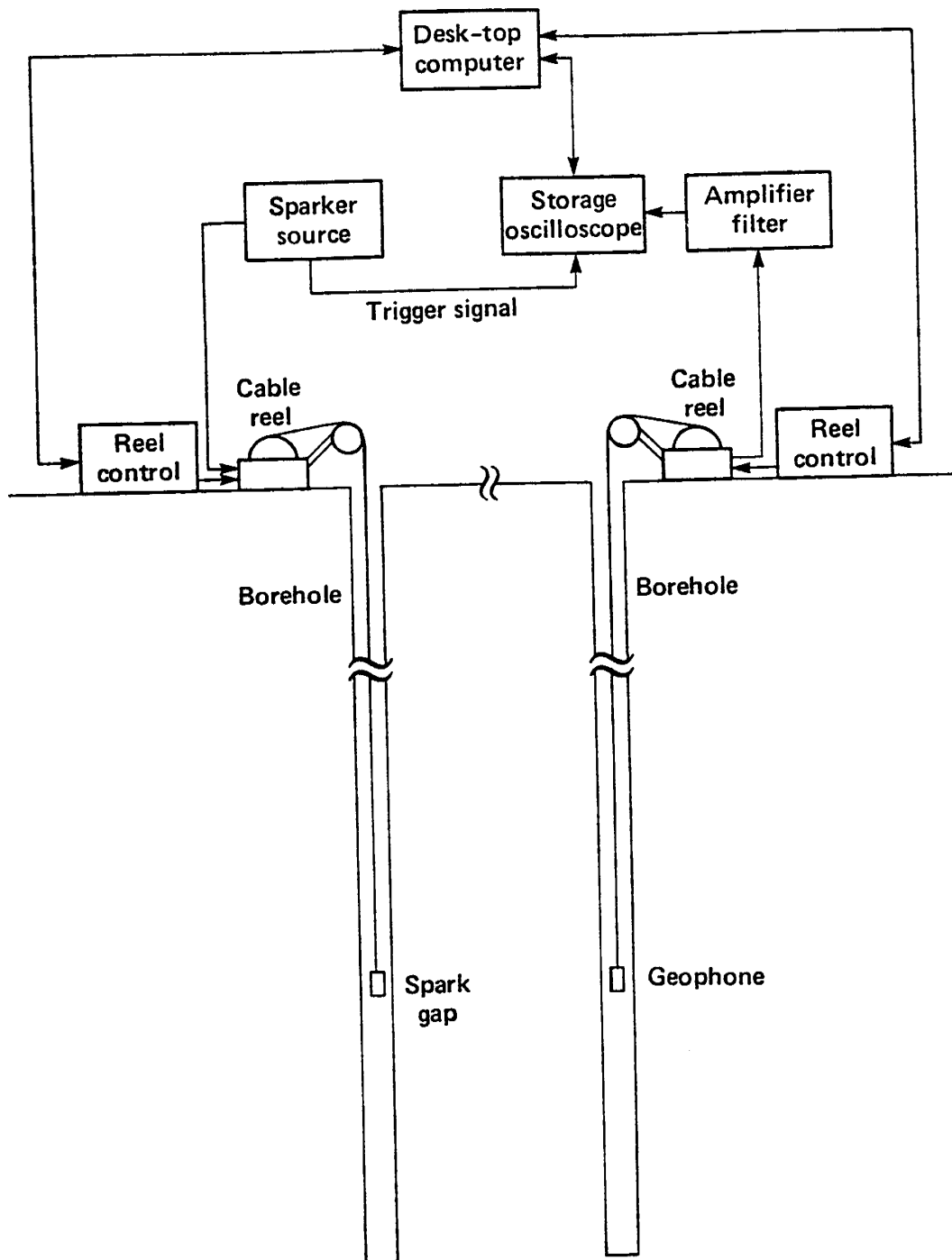


Fig. 9. Block diagram of seismic instrumentation system.

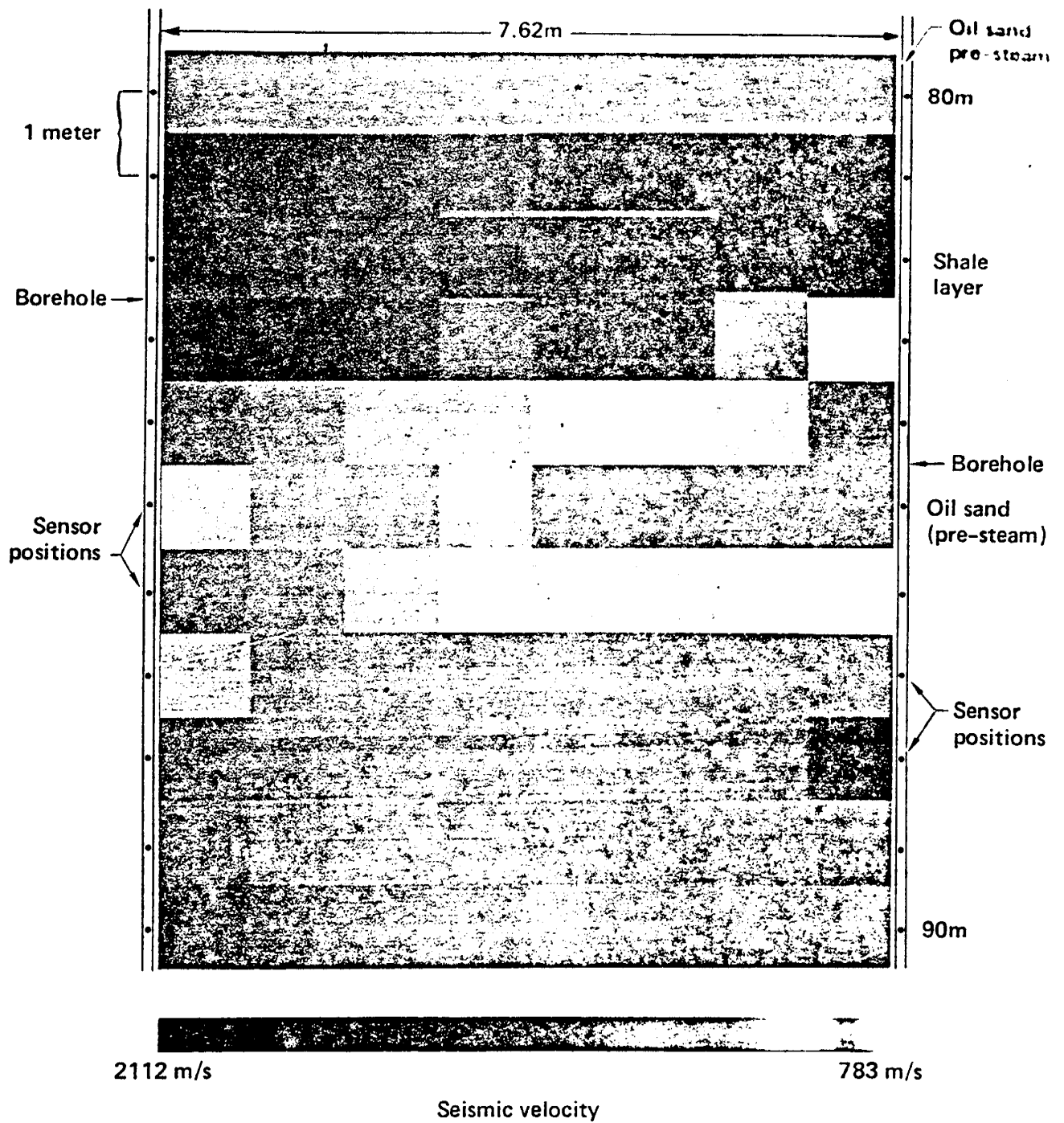


Fig. 10. Seismic velocity tomograph. Data were taken from boreholes Nos. 2 and 4 at depths from 80 m to 90 m at 1-m increments. borehole separation is 7.62m. Straight-line ray path is assumed.

ELECTROMAGNETIC TOMOGRAPH (15mhz)

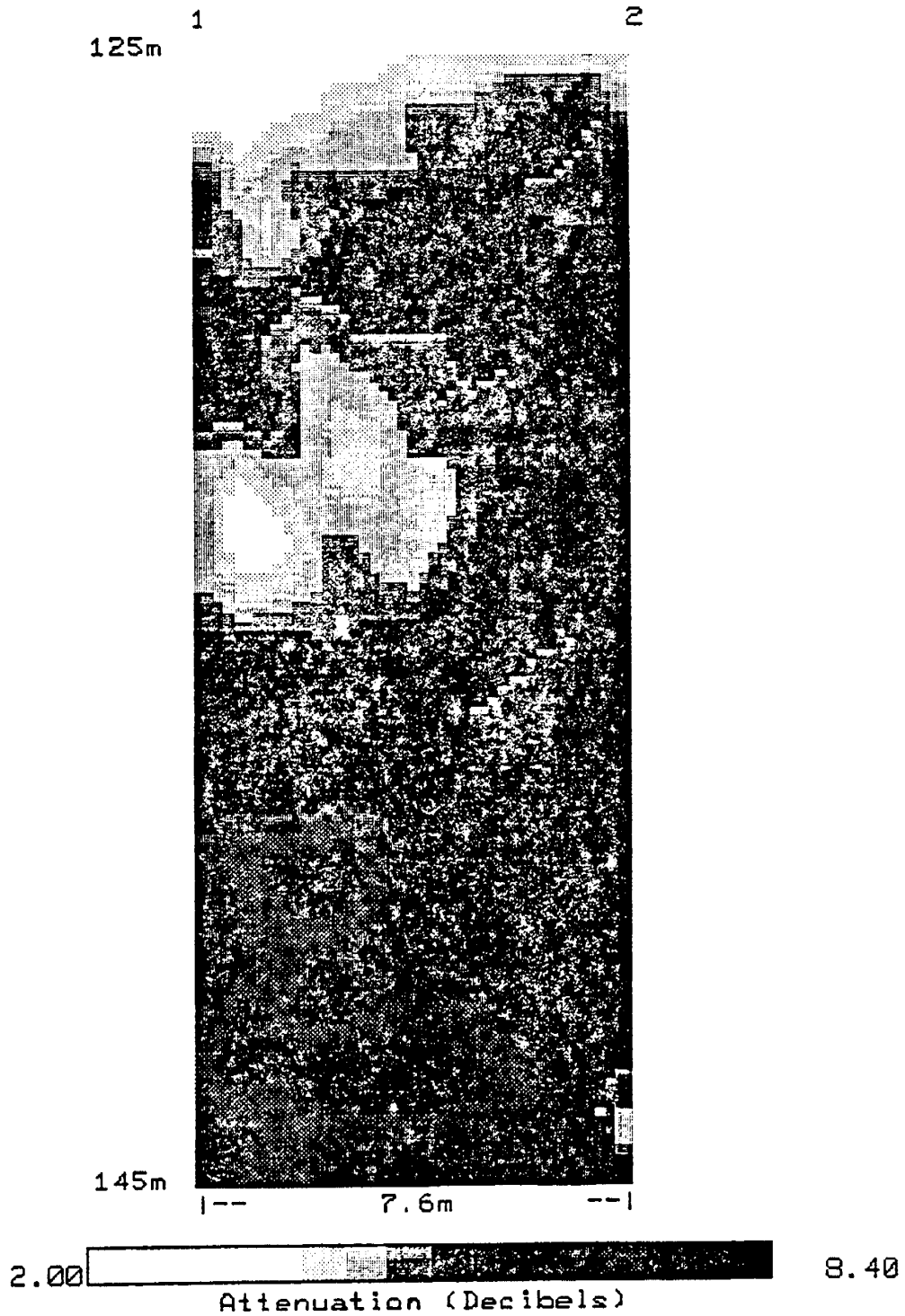


Fig. 11 Electromagnetic tomograph at 15 Megahertz, 0.25 m increments, showing possible steam channel

ELECTROMAGNETIC TOMOGRAPH (17mhz)

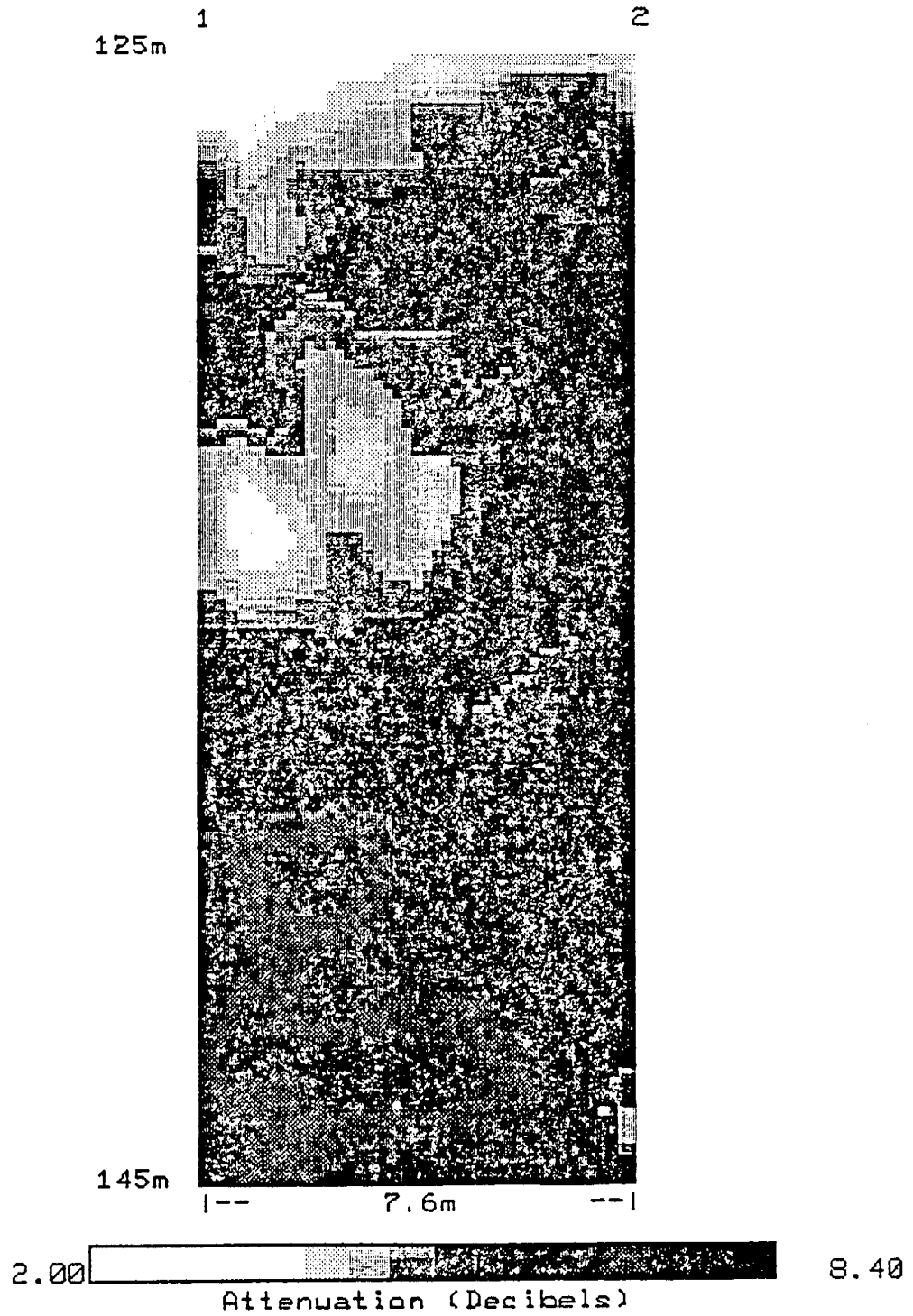


Fig. 12 Eletromagnetic tomograph at 17 Megahertz, 0.5 m increments.

Task 26 - INTEVEP shall provide with final information from its thermal front tracking acoustic signal experiments in the M-6 field.

ACOUSTIC SIGNAL THERMAL FRONT TRACKING TEST IN THE M-6 FIELD

(Task 26 of Annex IV of the Implementing Agreement)

Prepared by
Orlando Chacin
INTEVEP, S. A.

Los Teques, Venezuela
September 1986

CONTENTS

	Page
ABSTRACT	26-4
LIST OF ILLUSTRATIONS	26-5
1. INTRODUCTION AND OBJECTIVES	26-7
2. M-6 CORE SAMPLE ULTRASONIC MEASUREMENTS	26-9
3. M-6 CROSSWELL SEISMIC FIELD TEST	26-10
4. CONCLUSIONS AND RECOMMENDATIONS	26-11
REFERENCES	26-13

ABSTRACT

Thermal recovery projects in low to medium gravity oil reservoirs require a continuous control of the fluids spatial movements within the injection patterns in order to properly evaluate the process. Unfortunately, tools for in situ monitoring of actual flow distribution, movement rate and spatial heterogeneities of fire and steam fronts are still limited. Recently, high resolution geophysical methods have been introduced to assist in the related reservoir evaluation.

Using one of these geophysical methods, INTEVEP conducted a feasibility study in the M-6 steam drive project, in order to verify changes in seismic properties of a thermal developed reservoir. In this study, petrophysical analysis done with M-6 core samples showed that fairly large velocity and attenuation anomalies are related with steam injection, which suggested that the steam zone could be seismically located. However, results of a first cross-well seismic field test with actual production wells were discouraging due to downhole sparker failure. The acoustic source could not generate enough output energy to overcome the adverse conditions found within the selected injection pattern (cased wells, unconsolidated sands, wells distance and receiver-well noise).

Planning of future field tests in large scale steam projects, such as M-6, should include more rigorous acoustic and electrical control of the downhole sparker or alternately consider other non-destructive seismic sources such as a downhole vibrator. Additionally, lower resolution seismic techniques (VSP and surface seismic) which do not present downhole source restrictions should be included in a more integrated feasibility study of EOR thermal front tracking projects.

LIST OF ILLUSTRATIONS

	Page
Fig. 1. M-6 project location.	26-14
Fig. 2. Injection hexagons considered for the seismic field test.	26-15
Fig. 3. P wave velocity decrease with temperature in a 100% oil saturated core.	26-16
Fig. 4. S wave velocity decrease with temperature in a 100% oil saturates core.	26-17
Fig. 5. P wave amplitude decrease with temperature in a 100% oil saturated core.	26-18
Fig. 6. P and S wave velocities during steam transition in a 100% oil saturated core.	26-19
Fig. 7. P wave velocity change with temperature in a 0% oil saturated core.	26-20
Fig. 8. S wave velocity change with temperature in a 0% oil saturated core.	26-21
Fig. 9. P wave velocity decrease with steam transition in a 0% oil saturated core.	26-22
Fig. 10. P wave amplitude decrease with steam transition in a 0% oil saturated core.	26-23
Fig. 11. 1000 joule downhole sparker electrode and 8000 volt power supply at the LSE-1408 well.	26-24

	Page
Fig. 12. LSE-1408 well prepared for the field test.	26-25
Fig. 13. LSE-3056 well prepared for the field test.	26-26
Fig. 14. Crosswell seismic records without evidence of first arrivals.	26-27

1. INTRODUCTION AND OBJECTIVES

Evaluation of thermal EOR projects for low to medium gravity oil requires careful consideration of all factors influencing fluid migration within the injection patterns. One significant problem, arising in the design of thermal EOR projects is the accurate mapping and monitoring of reservoir fluids spatial distribution and properties so as to control the performance of the thermal process. Fluid saturations should be controlled at all times in order to modify the injection/production schedule, if necessary. Unfortunately, reservoir engineers still lack tools which can continuously determine the propagation direction, shape, movement rate and spatial heterogeneities of fire and steam fronts. Recently, new emerging techniques which make use of high resolution geophysical methods may provide accurate and complete evaluation of fluids distribution in reservoirs undergoing thermal EOR recovery processes.

The first two successful in situ monitoring of thermal EOR operations using geophysical methods applied surface seismic reflection and high-resolution crosshole electromagnetic transmission measurements. These operations were practiced on Conoco's Street Ranch pilot pattern ¹ and on Cities Service's pilot sites ². Both field measurements were still restrictive in terms of resolution (surface seismic) and penetration range (electromagnetic) for significantly mapping deep reservoirs and large scale thermal projects. Parallely, MARAVEN (operating affiliate of Venezuela PDVSA) also made attempts to detect steam fronts in the M-6 steam drive project by using surface and borehole (VSP) seismic techniques ^{3,4}. The results of these attempts were inconclusive. Therefore, Nur ⁵ suggested the application of the widely used high resolution seismic transmission

method 6, 7, 8 to detect changes in seismic properties of a thermal developed reservoir. Based on Nur's suggestion and MARAVEN results, INTEVEP decided to conduct a field seismic transmission test to validate the detectability of seismic waves changes induced by a steam drive project. Starting 1983 and after considering injection time, well break through, reservoir uniformity and ambient noise, INTEVEP, MARAVEN and Stanford Rock Physics Group selected an hexagon in the M-6 steam drive project (Fig. 1) to run the crosswell data experiment.

The crosswell feasibility study included the following steps: (1) Ultrasonic velocities and attenuation laboratory measurements at different pressure and temperature conditions on M-6 core samples. (2) Crosswell seismic field test in a selected hexagon of the M-6 field with both, seismic source and receiver down in the production wells. (3) Seismic processing and interpretation of the final transmission and reflection tomographs in combination with laboratory measurements, well logs, geological models and production information in order to provide reliable images of velocity and attenuation changes that may be related to fluid distribution in the M-6 reservoir.

2. M-6 CORE SAMPLE ULTRASONIC MEASUREMENTS

In mid 1983, INTEVEP sent core samples from the injector well LSE-3307 (Fig. 2) to Stanford University in order to measure P and S wave travel time and amplitude under real reservoir conditions of the M-6 area. A total of 2,605 measurements were done in the ultrasonic apparatus using 6 core samples, prepared with different oil/brine saturation ratios. For the 100% oil saturated samples, it was determined that a temperature increase from 25°C to 150°C resulted in a 40% decrease in the P wave velocity (Fig. 3) and a 35% decrease in S wave velocity (Fig. 4) for constant confining pressures. The temperature increase also affected the P wave amplitude, which decreased 90% (Fig. 5). To study the effect of steam, a steam-transition zone test was run in a 100% oil saturated core but the results (Fig. 6) showed no changes in the P and S wave velocities.

Later, tests runs in 100% brine saturated samples, showed that a temperature increase from 25°C to 150°C resulted in no changes in the P and S wave velocities (Figs. 7 and 8) for constant confining pressures. However, during the transition from brine to steam, a very marked decrease in the P and S wave velocities (Fig. 9) and P wave amplitude (Fig. 10) was observed. The above results summarize steam effect on acoustic wave transmission properties through cores. These data suggest we use seismic methods to locate steam saturated zones in oil reservoirs.

3. M-6 CROSSWELL SEISMIC FIELD TEST

Starting 1984, a team from INTEVEP and the Stanford Group designed the crosswell seismic experiment at the LSE-3054 hexagon (Fig. 2) after evaluating the completion condition of the selected production wells (LSE-1408 and LSE-3056), the 460 m distance between the two wells, the temperature and pressure conditions of the Lagunillas Inferior reservoir, and the presence of H₂S in the wells. The design included the following equipment: a 1000 joule downhole sparker (Fig. 11) specially built by Teledyne Exploration (Houston), a SWC-3 three-component downhole geophone, a EG&G Nimbus 1210 seismograph with a EG&G 1600 bpi SEG-D digital recorder, a Hewlett-Packard 3968A analog recorder and a LRS-100 surface geophone. After well preparation and equipment testing, the sparker was lowered down the LSE-1408 (Fig. 13) well, and the geophone down the LSE-3056 (Fig. 13) well, and several crosswell tests were run. No definite arrivals of those seismograms were recorded (Fig. 14), in spite of stacking various sparker shots at the same shot-receiver position. This first crosswell seismic survey system test in M-6 was a failure. Two main reasons were found to explain this result: First, the relation between the downhole sparker energy output and the production well distance was not high enough for the 2000 feet deep unconsolidated Lagunillas Inferior reservoir, and second, the unexpected high gas concentration present in the receiver well created too much acoustic noise making impossible the recording of any relevant signal.

4. CONCLUSIONS AND RECOMMENDATIONS

The feasibility study done by INTEVEP and Stanford University to detect steam fronts through the use of acoustic signals in the M-6 steam drive project has shown that:

- A significant change in velocity and attenuation of acoustic waves occurs when temperature increases in oil saturated sands. Moreover, the presence of steam (no oil saturation) in the pores magnifies this effect. These core measurements suggest that fairly large velocity anomalies are associated with steam injection, and that these anomalies can be mapped seismically if they are large enough in size.

- A more rigorous control of the acoustic capabilities of the downhole sparker is needed in order to record high resolution seismic data in a subsequent field test. Additionally, to perform a crosswell test in actual production wells is necessary to have a careful planning of the logistics needed, together with information of the "noise" level in the receiver well.

At present, INTEVEP's experience should suggest careful thinking before any future verification in the field of any further laboratory tests. The selection of a smaller scale steam drive project (50 to 100 m between production wells) is considered important if production wells have to be used in a future crosswell experiment. The drilling of observation wells at convenient places and shorter distances inside the injection patterns, should be considered if justifiable. Furthermore, other non-destructive downhole sound sources such as a downhole vibrator, a water gun or a bridged-gap electrode sparker should be examined. Finally, great importance should also be given to the use of PVC-cased observation wells as receivers in order to avoid the high noisy environment normally present in field due to gas and steam entering the vicinity of the production wells.

If experimental and logistic inconvenients are overcome, new crosswell seismic tests should lead to the construction of 2-D velocity and attenuation tomographs. These data shall be related to laboratory measurements, well logs, stratigraphic and production information to give accurate values of oil-water saturations in each region of the geotomographic reconstruction. A natural extension of these 2-D crosswell tomographs would be the construction of a full 3-D tomograph from various crosswell field seismic surveys in the same injection pattern.

Finally, to map seismic anomalies in a complete steam drive project, it is necessary to compare the above results with lower resolution seismic techniques (3-D surface seismic and offset VSP) in order to analyze the feasibility of lateral prediction of anomalies throughout the reservoir without the restrictions of a downhole source.

REFERENCES

1. Britton, M.W., Martin, W.L., Leibrecht, R.J. and Harmon, R.A. The Street Ranch Pilot Test of Fracture-Assisted Steamflood Technology. Presented at the SPE California Regional Meeting; San Francisco, 1982.
2. Witherholt, E.J., Kretschmar, J.L. and Jay, K.L. The Application of Crosshole Electromagnetic Wave Measurements to Mapping of a Steam Flood. Presented at the 33rd Annual Technical Meeting of the Petroleum Society of CIM; Calgary, 1982.
3. Geología de Producción. Determinación del Frente de Vapor en el Proyecto M-6 mediante Métodos Sísmicos. Informe Interno, MARAVEN, S. A., 1982.
4. Noel, J. M. An Experiment of Steamdrive Detection by Vertical Offset Seismic Profiles. Internal Report, MARAVEN, S.A., 1983.
5. Nur, A. Seismic Imaging in Enhanced Recovery. Presented at the DOE/SPE EOR Conference; Tulsa, 1982.
6. Bois, P., La Porte, M., Laverge, M. and Thomas, G. Well-to-Well Seismic Measurements. Geophysics, v.37, p. 471-480, 1972.
7. McCann, D.M., Grainger P. and McCann, C. Inter-Borehole Acoustic Measurements and Their Use in Engineering Geology. Geophysical Prospecting, v.23, p.50-69, 1975.
8. Thill, R.E. Acoustic Cross-Borehole Apparatus for Determining In Situ Elastic Properties and Structural Integrity of Rock Masses. Proc. 19th U.S. Rock Mech. Symposium, University Nevada-Reno Press, p. 121-129, 1978.

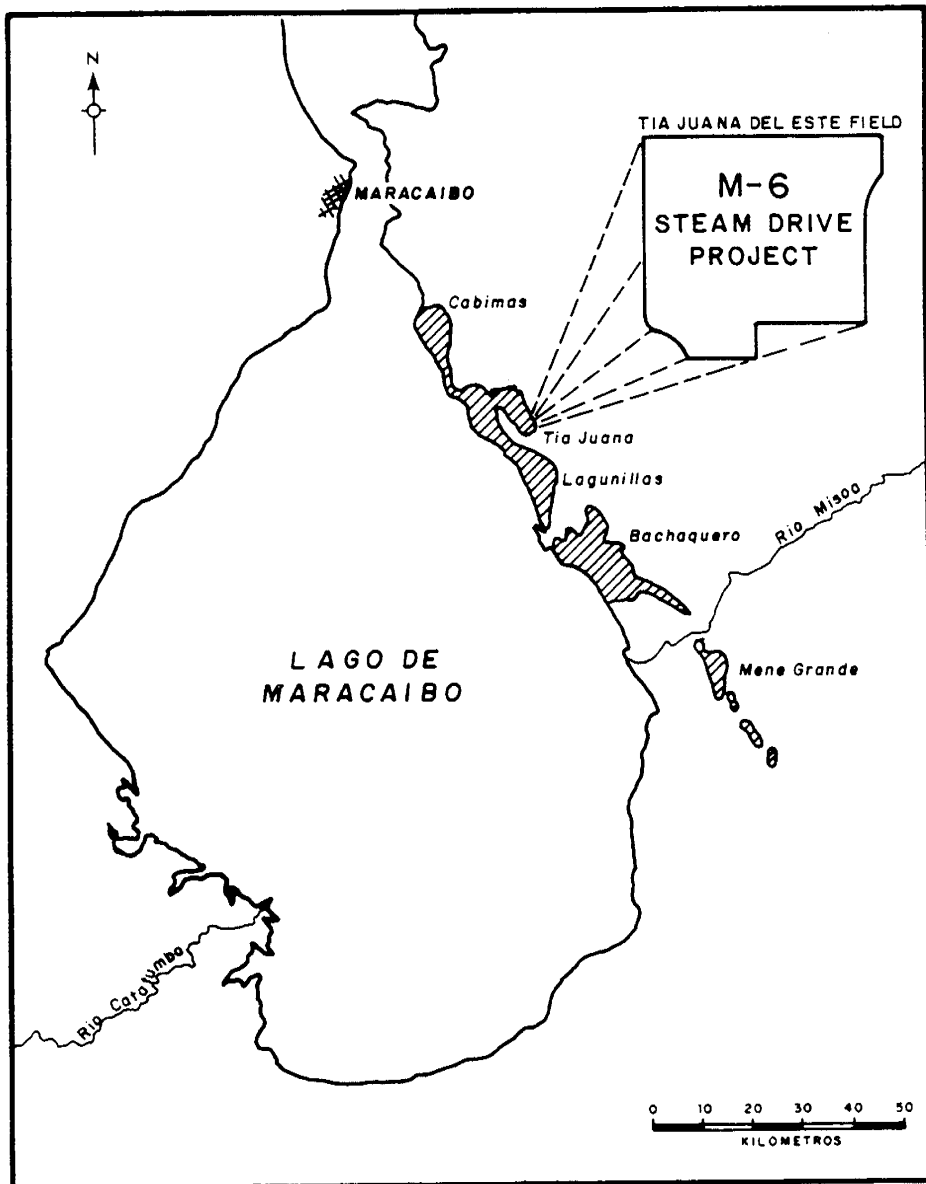


Fig. 1. M-6 project location.

M-6 STEAM DRIVE PROJECT (MARAVEN, S.A.)

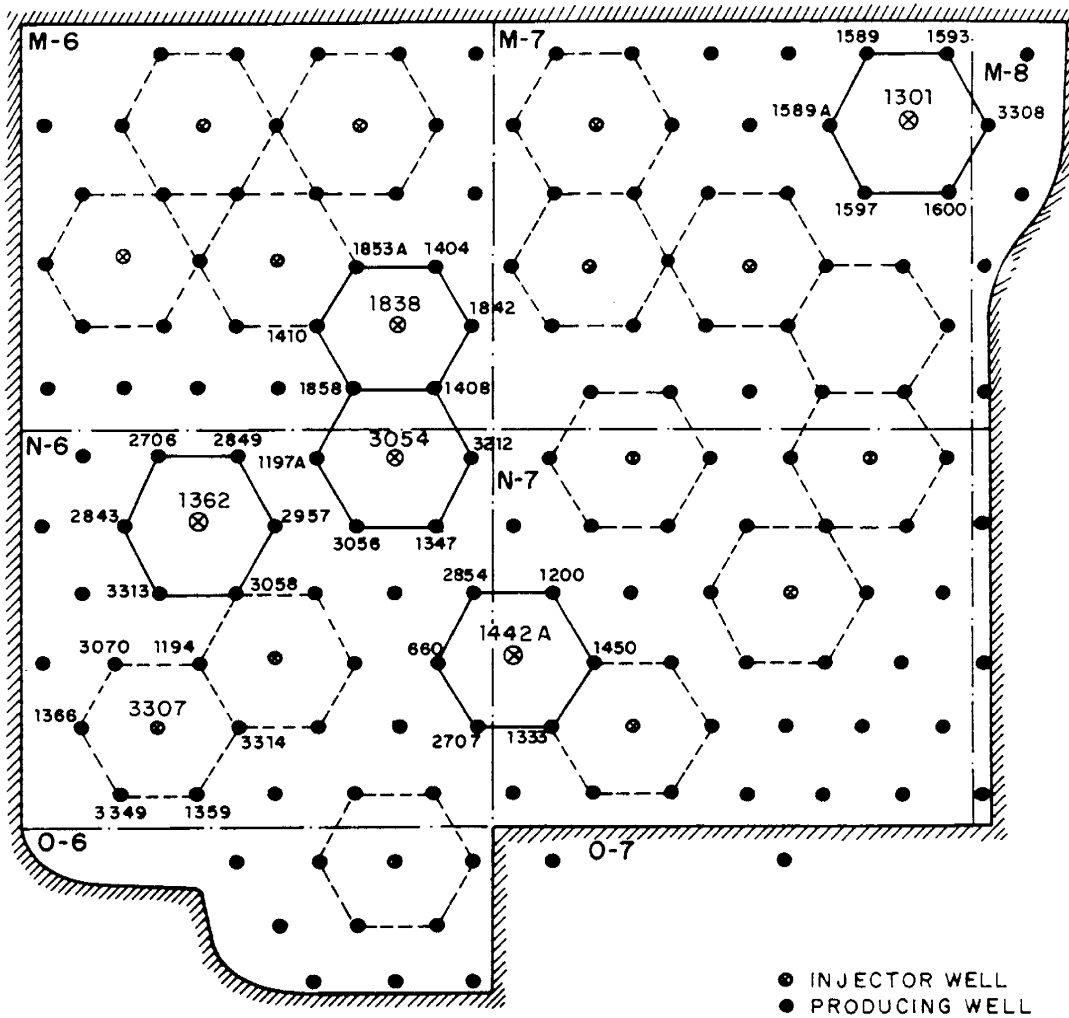


Fig. 2 Injection hexagons considered for the seismic field test.

WELL LSE-3307 (SAMPLE 7)

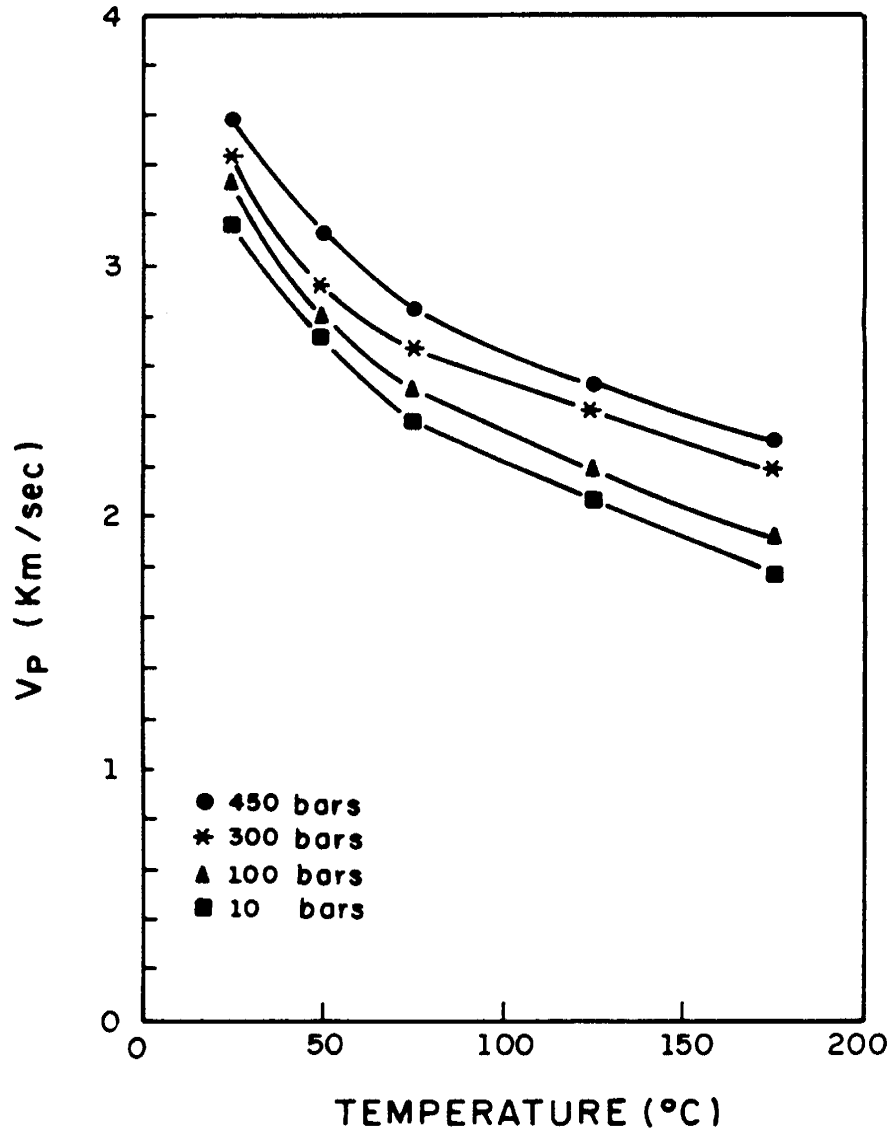


Fig. 3. P wave velocity decrease with temperature in a 100% oil saturated core.

WELL LSE-3307 (SAMPLE 7)

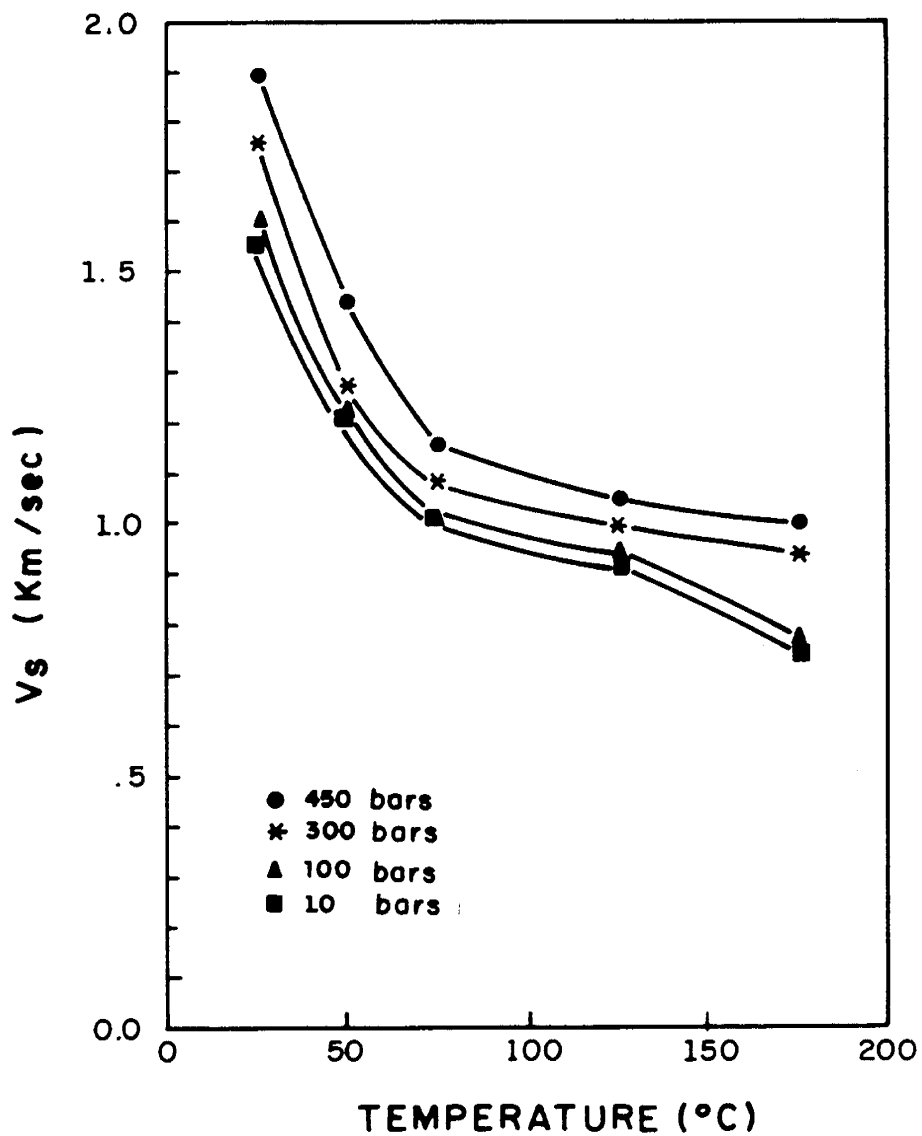


Fig. 4. S wave velocity decrease with temperature in a 100% oil saturated core.

WELL LSE-3307 (SAMPLE 7)

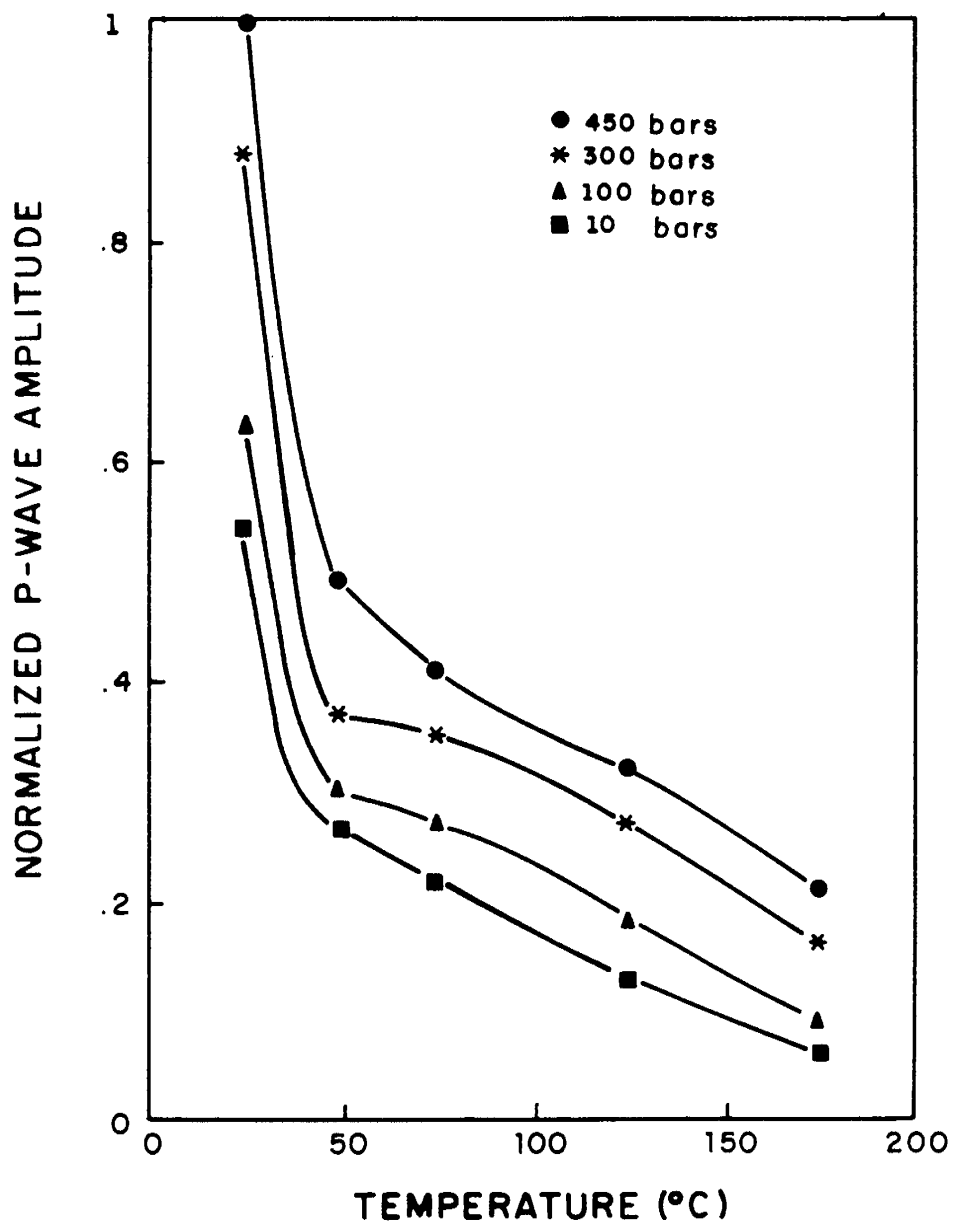


Fig. 5. P wave amplitude decrease with temperature in a 100% oil saturated core.

WELL LSE-3307 (SAMPLE 7)

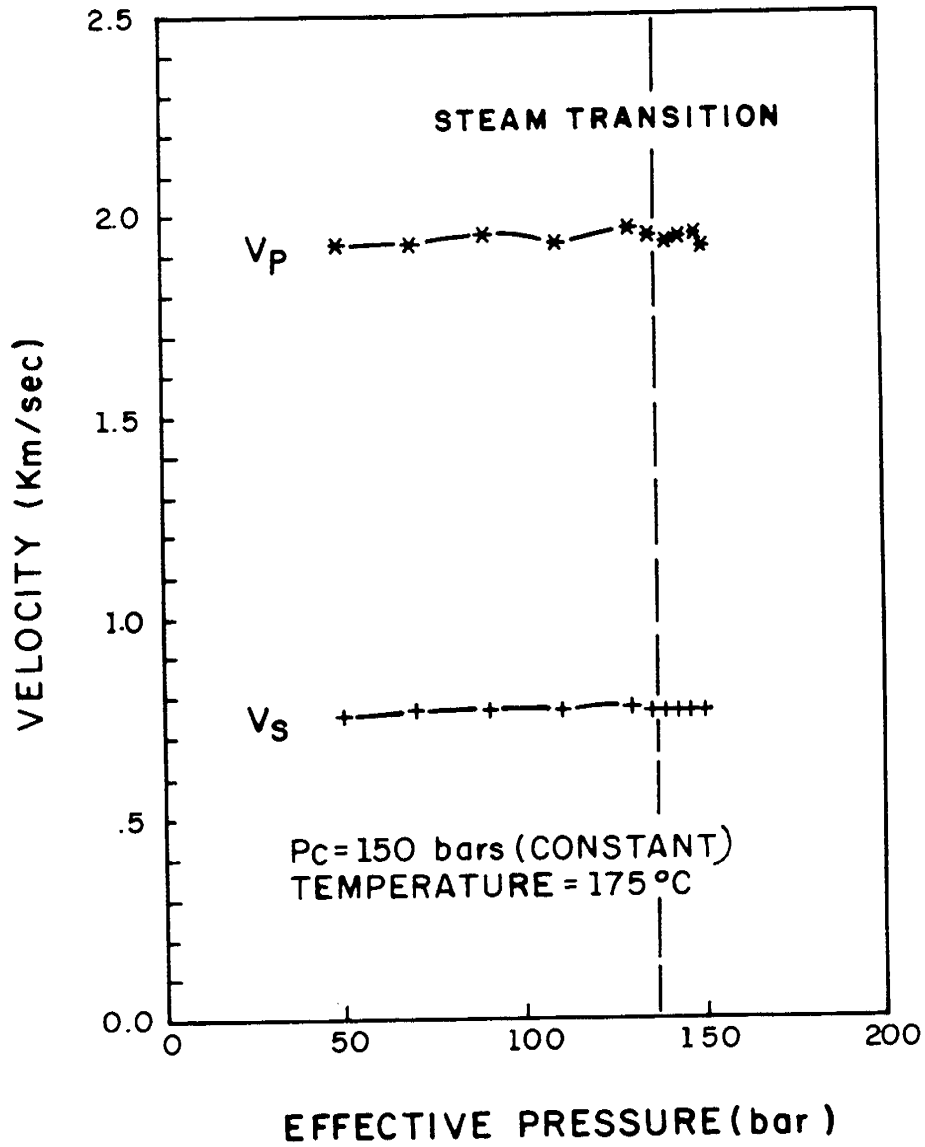


Fig. 6. P and S wave velocities during steam transition in a 100% oil saturated core.

WELL LSE-3307 (SAMPLE 3)

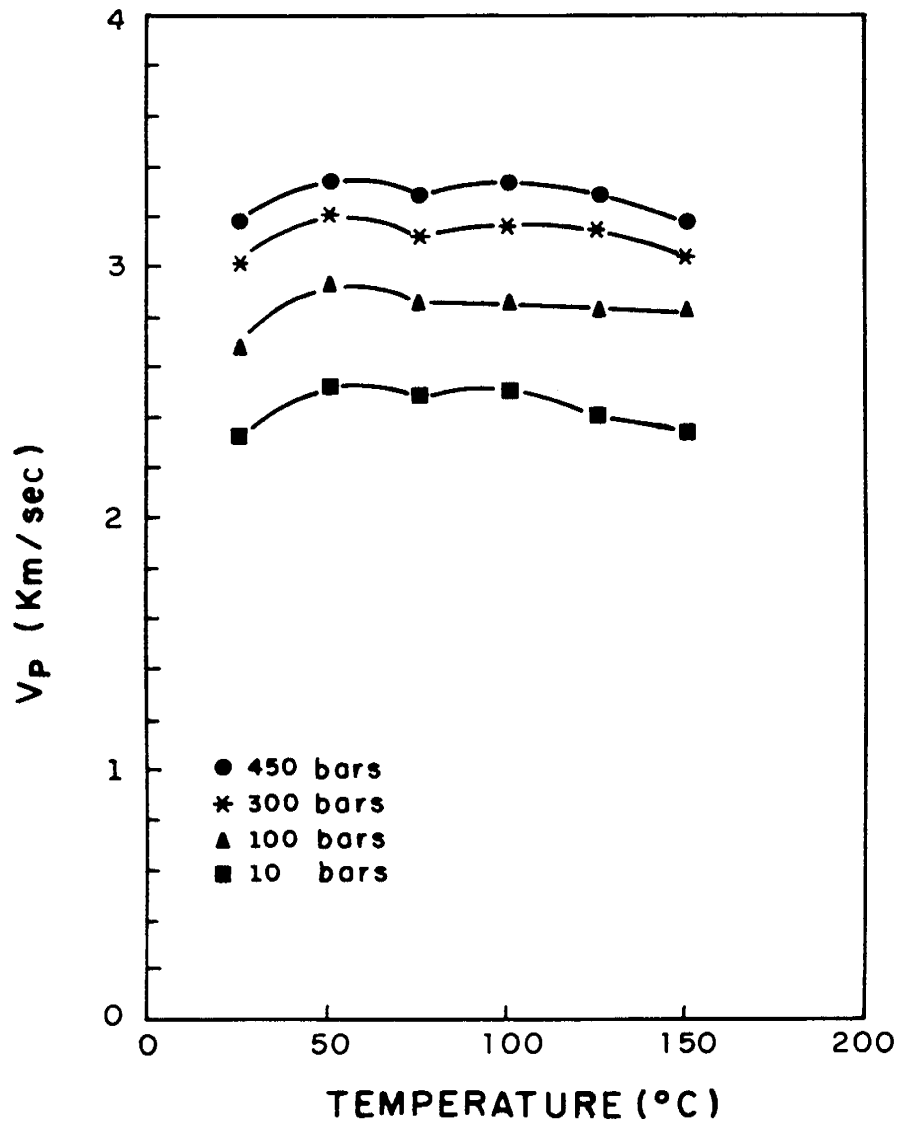


Fig. 7. P wave velocity change with temperature in a 0% oil saturated core.

WELL LSE-3307 (SAMPLE 3)

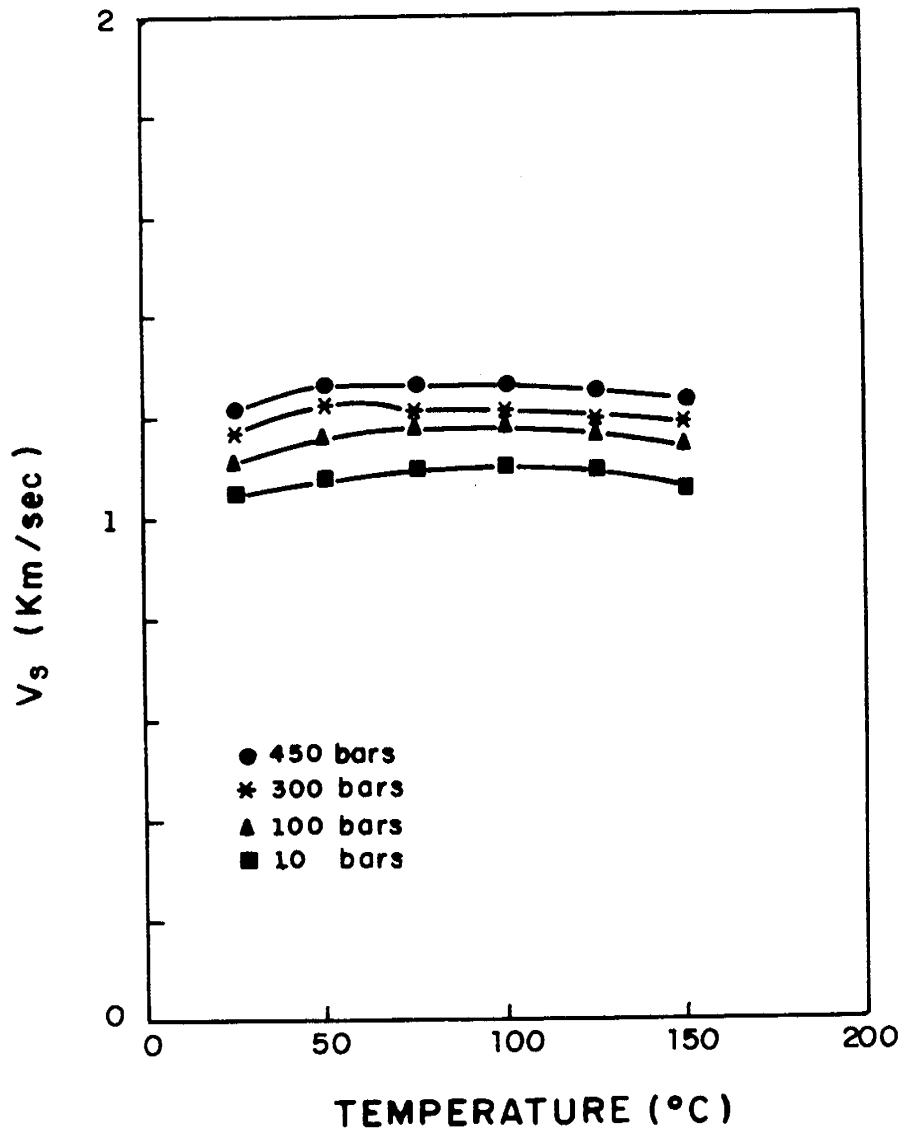


Fig. 8. S wave velocity change with temperature in a 0% oil saturated core.

WELL LSE-3307 (SAMPLE 3)

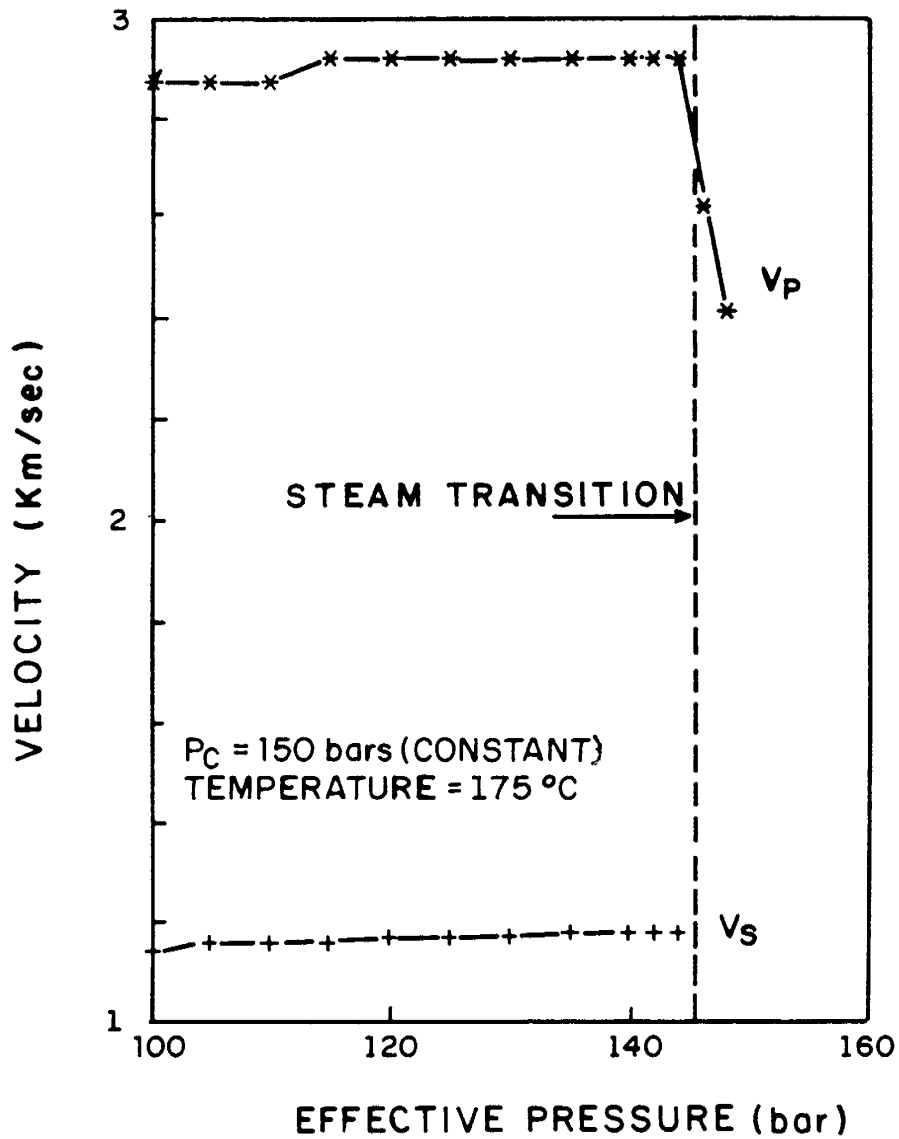


Fig. 9. P wave velocity decrease with steam transition in a 0% oil saturated core.

WELL LSE-3307 (SAMPLE 3)

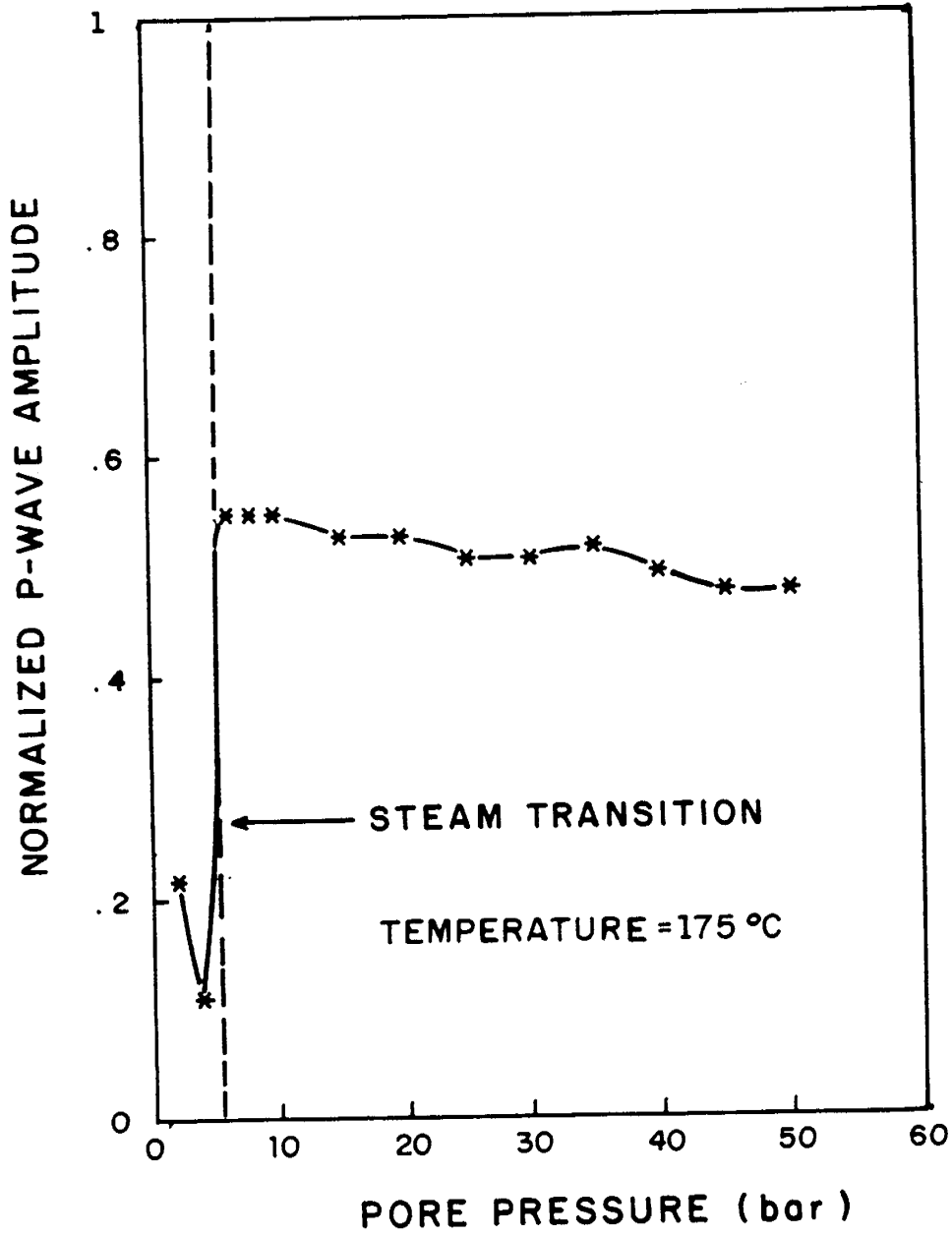


Fig. 10. P wave amplitude decrease with steam transition in a 0% oil saturated core.

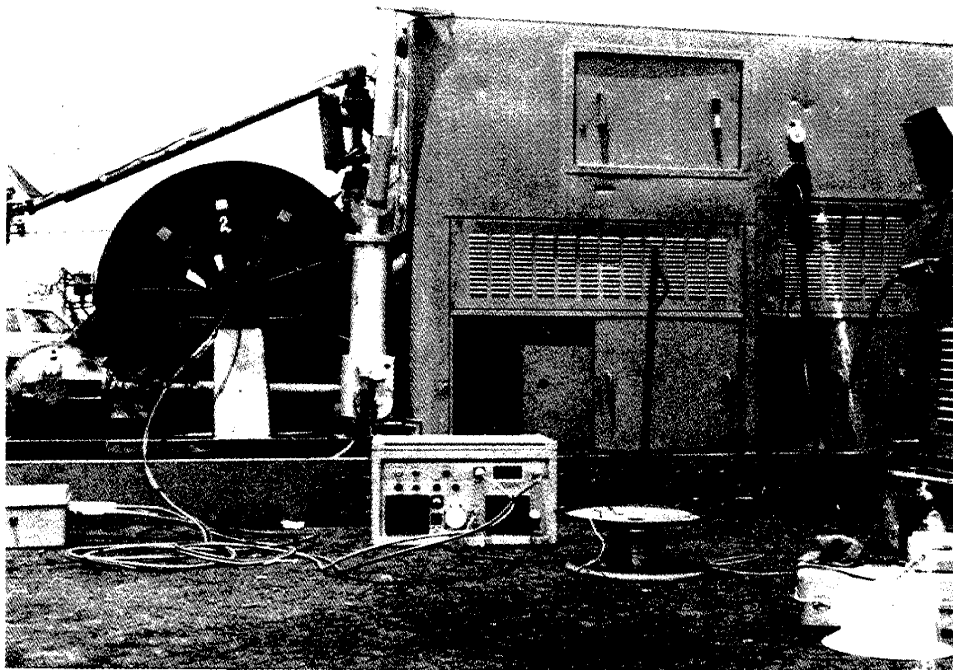
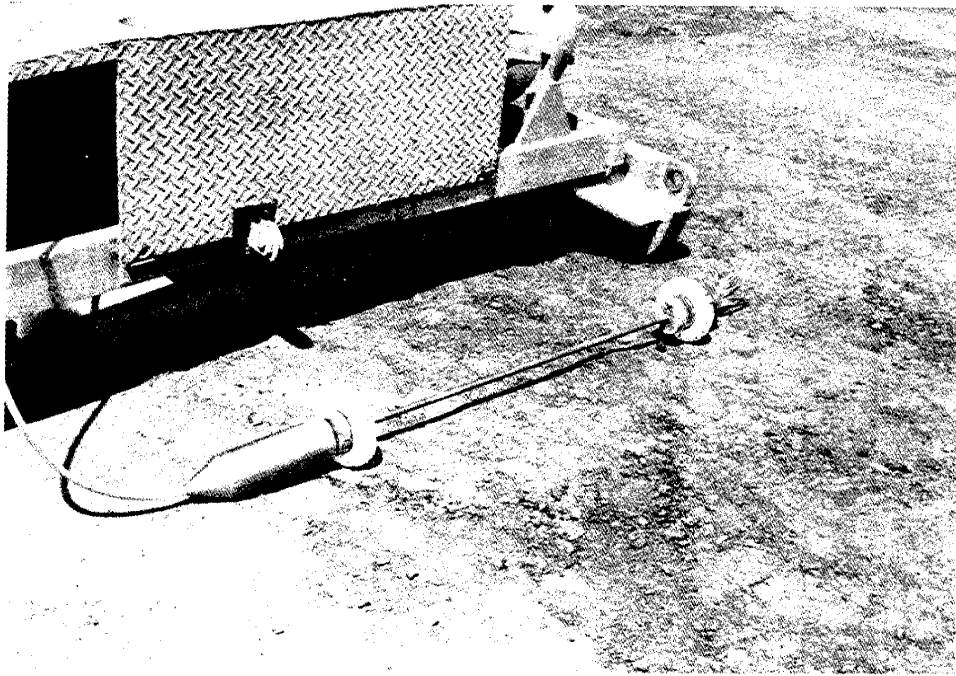


Fig. 11. 1000 joule downhole sparker electrode and 8000 volt power supply at the LSE-1408 well.

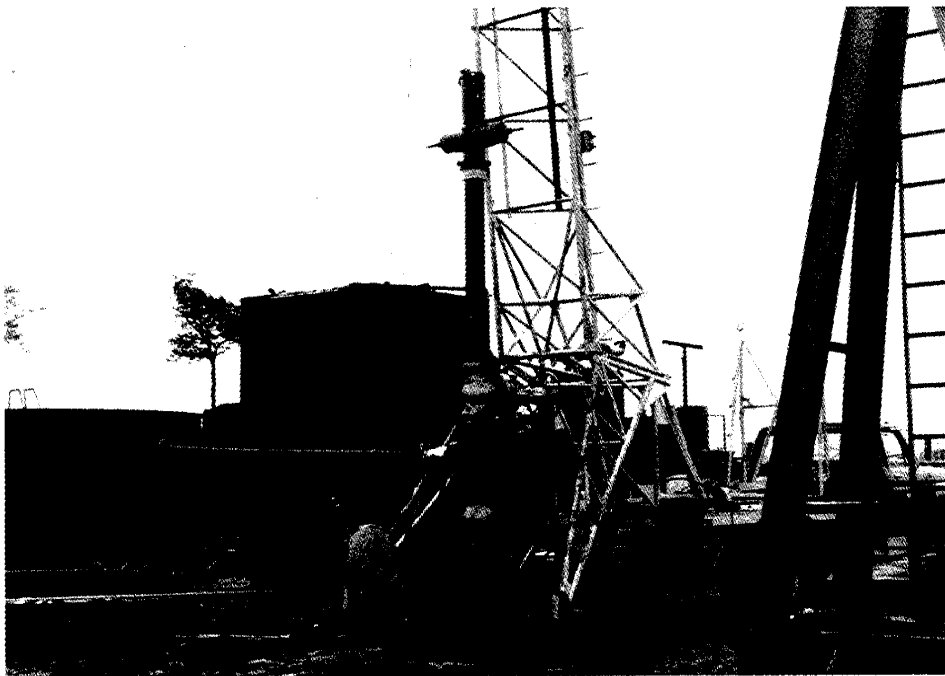


Fig. 12. LSE-1408 well prepared for the field test.



Fig. 13. LSE-3056 well prepared for the field test.

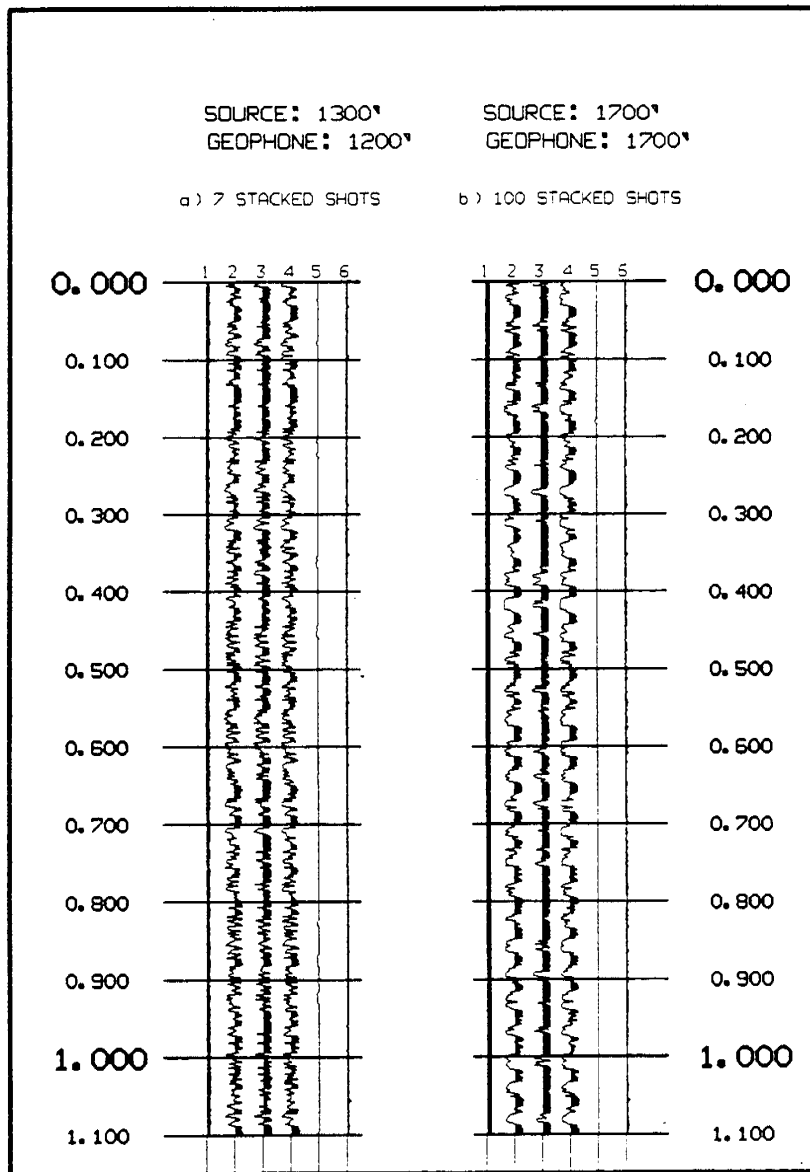


Fig. 14. Crosswell seismic records without evidence of first arrivals.

Task 27 - DOE shall provide INTEVEP with information from the project and field tests conducted by Sandia Laboratories on the use of Controlled Source AudioMagneticTelluric (CSMAT) surveys to determine the location of steam zones and fronts within a petroleum reservoir.

INTEGRATED, REAL-TIME, PROCESS-MAPPING INSTRUMENTATION SYSTEM

Sandia National Laboratories

INTRODUCTION

Sandia has been involved in developing techniques to map geologic discontinuities for over ten years. To date this work has focused on the development of hardware to detect and measure geophysical properties that are related to the discontinuity. In particular, Sandia has done developmental work on a borehole seismic system (BSS), a surface electrical potential system (SEP), and a controlled-source audio magnetotelluric technique (CSAMT). These tools have been demonstrated in full-scale field experiments including massive hydraulic fracturing, in situ coal gasification, coal mine fires, steam floods, fire floods, and in situ oil shale retorting. Moreover, the tools can, in fact, produce signals that can be used to infer some aspects of the geometry of the discontinuity associated with the process front.

This summary presents some results from two of these techniques and then addresses the problem of the real-time implementation of the individual subsystems and the integration of these subsystems into a complete, computer-linked instrumentation system.

TECHNIQUE RESULTS

Controlled Source Audio Magnetotelluric (CSAMT)

For thermal processes (fire floods and steam floods), and certain types of chemical floods, there will be significant changes in the electrical resistivity of the pay zone because of the changes in temperature, changes in the water saturation, and changes in the resistivity of the process fluids.

The CSAMT technique can be used to detect these electrical property changes. It is an electromagnetic (EM) geophysical technique where an electromagnetic field (EMF) is generated by a long wire dipole laid out on the surface of the earth and grounded at both ends to the earth. A transmitter operating at selected frequencies in the range of 0.01 to 5000 Hz excites the dipole at its center. The controlled source in the acronym CSAMT refers to the controlled frequencies used over the lower audio band down into the subaudio. Normally the transmitting antenna is located some distance from the area to be interrogated in order to minimize the nonlinear aspects of the generated EMF.

The incident EMF from the transmitting antenna will be scattered or reflected from the underlying structure. Preliminary laboratory experiments imply that the dominant contribution is from scattering. This scattered EMF will combine with the incident field and the total field will impinge on a receiving station located on the surface above the zone to be mapped. The receiving station consists of antenna that allows measurement of the electric and magnetic components of the signal. The oscillator used to control the transmitter is phase locked to the data acquisition unit at the receiving/mapping station. Thus, the incident field signal can be subtracted from the total field signal by making only measurements of signals that are not in phase with the transmitter. The magnitude and phase relative to the transmitted signal of all components of the electric and magnetic fields can be measured.

The depth of interrogation depends on the frequency; the lower the frequency, the deeper the penetration of the EM wave. The apparent resistivity depends on the resistivities of all of the formations penetrated by the EM wave. Thus if one measures the resistivities over a range of frequencies at a fixed observation point, the portion of the formation observed becomes larger as the frequency is lowered. Although this does give an indication of the depth dependency of the apparent resistivity, this approach is difficult to interpret exactly. Information about the geophysical characteristics can be used to resolve ambiguities in interpretation but sophisticated computer codes are required.

To date, two field experiments have been conducted on an EOR process. One was in conjunction with an in situ combustion, heavy oil recovery experiment conducted by the Bartlesville Energy Technology Center in the Bartlesville sand at a depth of approximately 350-360 ft.¹ Two surveys were conducted six months apart and differences in apparent resistivity during that interval were consistent with process and post-operation core data.

The other test was the first steam flood experiment (TS-1S) in the Northwest Asphalt Ridge Tar Sand (oil sand) near Vernal, Utah, conducted by DOE's Laramie Energy Technology Center.² The reservoir is about 45 ft thick and lies at a depth of 500-550 ft. Steam was injected into the center well of two concentric inverted five-spot patterns of 0.1 and 0.25 acres each (Figure 1). In the 160 days of operation until September 29, 1980, a total of 65,700 bbl of water equivalent steam were injected into the 45-ft thick, 500-ft deep tar sand zone. 1,150 bbl of oil and 6,250 bbl of water were produced during the course of the experiment. The permeability of the lower 5 ft of the pay zone was much higher than that of the upper portion. The post-operation core holes indicated that considerable steam had bypassed into a zone below the injection zone.

Steam injection began on April 23, 1980. The first CSAMT survey was run June 20-22 and a second, near the end of the test, on October 8-12, 1980. Apparent resistivity data are shown for two different frequencies in Figures 2 and 3 for the two different surveys. By skin depth arguments, the 512-Hz data indicate what is happening at the top of the zone, and the 128-Hz data indicate deeper penetration near the bottom of the zone.

The interpretation of these contoured maps requires the use of laboratory studies and full utilization of information generated by the more normal oil field experimental parameters. Preliminary lab steam flood studies show that the water bank produced a lowering of the formation resistivity. Thus, those regions where the value is decreased

correspond to areas where water has condensed or a water front is located. The area south of (below) 3P3 in the October data indicates a major water bank, as does the one surrounding 3P2.

Lab experiments have shown that uncondensed steam will increase the formation resistivity. Thus, the high values for the 128-Hz data about injection well 3I1 indicates an active steam zone, and suggests (a) that a volume in which the steam has swept out the formation oil but yet is hot enough that the steam has not condensed, and (b) that the dominant injection zone was at the bottom of the pay zone. This is in agreement with spinner flow measurements and data from the temperature observation wells. There is an indication that the hot water bank is beyond the 3P3, 3P7, and 3P2 line with the possibility of large-scale fingering developing between 3P3 and 3P7 and another finger past 3P2.

If this interpretation is correct, the response should indicate the bypass of steam into an underlying zone below the injection interval as observed in the post-operation drilling. A survey at a frequency of 64 Hz should contain not only the volume in the pay zone but also that below the pay zone. A substantial area of high resistivity was observed.

This work shows that measurements made from the surface by a noninvasive technique can indicate the changes that are occurring in the steamed pay zone. Use of this method with other oil-field information about production activities and, where available, temperature and pressure measurements has helped to give a more complete picture of what progressed in the TS-1S experiment. By careful choice of frequency and measurement techniques, it is possible to see through a conducting zone. These measurements could have been enhanced by (1) a series of background CSAMT measurements before injection began; (2) a well-defined, regularly spaced, rectangular grid to locate observation points; (3) laboratory measurement of the electrical parameter changes induced by the specific EOR processes; and (4) as much information from process operations as possible.

Borehole Seismic System (BSS)

Acoustic emissions resulting from a hydraulic fracture are thought to be caused by shear failures induced by the open, pressurized fracture, the localized high pore pressure zone surrounding the fracture, and the presence of planes of weakness in the rock surrounding the fracture. Although these acoustic emissions are not thought to be caused by tensile failure at the hydraulic fracture's propagating edge, it should be possible to use their location to infer the hydraulic fracture azimuth and height, because they should occur in a tight band near the hydraulic fracture face. The goal of the BSS is to determine the fracture azimuth and height by detecting and locating these microseismic events.

Recent redesign of the hardware, software, and data-reduction techniques associated with BSS have made possible better estimates of hydraulic fracture geometry.³ The redesigned triaxial system now incorporates three geophones per axis and provides 30 times the downhole gain of the replaced system, resulting in improved signal-to-noise ratios. This stronger signal, together with an increased digitization rate for each of the six simultaneously digitized channels from two borehole seismic tools, has made possible the acquisition and processing of data that were previously inaccessible. The new electronics makes use of a null system and an improved calibration system which includes a synthetic event generator to produce sinusoidal signals of specified amplitude, frequency, and phase. These make readjustments to maintain system balance possible while the tool is in place downhole.

The method of microseism location depends on the detection of primary (compressional) and secondary (shear) wave arrivals to compute the distance from the BSS tool to the microseism. The direction from which the wave arrives is determined from phase information contained in the triaxial geophone data.⁴ This method depends on the fact that a primary wave is polarized in the direction of propagation, so that a three-dimensional vector with components proportional to the output of

the three geophone axes points either towards or away from the direction of arrival.

If the primary and secondary wave arrival times can be determined, then the distance to a seismic source can be calculated by the different wave arrival times and a velocity factor. This factor can be determined empirically from seismic sources at known distances, without knowledge of the primary or secondary wave velocities. Since the primary wave travels faster than all other waves and is polarized parallel to the direction of travel, it is possible to determine the direction from which it arrives at a triaxial geophone of known orientation by analysis of the three components of the first arrival of the signal. First, the east and north components are analyzed by using spherical statistics to determine the azimuth of the direction of arrival.⁵ Then a three-dimensional spherical statistical analysis of the data is used to determine the elevation to the source. In addition to the azimuth and elevation of the direction of arrival, spherical statistics yield an estimate of the probable error in the form of standard deviations for both the azimuth and elevation.⁵

Given the azimuth, elevation, and distance to an event determined by two BSS tools in offset wells, it is desirable to refer the two single-tool locations and their error measures to a common coordinate system and determine a most probable single location and an error measure for that location. This can be done by assuming a triangular probability distribution about each location based on the mean, mode, and standard deviation for the azimuth, elevation, and distance, and solving for the position which minimizes the error measure.⁵ For a rectangular coordinate system, the error measure is expressed as a standard deviation for each of the coordinate axes and can be thought of as an ellipsoid with axes parallel to the coordinate axes. The minimum error position is the position which minimizes the volume of the error ellipsoid.

This improved system was used in conjunction with a hydraulic fracture stimulation conducted in November 1986 as part of DOE's

Multiwell Experiment.⁶ Over 100 microseismic events were recorded and digitized during pumping, shut-in and flowback of the treatment. The treatment consisted of 22,000 gal of 75 quality nitrogen foam, and 32,500 lbs of intermediate strength proppant, pumped at 10 bpm. The zone was the 23 ft thick fluvial B sandstone at a depth of 5822-5845 ft. Two BSS tools were used: one in each of two offset wells.

A total of 29 events were detected which were located from both BSS tools and resulted in locations that were close enough together in both time and space to reasonably be considered to represent the same microseismic event resulting from the stimulation. The individual event ellipses produced by the maximum likelihood event location scheme are shown in Figure 4. These events indicate a fracture azimuth of 68° west of north. All events lie between parallel lines 25 ft on either side of this line, as shown more clearly in Figure 5. The accuracy of the redesigned system, based on the ability to locate perforation shots, indicates a 25-ft uncertainty in the location of individual microseisms. This indicates that a fairly high level of confidence can be associated with the 68° west of north fracture azimuth determined from the two-well locations. This azimuth is in excellent agreement with previous measurements at this site. The vertical distribution of the signals is shown in Figure 6 and indicates possible upward growth of the fracture.

INTEGRATED PROCESS MAPPING SYSTEM

Although the proposed system has a broad-ranging application base, perhaps the best way to articulate the concepts associated with such a system is in the context of a specific application. One such application is hydraulic fracturing of oil and gas wells. Hydraulic fracturing has become an important technique in the stimulation of low-permeability hydrocarbon reservoirs. Historically, these low-permeability reservoirs were considered noncommercial, but with continuing advancements in hydraulic-fracturing technology, the reservoirs are becoming increasingly economic. At present, roughly 25% to 30% of total U.S. oil reserves are

economically producible because of hydraulic fracturing. Treatments have become so widespread that approximately 35% to 40% of all wells drilled today are hydraulically fractured at some point.⁸

Optimization of a hydraulic-fracture treatment requires an approach that takes into account those properties of the formation that affect reservoir performance and those properties of the fracture--in particular, the fracture geometry--that will lead to increased production. In principle, the creation of an optimal fracture geometry will maximize the return (enhanced revenues minus treatment cost) of a hydraulic-fracturing treatment. Therefore, the creation of a satisfactory fracture geometry is particularly important in hydraulic fracturing, because the fracturing can constitute a large portion of the total well costs.

Accurate knowledge of formation properties is essential for selecting suitable values for the treatment parameters.⁹ Unfortunately, the approach that is commonly used to select values for the treatment parameters is far from satisfactory. Except for pressure data collected during fracturing, this approach entails an almost total reliance on data generated from prefrac measurements in the laboratory and from prefrac observations and measurements in the field (including minifrac measurements).

The prefrac data, in the form of values for formation parameters such as porosity (ϕ), permeability (k), vertical distribution of minimum principal horizontal in situ stress (σ), material properties (e.g., Young's modulus (E) and Poisson's ratio (ν)), and probable fracture orientation, are used in conjunction with trial values for treatment parameters (e.g., viscosity (μ), leakoff rate (β), density (ρ), fluid volume (V), and injection rate (F) of the fracture fluid; size, crushing strength, and concentration of the proppant (sand)) as inputs to a fracture model from which estimates of fracture geometry (height (H), length (L), and width (W), in addition to probable orientation) can be made. Assuming that the physics incorporated in the fracture model is

correct, then the use of this modeling procedure for optimizing the treatment design with respect to the desired fracture geometry is currently still limited to finding a satisfactory set of initial values for the treatment parameters.⁸ The values for the formation parameters are fixed at the initial values obtained from prefrac measurements.

Initial values for the in situ viscosity and leakoff rate may be inaccurate, and these values may change during the fracturing process. Thus, the initial set of values for the treatment parameters may no longer be (and may never have been) optimal. Efforts to alter the treatment during fracturing, in such a way as to control or improve fracture geometry, must rely on judgments based on previous experience and on limited information (e.g., flow and, possibly, pressure and temperature data). In the absence of the means to measure the fracture geometry during fracturing, there is no way to update the values for the viscosity and leakoff rate by comparing fracture-model output with observed fracture geometry), and lacking these values, the fracture model cannot provide reliable information that can serve as a guide in controlling or altering the treatment to achieve the desired fracture geometry.

Control of the Treatment with Real-time Data

The use of a real-time fracture-diagnostics instrumentation system is essential for providing the information needed to control a fracture treatment and to determine whether or not the ongoing treatment is in fact appropriate. Figure 7 is a flow diagram that shows how a real-time instrumentation system might be used to optimize the fracture treatment and fracture geometry.

During treatment, continual comparison of the fracture geometry predicted by the fracture model with the fracture geometry sensed by the instrumentation system makes it possible to provide updated values for the in situ viscosity and leakoff rate. Provided that the fracture model

is correct and convergence is obtained in this model-convergence loop (yielding an altered but physically reasonable and self-consistent set of values for these parameters), then there exists sufficient information with which to use the model to test the effect on fracture geometry of modifying the fracturing treatment. With the desired fracture geometry as a goal, iterations within the treatment-parameter loop are potentially useful for providing the information needed to guide and control the course of the treatment. As indicated in Figure 7, it is, of course, possible that the iterative procedures will not lead to eventual agreement between observed and calculated fracture geometries. In this event, there is no model-derived rationale by which the ongoing treatment can be controlled or improved, and the empirical fracture geometry must be used in determining the course of the treatment.

The System

An integrated, real-time instrumentation system consisting of a number of diagnostic subsystems is proposed. A conceptual framework for the system is shown in Figure 8.

To provide this real-time instrumentation system, four diagnostic subsystems have been or are currently being developed. These subsystems, which are to be linked together by a microcomputer network, consists of (1) an internal-fracture-pressure measurement system, (2) a fluid-flow measurement system, (3) a borehole seismic system (BSS), and (4) a surface-electric-potential (SEP) or CSAMT measurement system.

Use of a combination of diagnostic subsystems is required to ensure that all pertinent fracture parameters, which define the fracture geometry, are measured. These subsystems are complementary and, in addition, they provide a certain amount of redundancy in the measurements, through the use of which it is possible to make consistency checks.

The composite instrumentation system will provide not only the at-the-wellbore measurement capabilities afforded by the use of the pressure and fluid-flow diagnostic systems but also the away-from-the-wellbore measurement capabilities made possible by the use of the BSS and the SEP or CSAMT systems. In addition, the composite system, in conjunction with the fracture model and the computer-driven diagnostic methodology, will provide the capability to subject the data acquired from all four measurement subsystems to real-time analysis and interpretation. It is these attributes of the proposed system that make it unique.

Diagnostic Subsystems

The vertical distribution of minimum horizontal in situ stress has the greatest influence on fracture height.¹⁰ Layers with low minimum in situ stress are fractured even with low fracture pressures, while those layers with high minimum in situ stress require high fracture pressures. As a fracture grows in height, pressures and temperatures within each fractured layer readjust in response to the introduction of fracturing fluid, thereby changing the pressure profiles of the fracture interval with time. These changes can be monitored at the wellbore. If sufficient contrasts with respect to horizontal in situ stresses exist, then real-time pressure measurements, coupled with prefrac determinations of these stresses, can be used to determine the fracture height (H). Pressure and in situ stress measurements for each layer can be used as inputs to a generalized version of the Simonson model,¹¹ from which an estimate of fracture height can be obtained.

For a vertical fracture with length greater than height, an estimate of fracture width (W) can be made using estimated fracture height, the real-time pressure measurements, and the prefrac measurements of Poisson's ratio and Young's modulus. Width is calculated using the equation of Perkins and Kern.¹²

Calculations of both fracture width and fracture height require that fracture pressures be known. Initially, the measured wellbore pressures

are used. Pressure at any given point in a fracture, though, depends on fracture height and width and on distance from the wellbore. To calculate far-field fracture parameters, it is necessary to adjust the wellbore pressures for the large pressure drop due to fluid flow along the length of the fracture.¹³ This adjustment requires that fracture length be known.

Fluid-flow measurements provide fracture volume (V), from which fracture length (L) is calculated. Additional parameters required in the calculation include fracture height, width, and the leakoff rate (β), which is determined during the prefrac well tests. Because fracture height and width are needed to calculate length and because fracture length is required to determine the fracture pressure (i.e., the fracture pressure away from the wellbore) used in the height and width calculations iteratively, until convergence is achieved giving both near- and far-field values for the fracture height, width, and length.

The real-time measurement of pressure and fluid flow is, of course, standard practice in a fracture treatment; however, the use of pressure and fluid-flow measurements in a real-time analytical context is not. Furthermore, using current modeling methods, these at-the-wellbore measurements cannot be used to determine fracture orientation (θ) or the ratio (α) of the lengths of the fracture wings (L_{maj} and L_{min}). To determine these parameters, BSS and SEP or CSAMT measurements are made in the near and far fields, respectively. These measurements are essentially away-from-the-wellbore measurements, and their incorporation within a real-time instrumentation system is what distinguishes the proposed diagnostic system from that used in standard practice.

The BSS and CSAMT have been described in previous sections. In the SEP technique, pulses of current are injected into the treatment well/fracture combination, and a remote well casing 1 to 2 miles away acts as the return electrode. The induced potential distribution is measured by a set of potential probes at the earth's surface on

concentric circles located around the fracture well. As a fracture grows, the conductive frac fluid filling it alters the induced surface electrical potentials around the fracture well. The potential gradients associated with pairs of probes (one probe at each radius) are measured as the fracture develops.

A composite instrumentation system that includes BSS and SEP capabilities has been discussed for a stimulation experiment.¹⁴ The fielding of the composite system and the operational procedures associated with its use are described. This description provides an example of how the proposed real-time instrumentation system might be deployed in the field.

System Summary

A fracture-diagnostics system with real-time capability offers an opportunity to control the treatment during fracturing. In the real-time system, fracture parameters are predicted prefrac just as they are in current treatments. However, once fracturing has commenced, the real-time instrumentation, consisting of an integrated system of fracture-diagnostic subsystems, measures the fracture parameters in real time. Measured and predicted parameters are compared and necessary revisions of the treatment are made to ensure that the fracturing process is leading to the desired fracture geometry.

Efforts to develop a real-time instrumentation system should be focused on (1) developing the real-time capabilities of each of the separate diagnostic subsystems, (2) solving the problems associated with the integration of these subsystems into a complete real-time system, and (3) testing the system in the field.

CONCLUSIONS

An integrated process mapping system has been proposed. Two potential components of such a system, one based on controlled-source

audio magnetotellurics and another on borehole seismics, have been described and examples of field results given. Clearly, advances towards such an overall process mapping system are being made.

REFERENCES

1. Wayland, J. R. and Bartel, L. C. Measurements for the BETC In Situ Combustion Experiment, SAND82-1699, November 1982.
2. Wayland, J. R., Lee, D. O., and Cabe, T. J., CSAMT Mapping of a Utah Tar Sand Steamflood, J. Pet Tech., p. 345, March 1987.
3. Thorne, B. J. and Morris, H. E., "Advances in Borehole Seismic Diagnostics," Paper SPE/DOE 16405 presented at the 1987 SPE/DOE Joint Symposium on Low Permeability REservoirs, Denver, May 17-19, 1987.
4. Gal'perin, E. I., The Polarization Method of Seismic Exploration, D. Reidel Publishing Co., Dordrecht/Boston/Lancaster, 1984.
5. Engi, D., A Numerical Signal Processing Technique for Borehole Seismic Fracture Diagnostics, SAND86-1865, January 1987.
6. Northrop, D. A. and Sattler, A. R., The Multiwell Experiment: A Field Laboratory for Tight Gas Sands Research, Presented at the 17th Intersociety Energy Conversion Engineering Conference, Los Angeles, August 1982.
7. Teufel, L. W., C. M. Hart, A. R. Sattler and J. A. Clark, Determination of Hydraulic Fracture Azimuth by Geophysical, Geological and Oriented Core Methods at the Multiwell Experiment Site, Rifel, Colorado, SPE 13226, 59th Annual SPE Meeting, Houston, TX September 1984.

8. Veatch, R. W., Overview of Current Hydraulic Fracturing Design and Treatment Technology--Part 1, J. Pet. Tech., April 1983, pp 677-87.
9. Pai, V. and Garbis, S., Tight Sands Require Detailed Planning, Oil & Gas Journal, July 25, 1983, pp 135-39.
10. Warpinski, N. R., Schmidt, R. A., and Northrop, D. A., In Situ Stresses: The Predominant Influence on Hydraulic Fracture Containment, J Pet Tech, March 1982.
11. Simonson, E. R, Abou-Sayed, A. S., and Clifton, R. J., Containment of Massive Hydraulic Fractures, Soc. Pet. Eng. J., February 1978, pp 27-32.
12. Perkins, T. K. and Kern, L. R., Widths of Hydraulic Fractures, J. Pet. Tech., September, 1961, pp 937-49.
13. Warpinski, N. R., Measurement of Width and Pressure in a Propagating Hydraulic Fracture, Paper SPE/DOE 11648 presented at the 1983 SPE/DOE Joint Symposium on Low Permeability Gas Reservoirs, Denver, March 13-16, 1983.
14. Hart, C. M., Engi, D., and Morris, H. E., A Comprehensive Fracture Diagnostics Instrumentation Fielding Program, Paper SPE/DOE 11650 presented at the 1983 SPE/DOE Joint Symposium on Low Permeability Gas Reservoirs, Denver, March 13-61, 1983.

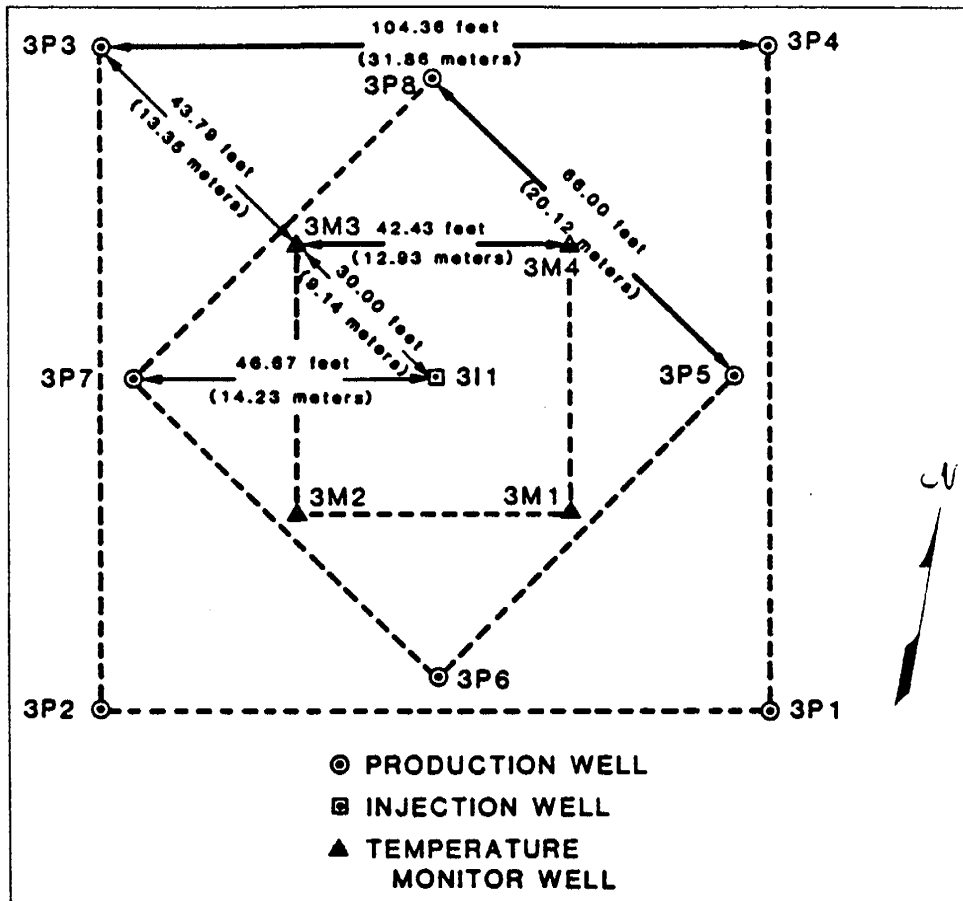
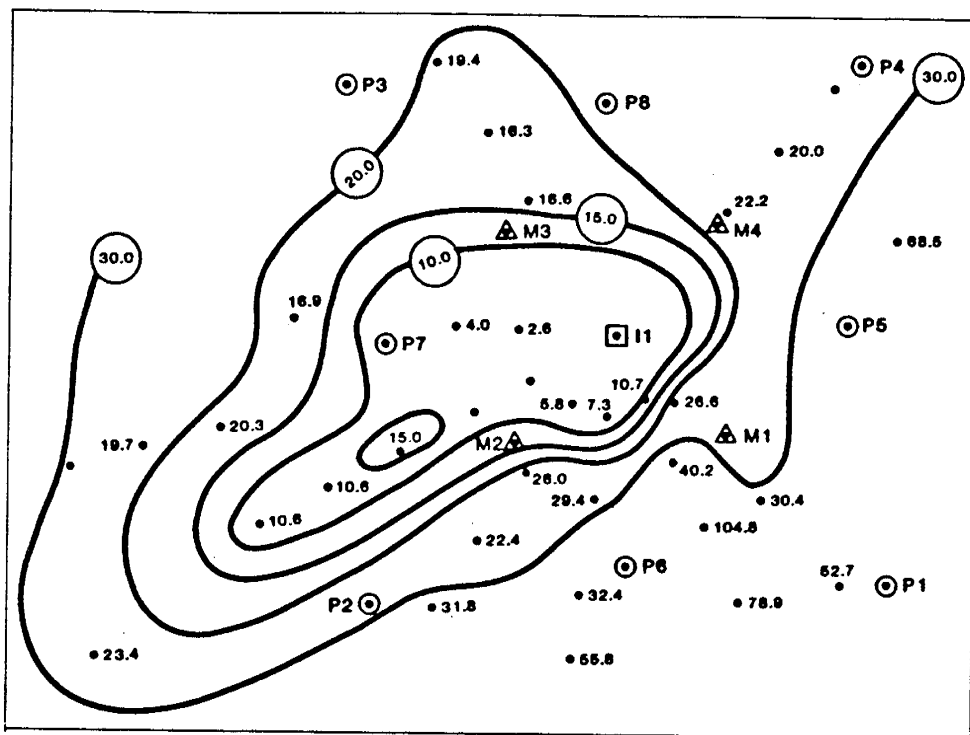
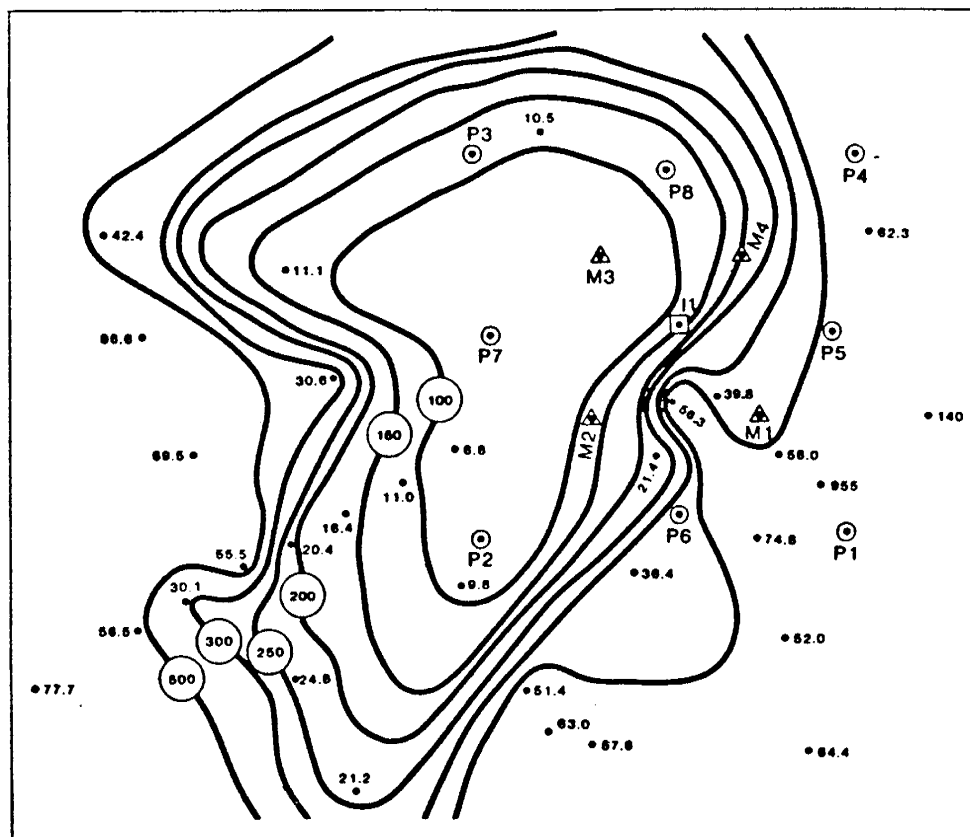


Figure 1. LETC TS-1S well pattern.

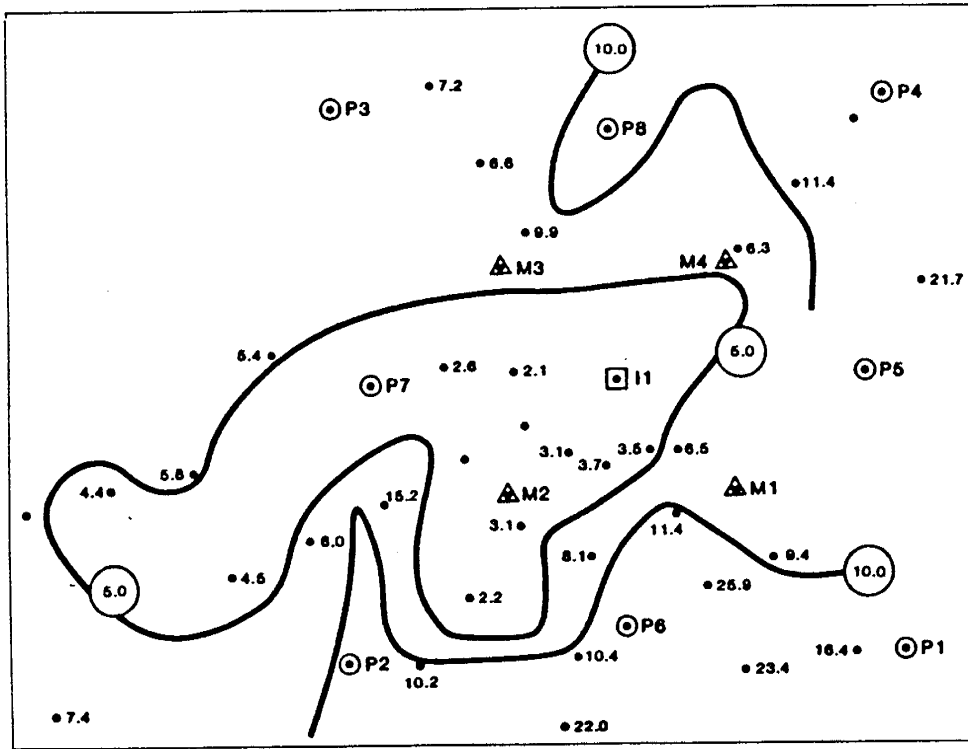


(a)

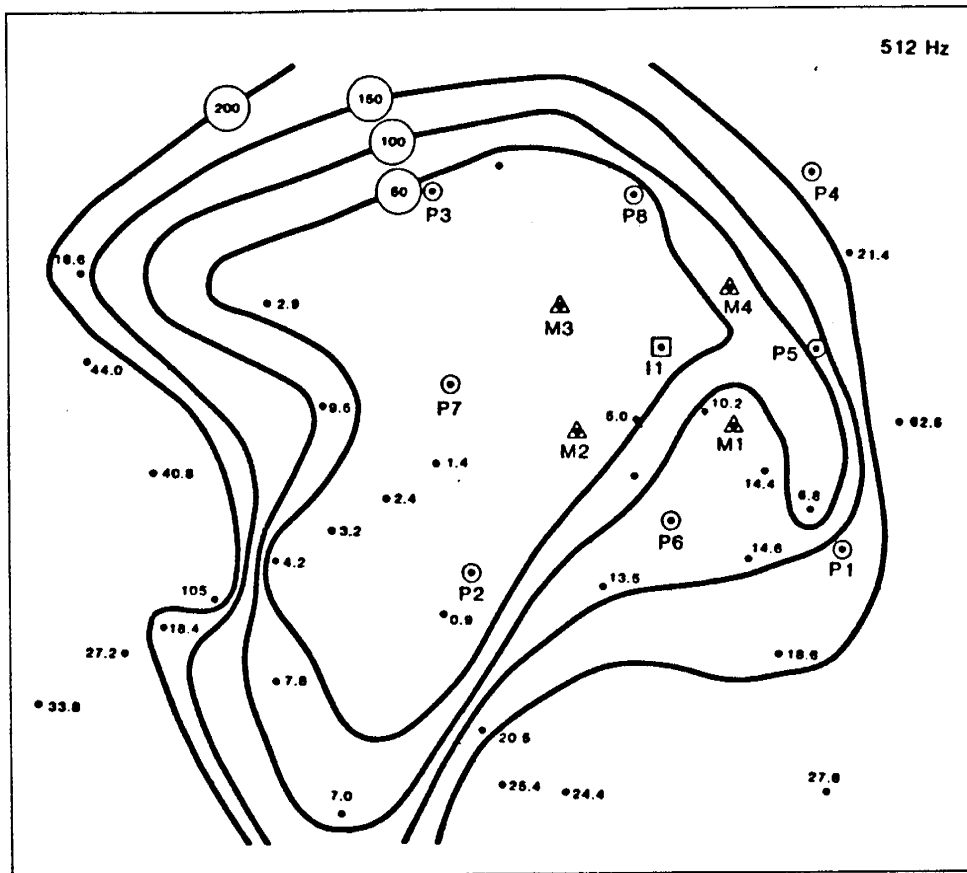


(b)

Figure 2. CSAMT Resistivity at 128 Hz (a) June 20-22, 1980; (b) October 8-12, 1980.



(a)



(b)

Figure 3. CSAMT Resistivity at 512 Hz (a) June 20-22, 1980;
(b) October 8-12, 1980.

Horizontal Event Map, 1986 Main Frac

68.2 Degrees West of North
Standard Deviation 21.3

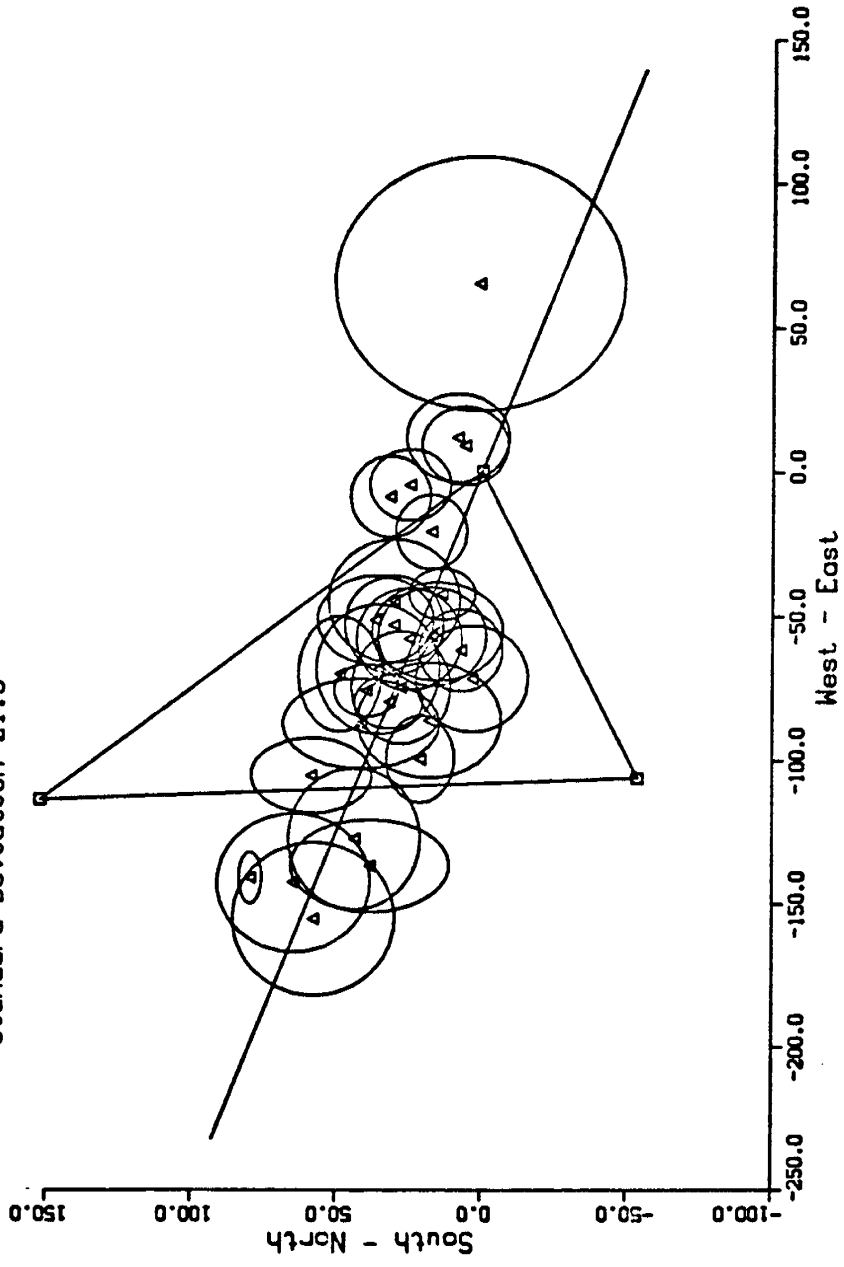


Figure 4.

Vertical Event Map, 1986 Main Frac

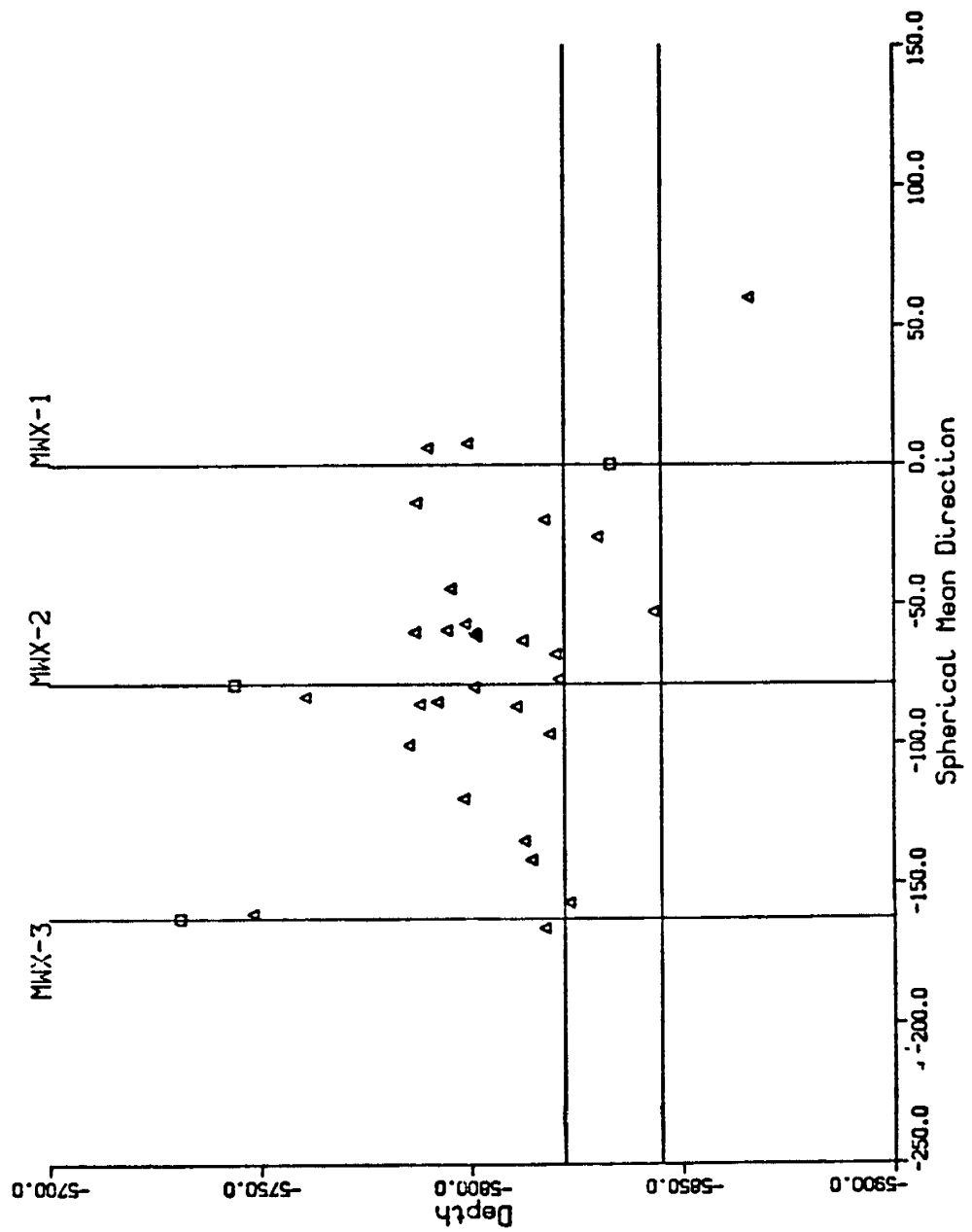


Figure 5.

Horizontal Event Map, 1986 Main Frac

68.2 Degrees West of North
Standard Deviation 21.3

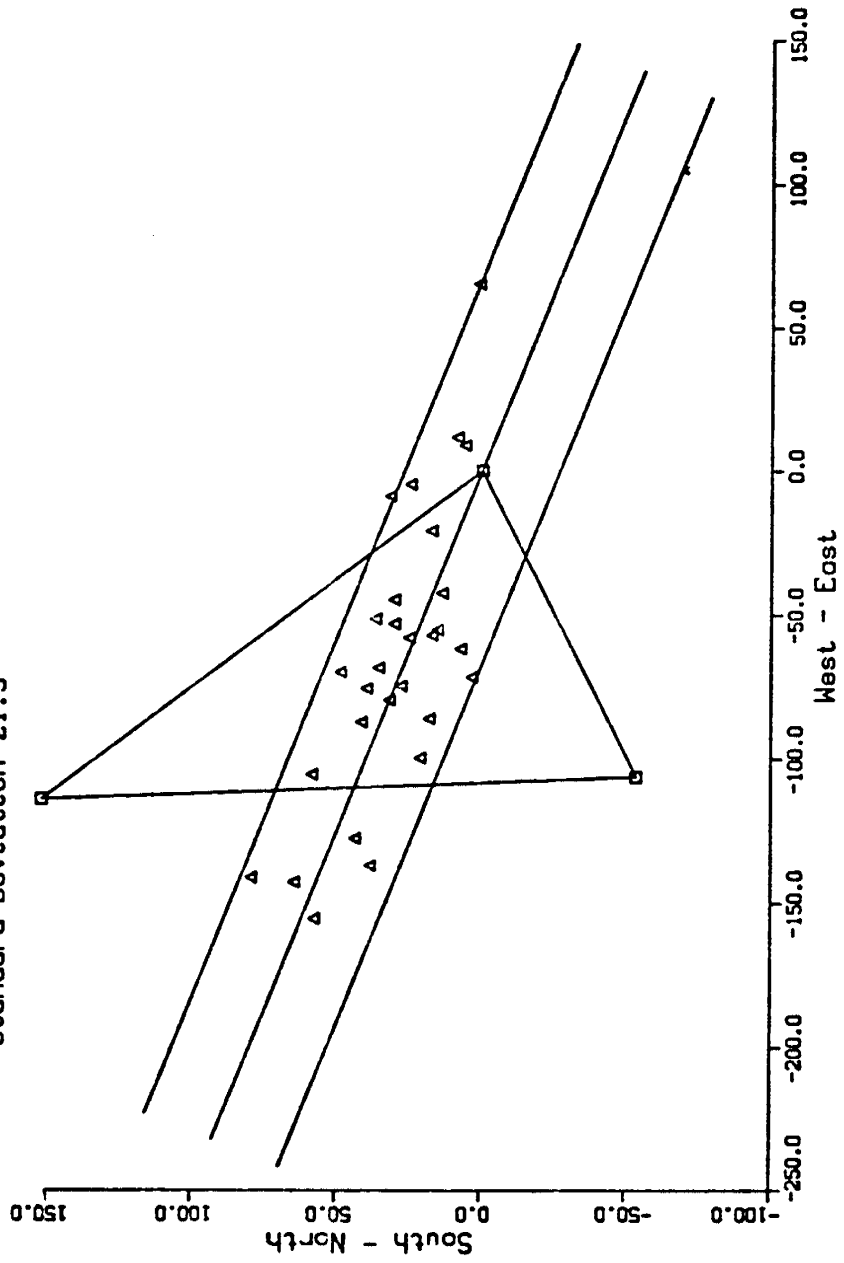


Figure 6.

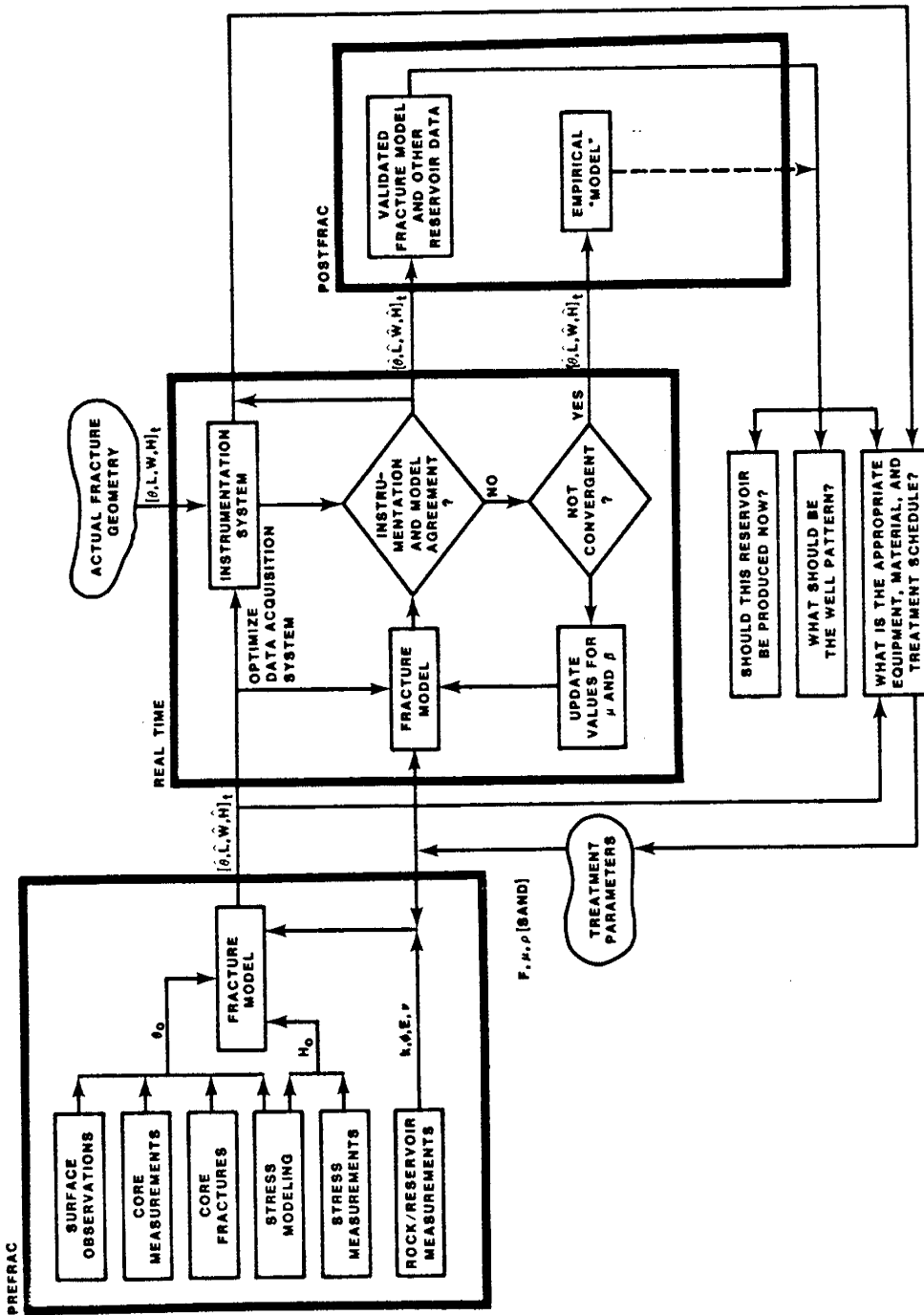


Figure 7. Flow Diagram Showing the Use of a Real-Time Instrumentation System in the Control of the Fracturing Treatment and Fracture Geometry

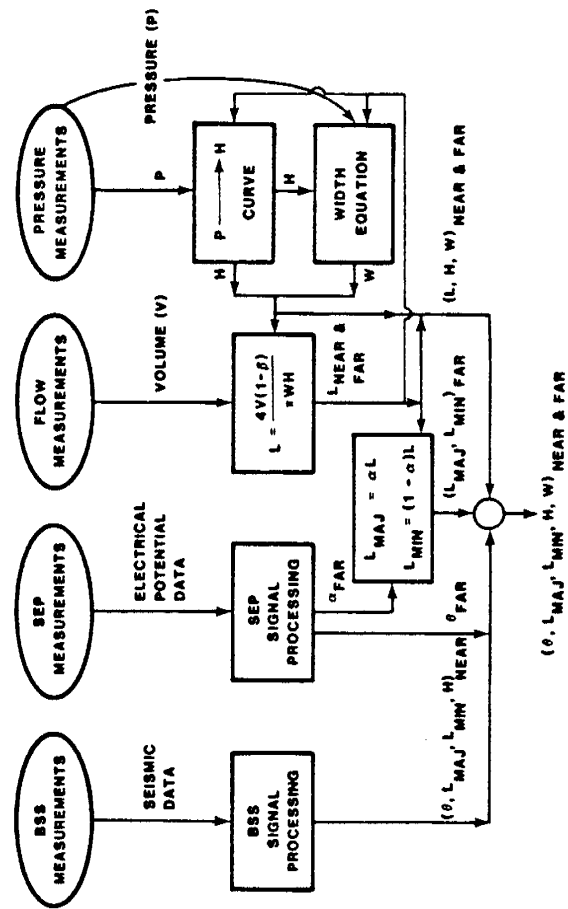


Figure 8. Real-Time Fracture-Diagnostics Instrumentation System

Task 28 - DOE shall provide INTEVEP with information from the foam diversion research and steam additive computation model development conducted by the Stanford University Petroleum Research Institute. The Project Managers will consult with one another on foam diversion research and computational modeling being conducted at SUPRI and INTEVEP laboratories with a view toward avoiding duplication of effort and enhancing the respective research effort.

<u>Included in this task are:</u>	Page
A Study of Heat Transfer of Steam Displacement	28-3
A Laboratory Study of Surfactants As Foaming Agents	28-4
Two-Dimensional Displacement by Gas and Surfactants Under Foaming Conditions	28-8
Foam/Emulsion Displacement of Oil in Unconsolidated Sandpacks	28-10
Flow of Foam Through Micromodels	28-14
The Transient Behavior of Surfactant Foam Flow in Porous Media	28-18
Apparent Viscosity Measurements of Surfactants Foam Flow in Porous Media	28-39
Foams in Porous Media - A Literature Survey	28-76

A STUDY OF HEAT TRANSFER OF STEAM DISPLACEMENT

A technical report by Fred Wang and W.E. Brigham (TR 55, 1986) was published on this topic; the following is an abstract of these results.

ABSTRACT

A system of differential equations describing the temperature distribution in the insulation and the heat frontal movement in a cylindrical core during steam injection is derived and solved in Laplace space. The real-time solution is obtained by using the Stehfest algorithm. The solution shows that movement of the heat front is strongly dependent on the heat transfer coefficients at the inner and outer boundaries.

Experimental results of steam injection are shown at pressures varying from 0.11 to 1.42 MPa (16 to 206 psia). The apparent thermal conductivity of the insulation as a function of temperature was obtained by comparing experimental data with an analytic solution. When the pressure of the steam zone changed during a run, it was found that changes of volumetric heat content in the heated core and the insulation may be treated as though they were changes in heat injection rate. The method of succession of steady states can also be used to approximate the heat frontal movement for cases of variable pressure. For displacements using Kaydol as the in-place oil, the initial oil saturation had little effect on irreducible oil saturation.

A method for approximating the steam swept volume is presented using an adjustment to the Marx and Langenheim equation and a new definition of the critical time. This method is to change the time scale using f_{hv}^n as a factor to adjust the time scale after the critical time, where f_{hv} is the fraction of total heat which is latent heat, and where n is determined empirically. The f_{hv} varies from 0.1 to 0.9 and n varies from 0.4 to 1.9. This method improves the approximation of the steam swept volume.

The steam mobility can be reduced by alternate injection of steam and surfactant slugs. The steam mobility decreased with an increase of surfactant concentration and with an increase in the slug sizes of the surfactant solutions. The number of surfactant slugs required to obtain the maximum mobility reduction was found to be a function of surfactant concentration and backpressure. The addition of nitrogen in the injected steam further reduced the steam mobility, with very little effect seen at concentrations of nitrogen above about one mole percent.

A LABORATORY STUDY OF SURFACTANTS AS FOAM DIVERTING AGENTS

INTRODUCTION

An insulated cylindrical core packed with unconsolidated sand was used to study and compare commercially manufactured surfactants. Each surfactant was injected with steam and nitrogen simultaneously to generate a foam in-situ. The diverting capability of the foam was measured in terms of pressure drops along the cylindrical core. The surfactants that will be studied in this experiment are Chevron's SD1000 and Shell's Enordet AOS 1618.

APPARATUS

The experimental equipment used was designed and built by Wang (1986) as part of his PhD dissertation. A schematic diagram of the steam/foam displacement apparatus is shown in Fig. 1. Two Constametric Model II pumps were used to inject fluids into the sandpack. One pump was used solely to pump water for steam generation and the other was used for surfactant or mineral oil injection.

Steam was generated by a tubular furnace capable of elevating the steam temperature above 600°F. Heat tape and a heating band were used to compensate for heat losses along the injection line and the inlet flange, respectively.

Nitrogen injection was controlled by a Matheson 8240 flow controller which consists of a flow transducer, a flow control valve, a power supply/readout box and an interconnecting cable. A pressurized tank with a pressure regulator was used as the nitrogen source.

The linear sandpack consisted of a 6 ft. stainless steel tube packed with commercially-graded Ottawa sand. Along the tube are various thermocouples and five pressure taps to measure the temperature and pressure profile, respectively.

The produced fluids were collected by a fraction collector (Buchler Model Fractomettte Alpha 200) based on volume. Backpressure on the system was maintained by a Grove Valve and Regulation Co. Model 591W backpressure regulator.

DATA COLLECTION

The data collection consisted of strip chart recorders and a data logger connected to a computer. Thermocouple measurements along the cylindrical core were recorded by a 24 channel strip chart recorder. Pressure data were measured by transducers with corresponding demodulators to transform the signals into a DC output. These voltage were recorded by two three-pen strip chart recorders.

Both temperature and pressure measurements were also connected to a data logger which was linked to Tektronics 4054 computer. The measured data was stored on tape and later transferred to a Vax 11/750 computer for analysis.

SAND PACK PREPARATION

A commercially graded Ottawa sand (mesh 170-200) was washed and oven dried before packing. The weight of the packed sand was carefully recorded to determine the sandpack porosity. Vibrators and a rubber mallet were used to expedite the settling of the sand.

The stainless steel tube was sealed by a flange and copper O-ring assembly on each end and then pressure tested with nitrogen to 300 psig for 24 hours. The sandpack was then evacuated and filled with water under a vacuum. The pore volume was determined from the volume of water used to fill the sandpack and compared favorably to the value obtained from the sand volume.

The water saturated sandpack was next flooded with mineral oil to the irreducible water saturation. Steam was then injected until steam-out conditions to simulate a steam channel. Table 1 shows the properties of the sandpack.

TABLE 1
SANDPACK PROPERTIES

Porous medium - Ottawa Sand (mesh 170-200)

Sandpack length, $L = 6$ ft.

Sandpack inside diameter, ID = 2.15 in.

Porosity, $\phi = 35.3\%$

Permeability, $K = 4.97$ darcys

Residual oil saturation, $S_{or} = 18.7\%$

Mineral oil - Kaydol

EXPERIMENTAL RUNS

The surfactant/foam runs initially began by injecting steam into the linear sandpack at a constant rate (4 cc/min of equivalent water) until steam breakthrough. After breakthrough, slugs of surfactant solution were injected simultaneously with the steam.

The first run consisted of injecting 2 slugs of 0.1 PV of 0.1% by weight SD 1000 at 4 cc/min simultaneously with steam at 4 cc/min of equivalent water. The second surfactant slug was not injected until the pressure profile in the system had fallen to pre-surfactant injection pressures. No back pressure was held on the system for this run. Temperature and pressure profiles along the sandpack were recorded along with the concentration of any surfactant in the produced fluid.

The second run was a repeat of the first run except that a 70 psig back pressure was held on the system and a third slug of water and steam was injected at the same rates as the two surfactant solution slugs. Preliminary results indicate that the back pressure has little affect on the pressure drop along the sandpack.

The same procedure was used for the third run except that 1.0% by weight of SD 1000 was used rather than the 0.1% by weight used in the two previous runs, and the water slug was injected first followed by the two surfactant solution slugs. The preliminary results indicate that there was no significant change in the pressure drop along the sandpack with the higher

concentration of surfactant. The fourth run made this year was a repeat of the third run to confirm the results and show the reproducibility of the runs. Table 2 sums up these four runs.

TABLE 2
SURFACTANT RUNS

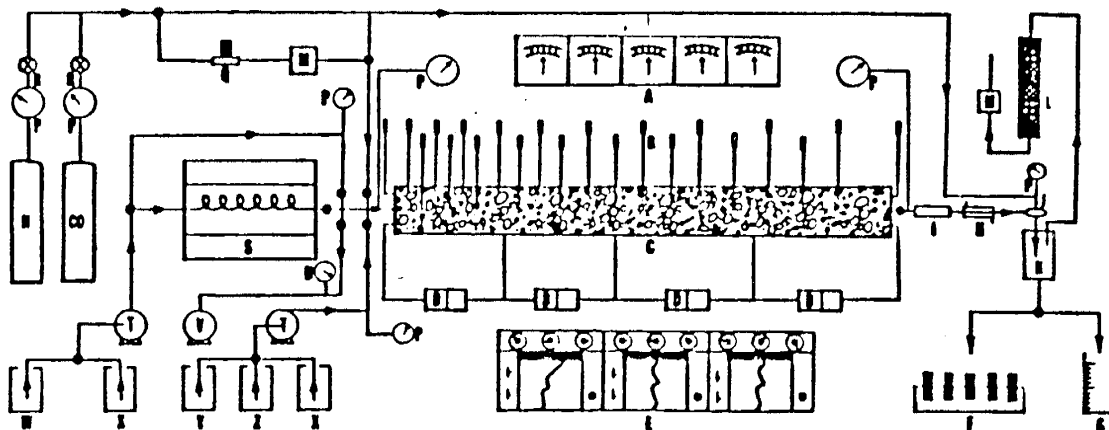
Run No.	Slug 1	Slug 2	Slug 3	Back Pressure
1	0.1%	0.1%	--	0
2	0.1%	0.1%	water	70
3	water	1.0%	1.0%	70
4	water	1.0%	1.0%	70

FUTURE RUNS

Future runs include injecting nitrogen simultaneously with the surfactant and steam, and possibly continue injecting nitrogen with the steam for a period of time after surfactant injection has stopped.

REFERENCES

1. Wang, F.P.: "A Study of Heat Transfer of Steam Injection and the Effect of Surfactants on Steam Mobility Reduction," PhD Dissertation, Stanford University, Stanford (1986).



- | | |
|--------------------------------------|---|
| A: temperature controllers | N: nitrogen cylinder |
| B: thermocouples | O: carbon dioxide cylinder |
| C: sandpack | P: pressure gauge |
| D: pressure transducers | Q: gas flow controller |
| E: recorders | R: gas flow regulator |
| F: fractional collector | S: steam generator |
| G: graduated cylinder | T: pump |
| H: heat exchanger (condenser) | U: vacuum gauge |
| I: side glass | V: vacuum pump |
| J: back pressure regulator | W: water container |
| K: gas/liquid separator | X: cleaning fluid |
| L: moisture drier | Y: oil container |
| M: gas flow meter | Z: surfactant solution container |

Fig. 1. Schematic Diagram of Steam Displacement Apparatus.

TWO-DIMENSIONAL DISPLACEMENT OF OIL BY GAS AND SURFACTANT UNDER FOAMING CONDITIONS

A technical report by Syed M. Mahmood and W.E. Brigham (TR 58, 1986) was published on this topic; the following is a summary of these results.

CONCLUSIONS AND RECOMMENDATIONS

A number of conclusions, both qualitative and quantitative have been arrived at as a result of this research. The qualitative conclusions are somewhat speculative in nature and thus lead to the recommendations for further research to better define the general nature of foam flow behavior when gravity force is also important.

CONCLUSIONS

In this two-dimensional sandpack, gravity was always an important force for all injection rates. The rates used were in the range that would scale to the rates of typical oil field reservoirs. In all cases it was found that the gas rose to the top of the sandpack and rapidly formed a thin Dietz-type tongue extending up to the producing end. The rate of gas injection had virtually no effect on the behavior of this gas finger.

The surfactant solution always segregated toward the lower part of the model. The nature of its flow depended on the rate, the surfactant concentration and the mobility ratio between the surfactant solution and the oil. When the mobility ratio was favorable, the surfactant moved as a nearly vertical front at the rates tested.

When the mobility ratio was unfavorable, and the surfactant solution rate was low, it moved along the bottom as a Dietz tongue. When the mobility ratio was unfavorable, and the surfactant solution injection rate was high, viscous fingers were formed at the surfactant solution-oil displacement front.

The surfactant concentration affected these liquid fronts, apparently due to the reduction in capillary forces. Low concentration surfactant solutions showed a more diffused interface, while higher concentration solutions showed sharper fronts.

Many different modes of injection and production were tried initially in an attempt to reduce gravity segregation and to cause foam flow to begin sooner in the reservoir. These included:

- (1) A single slug of surfactant solution followed by gas,
- (2) Alternate slugs of surfactant solution and gas with the surfactant solution injected into the top and the gas into the bottom,
- (3) Preformed foam injection, and
- (4) Simultaneous injection of surfactant solution with gas.

In all cases segregation occurred, but the best recovery was found when the surfactant and gas were injected simultaneously. Thus all subsequent experiments were run in this mode.

An attempt was made to model these subsequent runs using the scaling laws and dimensionless groups which relate capillary, viscous and gravity forces. The results were inconsistent. In particular it could be seen that, in the middle of many runs, the oil production rate began to rise rapidly. This always occurred at the time when foam generation was seen to begin in the sandpack, forming a third front in the gas-swept zone. It became clear that this delay in foam generation was a key to understanding the behavior, and was also the reason that the simple dimensionless variables did not adequately define the system.

This delay in the onset of in-situ foam generation has been termed the mass effect. It was speculated that the foamicidal behavior would be a function of the rates of gas and surfactant solution injection, the surfactant concentration, and the geometry of the system; and also the natures of the porous medium, the in-place fluids, and the surfactant solution. Although several oils were used in this experimental work, they were all refined oils of different viscosities which seemed to have similar behavior. Also the porous medium and geometry were constant in this work and the same surfactant was always used. Thus the variables of importance found for these experiments were the gas and surfactant injection rates and the surfactant concentration. All three variables affected the time of in-situ foam generation. An empirical equation was developed which successfully predicted the onset of foam generation in the sandpack.

Most of the data indicated two gravity tongues, gas and surfactant solution; and after the mass effect was overcome, a third foam front formed in the gas tongue. A simplified equation was derived to calculate the recovery from these tongues using a modified Buckley-Leverett formulation combined with a Dietz tongue in the gas, and a simple Dietz tongue in the surfactant solution. This is called the Combination-Drive Model herein. Once in-situ foam started to flow in the gas tongue, mobility in the model was modified to take the reduced gas mobility into account. This model was successful in predicting the recovery history of most of the runs. The exceptions occurred only in those runs where the displacement behavior differed markedly from the model. To make these calculations, the terms that were inserted into the equation were the oil saturation change in the gas and surfactant solution tongues, and the mobilities of surfactant solution, gas and foam. The same values could be used in all runs.

This same formulation concept was used to calculate the pressure drop history of the runs, and the success was far less pronounced. For several runs, the pressure drop history was well matched, but the behavior differed widely for many others. The poorer matches are probably due to the assumptions used in the model that the gas foam mobility was constant once foam was formed. Actually, as the foam moved through the model, the gas foam mobility decreased with time. No method was found to predict the rate of movement of the foam front; however, it is expected to be a complex function of the same variables which affect the onset of in-situ foam generation.

RECOMMENDATIONS

Since only one surfactant, and one porous medium with one geometry were used in the experiments, it would be useful to pursue other experiments where these factors were varied. With such systems, both the mass effect equation and the combination-drive displacement model could be tested, and modified if necessary.

A series of runs should be made to better define the foam front movement in the gas finger. From these data an equation of foam movement should be developed. Pressure drop measurements near the top of the model could help define these mobilities. The same variables mentioned in the paragraph above could be included in the foam front equation. If this were successful, the pressure drop history of foam floods could be better matched.

FOAM/EMULSION DISPLACEMENT OF OIL IN UNCONSOLIDATED SANDPACKS

INTRODUCTION

The aim of this research is to try and separate the different effects that a gas driven surfactant slug has on oil recovery. Three chemically similar surfactants whose properties range from foaming agents to emulsifying agents are being used to separate the effects of wettability changes and reduced oil-water interfacial tension from the other effects that a foam phase has as an oil displacing aid.

It was initially intended that this research be carried out using Plexiglas sandpacks. A partial vacuum at the outlet of the model was to be the driving force for the oil production. Moderate success was obtained using a small (18" × 6" × 1/4") prototype Plexiglas model, but when a larger model (36" × 12" × 1/4") was constructed, unresolvable problems arose. The major problem arose in the packing of the Plexiglas model in that it was impossible to get a close pack between the sand and the walls of the model. Despite measures of prevention, the walls of the model would bow out under the slight pressure exerted by the sand. After efforts to correct the problem, it was decided that it would be best to use a more conventional metal reinforced glass model.

At present the low HLB number surfactant runs have been completed and the intermediate HLB number surfactant effects are being investigated. In addition, a polysaccharide biopolymer is being added to the surfactant solution slug in hopes of stabilizing the foam lamellae.

The results with the low HLB number surfactant show that only at the highest concentration used (0.1% by wt.) did the surfactant solution increase oil recovery. At all other surfactant concentrations the oil recovery was exactly the same as when no surfactant was present in the injected slug. However, at all concentrations (0.01%, 0.03%, 0.1%) the aqueous phase recovery from the sandpack increased over that when a 0.0% surfactant slug was used.

The early results from the runs where the polymer was included in the surfactant slug indicate that the polymer slows down the rate of oil recovery initially, but produces the oil at a more even rate and results in higher ultimate recovery. Another effect of the addition of the polymer to the surfactant solution was a dramatic decrease in the aqueous phase recovery. In each instance, the addition of polymer reduced the aqueous phase recovery to about 10% of its value when no polymer was added.

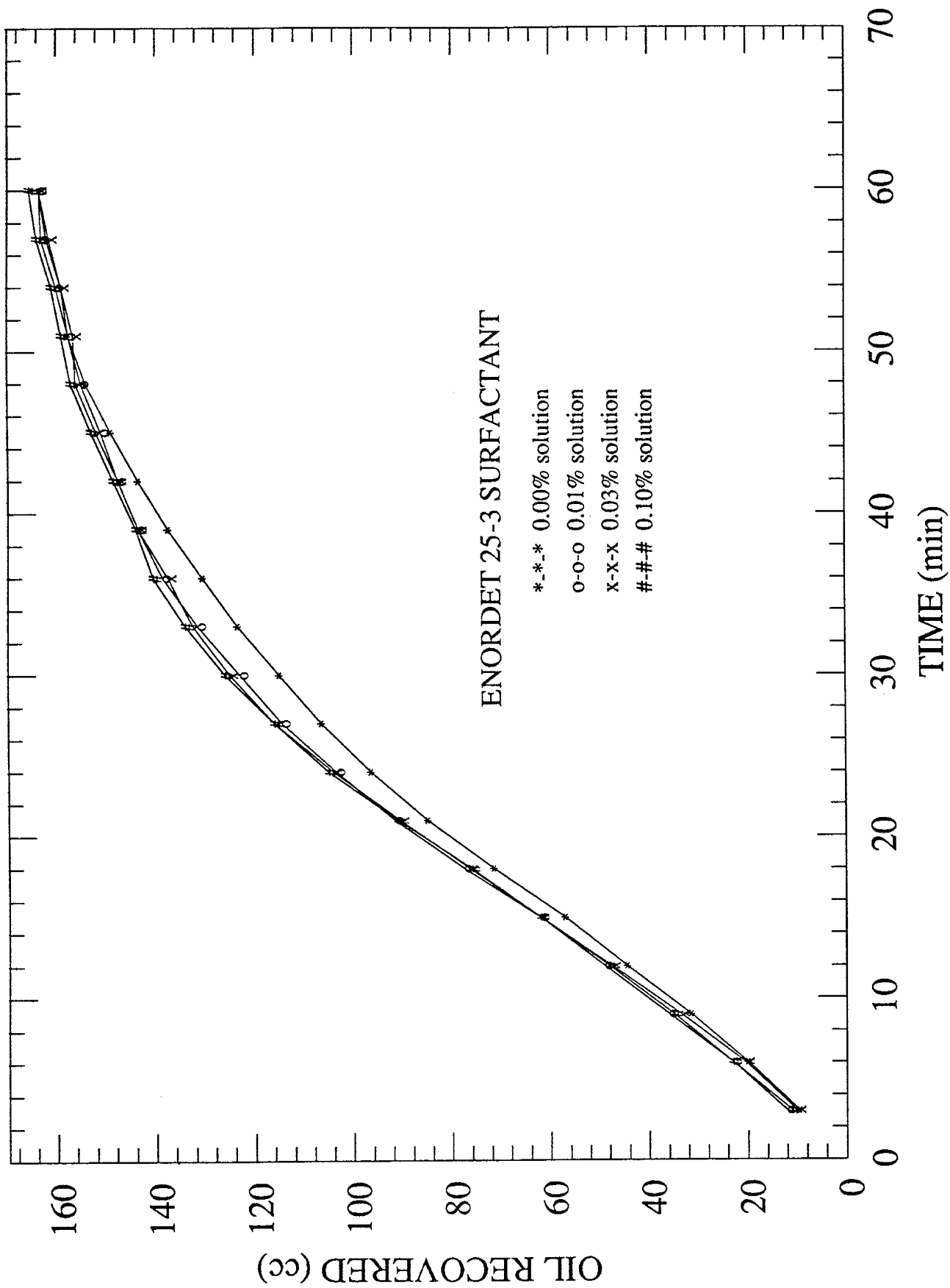


Fig. 1. Oil Recovery versus Time

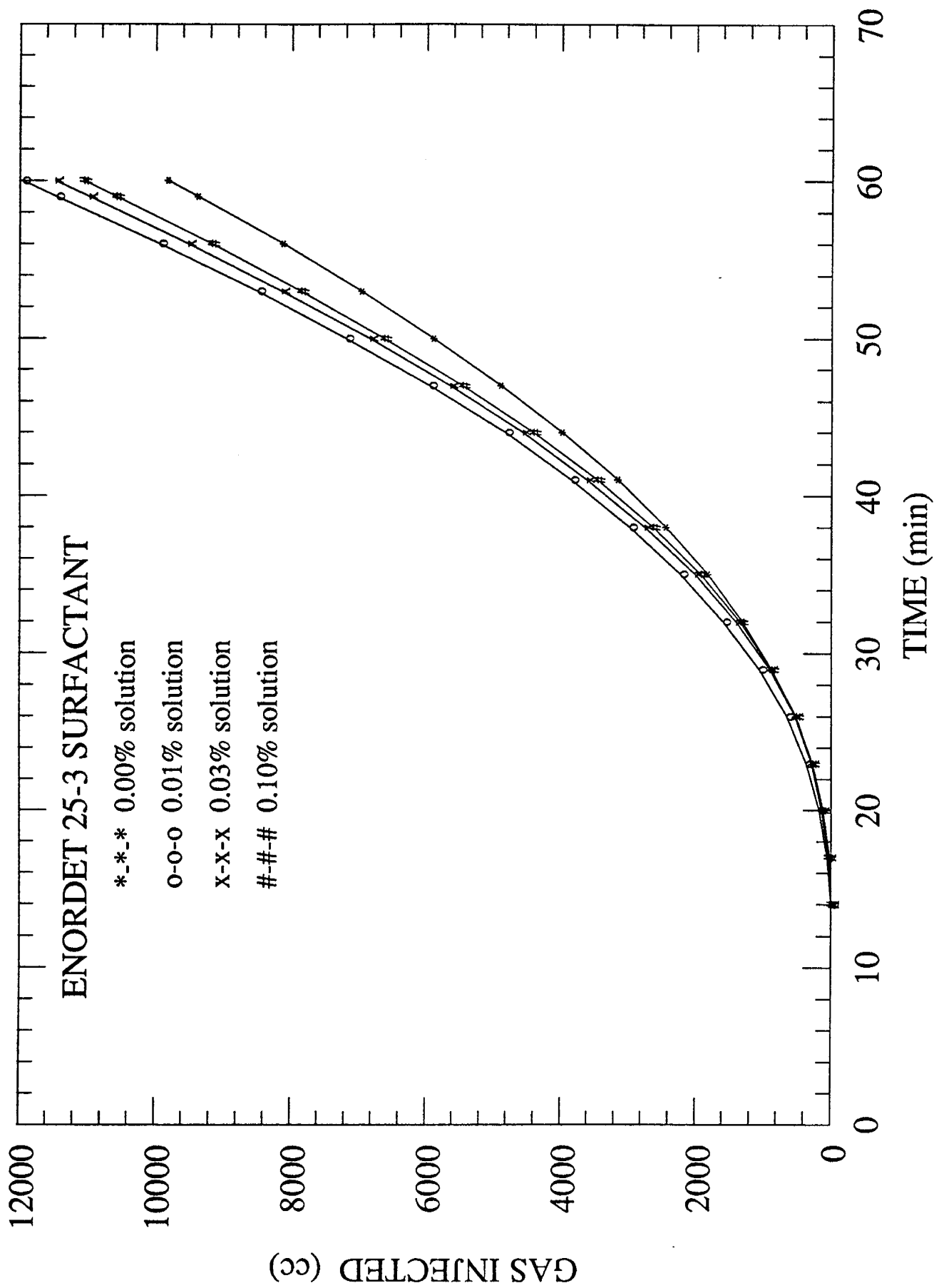


Fig. 2. Gas Injected versus Time

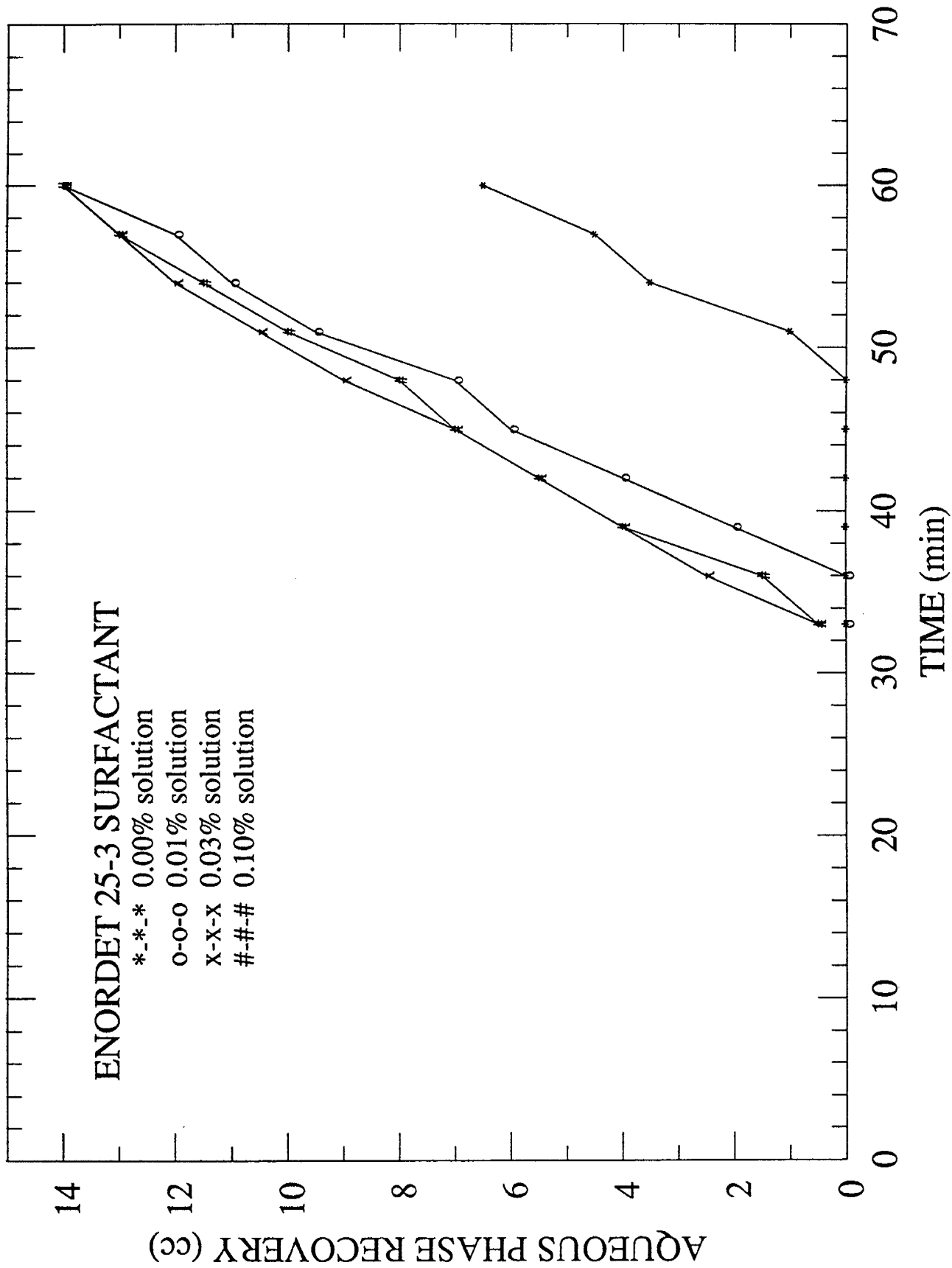


Fig. 3. Aqueous Phase Recovery versus Time

FLOW OF FOAM THROUGH MICROMODELS

INTRODUCTION

This work started in the summer of 1986. The objective is to study the flow of foam through a micromodel as an extension of the work done by Owete and Brigham (1984). In his research, Owete used etched silicon wafers to represent a monolayer of porous matrix. He used two types of models, one with homogeneous pore structures and one with randomly distributed pore structures. In his experiments, Owete injected air into the surfactant saturated models and observed the "flow characteristics of foam under varying air injection rates, pore dimensions and surfactant concentration." However, he never introduced oil in his models. We are attempting to observe the more complex behavior of flow of foam with oil.

This work involves the same procedure as Owete's with a few exceptions. Instead of using etched silicon wafers, a single layer of sand is used as the porous medium. Instead of injecting air, CO₂ is injected to reduce the amount of residual gas in the micromodel. The runs are made at room temperature and atmospheric pressure. Under these conditions, CO₂ is immiscible. Surfactant followed by CO₂ is injected into the model which had previously been saturated with oil. Observations were made of the foam flow mechanisms under varying injection rates and surfactant concentration.

EXPERIMENTAL APPARATUS

The apparatus consists of a high powered microscope, a photo camera to take slides, a television camera connected to a video monitor and video recorder. The micromodel has tubing lines connecting it to the syringe pump and the pressure transducer which is connected to the demodulator, voltmeter and pressure recorder. A schematic diagram of the experimental apparatus is shown in Fig. 1.

A filter was used to reduce the glare from the refraction of light through the sand grains. The fluids were dyed different colors to help distinguish the interfaces and the wettabilities. The oil was dyed red and the surfactant was dyed blue.

THE MICROMODEL

Various micromodel constructions were attempted before we found one suitable to our needs. We first tried using a Teflon gasket situated between two Plexiglas plates with the sand contained within the gasket. Problems arose because the sand grain size was very small, 120 mesh, making it very difficult to obtain a single layer of sand. Also, the Teflon was held in place using Room Temperature Vulcanizing Silicone Rubber (RTV). RTV contains silicon and our concern was it would kill any foam generated by the surfactant. The Teflon also failed to provide a good seal thus allowing the fluids to escape. We also attempted to use modeling clay to obtain an imprint of the sand grains and then use resin to obtain a cast. Wax was used to fill the pore space while the top cast was allowed to cure. Two ports were drilled and the wax was melted and allowed to flow out leaving void pore spaces. We were unable to extract all of the wax and the quality of the imprint from the modeling clay was poor.

The final construction was a modification of our initial attempt. It consists of two Plexiglas plates measuring 3-1/4 in. in length, 1-7/8 in. in width and 1/2-in. in height. Instead of Teflon, a rubber gasket was placed between the plates. The plates were tightened with six bolts, compressing the rubber and thus providing a seal for the fluids passing through the matrix. Two ports, an inlet and an outlet, on the top plate are used to pass the fluids through the porous matrix. Figure 2 is a diagram of the micromodel.

The sand grain size is 35 mesh (U.S. equivalent) equal to a mesh opening of 0.495 micrometers. The absolute permeability of the matrix was calculated using Darcy's Law for radial flow at the inlet and outlet and linear flow for the area between the ports. The absolute permeability is approximately equal to 19 Darcys.

EXPERIMENTAL PROCEDURE AND OBSERVATIONS

The surfactant used for the experiments was Shell Enordet AOS 1618. The first run recorded was the displacement of 1.1% surfactant with CO_2 . The generation of lamellae could be observed as the gas broke through. Other runs were of oil displaced by surfactant followed by CO_2 . Some runs were made using 1.1% surfactant concentration and other runs using 0.1% surfactant concentration. For the higher concentration the oil was displaced in large droplets and as the gas broke through there was some formation of lamellae. For the lower surfactant concentration, the oil was displaced in smaller droplets. The change was very gradual as the surfactant displaced the oil and as the gas broke through, there was not as much lamellae generation as with the higher surfactant concentration.

For the surfactant run the maximum pressure drop was 1.6 psi at a pump rate of $1.28 \times 10^{-3} \text{ cm}^3/\text{min}$. For the oil and 1.1% surfactant concentration, the maximum pressure drop was 0.73 psi while the surfactant was displacing the oil at a pump rate of $1.28 \times 10^{-3} \text{ cm}^3/\text{min}$. For the oil and 0.1% surfactant concentration, the maximum pressure drop was 0.31 psi at a pump rate of $1.28 \times 10^{-3} \text{ cm}^3/\text{min}$.

FUTURE WORK

In the future, runs will be made to observe the effects caused by varying rates, surfactants, and oils.

REFERENCE

1. Owete, O.S. and Brigham, W.E.: "A Micromodel Study of Foam Flow Through Porous Media," SUPRI TR 37 [DOE/ET/1564-6] (July 1984).

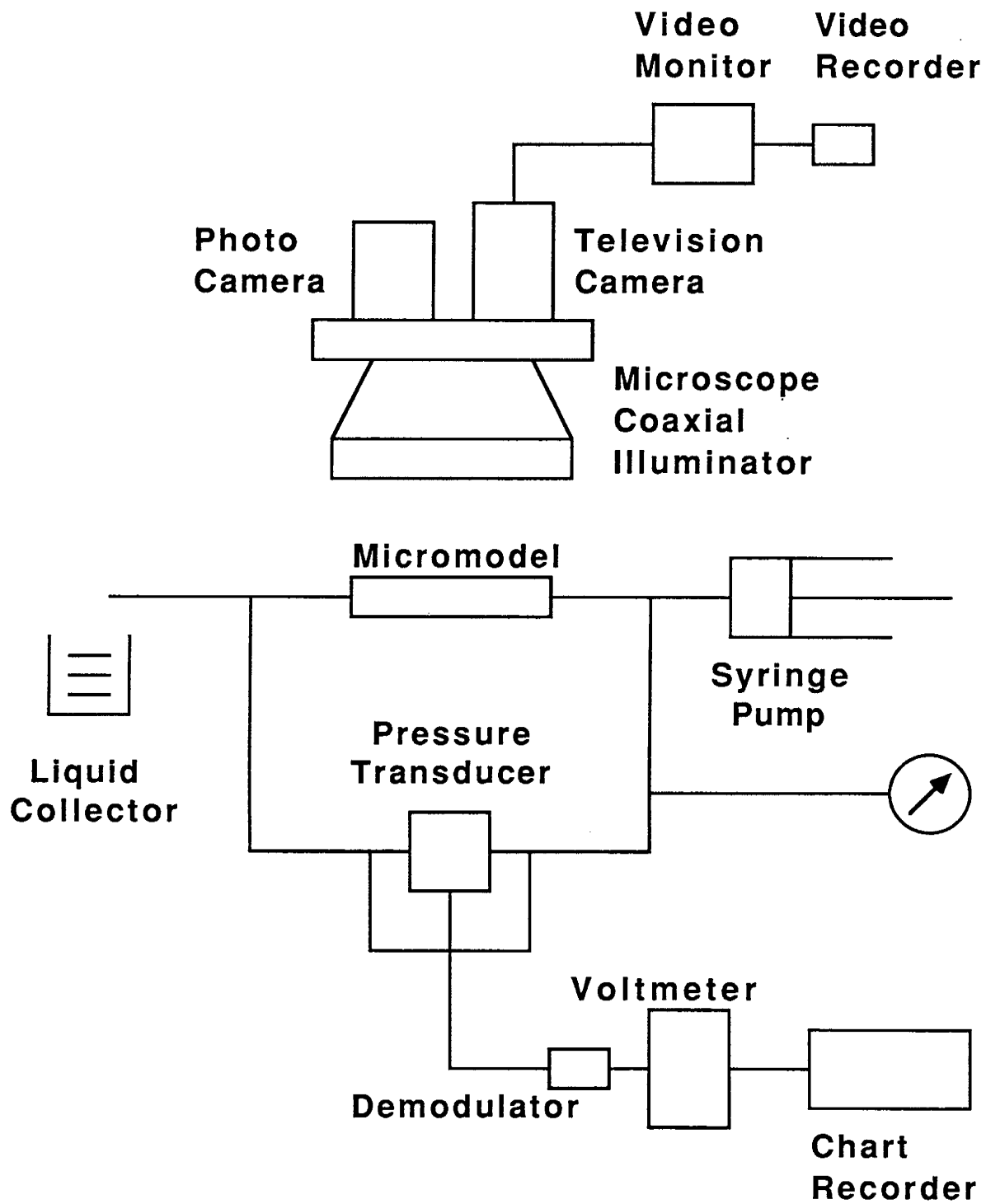
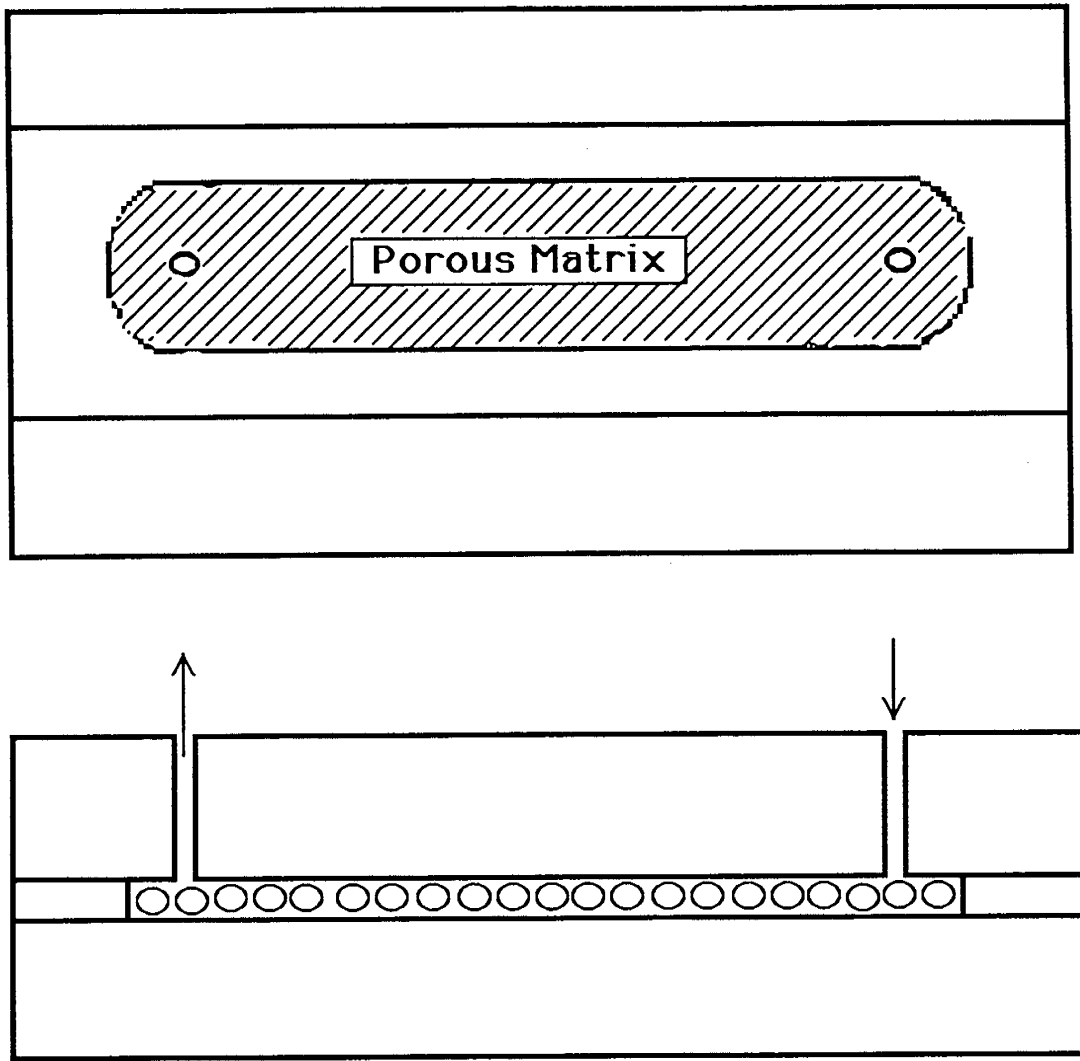


Fig. 1 Schematic Diagram of Apparatus



Sand Grain Size: 35 mesh U. S. Equivalent
0.495 micrometers

Absolute Permeability, $k = 19.2$ Darcys

Fig. 2 Diagram of Micromodel

THE TRANSIENT BEHAVIOR OF SURFACTANT FOAM FLOW IN POROUS MEDIA

INTRODUCTION

One promising method to improve a steam drive is by the formation of an in-situ foam. This is accomplished by injecting a small amount of a surfactant along with the steam. Sometimes also, a noncondensable gas such as nitrogen is mixed in. Foam's high apparent viscosity could greatly improve the mobility ratio, and the blocking ability of foam is useful in reducing the thieving effect of high permeability streaks on premature steam breakthrough. As reported by Lescure and Claridge (1986), these beneficial characteristics could also be utilized to improve the efficiency of other enhanced recovery methods, namely carbon dioxide flooding.

The utilization of foam as a displacing medium was first proposed by Bond and Holbrook (1958). Not long after this Fried (1961) conducted a number of experiments using foam to displace brine and/or oil from porous media. For his purposes Fried generated an aqueous foam external to the porous medium, injected a slug of foam into the medium, and then drove this slug along by continuous injection of air. Fried showed that the low mobility of the foam as well as its gas blocking ability contribute to a higher oil recovery and lower gas-oil ratio than with conventional displacement methods.

The literature survey conducted by Marsden *et. al* (1977) indicated that the prime candidate for a blocking agent in steam drives was foam. Subsequently Chiang *et. al* (1980) investigated different surfactants and found that indeed, gravity override of gas could be sharply reduced. They also found that in-situ foaming generally increased with surfactant concentration until the critical micelle concentration (CMC) was reached. Additional surfactant beyond the CMC did not affect the foaming process. Wang *et. al* (1982) studied the ability of several surfactants to generate foams at steam injection temperatures and pressures. They achieved promising results with several foamers. Dilgren *et. al* (1982) described reduction of steam mobility by foam in terms of a permeability reduction factor defined as the ratio of the permeability of steam in the presence of foam to the permeability of steam in the absence of foam. They found these factors ranging from 1.0 to 0.025. For their purposes Dilgren *et. al* assumed that the mobility reduction was due to lowered permeability only; no change in viscosity was considered.

In reality, foam has a measurable viscosity much higher than the viscosity of either its gas or liquid components. Marsden and Khan (1966) measured foam viscosities using a modified Fann VG Meter. They found the foam viscosity increased with increasing quality at a given shear rate. Foam was concluded to be a non-Newtonian fluid by virtue of the fact that the viscosity decreased with increased shear rate. Marsden and Khan also found that increasing the surfactant concentration increased the viscosity slightly. These three basic properties of the viscosity of foam have been confirmed in further studies by other researchers including Marsden *et. al* (1967), Raza and Marsden (1967), Mitchell (1969), Minssieux (1974), Holbrook *et. al* (1981), and Treinen (1985).

With such general agreement as to the behavior of foam in porous media, more recent research has concentrated on understanding the causes of such behavior and the key factors which control it. Beginning with Holm (1968), attempts have been made to establish the flow paths of gas and liquid when foam is injected into a porous medium. Holm concluded that foam does not flow as a body even when the liquid and gas were combined and injected as

foam. There was no free gas flow; the gas moved through the system by progressively breaking and reforming bubbles through the length of the medium. The liquid was found to move via the interconnected film network of the bubbles. The respective flow rates were a function of the number and strength of the films. Owete (1984) observed this mechanism in micromodels. The stability and bubble making ability of liquid films (lamellae) has therefore become the crux of many recent studies. The behavior of foam lamellae in smooth capillary tubes was the subject of a project undertaken by Hirasaki and Lawson (1983). They discovered the importance of foam texture, or average bubble size in relation to the capillary tube size; foam quality, or the gas volume divided by the total volume; and the surface tension gradients created when surfactant is swept from the front of a bubble to its rear. The most recent work on the subject has dealt with the conditions under which foam bubbles are formed and/or destroyed using simplified models such as a toroidally constricted capillary tube used by Sanchez *et. al* (1986). They formulated an expression for the generation rate of foam bubbles based on geometric and fluid properties. Radke and Ransohoff (1986) categorized the mechanisms of foam generation within glass bead packs. The snap-off mechanism was concluded to be the primary mechanism responsible for the formation of a strong foam. They developed a simple model to predict the onset of snap-off. The stability of foam lamellae as determined by capillary pressure was the subject of a recent study by Khatib *et. al* (1986). The destabilization of foam lamellae by oil droplets was observed by Nikolov *et. al* (1986) using sophisticated microscopic techniques. They have demonstrated that the surfactant type and concentration directly influence the stability of the three phase emulsion structure.

Most studies up until now have dealt with the steady state operation of foam injection. One approach not yet thoroughly reported is the investigation of the transient flow behavior of a foam displacement process. Because many investigators have found that truly steady state conditions cannot be achieved before a considerable amount of foam has been introduced into a porous medium, the transient forces are likely to dominate over most or all of the duration of a field project. A useful tool for planning a foam enhanced injection project would be a predictive model for the behavior and duration of the transient period of foam generation and flow in porous media. The first step in creating such a model is, of course, accumulating basic experimental data. The work reported here is a first attempt to determine the usefulness of an apparatus redesigned to yield transient foam flow data. The system studied is a one dimensional, low temperature, low pressure environment.

EXPERIMENTAL EQUIPMENT

The equipment used for this study was the same apparatus originally designed and used by Treinen (1985) for his study of the apparent viscosity of foam in porous media. Some modifications have been made for the current experiment. In the interest of continuity the entire apparatus will be herein described with no distinction between the original version and the modifications. The following description, therefore, contains some duplication of Treinen's efforts.

The schematic in Fig. 1 illustrates the equipment used to produce foam and displace fluid in a porous medium. Foam of known quality and flowrate was generated from nitrogen and surfactant solution passing through a foam generator. The foam was then injected into a sandpack 100% saturated with water. While this displacement was taking place, the absolute pressure at various points along the sandpack was monitored. Also at this time, the effluent liquid was collected and running totals of its volume and surfactant concentration were noted.

A more detailed diagram of the equipment is given in Fig. 2. A Matheson Model 8240 mass flow controller was used to regulate the flow of nitrogen. The liquid flow was controlled

using a Constametric model 3G liquid chromatography pump. To produce foam, nitrogen and surfactant solution were introduced into a foam generator illustrated in Fig. 3. This generator is actually a short version of the sandpack, 1 in. in diameter and 3 in. in length, packed with 120-140 mesh Ottawa sand. By controlling the gas and liquid flow rates into this generator, a uniform foam of desired quality was produced. Before flowing into the sandpack, the foam went through an observation cell. This cell was constructed by sandwiching a thin Teflon gasket between two thick, acrylic plastic plates. The thickness of the Teflon gasket, and hence the separation between the plastic plates, is 0.01 in. An identical observation cell is located at the outlet of the sandpack.

The sandpack consists of a clear acrylic plastic tube 1 in. in diameter and 24 in. in length. End butts were designed to promote one-dimensional flow at the sandpack ends by distributing flow through a number of radial and circular channels. This arrangement is shown in Figure 4. The sand used in the sandpack was 120-140 mesh Ottawa sand which had been acid and base washed. Sand migration was prevented by 200 mesh stainless steel screens at the inlet and outlet, and by in line filters with 60 micron porous elements at the pressure tap fittings.

To minimize the variation in foam quality due to the expansion of gas, the system was initially run at an elevated downstream pressure of 50 psig. This was achieved by using a backpressure regulator. To measure the absolute pressure along the sandpack eight pressure taps were located at 2, 4, 6, 9, 12, 15, 18, and 21 in. from the inlet. Pressure taps were also located near the inlet and outlet of the sandpack. Since the number of pressure transducers initially available was limited to eight, not all of the sandpack pressure taps were utilized. The inlet and outlet, along with six of the sandpack taps, were connected to differential pressure transducers. In order to read absolute pressure from a differential pressure transducer, one must expose the negative side of the transducer to a known, constant pressure. In this case that pressure could have been atmospheric pressure, but because of the elevated system pressure this would have necessitated using pressure transducer plates in the 0 to 100 psi range. With a total flowing pressure drop across the sandpack in the range of 5 psi, these plates would not have been sensitive enough. For this reason the pressure transducers were connected to a constant pressure source of 50 psig allowing the use of 5 psi differential pressure plates in the pressure transducers. In the existing design, the same pressure line is connected to both the backpressure regulator and the transducer constant pressure. This arrangement was found to be less than satisfactory because the pressure at which the backpressure regulator allowed fluids to pass was two to three psi less than the regulator's control pressure. Although this pressure discrepancy may seem small, it eliminated most of the 5 psi scale available from the transducers. An alternative design would be to simply separate these two lines, thereby allowing for different pressures in each.

The response from the transducers was monitored by an Apple II+ personal computer. The interface between the two devices was an Applied Engineering Twelve Bit Analog-to-Digital Converter. The main purpose of this computerized setup was to allow for unmanned operation of the experiment. This capability was not fully utilized in the early experiments, however, because an important facet of the data was the correlation of pressure behavior with the observed position of the foam front. The ability to automate the apparatus should still prove valuable in its future operation.

Samples of the liquid produced were collected in test tubes during each run using an ISCO Golden Retriever. This device allows samples to be collected on either a volumetric basis or on a timed interval basis. Using the timing option, the liquid production rate can be calculated by measuring the volume produced during each time interval.

PROCEDURE

Prior to each experimental run, the pressure transducers were calibrated. Each experimental run was begun with a new sandpack. Dry sand was packed into the tube while in an upright position, while vibration and an induced vacuum were used to enhance settling of the sand. To ensure consistency, each sandpack's porosity and permeability were measured before each run. An estimated porosity was obtained by weighing the tube before and after packing; the difference being the weight of the sand. Assuming a grain density of 2.65 g/cc, total pore volume and porosity could be calculated. While still dry, the sandpack's gas permeability was then measured using nitrogen, a water manometer, and a bubble flow meter. After this measurement, the sandpack was alternately flushed with CO_2 and evacuated several times. After several of these cycles, the sandpack was flooded with distilled water. Water was then pumped through at elevated backpressure for about one pore volume. An important factor in obtaining accurate pressure readings was to be sure that the line leading from each pressure tap to its transducer was completely water-filled. To do this, the drain screw on each transducer was opened and left open until water dripped out at a constant rate and no gas slugs appeared to be escaping. After all transducers had been cleared, the sandpack was repressurized by pumping more water into it, and the drainage process repeated. The water permeability was then measured with a water manometer and a graduated cylinder. The water permeability values obtained were invariably lower than the gas permeability for a given sandpack. This characteristic was consistent with Treinen's experience.

A foam flow rate, quality, surfactant concentration, and backpressure were then selected for each experiment. Foam quality could be calculated by a ratio of volumes.

$$\text{Quality } \Gamma = \frac{\text{Gas Volume}}{\text{Gas Volume} + \text{Liquid Volume}} \quad (1)$$

The difficulty in obtaining a desired quality is the compressible nature of a gas phase. The foam quality and flow rate were therefore calculated at the midpoint of the sandpack using an anticipated pressure gradient, Δp . These expected pressure gradients were derived from Treinen's steady state data. Soon after the transient data began to come in, the advisability of using these pressure drops for the present purpose was called into question. There being no other better means however, this method was continued. The gas flow rate was then found.

$$q_g = \frac{14.7q_{gsc}}{14.7 + \Delta p/2 + \text{backpressure}} \quad (2)$$

The liquid phase was assumed to be incompressible. The total foam flow rate is a simple addition.

$$q_{\text{foam}} = q_{\text{liquid}} + q_{\text{gas}} \quad (3)$$

All parameters were chosen initially so as to attempt to eventually match steady state results. The observed behavior then provided the impetus for the values chosen in subsequent runs.

The surfactant used in this study was Suntech IV from the Sun Petroleum Products Company. The surfactant is an anionic sulfonate manufactured from normal hydrocarbons ($C_{15} - C_{18}$) and toluene. The average molecular weight was 425 with a critical micellar concentration (CMC) of 0.28 wt%.

The desired foam was generated and allowed to flow through the upstream observation cell and out the auxiliary inlet, while the sandpack remained water saturated, sealed, and pressurized. When the foam flow was constant and stabilized, the auxiliary inlet was closed and the foam pressure was allowed to build up to the sandpack pressure. The foam was then introduced into the sandpack and pressure monitoring and observations begun.

When choosing a time interval for liquid collection, three points should be remembered:

1. Until gas breakthrough, the liquid production rate equals the total foam injection rate;
2. After gas breakthrough, the liquid production rate approximately equals the liquid injection rate; and
3. The minimum volume needed for a surfactant concentration titration in the expected range will be about two milliliters.

The collected liquid samples were titrated using a chloroform-hyamine procedure to find the surfactant (sulfonate) concentration. By knowing the volumes of the samples, their surfactant concentrations, and the times over which they were taken, a material balance could be performed for the surfactant in order to determine average in-situ concentration.

RESULTS AND DISCUSSION

When the apparatus was completed, two test runs were made during which various problems were encountered that rendered the data obtained erroneous. After these problems were remedied, one valid run was performed the results of which are presented here. Due to time limits, a complete history for the system from beginning to steady state conditions was not obtained. A foam of 90% quality was injected at a rate of 0.1 cc/min. into a sandpack having a permeability of 6.97 darcies and a porosity of 32%. The surfactant concentration was 0.05 wt%, and the experiment was run at a backpressure of approximately 50 psig. The clear acrylic tube allowed easy visual observation of the foam front as it progressed through the sand. Small gas fingers could be seen slightly ahead of a region of apparent uniform gas saturation. This front traveled through the sandpack relatively quickly and gas broke through at the outlet after 0.793 pore volumes of foam had been injected. At that time the foam front was 4.76 cm upstream of the outlet. Fig. 5 shows the exact position of the observed foam front plotted against the number of pore volumes of foam injected at several times before gas breakthrough.

The position of the front could also be inferred by noting the higher pressure gradient in the foam region. Fig. 6 shows the pressure profile in the sandpack at several times prior to gas breakthrough. The visually observed foam front position is also marked. The large pressure drop from the inlet to the first pressure tap at 4 in. is believed to occur primarily across the inlet butt and is not truly indicative of the viscous foam behavior within the sandpack. As can be seen, the pressure gradient behind the foam front was noticeably steeper than the pressure gradient in the water zone. The other important feature of this figure is the steepening of the pressure gradient with time. In other words, as more foam passed through the sand near the inlet the pressure drop in that region increased. This behavior could also be observed on a larger scale by plotting the pressure profile across the entire sandpack at times after breakthrough, as in Fig. 7.

To check for consistency it is possible to discretize the sandpack into sections of different lengths. Assuming no change in permeability once foam has saturated a region, an effective viscosity, μ_{eff} , can be found from the pressure drop.

$$\mu_{\text{eff}} = \frac{kA}{q_{\text{foam}}L} \Delta p \quad (4)$$

According to the pressure behavior, as more foam passes through a given volume of sand the μ_{eff} should rise. The results of this calculation for the entire sandpack are shown in Fig. 8. The effective viscosity was then calculated for several sections of the sandpack. The comparison was poor for sections close to the inlet. The reason for this could be the rather large, constant pressure drop across the inlet butt which masked the foam viscosity effects. Figure 9 shows the results of this calculation for the first 12, 18, and 21 in. of the sandpack. As can be seen, these sections compared fairly well to each other and to the entire sandpack. This seems to indicate that the foam viscosity is a function of the throughput of foam, and that this dependence did not vary with scale.

Certainly this behavior is due in part to surfactant adsorption onto the sand grains. In an attempt to find the amount of surfactant adsorbed, two parameters must be estimated: the average liquid saturation and the total amount of surfactant within the system. By finding the surfactant concentration in the liquid produced, a material balance can be performed on the surfactant to yield the amount in the sandpack at any time.

Figure 10 shows the volume of liquid produced as a function of the volume of foam injected. From this figure it is clear that at early times the volume of liquid produced is nearly equal to the volume of foam injected. After breakthrough of gas, the liquid production rate decreases. Notice that the curve is slightly concave downwards, thus indicating a gradually increasing gas saturation.

Figure 11 shows the effluent surfactant concentration as a function of the volume injected. Notice that 8-10 pore volumes of foam were injected before the surfactant concentration started to rise significantly. This shows that the surfactant was retained in the porous medium, presumably by adsorption. Material balances on the data from Figs. 10 and 11 could be used to calculate the amount of surfactant retained in the core. This has not been done as yet; but will be in the future.

A difficult value to get a handle on is the average liquid saturation in the foam-filled region. An estimate can be obtained, however, by assuming an average gas saturation within the short region of gas fingers extending from the foam front to the outlet. An estimate for this gas saturation can be obtained using Buckley-Leverett fractional flow theory along with an empirical relative permeability curve for the sandpack.

Using the relative permeability curves of Fig. 12, the gas fractional flow curve predicts an average gas saturation of 0.24 ahead of the foam front (Fig. 13). Using this value, it should thus be possible to calculate the average gas saturation in the foam zone both prior to, and after, breakthrough. This type of calculation would be useful to relate the saturation and mobility data in the experiment, and such calculations will be made in future runs.

REFERENCES

1. Bond, D.C. and Holbrook, O.C.: "Gas Drive Oil Recovery Process," U.S. Patent No. 2,866,507 (1958).
2. Buckley, S.E. and Leverett, M.C.: "Mechanism of Fluid Displacements in Sands," *Trans.*, AIME (1942) 146, 107-116.
3. Chiang, J.C., Sanyal, S.K., Castanier, L.M., Brigham, W.E., and Sufi, A.: "Foam as a Mobility Control Agent in Steam Injection Processes," paper SPE 8912 presented at the SPE 50th Annual California Regional Meeting, Los Angeles, April 9-11, 1980.
4. Corey, A.T., Rathjens, C.H., Henderson, J.H., and Wyllie, R.M.J.: "Three Phase Relative Permeability," *Trans.*, AIME (1956) 207, 349-351.
5. Dilgren, R.E., Deemer, A.R., and Owens, K.B.: "The Laboratory Development and Field Testing of Steam/Noncondensable Gas Foams for Mobility Control in Heavy Oil Recovery," paper SPE 10774 presented at the 52nd Annual California Regional Meeting, San Francisco, March 24-25, 1982.
6. Fried, A.N.: "The Foam Drive Process for Increasing the Recovery of Oil," USBM Report of Investigations 5866, 1961.
7. Hirasaki, G.T. and Lawson, J.B.: "Mechanism of Foam Flow in Porous Media - Apparent Viscosity in Smooth Capillaries," paper SPE 12129 presented at the SPE 58th Annual Technical Conference and Exhibition, San Francisco, Oct. 5-8, 1983.
8. Holbrook, S.T., Patton, J.T., and Hsu, W.: "Rheology of Mobility Control Foams," paper SPE 9809 presented at the SPE/DOE Second Joint Symposium on Enhanced Oil Recovery, Tulsa, OK, April 5-8, 1981.
9. Holm, L.W.: "The Mechanism of Gas and Liquid Flow Through Porous Media in the Presence of Foam," *Soc. Pet. Eng. J.* (Dec. 1968)359-369.
10. Khatib, Z.I., Hirasaki, G.J., and Falls, A.H.: "Effects of Capillary Pressure on Coalescence and Phase Mobilities in Foams Flowing Through Porous Media," paper SPE 15442 presented at the SPE 61st Annual Technical Conference and Exhibition, New Orleans, Oct. 5-8, 1986.
11. Lescure, B.M. and Claridge, E.L.: "CO₂ Foam Flooding Performance vs. Rock Wettability," paper SPE 15445 presented at the SPE 61st Annual Technical Conference and Exhibition, New Orleans, Oct. 5-8, 1986.
12. Marsden, S.S., Eerligh, J.J., Albrecht, R.A., and David, A.: "Use of Foam in Petroleum Operations," *Proc.*, Seventh World Petroleum Congress, Mexico City (April 1967) 235.
13. Marsden, S.S., Elson, T., and Guppy, K.: Literature Review of the Selective Blockage of Fluids in Thermal Recovery Projects, SUPRI-TR-3, Stanford U. Petroleum Research Inst., Stanford, CA (Dec. 1977).

14. Marsden, S.S. and Khan, S.A.: "The Flow of Foam Through Short Porous Media and Apparent Viscosity Measurements," *Soc. Pet. Eng. J.* (March 1966)17-25.
15. Minssieux, L.: "Oil Displacement by Foams in Relation to Their Physical Properties in Porous Media," *J. Pet. Tech.* (Jan. 1974)100-108.
16. Mitchell, B.J.: "Viscosity of Foam," PhD dissertation, U. of Oklahoma, Norman (1969).
17. Nikolov, A.D., Wasan, D.T., Huang, D.W., and Edwards, D.A.: "The Effect of Oil on Foam Stability: Mechanisms and Implications for Oil Displacement by Foam in Porous Media," paper SPE 15443, proceedings, 61st Annual Technical Conference and Exhibition, New Orleans, Oct. 5-8, 1986.
18. Radke, C.J. and Ransohoff, T.C.: "Mechanisms of Foam Generation in Glass Bead Packs," paper SPE 15441 presented at the SPE 61st Annual Technical Conference and Exhibition, New Orleans, Oct. 5-8, 1986.
19. Raza, S.H. and Marsden, S.S.: "The Streaming Potential and Rheology of Foam," *Soc. Pet. Eng. J.* (Dec. 1967) 359-368.
20. Sanchez, J.M. and Schechter, R.S.: "The Effect of Trace Quantities of Surfactant on Nitrogen/Water Relative Permeabilities," paper SPE 15446, proceedings, 61st Annual Technical Conference and Exhibition, New Orleans, Oct. 5-8, 1986.
21. Treinen, R.J.: "Apparent Viscosity Measurements of Surfactant Foam in Porous Media," MS Report, Stanford U., Stanford, CA (1985).
22. Wang, P.F., Al-Khafaji, A., Castanier, L.M., and Brigham, W.E.: "Steam-Surfactant Systems at Reservoir Conditions," DOE Fossil Energy Report No. CONF-820712 (July 1982)216-226.

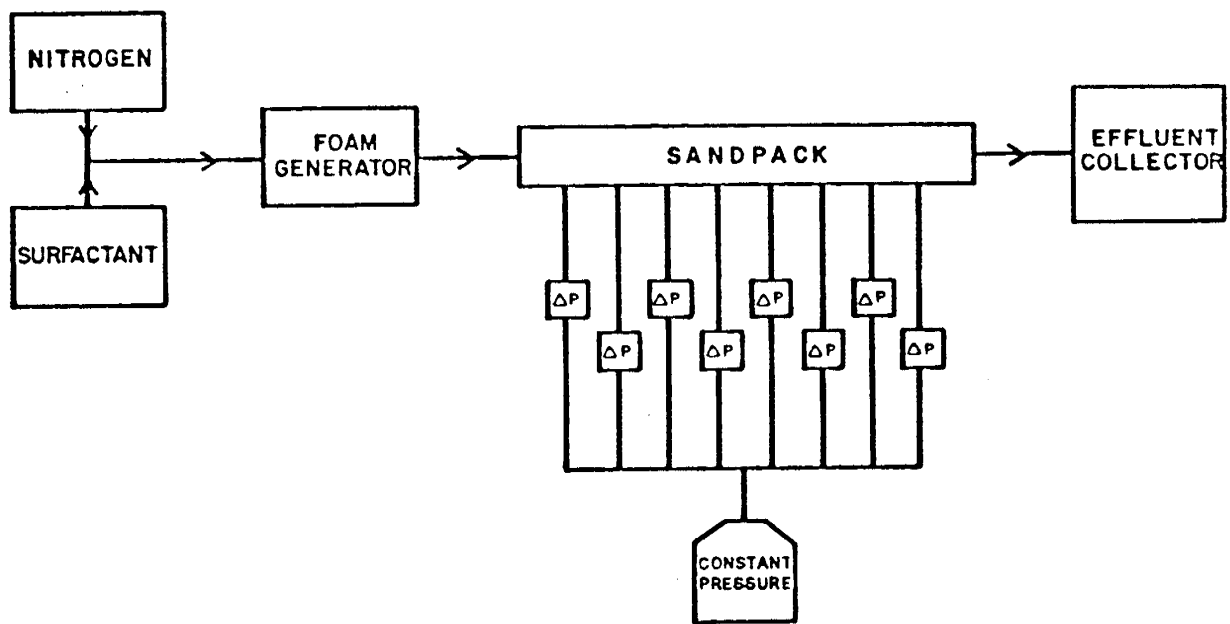


Figure 1. Simplified System Diagram.

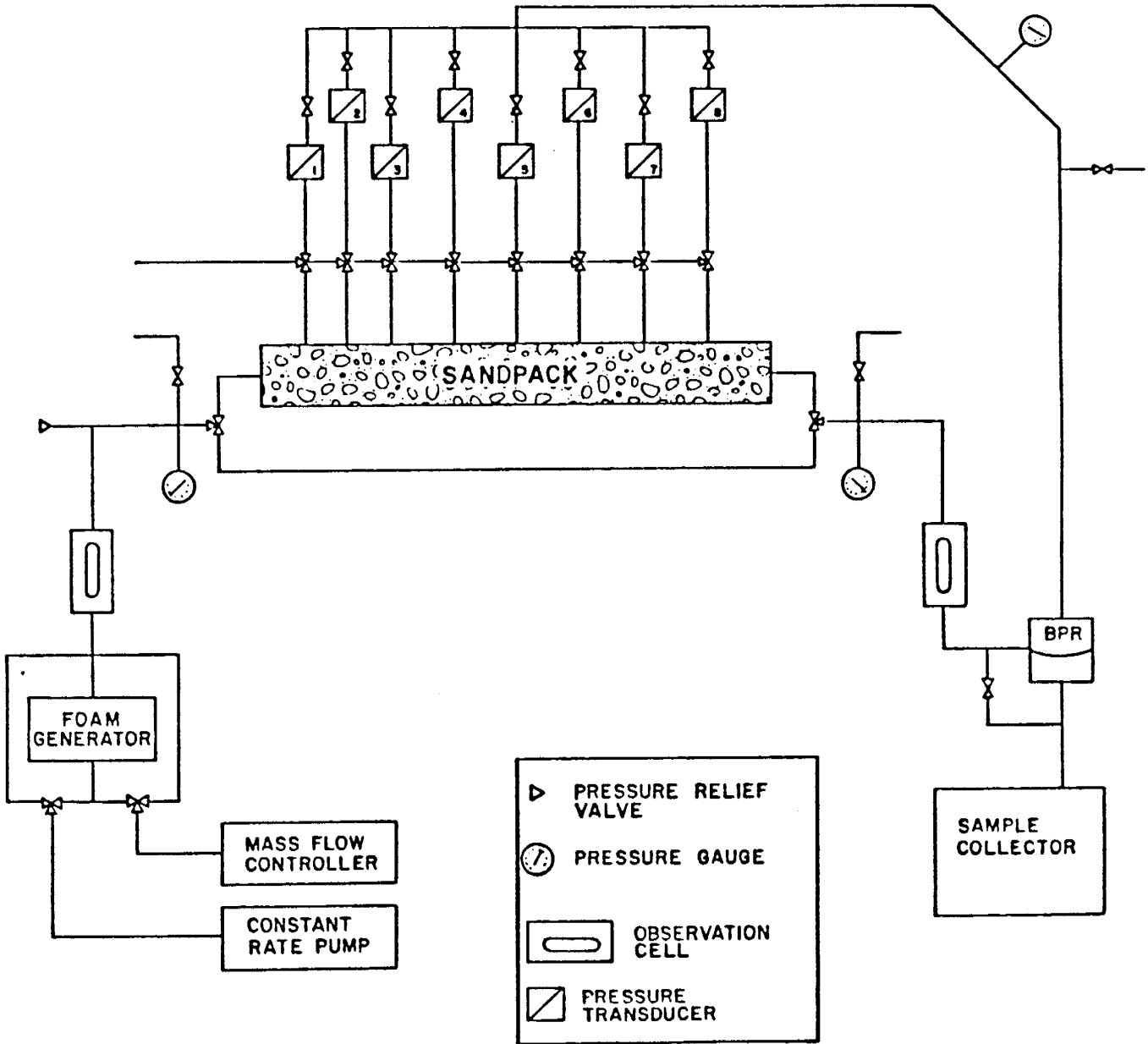


Figure 2. Detailed System Diagram.

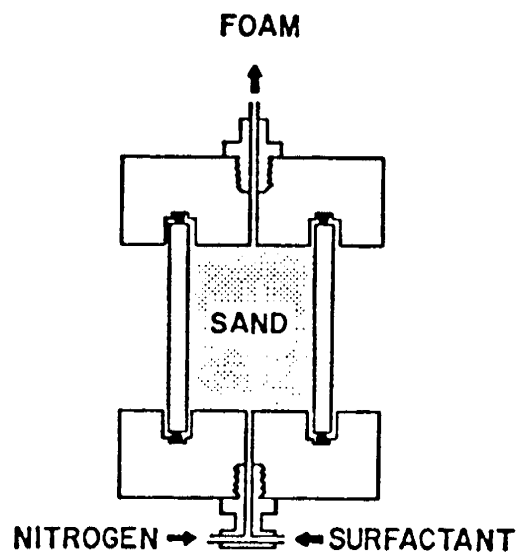


Figure 3. Foam Generator.

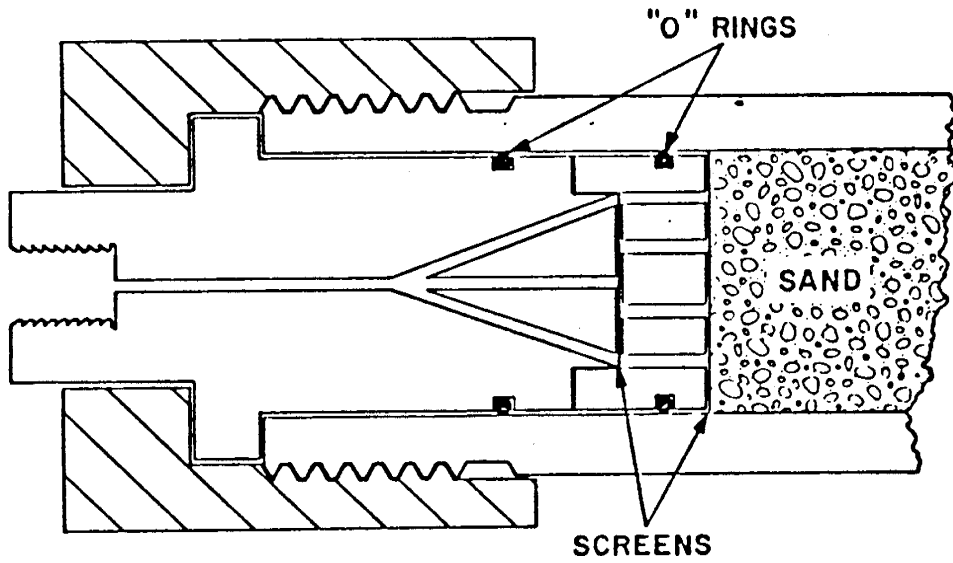


Figure 4. End Butt Design.

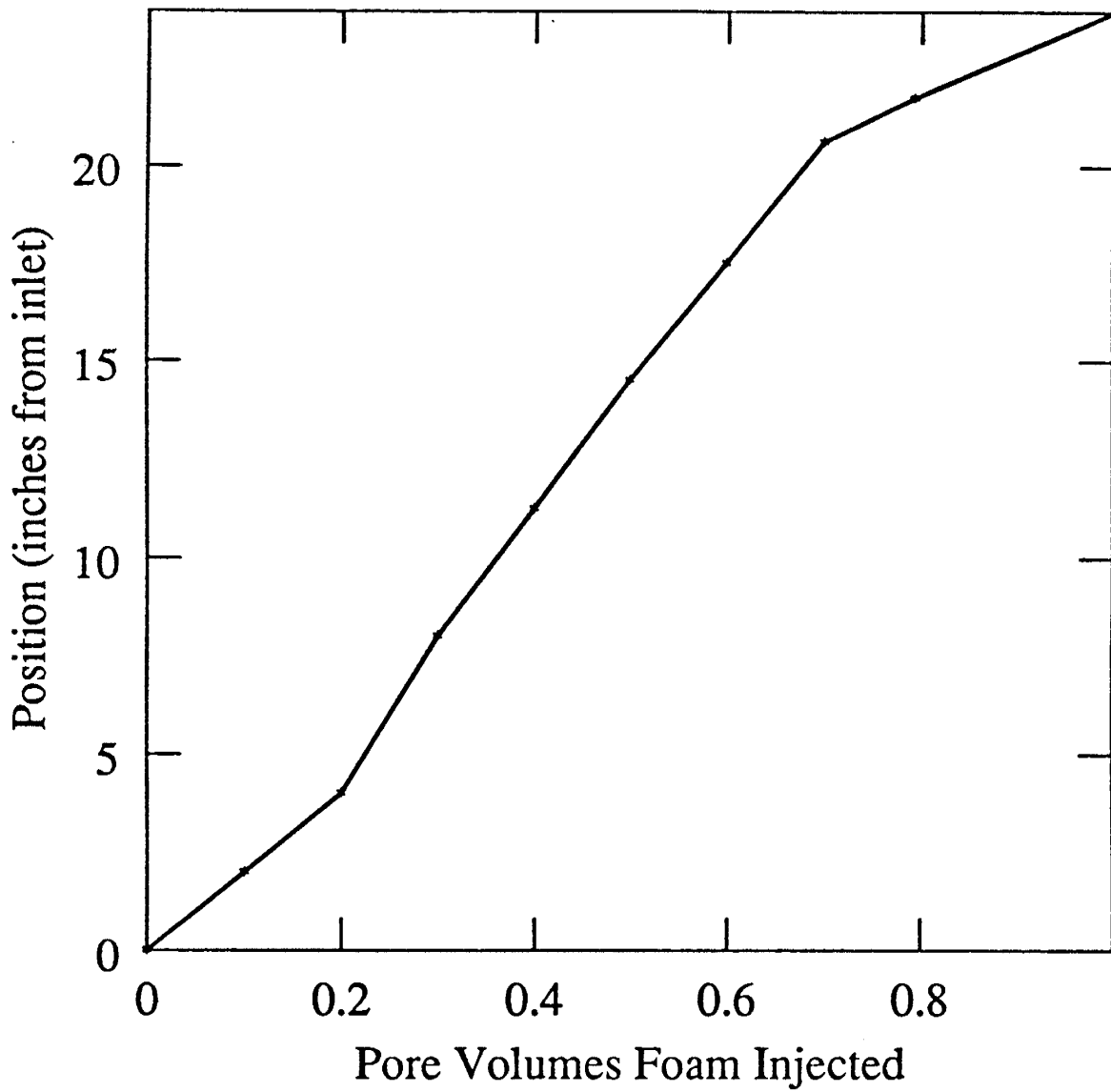


Figure 5. Observed Position of Foam Front

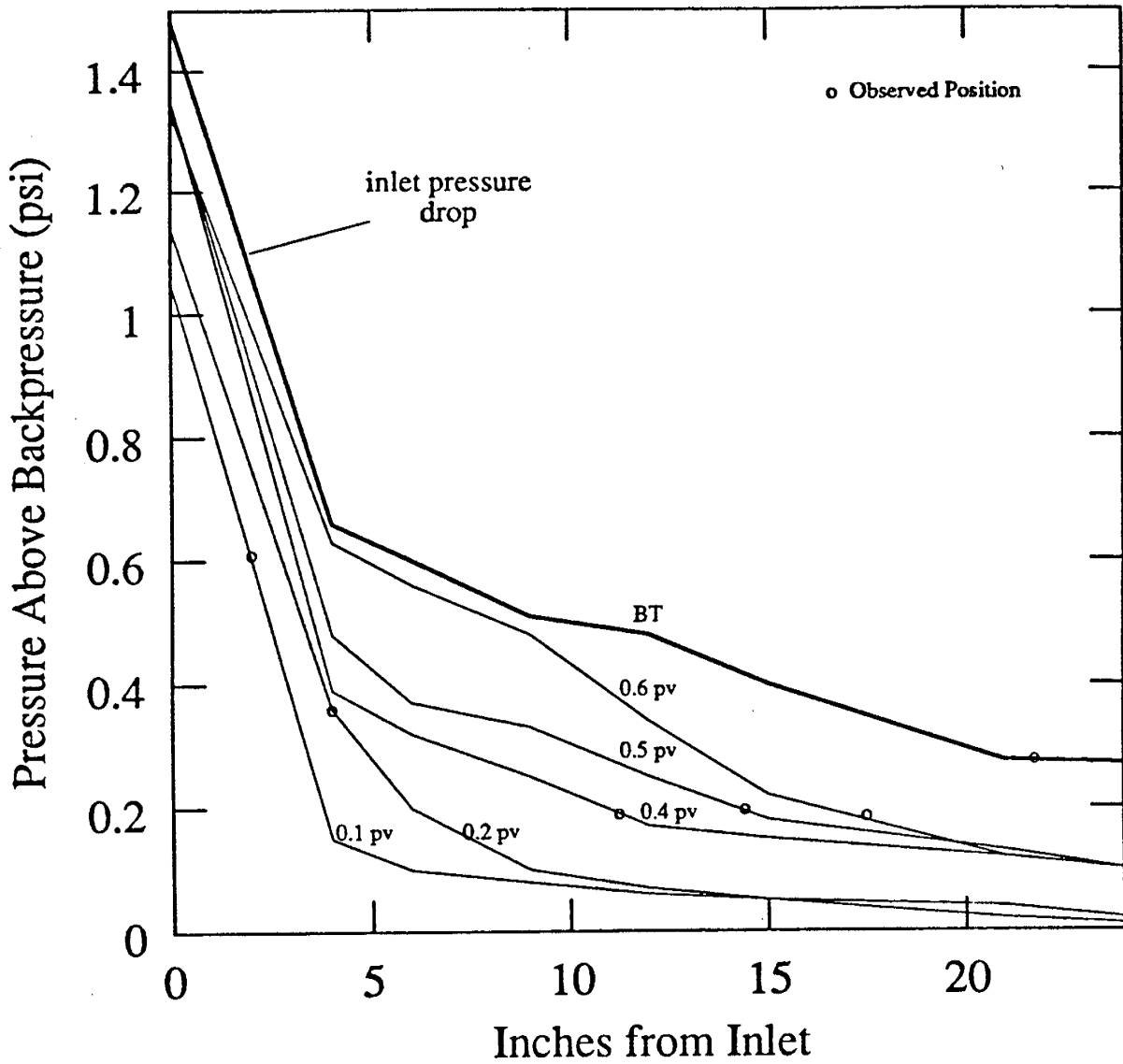


Figure 6. Foam Front Progression

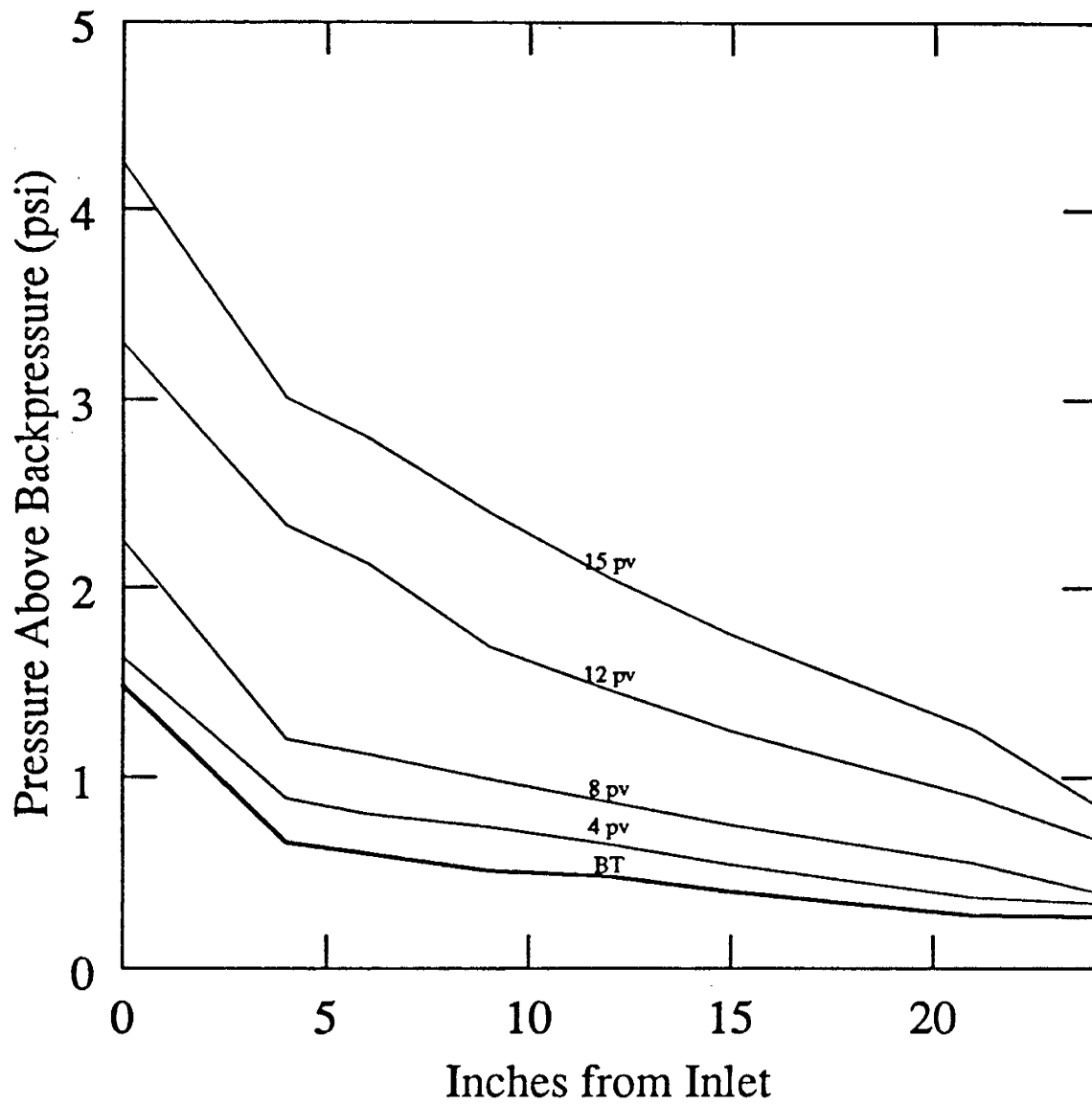


Figure 7. Pressure Profiles After Breakthrough

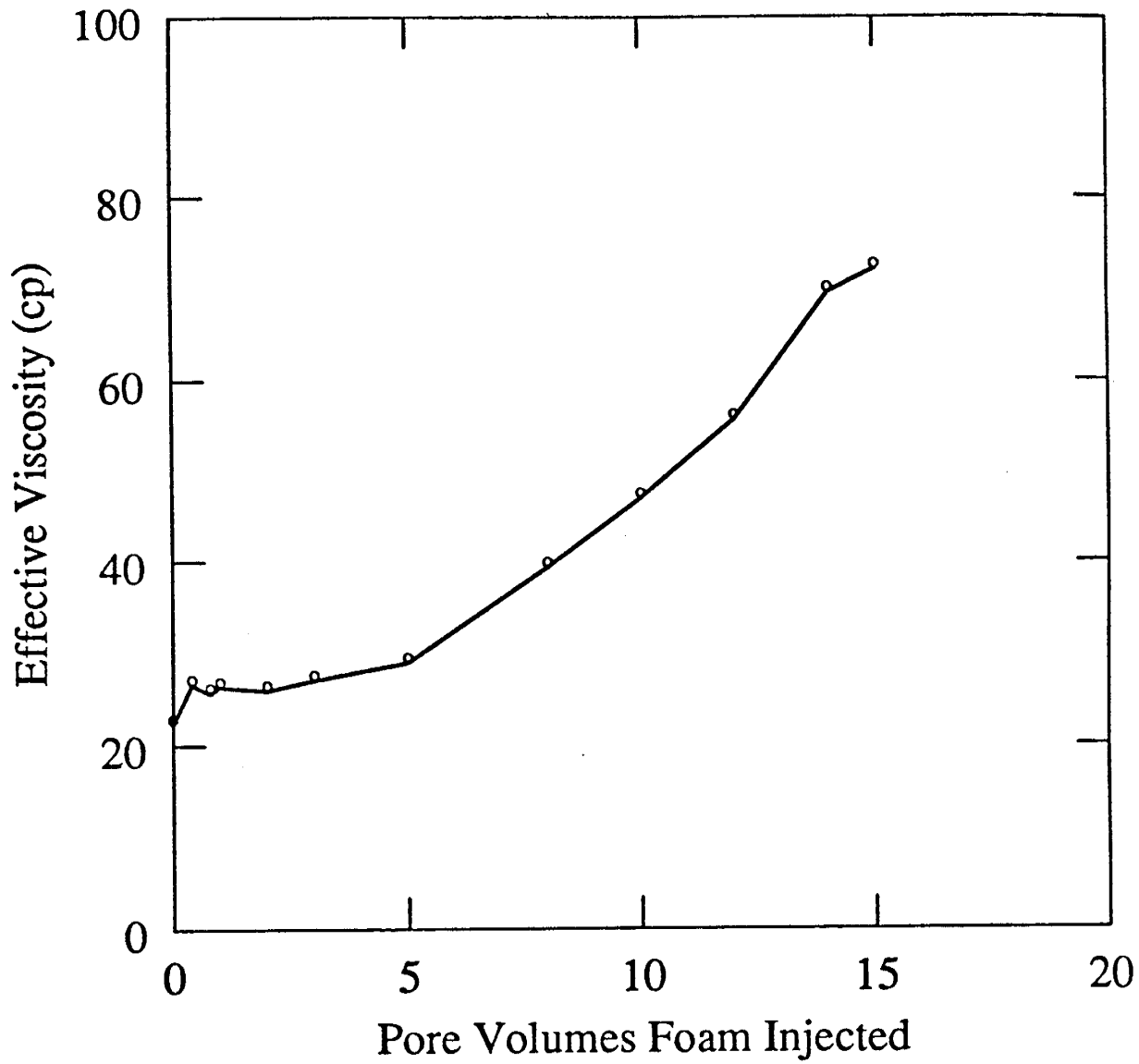


Figure 8. Effective Viscosity for Entire Sandpack

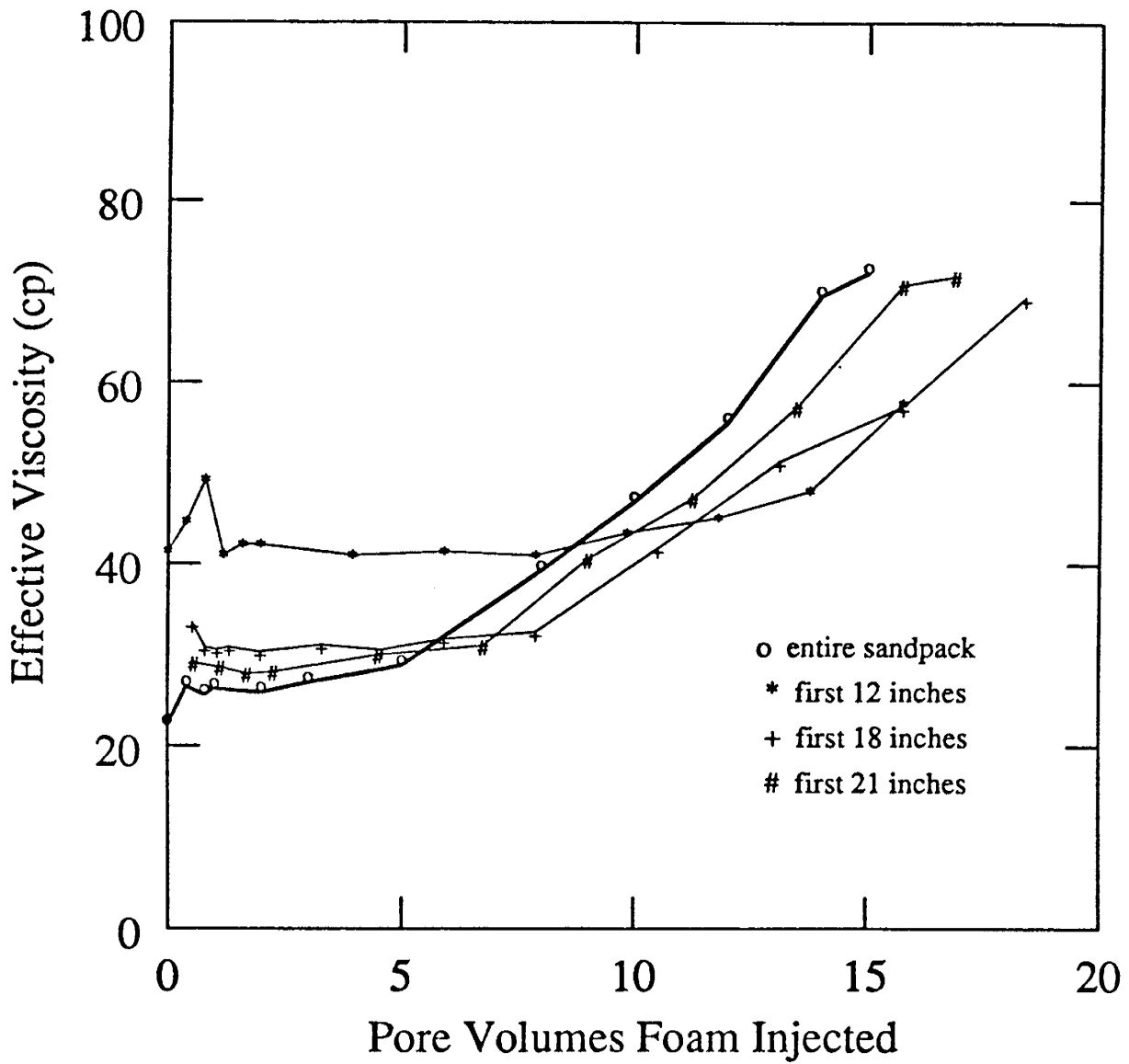


Figure 9. Comparison of Effective Viscosities

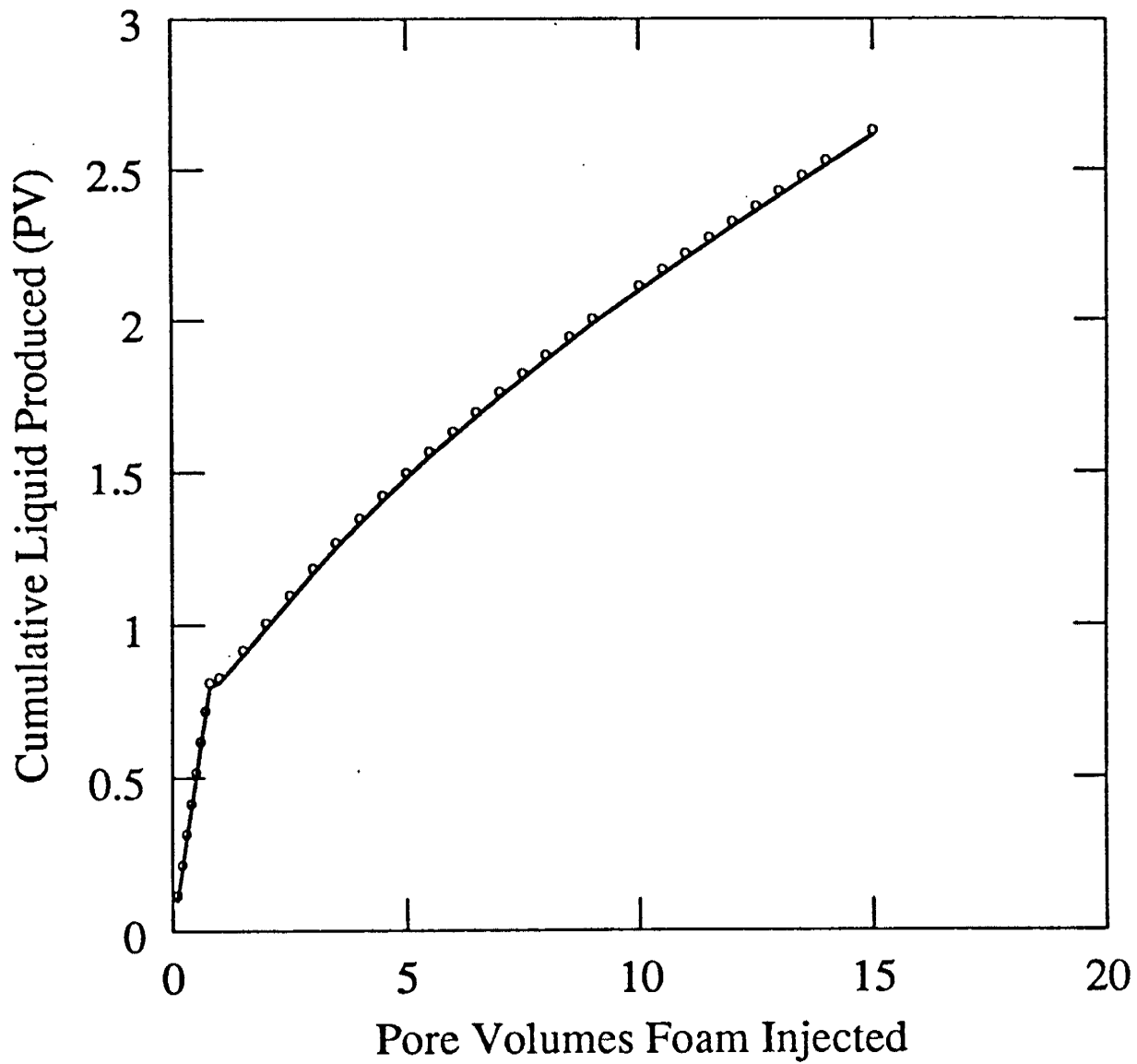


Figure 10. Cumulative Liquid Production

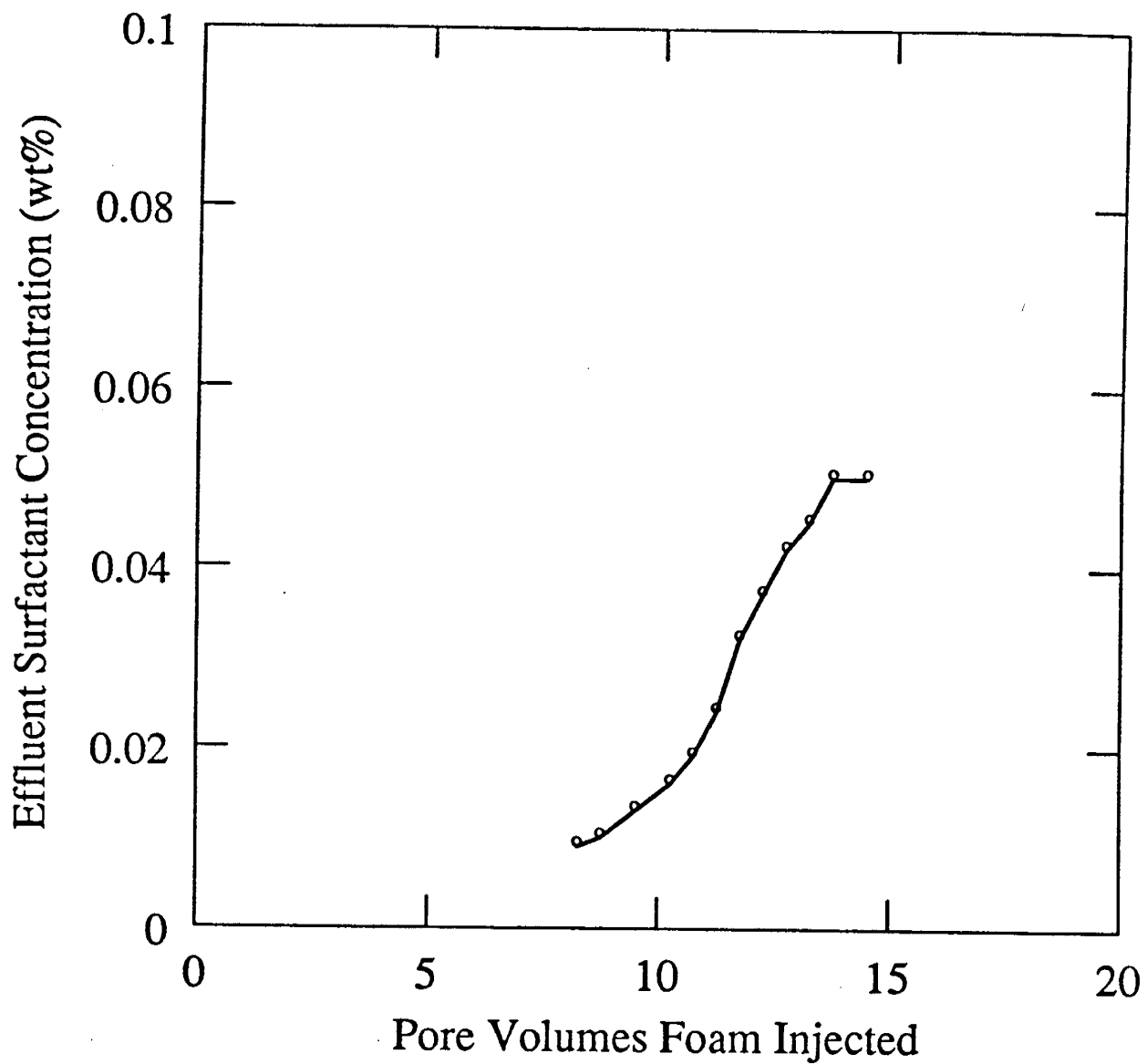


Figure 11. Produced Liquid Concentration

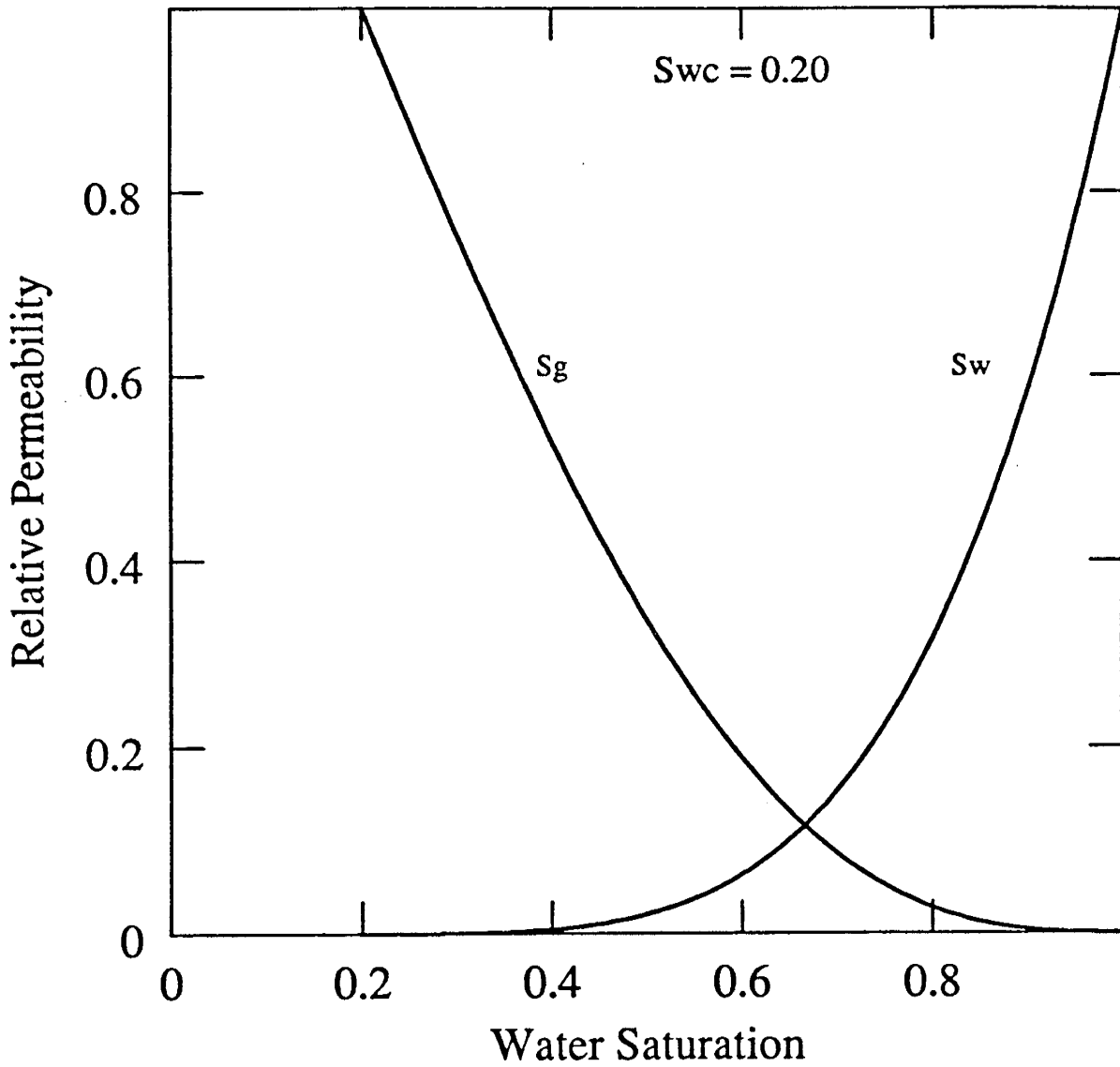


Figure 12. Corey Relative Permeabilities

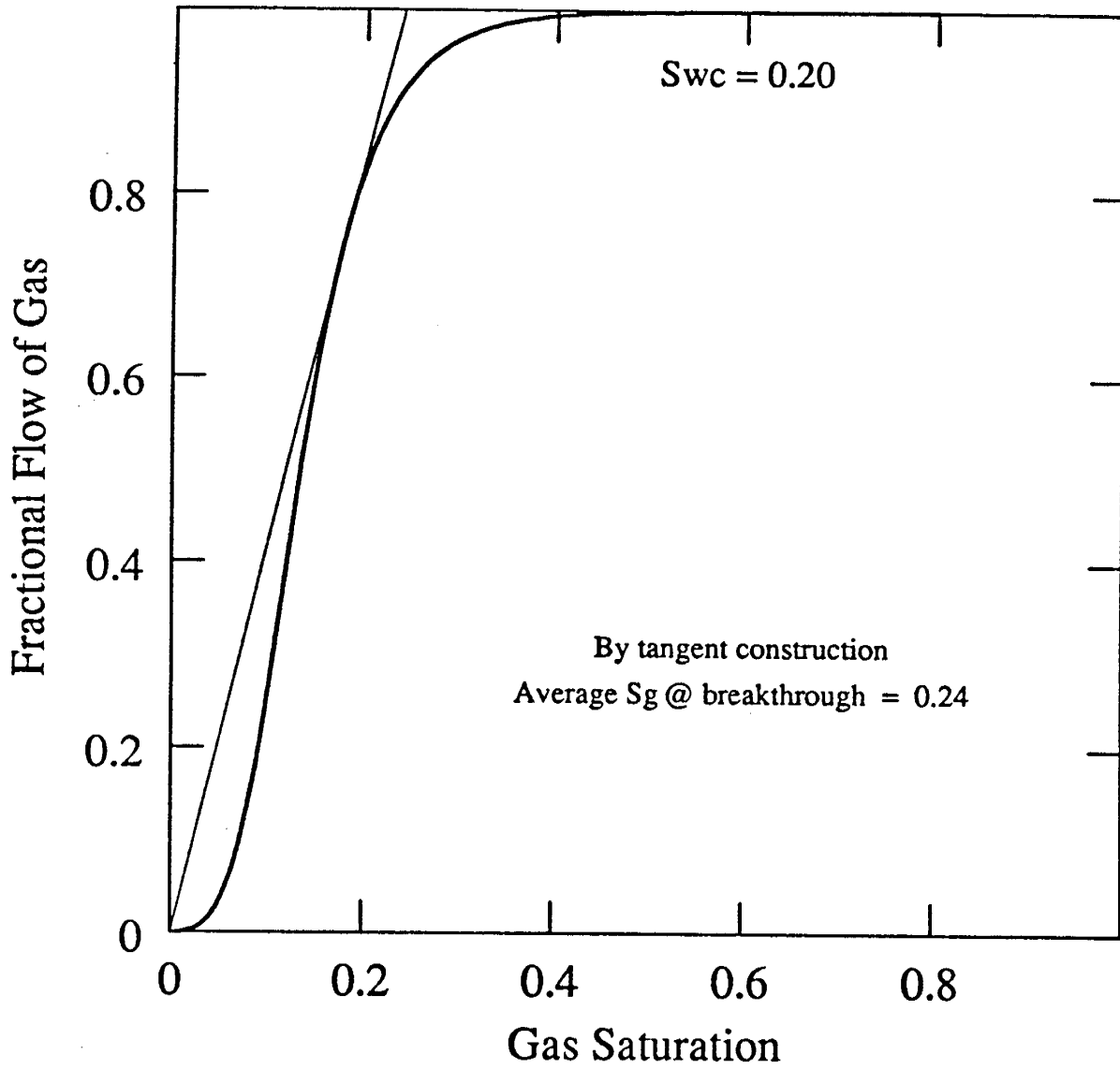


Figure 13. Fractional Flow Curve

APPARENT VISCOSITY MEASUREMENTS OF
SURFACTANT FOAM IN POROUS MEDIA

By
Richard J. Treinen
W. E. Brigham
L. M. Castanier

LIST OF TABLES

	<u>Page</u>
1. Back Pressure Effects on Foam Quality.....	6
2. Sand Pack Properties.....	8
A-1 Differential Pressure Data	25
A-2 Normalized Pressure Data	27
A-3 Apparent Viscosity Data	29
A-4 Permeability Effects on Apparent Viscosity	30
A-5 Surfactant Concentration Effects on Apparent Viscosity	31
A-6 Flow Velocity Effects on Apparent Viscosity	32
A-7 Flow History Effects on Apparent Viscosity	32
A-8 Surface Tension of Suntech IV	33

LIST OF FIGURES

	<u>Page</u>
1. Simple Flow Diagram	3
2. Apparatus Schematic	4
3. Foam Generator	4
4. End Butt Design.....	5
5. Back Pressure Regulator Modification.....	7
6. Foam Displacing Water/Surfactant	10
7. Effects of Foam Quality on Texture for Surfactant Concentrations from 0.05 to 0.3 wt%	12
8. Effects of Foam Quality on Texture at a Surfactant Concentration of 0.01 wt%.....	13
9. Permeability Effects on the Apparent Viscosity of Foam at a Velocity of 2.8 ft/D and Surfactant Concentration of 0.05 wt%.....	14
10. Surfactant Concentration Effects on Apparent Viscosity of Foam for a Quality of 70% at a Velocity of 2.8 ft/D.....	16
11. Quality and Surfactant Concentration Effects on Apparent Viscosity of Foam at a Velocity of 2.8 ft/D	16
12. Surface Tension of Suntech IV.....	17
13. Apparent Viscosity and Foam Quality Relationship at a Velocity of 2.8 ft/D for Surfactant Concentrations from 0.05 to 0.03 wt%.....	17
14. Flow Velocity Effects on Apparent Viscosity at a Foam Quality of 90% and a Surfactant Concentration of 0.05 wt%	18
15. Flow History Effects on Apparent Viscosity for a Surfactant Concentration of 0.05 wt%.....	18

TABLE OF CONTENTS

	<u>Page</u>
LIST OF TABLES	iii
LIST OF FIGURES	iii
ACKNOWLEDGEMENTS	iii
ABSTRACT	iv
1. INTRODUCTION	1
2. EXPERIMENTAL EQUIPMENT	3
3. PROCEDURE	8
4. OBSERVATIONS OF FOAM FLOW	10
5. APPARENT VISCOSITY MEASUREMENTS	14
6. CONCLUSIONS	20
7. RECOMMENDATIONS FOR COMPLEMENTARY WORK	21
8. REFERENCES	22
APPENDIX	24

ABSTRACT

The apparent viscosity of surfactant foam in a sand pack model was measured at reservoir flow velocities. The effects of foam quality, surfactant concentration, and flow rate were investigated.

Ottawa sand, 120 to 140-mesh, was packed into a 1 by 24 inch tube. Porosity was 38%, and permeability ranged from 5 to 8 darcies. Foam of a known quality and flow rate was continuously injected into the sand pack until a steady state condition was reached. Pressure drop was measured across three different segments of the sand pack. A system back pressure of 50 psig was applied to minimize changing foam quality caused by gas expansion. The surfactant used in this study was Suntech IV. All measurements were made at room temperature.

Results show that the apparent viscosity of surfactant foam ranges from 50 to 70 centipoise at reservoir flow velocities. Increasing the foam quality corresponded to a small increase in the apparent viscosity of foam. Changes in surfactant concentration from 0.005 to 0.05 wt% caused a rapid increase in apparent viscosity. Changes in concentration above 0.05 wt% had little effect on apparent viscosity. Increasing the flow rate resulted in a reduction of the apparent viscosity of foam. This pseudo-plastic flow behavior has been widely reported in the literature. The apparent viscosity of foam in porous media was significantly effected by flow rate history.

1. INTRODUCTION

In 1958 Bond and Holbrook proposed that a mixture of gas and surfactant solution could be used as an oil recovery agent. Since that time surfactant foams have been applied in many areas of the petroleum industry. In steam injection pilot studies, improved recovery of oil with surfactant foams have been reported by Doscher and Kuuskraa (1982), Dilgren (1982), Strom and Brigham (1984), and Ploeg and Duerksen (1985). Applications of surfactant foams as a sealant in gas storage reservoirs have been reported by O'Brien (1967), Bernard (1967), Holm (1968), and Albrecht and Marsden (1970). Foam has also been applied in drilling, well bore clean up, and well stimulation.

An important property of foam is its viscous behavior in porous media. Sibre (1943) was probably the first to note the markedly greater viscosity of foam in comparison to its gaseous and liquid components. The mechanism responsible for the viscous behavior of foam is not completely understood.

Several authors have proposed mechanisms or observed flow patterns pertinent to the viscous behavior of foam in porous media. Fried (1961) proposed that foam moves through pore spaces as a body. Raza and Marsden (1965) reported pseudo plastic behavior for foam flow in capillary tubes. Holm (1968) suggested that different flow patterns exist for gas and surfactant solution. Holm proposed that gas flows as a discontinuous medium separated by liquid lamella. The lamella could break and reform as gas passes through pore channels. Separate fixed channels allow independent liquid flow. Holm also claimed that the contribution to the liquid flow in the form of lamella was negligible in comparison to that of the liquid channels. Hirasaki and Lawson (1983) concluded that the viscous behavior was the result of three phenomenon; liquid slug flow between bubbles, bubble deformation at pore constrictions, and surface tension gradients near gas liquid interfaces.

In the literature the viscous behavior of foam has been reported in many ways. Bernard and Holm presented the effects of foam in porous media as fractional permeabilities for gas (1964) and water (1965). Marsden and Kahn (1966) reported ratios of effective permeability to apparent viscosity as well as ratios of relative permeability to apparent viscosity. Minssieux (1974) used Darcy's law to calculate the apparent viscosity of foam in porous media. Dilgren *et al.* (1982) presented the results of foam flow experiments in terms of permeability reduction factors. Heller *et al.* (1982) reported mobility ratios and relative mobility ratios equivalent to the ratios of Marsden and Kahn (1966). In the same paper, Heller also compared the results from several papers and found general agreement if the data was expressed as relative mobility.

As it is not clear that any one method of representing the viscous behavior of foam is superior to the others, apparent viscosity has been chosen as the parameter to report the behavior of foam in this paper. This is not meant to imply that foam flows as a body through porous media, since it has been shown on a microscopic scale that the flow behavior of foam is quite complex. However, on a macroscopic scale bulk flow of foam may not be a bad assumption. Apparent viscosity has been chosen since the magnitude of the viscosity reflects the viscous behavior of foam in comparison to the gas and surfactant phases.

The magnitude of the viscous behavior of foam in porous media as reported in the literature covers a large range. Several papers reported apparent viscosity of foam in porous media or provided data from which apparent viscosity could be calculated. Aizad and Okadan (1977) reported values from 3 to 12 centipoise for one surfactant and 20 to 90 centipoise for a different surfactant. Ali *et al.* (1983) recorded differential pressures from which apparent viscosities of 3 to 7 centipoise could be calculated. Heller *et al.* (1982) summarized the results of several previous papers by reporting relative mobilities. The units of Heller's relative mobility is reciprocal centipoise. By inverting Heller's values, a range of 1.5 to 840 centipoise was obtained.

Previous work in the literature on foam flow in porous media had been conducted at flow velocities from 200 to 1500 feet per day. This range of flow velocities may be applicable near the well bore and in high permeability streaks; however, this range would not apply once mobility control or streak blockage has been attained, which is the desired effect of surfactant foam. The goal of this project was to measure the viscous behavior of surfactant foam at reservoir flow rates. The effects of foam quality, surfactant concentration, and flow rate were also studied.

2. EXPERIMENTAL EQUIPMENT

The simple diagram in Fig. 1 illustrates the method used to measure the apparent viscosity of foam in porous media. Foam of a known quality and flow rate was generated from nitrogen and surfactant solution passing through a foam generator. The foam was then passed through a sand pack of known permeability. After a period of time needed to reach steady state conditions, the differential pressure across the sand pack was recorded. The apparent viscosity was then calculated using Darcy's law.

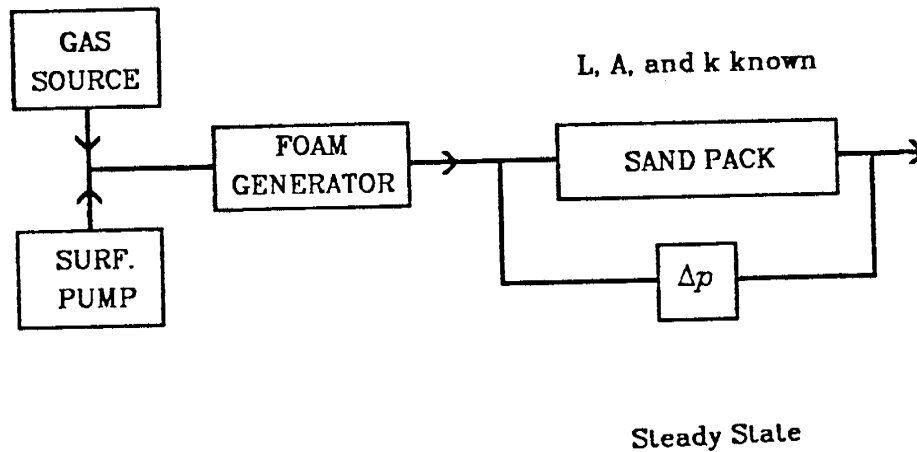


Fig. 1. Simple Flow Diagram

The equipment used in this study is more complex than that of the simple diagram. Figure 2 is a schematic of the actual equipment used in this study. The components were chosen to achieve two design criteria, flow velocities on the order of 1 ft./day and one dimensional flow of foam.

A Matheson model 8240 mass flow controller was used to regulate the flow of nitrogen. The surfactant flow was controlled using a Constametric model 3G liquid chromatography pump. The two phases were introduced into a foam generator (Fig. 3). The foam generator is actually a short sand pack, 1 inch in diameter and 3 inches in length, packed with 120-140 mesh Ottawa sand. As the two phases percolate through the sand a uniform foam is produced. By precise regulation of the nitrogen and surfactant flow rates, foam of a desired quality and flow rate can be produced.

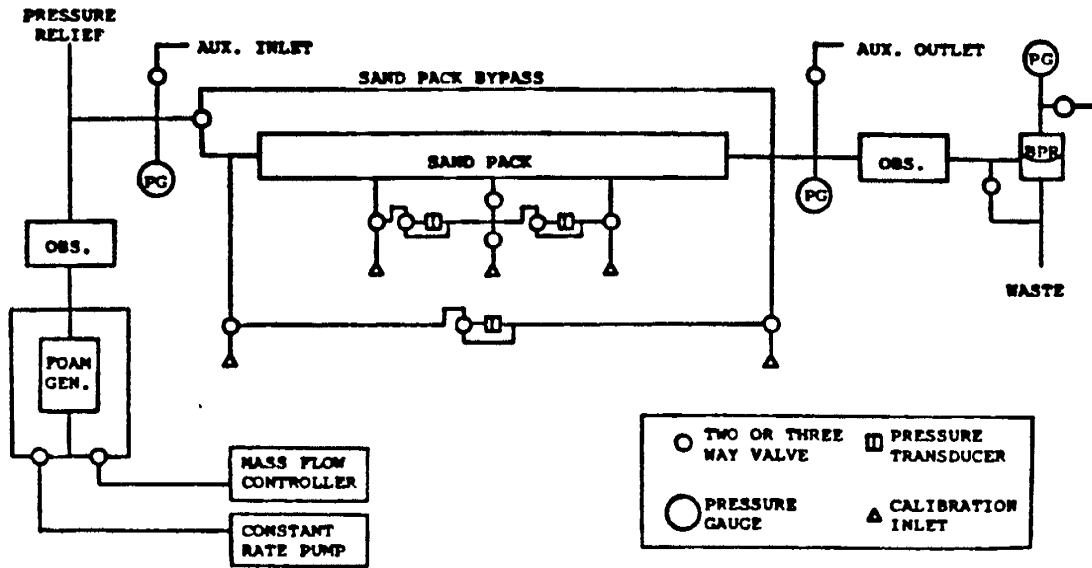


Fig. 2. Apparatus Schematic

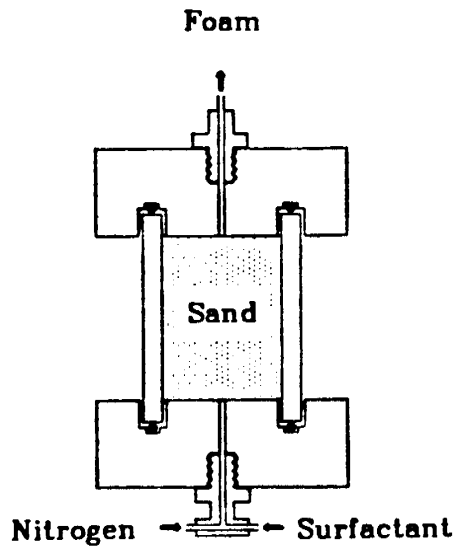


Fig. 3. Foam Generator

The produced foam then flows through an observation cell, where the texture of the foam can be observed and photographically recorded. The observation cell was constructed by sandwiching a thin Teflon template between two thick acrylic plastic plates. The separation between the plates was fixed by the thickness of the Teflon template. By trial and error a thickness of 0.01 inches was found to be suitable for the observation of foam.

The dimensions of the sand pack were chosen to be 1 inch in diameter and 24 inches in length. Based on the minimum controlled flow rate available from the surfactant pump, which was the limiting factor, 1 inch was found to be the smallest workable diameter. This diameter allowed a flow velocity of 2.8 ft/day at a quality of 90%. It was initially felt that surfactant flow rates could be achieved to produce a 95% quality foam, however this was found not to be possible. Based on expected apparent viscosities, the 24 inch length was picked to produce measurable pressure drops. End butts were designed to promote one dimensional flow at the sand pack ends (Fig. 4). The tube used for the sand pack was made of acrylic plastic, allowing observation of foam movement in the sand pack.

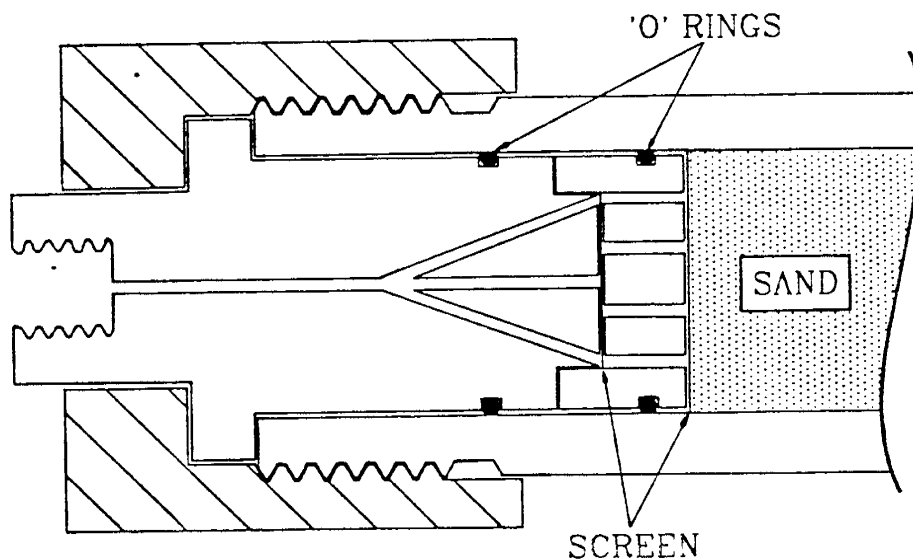


Fig. 4. End Butt Design

The sand used in the sand pack was 120-140 acid and base washed Ottawa sand. This was the same sand that was used in the foam generator. Stainless steel screen of 200 mesh was placed at the inlet and outlet to prevent sand migration. Pressure tap fittings in the sand pack wall were stuffed with glass wool to serve this same purpose.

Pressure measurement was achieved with three differential pressure transducers placed across different segments of the sand pack. One transducer recorded the pressure drop across the entire sand pack. The other two transducers were used to record differential pressures across six inch sections comprizing the second and third quarters of the sand pack. The response from the transducers was continuously recorded on a triple pen strip chart recorder. Sporadic trouble was encountered with one and occasionally both of the inner sand pack transducers. For some reason which has not been completely resolved, the differential pressure across these transducers sometimes became locked at some low value. The only method found to relieve this problem has been by the removal of the sand pack. For this reason it is suspected that the cause of the problem occurs at the pressure tap connection to the sand pack. A possible source of this problem could be the dense wad of glass wool stuffed into the sand pack wall fittings. The glass wool prevents migration of sand into the pressure tap lines. If this glass wool becomes impregnated with foam the transmission of pressure to the transducers may be impaired. In the experiments where the transducers responded normally, average pressure drops were calculated from normalized differential pressures. This data is presented in the appendix of this report. In a significant number of experiments the values obtained from the differential transducers showed substantial variation. The pattern of variation was fairly constant throughout experiments in each sand pack. This variation could be caused by either inaccurate transducer calibration or stable heterogeneous flow behavior of foam. In summary consistent data from all three pressure transducers at once was difficult to obtain and judgement was necessary in the analysis of the differential pressure data.

A second observation cell, identical to that described previously, was used to view the texture of the foam after passing through the sand pack.

Elevated system pressures were found to be necessary to minimize the change in foam quality due to the expansion of gas. The importance of high system pressures is shown in Table 1. This table shows the variation in foam quality

TABLE 1. BACK PRESSURE EFFECTS ON FOAM QUALITY VARIATION

Back Pressure	Atmospheric			50 psig		
	Inlet	Midpoint	Outlet	Inlet	Midpoint	Outlet
Pressure (psia)	18.3	16.5	14.7	68.3	66.5	64.7
Quality (%)	67.8	70.0	72.4	69.4	70.0	70.6

for a system with an outlet pressure at atmospheric pressure and also at 50 psig. This data has been calculated using Boyle's law for the ideal expansion of gas. The flow rates of nitrogen and surfactant are set to produce a target quality of 70% at the sand pack midpoint. The pressure drop of 3.6 psi is typical of the data recorded in this study. For the system operated at atmospheric pressure,

the foam quality departs from the target quality by more than 2 percentage units. However by applying 50 psig of backpressure, this departure from the desired quality has been reduced to less than 1%. Thus by using 50 psig of back pressure, the quality of foam throughout the sand pack can be kept reasonably constant. A back pressure of 50 psig was used in all tests of this study.

Although the application of a back pressure regulator reduces changing quality problems, it also introduces fluctuating system pressures. For diaphragm type back pressure regulators, the rise and fall of the system pressure is directly related to the differential pressure required to open and close the diaphragm seal. In typical back pressure regulators this pressure oscillation is about 5 to 10 psi. When trying to measure differential pressures of 3 psi, this can be a major problem. Figure 5a shows a schematic of the back pressure regulator used in this study as initially received from the manufacturer. The diaphragm material is a 1/4 inch thick Teflon disk. To reduce the magnitude of the pressure fluctuation, the Teflon was replaced by a thin Neoprene gasket (Fig. 5b). To prevent extrusion of the gasket, a brass 'thumbtack like' pin was placed in the outlet port. The surface of the metal under the pin was also roughened to prevent the pin from sealing the outlet. With this modification, the back pressure regulator will open and close over a 1/4 psi pressure change.

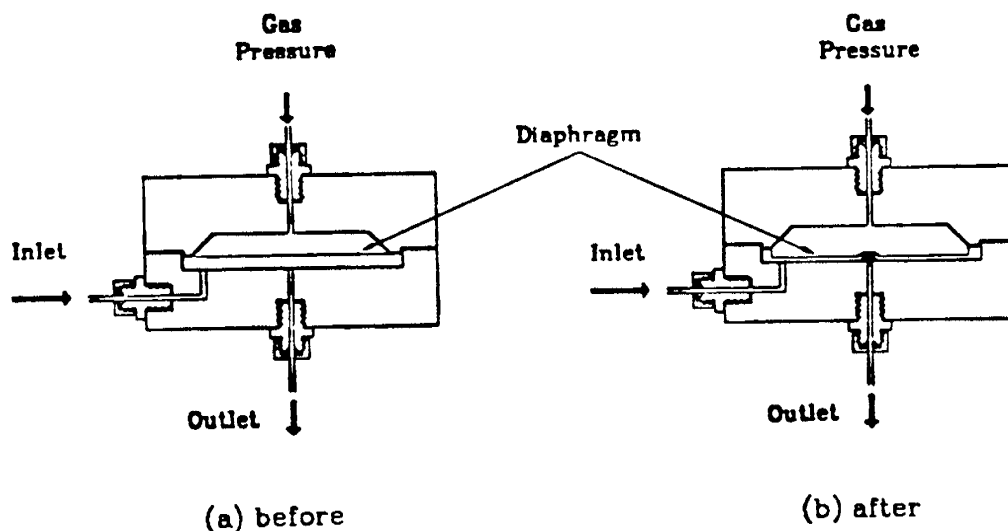


Fig. 5. Back Pressure Regulator Modification

Additional features of the apparatus include numerous valves for the preparation of the sand pack and calibration of pressure transducers. The system has been designed to operate at room temperature and pressures up to 125 psig. A resealing pressure relief valve has been preset to release at 125 psig. Pressure testing of components was conducted at 200 psig.

3. PROCEDURE

Experiments were conducted in four sand packs. Dry sand was packed into the tube while in a vertical position; vibration and air flow were used to promote close packing of sand grains. Air flow was obtained by attaching a vacuum line to the bottom of the tube. An estimate of the sand pack porosity was made from the weight of the sand and the volume of the tube. This calculation assumed a sand grain density of 2.65 g/cm³. Air permeability was measured using a water manometer and a bubble flow meter.

The sand packs were saturated with either water or surfactant solution. This was achieved by several cycles of evacuation and CO₂ flushes, and then a final evacuation and flush with the fluid of choice. Water permeability was measured with a water manometer and a graduated cylinder. A second estimate of porosity was obtained from the difference in weight between the dry and saturated sand pack. Although the measured air and water permeabilities agree to a reasonable extent, calculations using absolute permeability used the air permeability value since these values were measured with greater accuracy. Table 2 lists the recorded sand pack properties.

TABLE 2. SAND PACK PROPERTIES

Sand Pack	Length (cm)	Area (cm ²)	Φ_{dry} (%)	Φ_{wet} (%)	k_a (d)	k_w (d)
1	60.01	4.48	37.8	39.9	5.16	-
2	60.01	4.48	38.5	-	8.55	8.04
3	60.60	4.48	37.2	39.3	7.18	6.62
4	60.60	4.48	37.9	39.2	8.08	7.08

By precise regulation of nitrogen and surfactant flow rates, foam of a known quality and flow rate was injected into the sand pack. Foam quality was defined on a volumetric basis from the gas and surfactant phases.

$$\text{Quality, } \Gamma = \frac{\text{Gas Volume}}{\text{Gas Volume} + \text{Surfactant Solution Volume}} \quad (1)$$

The flow rate of foam was calculated at the sand pack midpoint and is simply the sum of the gas and surfactant solution rates.

$$\text{Volumetric Flow Rate, } q = q_s + q_g \quad (2)$$

Since gas is highly compressible, the gas flow rate at the midpoint must be calculated using Boyle's law for the ideal expansion of gas.

$$q_g = \frac{14.7 q_{g_{sc}}}{14.7 + \frac{\Delta p}{2} + \text{Back Pressure (psig)}} \quad (3)$$

The surfactant solution was treated as an incompressible phase. The flow velocity reported in this study was calculated from the volumetric flow rate and the sand pack properties,

$$\text{Flow Velocity, } q_{1d} = \frac{q}{A \phi} \quad (4)$$

where A is the cross sectional area and ϕ is the porosity.

Depending upon the foam quality, flow rate, surfactant concentration, and the initial conditions, a variable period of time was required to reach steady state flow in the sand pack. In the first experiments low surfactant concentration foam displaced water. In this case adsorption of surfactant on the sand grains combined with the slow rate of surfactant injection significantly increased the time required to achieve steady state flow. By starting with a surfactant saturated sand pack, adsorption of the surfactant from foam was eliminated and steady state was reached in a much shorter period of time.

Once steady state flow of foam through the sand pack was established, the differential pressure was recorded. The apparent viscosity of foam was calculated using Darcy's law.

$$\text{Apparent Viscosity, } \mu_a = \frac{k A \Delta p}{q L} \quad (5)$$

To produce a foam of a different quality and/or flow rate, the rates of nitrogen and surfactant were changed. This new foam displaced the previous foam. Steady state conditions under these new conditions were always attained when approximately one pore volume of new foam had been injected. Care was taken to maintain steady flow rates during foam quality or surfactant concentration changes since it was found that flow rate changes can significantly alter the viscous behavior of foam. Changes in surfactant concentrations were always made toward more concentrated solutions. This pattern was followed to avoid any irreversible adsorption characteristics of the surfactant.

The surfactant used in this study was Suntech IV from the Sun Petroleum Products Company. The surfactant is an anionic sulfonate manufactured from normal hydrocarbons ($C_{15} - C_{18}$) and toluene. The average molecular weight was 425 with a critical micellar concentration of 0.28 wt%.

4. OBSERVATIONS OF FOAM FLOW

The acrylic tube used for the sand pack allowed visual observation of foam displacing fluid. In the experiments where foam displaced water, two distinct fronts in the sand pack were observed, a sharp piston like foam front and a fingering gas front. The development of two fronts is the result of adsorption of surfactant on sand grains. As the quantity of surfactant in the fluid phase of the foam decreases below some minimum foaming concentration, gas is no longer held in the foam and can finger ahead into the water saturated region. This behavior is illustrated in Fig. 6a. The position of the foam front was evident, since a homogeneous foam filled sand was sharply separated from the region where both gas and water pockets could be observed. Incident to the position of the foam front, sharply increased differential pressures were observed. This pressure increase is believed to be a relative permeability effect separate from the viscous behavior of foam. Steady state conditions in the sand pack were reached at some time after the foam front traversed the length of the sand pack, indicating that surfactant adsorption was still continuing behind the front. Steady state was not achieved until approximately 10 pore volumes of foam had been injected into the sand pack.

In experiments where foam was injected into a surfactant saturated sand pack, steady state conditions were achieved after only 1.5 pore volumes of injection. By saturating the sand pack with surfactant solution, adsorption processes were complete before foam displacement. Foam fronts were not degraded by adsorption and piston-like displacement was observed in the sand pack as illustrated in Fig. 6b.

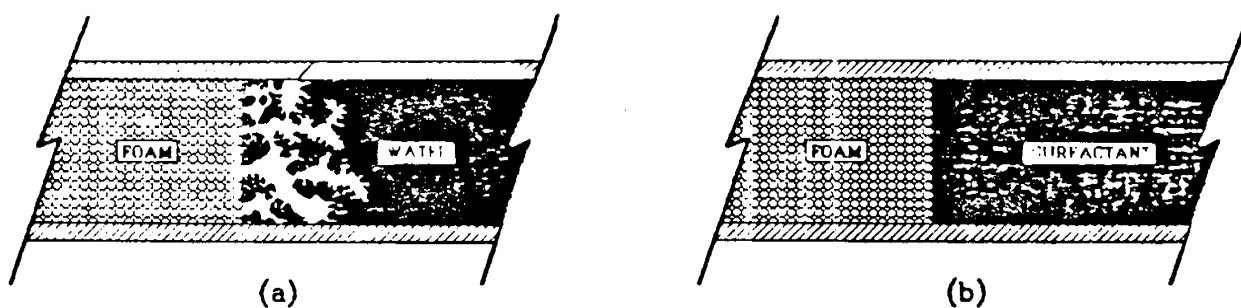


**Fig. 6. (a) Foam Displacing Water
(b) Foam Displacing Surfactant**

In experiments where foam displaced a foam of different quality and/or surfactant concentration, a discernable front could not be observed in the sand pack. In fact due to the small grain size of the sand used, movements of foam bubbles or lamella could not be observed. If only foam quality was changed

steady state was reached after one pore volume of injection. If the surfactant concentration was changed, three pore volumes of injection were usually required to achieve steady state.

Foam quality and surfactant concentration have significant effects on the texture of foam as observed in the observation cells. It must be noted that foam behavior in the observation cell may not reflect the true behavior in the porous media. For instance, the physical size of the bubbles in the observation cell are usually 10 to 15 times larger than the pore spaces of the sand pack. Nevertheless, an observed change in foam texture usually corresponded to changing apparent viscosity in the sand pack.

Considering the bubble size observed in the visual cells, one can speculate on the bubble size of surfactant foam in porous media. Since bubbles smaller than pore size were never seen in the visual cells, it appears certain that bubbles smaller than pore size do not occur in the porous media. As the gas exits the sand pack, lamella should form more often than they are broken. This pattern would generate bubbles that are smaller than the bubbles in the porous media. This observation is important, since it supports the theory that the viscous behavior of foam is caused by the breaking and reforming of lamella at pore throats. The fact that the bubble size observed was always greater than the pore size of the porous media precludes bulk movement of very small bubbles through the porous medium.

At high surfactant concentrations (0.05 to 0.3 wt%) foam texture was independent of concentration. Over this concentration range the following observations were made as foam quality increased (refer to Fig. 7). At a quality of 70% bubble size was uniform and approximately 0.010" in diameter. Bubble shape was approximately spherical. Increasing foam quality was marked first by distortion of bubble shape, a flattening of the surface where two bubbles touch. At 80% quality a small bubble was present in the nook between three bubbles. When quality reached 90% clusters of small bubbles were present along with groups of larger bubbles of up to 0.070" across. In the larger sizes, bubble walls were often shared between adjacent bubbles. As flow velocity increased, bubble size decreased for high surfactant concentration foam. Measurements of bubble size are not available since photographs, regrettably, were not taken of these experiments.

For low surfactant concentrations (0.005 and 0.01 wt%) increasing foam quality had dramatic effects on foam texture. At 70% quality the foam was not uniform. Bubble size ranged from approximately 0.025 to 0.002" in diameter. Bubble shape was spherical. As quality increased, bubble size and size distribution increased. Foam broke down into a free gas and a fluid with large distorted bubbles at 75% quality for the 0.005 wt% solution and at 85% wt% for the 0.01 wt% solution. Figure 8 illustrates the behavior of the 0.01 wt% surfactant foam. The obvious reason for this behavior is insufficient surfactant in solution for stable foam as the gas-liquid surface area increases and the volume of solution decreases, the result of increasing foam quality. Flow velocity experiments at low surfactant concentration were not made.

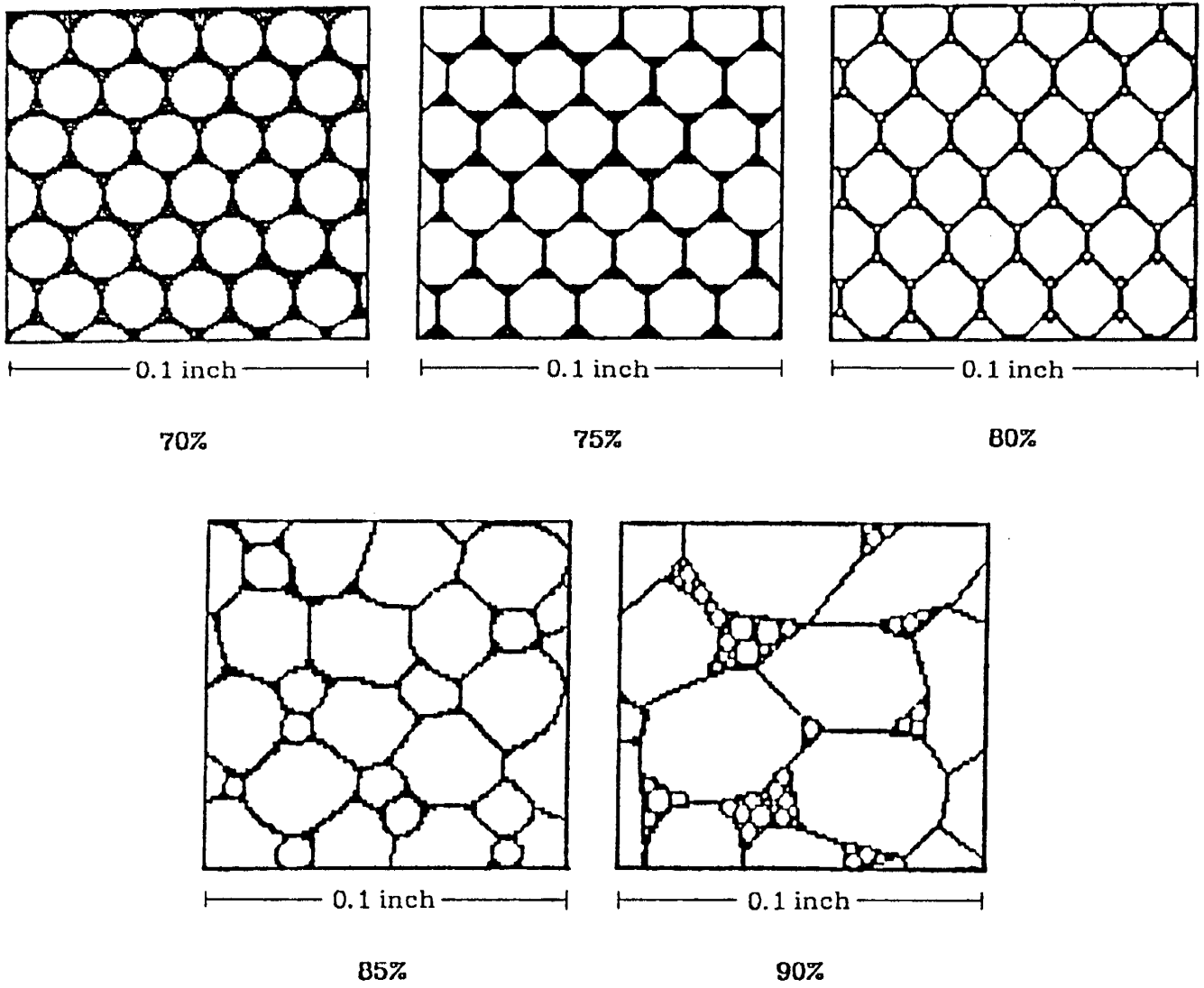


Fig. 7. Effects of Foam Quality on Texture for Surfactant Concentrations from 0.05 to 0.3 wt%.

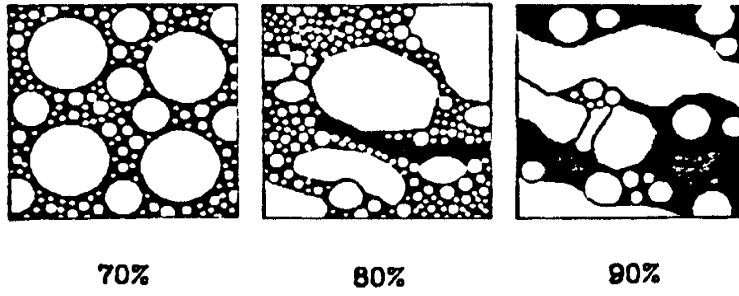


Fig. 8. Quality Effects on Texture in Low Surfactant Concentration Foam

5. APPARENT VISCOSITY MEASUREMENTS

Although the same sand and packing techniques were used in the preparation of all sand packs, a small distribution in the sand pack permeability was observed (see Table 2). To evaluate the effects of this permeability range on apparent viscosity the same experiment was conducted in three sand packs and the results were compared. Apparent viscosities were measured at a flow velocity of 2.8 ft/D using 0.05 wt% surfactant solution at foam qualities from 70 to 90%. The results are shown in Fig. 9. Note that the data from the 5.2 darcy sand pack lies between the data from the 7.4 and 8.6 darcy sand packs. Thus for this range in permeability the scatter in the data mask any effects of permeability on apparent viscosity.

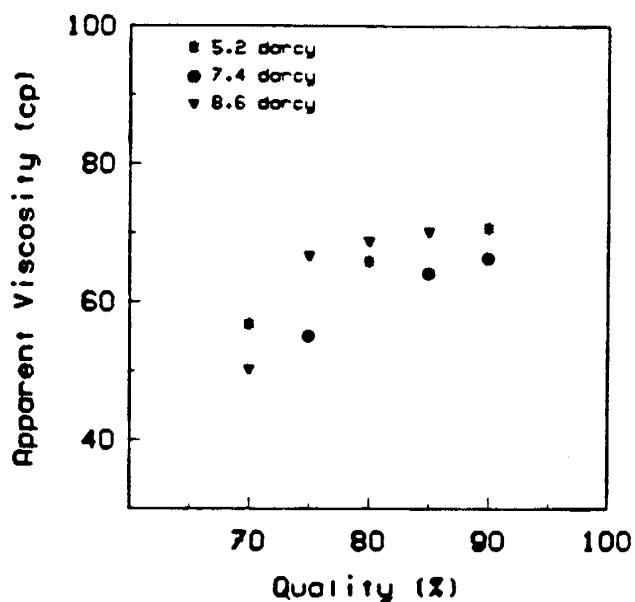


Fig. 9. Permeability Effects on the Apparent Viscosity of Foam

By the simplest of methods, merely shaking solutions of surfactant, the minimum foaming concentration of Suntech IV in water was found to be 0.005 wt%. Measurements of apparent viscosity were conducted on surfactant solutions varying in concentration from the minimum foaming concentration up to 0.3 wt%. The flow velocity for these experiments was 2.8 ft/D. The results for a foam quality of 70% are shown in Fig. 10. Initially the apparent viscosity increases rapidly with concentration, however the data indicate that at high concentrations apparent viscosity becomes independent of surfactant concentration. This is observed as a plateau in the data as concentration exceeds 0.05 wt%. The results of increasing foam quality on apparent viscosity are shown in Fig. 11. In this plot apparent viscosity is plotted against quality for surfactant concentrations from 0.005 to 0.3 wt%. Again the independence of apparent viscosity on concentration is observed at the concentrations of surfactant above 0.05 wt%. The data for the 0.01 wt% solution however shows an interesting behavior. At lower qualities apparent viscosity is significantly larger than the 0.005 wt% data, but at qualities greater than 80% the apparent viscosity for 0.01 wt% drops to that of the 0.005 wt% solution. This behavior corresponds with observations made in the visual cells. For this particular concentration free gas was observed when quality exceeded 85%. This drop in apparent viscosity with increasing quality could be caused by an insufficient surfactant concentration to maintain stable foam as quality increases.

Figure 12 shows the relationship between surface tension and the concentration of Suntech IV. The surfactant concentrations used in this study all lie in the region of the curve where the interfacial tension between gas and surfactant solution becomes independent of surfactant concentration. In particular the high surfactant concentrations, 0.05 to 0.3 wt%, are near the critical micellar concentration for Suntech IV which is 0.28 wt%. Since the formation of micelles places an upper limit on the surfactant available for the generation of foam, it follows that apparent viscosity would be expected to plateau as surfactant concentration approaches the critical micellar concentration.

Figure 13 shows the relationship found between apparent viscosity and foam quality. Four or more data points were used to calculate an average and standard deviation (error bars) at each quality. This data set combines all data collected for surfactant concentrations of 0.05 wt% and greater. The flow velocity for all data was 2.8 ft/D. From the graph, apparent viscosity increases slowly with foam quality. The shape of the curve is important, as the slope of the curve is nearly uniform throughout the quality range measured. This is quite different from the capillary tube data of Holbrook, Patton, and Hsu (1981) where the slope of the apparent viscosity curve increases dramatically over the same quality range. This difference suggests that the behavior of foam measured outside of porous media may have little bearing on behavior inside of porous media.

The data on the effects of flow velocity on apparent viscosity are shown in Fig. 14. Measurements were made with 90% quality foam at 0.05 wt% surfactant, at flow velocities ranging 2.8 to 28 ft/D. The data show the non-Newtonian behavior of foam reported by Raza and Marsden (1965). A one order magnitude increase in flow velocity resulted in a 50% reduction in the apparent viscosity of foam. The relationship between apparent viscosity and flow rate appears to be linear, however more data would be necessary to confirm this trend.

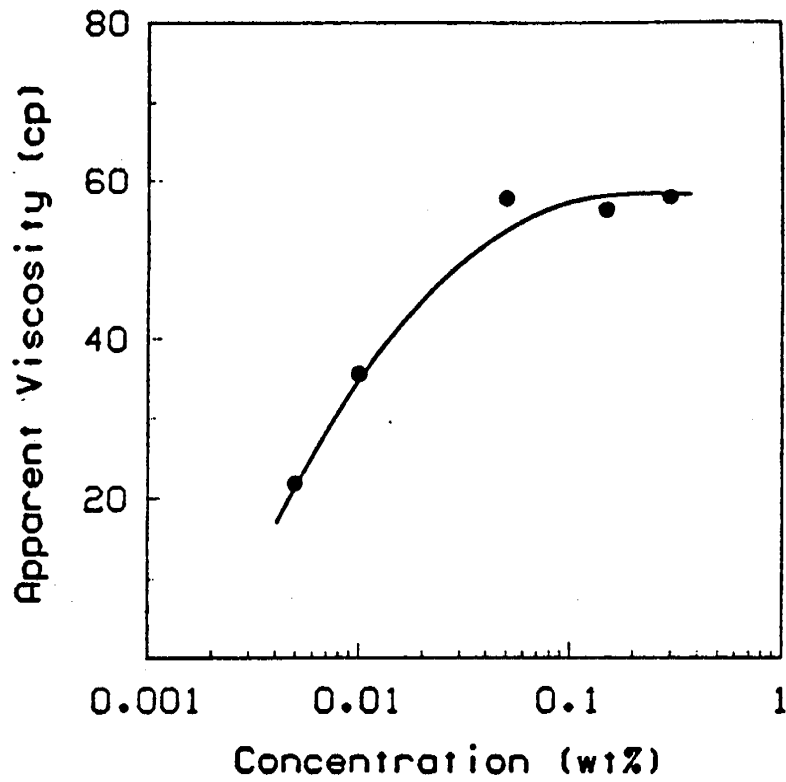


Fig. 10. Surfactant Concentration Effects on Apparent Viscosity of Foam

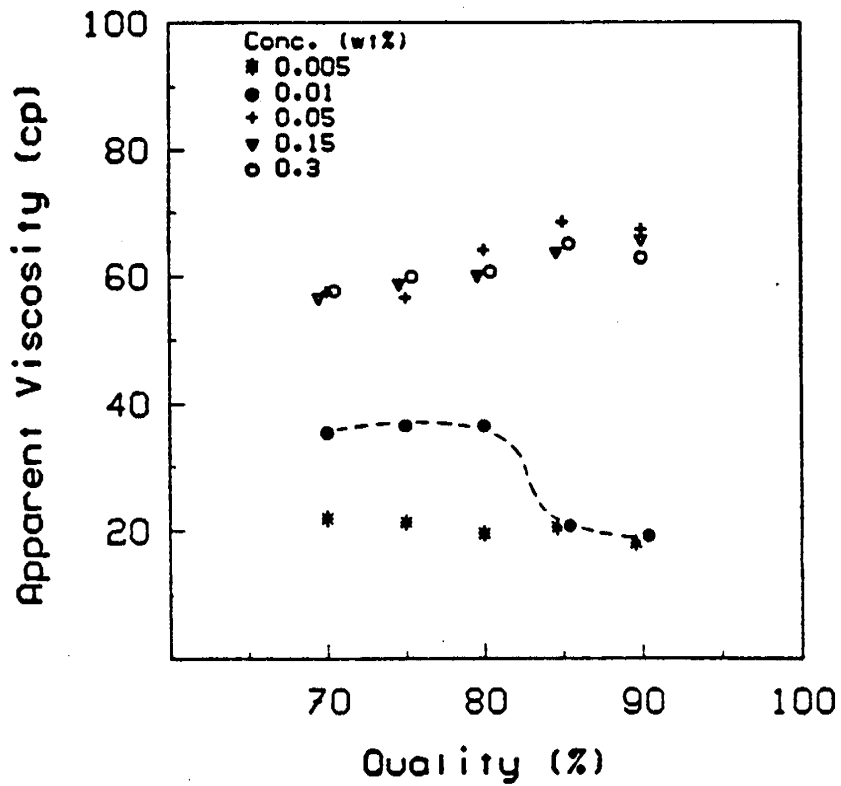


Fig. 11. Quality and Surfactant Concentration Effects on Apparent Viscosity of Foam

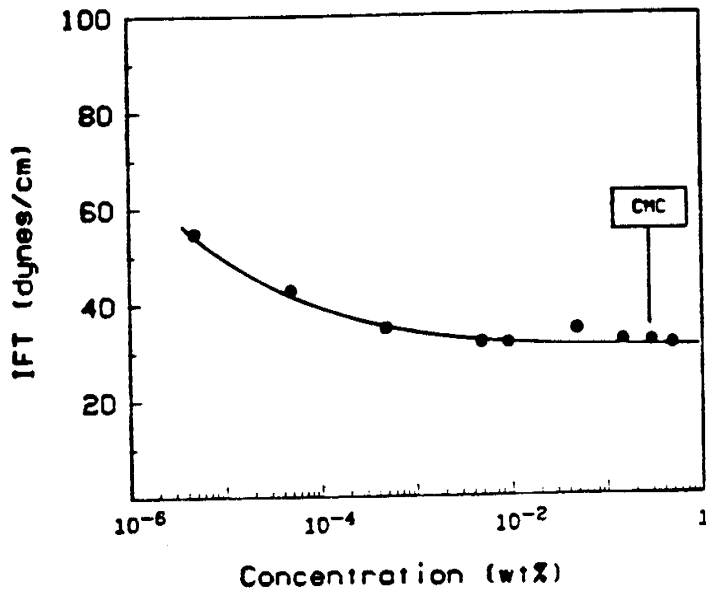


Fig. 12. Surface Tension of Suntech IV

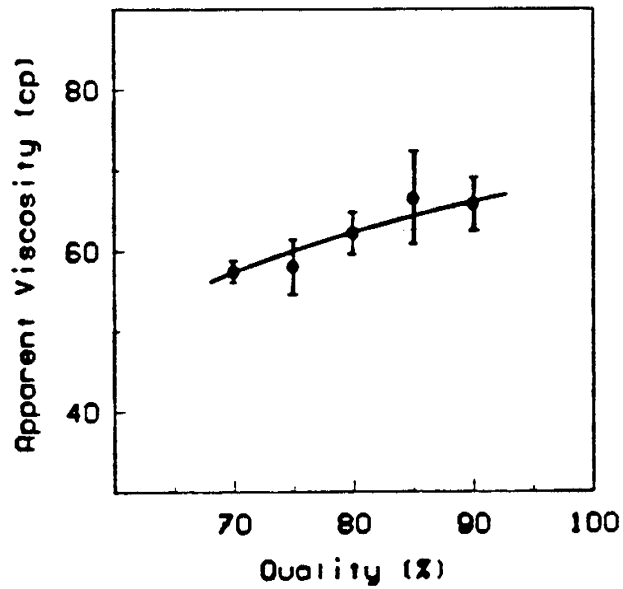


Fig. 13. Apparent Viscosity and Foam Quality Relationship

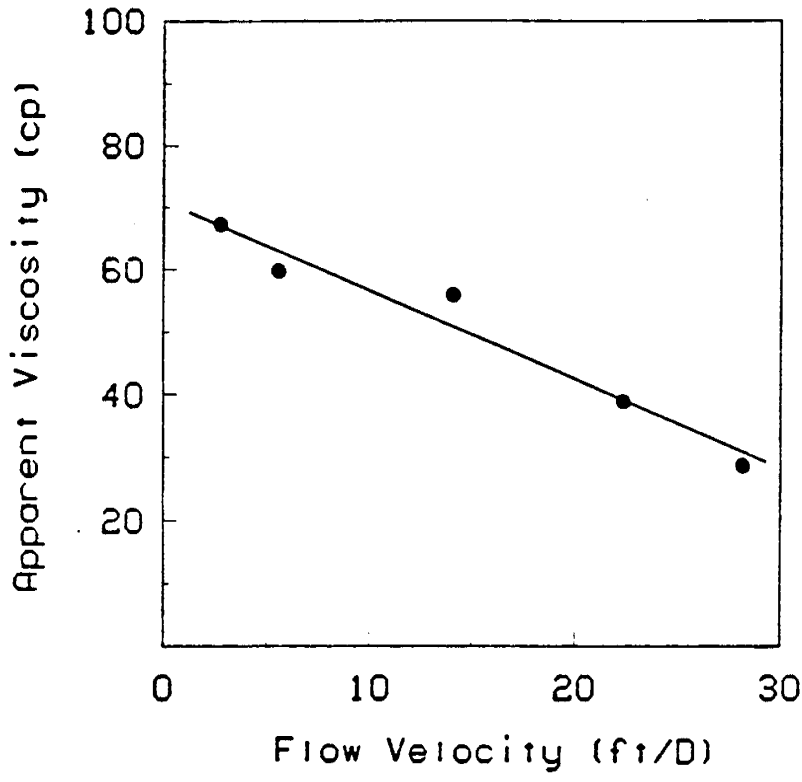


Fig. 14. Flow Velocity Effects on Apparent Viscosity

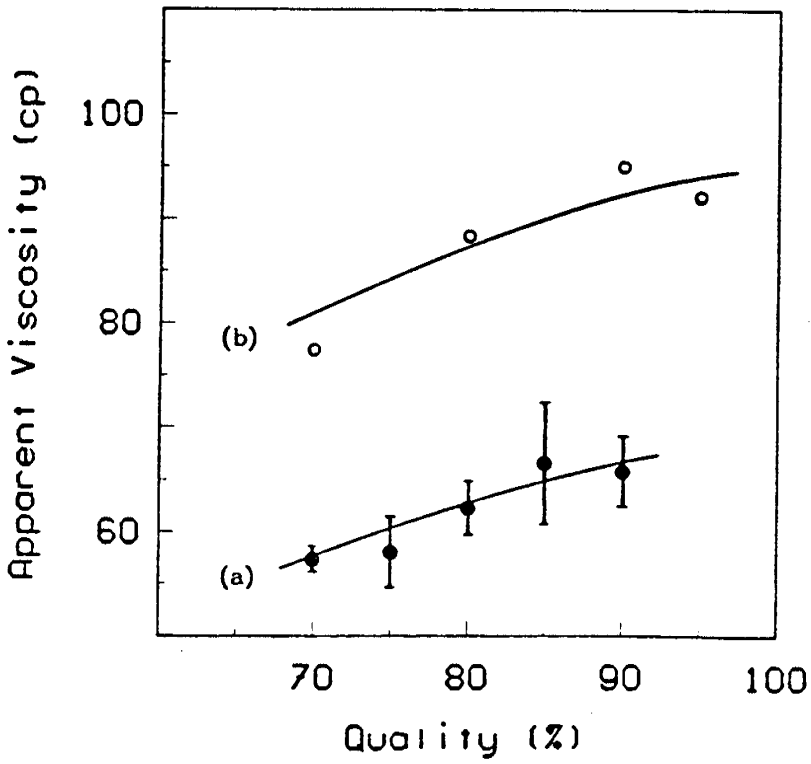


Fig. 15. Flow History Effects on Apparent Viscosity
 (a) 2.8 ft/D (b) 2.8 ft/D preceded by 28 ft/D

Figure 15 shows an effect of flow rate history on apparent viscosity. Apparent viscosity is graphed against foam quality. The data in the lower curve has been previously shown in Fig. 13, and represents the behavior of foam at a flow rate of 2.8 ft/D. The data in the upper curve were also collected at a flow rate of 2.8 ft/D, however this flow velocity was preceded by a flow velocity of 28 ft/D. The mechanism causing the flow rate history effect is not known, nor have any reasonable explanations been proposed. This property of foam has promising applications. The viscous behavior of foam is the important property of foam necessary to control mobility. By changing the flow velocity of foam in porous media, it appears that a low viscosity foam can be transformed into a higher viscosity foam. Techniques based on this behavior could be employed to reduce the injectivity problems associated with foam while placing high viscosity foam in regions where mobility control is desired.

6. CONCLUSIONS

Based on the results of this study the following conclusions can be made on the flow of surfactant foam in porous media:

- (1) At low concentrations apparent viscosity of foam increases sharply with surfactant concentration.
- (2) At concentrations near the surfactant critical micellar concentration (CMC), apparent viscosity of foam becomes independent of surfactant concentration.
- (3) At concentrations approaching the CMC, apparent viscosity increases slowly with foam quality.
- (4) The texture of foam is significantly effected by quality.
- (5) At low surfactant concentrations, apparent viscosity can decrease with increasing foam quality.
- (6) Apparent viscosity of foam varies from 50 to 70 centipoise in darcy sand packs at reservoir flow rates.
- (7) Increasing flow velocity causes a significant decrease in the apparent viscosity of foam.
- (8) The flow history of surfactant foam in porous media has significant effects on the apparent viscosity of foam.

7. RECOMMENDATIONS FOR COMPLEMENTARY WORK

This study has only scratched the surface of the information necessary to understand the flow behavior of surfactant foam in porous media. The following recommendations for future work are presented for three areas; equipment modifications, experiments to complete the work of this study, and complementary studies on the behavior of foam in porous media.

The equipment worked well except for the inner sand pack pressure transducers, which often gave erroneous readings. The suspected cause of this malfunction is the wad of glass wool placed in the pressure tap fittings to prevent sand migration. Fittings with an integral stainless steel screen are suggested as a possible solution to this problem. The limiting factor in the generation of high quality foam was the minimum stable flow rate of the surfactant pump. An adjustment in the operation of the system that may allow a lower surfactant flow rate would be an increase in the system back pressure. The pump used in this system employs pistons and check valves. At low flow rates the check valves seal too slowly and significant back flow occurs. Operating the system at higher pressure can reduce this problem. For the current system the recommended system back pressure is 120 psig. Operation at this system pressure may allow the generation of a 95% quality foam at a flow velocity of 2.8 ft/D. Further increases in foam quality require either pump modification or replacement, or alternatively higher total flow rates.

To completely define the surfactant concentration effects, additional data are needed at both low and intermediate concentrations. Additionally, gas and water data without surfactant would provide a base line for the surfactant concentration data. There is also a need to extend the data set to include 95% and possibly 98% foam quality data. As discussed earlier, this can be done with pump modifications or at higher total flow rates. The data on the effects of flow velocity on apparent viscosity should be extended to velocities of 100 to 150 ft/D. This additional data would better define the shape of the apparent viscosity curve for flow velocity effects.

Future studies to complement this work should include studies over a wide range of permeability. Interesting work might include low quality foam injection to study the critical gas saturation behavior of foam. The acrylic sand pack tube is ideal for this study since the velocity of the foam front can be directly observed. To avoid confusing adsorption effects this work should be conducted in surfactant saturated sand packs. In order to apply the flow behavior of foam in this study to surfactants other than Suntech IV, the relationship between viscous behavior of foam and surfactant chemical structure should be studied in detail.

Since significant volume of injected surfactant was required to reach steady state and since this behavior is probably due to adsorption effects; studies on the transient nature of the flow viscosity of foam in porous media are necessary. The parameters that are expected to have a significant effect on the transient viscosity behavior of foam are velocity, quality, the nature of the porous media, and the nature of the fluids in place.

8. REFERENCES

1. Aizad, T. and Okandan, E., "Flow Equation for Foam Flowing Through Porous Media and its Application as a Secondary Recovery Fluid", SPE 6599, presented at the SPE-AIME International Symposium on Oil Field and Geothermal Chemistry, La Jolla, California, June 27-28, 1977.
2. Ali, J., Burley, R., and Nutt, C. W., "Foam Enhanced Oil Recovery from Sand Packs", personal communication, 1983.
3. Albrecht, R. A. and Marsden, S. S., "Foams as Blocking Agents in Porous Media", *SPEJ* (March 1970), 51-55.
4. Bernard, G. G., U. S. Patent 3,330,351 (1967).
5. Bernard, G. G. and Holm, L. W., "Effect of Foam on Permeability of Porous Media to Gas", *SPEJ* (September 1964), 267-274.
6. Bernard, G. G. and Holm, L. W., "Effect of Foam on Trapped Gas Saturation and Permeability of Porous Media to Water", *SPEJ* (December 1965), 295-300.
7. Bond, D. C. and Holbrook, O. C., "Gas Drive Oil Recovery Process", U. S. Patent 2,866,507 (1958).
8. Dilgren, R. E., Deemer, A. R., and Owens, K. B., "The Laboratory Development and Field testing of Steam/Noncondensable Gas Foams for Mobility Control of Heavy Oil Recovery", SPE 10774, presented at the SPE California Regional Meeting, San Francisco, California, March 24-26, 1982.
9. Doscher, T. M. and Kuuskraa, V. A., "Reviving Heavy Oil Reservoirs with Foam and Steam", *Oil and Gas Jour.* (February 1, 1982), 99-105.
10. Fried, A. N., "The Foam Drive Process for Increasing the Recovery of Oil", Report of Investigations 5866, U. S. Bureau of Mines 1961.
11. Heller, J. P., Lien, C. L., and Kuntamukkula, M. S., "Foam-Like Dispersions for Mobility Control in CO_2 Floods", SPE 11233, presented at the SPE 57th Annual Fall Meeting, New Orleans, Louisiana, September 26-29, 1982.
12. Hirasaki, G. J. and Lawson, J. B., "Mechanism of Foam Flow in Porous Media--Apparent Viscosity in Smooth Capillaries", SPE 12129, presented at the SPE 58th Annual Fall Meeting, San Francisco, California, October 5-8, 1983.
13. Holbrook, S. T., Patton, J. T., and Hsu, W., "Rheology of Mobility Control Foams", SPE/DOE 9809, presented at the SPE/DOE Second Joint Symposium on Enhanced Oil Recovery, Tulsa, Oklahoma, April 5-8, 1981.

14. Holm, L. W., "The Mechanism of Gas and Liquid Flow through Porous Media in the Presence of Foam", *SPEJ* (December 1968), 359-369.
15. Marsden, S. S. and Kahn, S. A., "The Flow of Foam through Short Porous Media and Apparent Viscosity Measurements," *SPEJ* (March 1966), 17-25.
16. Minssieux, L., "Oil Displacement by Foams in Relation to Their Physical Properties in Porous Media," *JPT* (January 1974), 100-108.
17. O'Brien, L. J., U. S. Patent 3,306,354 (1967).
18. Ploeg, J. F. and Duerksen, J. H., "Two Successful Stream/Foam Field Tests, Sections 15A and 26C, Midway-Sunset Field," presented at the SPE California Regional Meeting, Bakersfield, California, March 27-29, 1985.
19. Raza, S. H. and Marsden, S. S., "The Streaming Potential and Reology of Foam", *SPEJ* (December 1967), 359-368.
20. Sibre, T. O., "The Viscosity of Froth", Transactions of the Faraday Society (1943), Volume 30, 325.
21. Strom, J. L. and Brigham, W. E., "An Engineering and Economic Analysis of a Steamflood Plus Surfactant Field Project," Department of Energy Contract No. DE-AC03-80SF11445, 1984.

APPENDIX

DATA TABLES

This appendix contains the raw data collected in this study. Also contained in this appendix are tables which contain the data presented in the graphs of this report.

Table A-1

Differential Pressure Data

Experiment #	Sand Pack	Differential Pressure (psi)		
		Entire Sand Pack	2 nd Quarter	3 rd Quarter
2	1	3.61	0.91	-
3	1	4.12	1.08	-
4	1	4.48	1.14	-
5	1	17.8	4.79	-
6	1	4.83	1.27	-
7	1	5.45	1.47	-
8	1	5.70	1.62	-
9	1	5.18	1.66	-
10	1	20.1	5.81	-
11	1	14.7	-	-
16	2	-	0.61	-
17	2	-	0.57	-
18	2	-	0.59	-
19	2	3.33	0.62	-
20	2	5.38	0.89	-
21	2	5.30	0.84	-
22	2	5.25	1.00	-
23	2	9.48	2.34	-
24	2	10.1	2.35	-
25	2	11.3	2.59	-
26	2	12.7	2.87	-
29	3	3.13	0.55	0.51
30	3	3.63	0.63	0.62
31	3	3.75	0.65	0.64
32	3	3.53	0.52	0.56
33	3	3.73	0.55	0.55
34	3	3.73	0.59	0.56
35	3	3.80	0.62	0.64
36	3	3.88	0.66	0.65
37	3	3.60	0.54	0.53
38	3	3.80	0.57	0.56
39	3	3.80	0.59	0.57
40	3	3.98	0.64	0.63
41	3	3.83	0.62	0.61
42	3	3.73	0.55	0.56

Table A-1 Continued

Differential Pressure Data

Experiment #	Sand Pack	Differential Pressure (psi)		
		Entire Sand Pack	2 nd Quarter	3 rd Quarter
46	4	0.90	-	-
47	4	0.88	-	-
48	4	0.80	-	-
49	4	0.85	-	-
50	4	0.74	-	-
51	4	1.45	-	-
52	4	1.50	-	-
53	4	1.47	-	-
54	4	0.85	-	-
55	4	0.78	-	-

Table A-2

Normalized Pressure Data

Exp. #	Length (cm)		Normalized Δp (10^{-3} atm/cm)			Average $\Delta p/L$ (10^{-3} atm/cm)
	Entire Sand Pack	2 nd and 3 rd Quarters	Entire Sand Pack	2 nd Quarter	3 rd Quarter	
2	60.01	15.24	4.09	4.06	-	4.08
3	60.01	15.24	4.67	4.82	-	4.75
4	60.01	15.24	5.08	5.09	-	5.09
5	60.01	15.24	20.1	21.4	-	20.8
6	60.01	15.24	5.48	5.67	-	5.58
7	60.01	15.24	6.18	6.56	-	6.37
8	60.01	15.24	6.46	7.23	-	6.85
9	60.01	15.24	5.87	7.41	-	6.64
10	60.01	15.24	22.7	25.9	-	24.3
11	60.01	15.24	16.6	-	-	16.6
16	60.01	15.24	-	2.72	-	2.72
17	60.01	15.24	-	2.55	-	2.55
18	60.01	15.24	-	2.63	-	2.63
19	60.01	15.24	3.78	2.77	-	3.28
20	60.01	15.24	6.10	3.97	-	5.04
21	60.01	15.24	6.01	3.75	-	4.88
22	60.01	15.24	5.95	4.46	-	5.21
23	60.01	15.24	10.7	10.4	-	10.6
24	60.01	15.24	11.5	10.5	-	11.0
25	60.01	15.24	12.8	11.6	-	12.2
26	60.01	15.24	14.4	12.8	-	13.6
29	60.60	15.24	3.51	2.46	2.28	2.75
30	60.60	15.24	4.08	2.81	2.77	3.22
31	60.60	15.24	4.21	2.90	2.86	3.32
32	60.60	15.24	3.96	2.32	2.50	2.93
33	60.60	15.24	4.19	2.46	2.46	3.04
34	60.60	15.24	4.19	2.63	2.50	3.11
35	60.60	15.24	4.27	2.77	2.86	3.30
36	60.60	15.24	4.36	2.95	2.90	3.40
37	60.60	15.24	4.40	2.41	2.37	2.94
38	60.60	15.24	4.27	2.55	2.50	3.11
39	60.60	15.24	4.27	2.63	2.55	3.15
40	60.60	15.24	4.47	2.86	2.81	3.38
41	60.60	15.24	4.30	2.77	2.72	3.26
42	60.60	15.24	4.19	2.46	2.50	3.05

Table A-2 Continued

Normalized Pressure Data

Exp. #	Length (cm)		Normalized Δp (10^{-3} atm/cm)			Average $\Delta p/L$ (10^{-3} atm/cm)
	Entire Sand Pack	2 nd and 3 rd Quarters	Entire Sand Pack	2 nd Quarter	3 rd Quarter	
46	60.60	15.24	1.01	-	-	1.01
47	60.60	15.24	0.99	-	-	0.99
48	60.60	15.24	0.90	-	-	0.90
49	60.60	15.24	0.95	-	-	0.95
50	60.60	15.24	0.83	-	-	0.83
51	60.60	15.24	1.63	-	-	1.63
52	60.60	15.24	1.68	-	-	1.68
53	60.60	15.24	1.65	-	-	1.65
54	60.60	15.24	0.95	-	-	0.95
55	60.60	15.24	0.88	-	-	0.88

Table A-3

Apparent Viscosity Data

Exp. #	Surf. Conc. (wt%)	Flow Rate (cm^3/min)	Flow Velocity (ft/D)	Quality (%)	Average $\Delta p/L$ (10^{-3} atm/cm)	k_a (d)	μ_a (cp)
2	0.05	0.1	2.8	70	4.08	5.16	56.6
3	0.05	0.1	2.8	80	4.75	5.16	65.9
4	0.05	0.1	2.8	90	5.09	5.16	70.6
5	0.05	1.0	28.0	90	20.8	5.16	28.8
6	0.3	0.1	2.8	70	5.58	5.16	77.4
7	0.3	0.1	2.8	80	6.37	5.16	88.4
8	0.3	0.1	2.8	90	6.85	5.16	95.0
9	0.3	0.1	2.8	95	6.64	5.16	92.1
10	0.3	1.0	28.0	90	24.3	5.16	33.7
11	0.3	0.5	14.0	90	16.6	5.16	46.0
16	0.05	0.1	2.8	80	2.72	8.55	62.5
17	0.05	0.1	2.8	70	2.55	8.55	58.6
18	0.05	0.1	2.8	75	2.63	8.55	60.4
19	0.05	0.1	2.8	85	3.28	8.55	75.4
20	0.05	0.2	5.6	80	5.04	8.55	57.9
21	0.05	0.2	5.6	70	4.88	8.55	56.1
22	0.05	0.2	5.6	90	5.21	8.55	59.9
23	0.05	0.5	14.0	70	10.6	8.55	48.7
24	0.05	0.5	14.0	80	11.0	8.55	50.6
25	0.05	0.5	14.0	90	12.2	8.55	56.1
26	0.05	0.8	22.4	86	13.6	8.55	39.1
29	0.05	0.1	2.8	75	2.75	7.18	53.1
30	0.05	0.1	2.8	85	3.22	7.18	62.1
31	0.05	0.1	2.8	90	3.32	7.18	64.1
32	0.15	0.1	2.8	70	2.93	7.18	56.5
33	0.15	0.1	2.8	75	3.04	7.18	58.7
34	0.15	0.1	2.8	80	3.11	7.18	60.0
35	0.15	0.1	2.8	85	3.30	7.18	63.7
36	0.15	0.1	2.8	90	3.40	7.18	65.6
37	0.3	0.1	2.8	70	2.94	7.18	56.7
38	0.3	0.1	2.8	75	3.11	7.18	60.0
39	0.3	0.1	2.8	80	3.15	7.18	60.8
40	0.3	0.1	2.8	85	3.38	7.18	65.2
41	0.3	0.1	2.8	90	3.26	7.18	62.9
42	0.3	0.1	2.8	70	3.05	7.18	58.9

Table A-3 Continued

Apparent Viscosity Data

Exp. #	Surf. Conc. (wt%)	Flow Rate (cm ³ /min)	Flow Velocity (ft/D)	Quality (%)	Average $\Delta p/L$ (10 ⁻³ atm/cm)	k_a (d)	μ_a (cp)
46	0.005	0.1	2.8	70	1.01	8.08	21.9
47	0.005	0.1	2.8	75	0.99	8.08	21.3
48	0.005	0.1	2.8	80	0.90	8.08	19.5
49	0.005	0.1	2.8	85	0.95	8.08	20.6
50	0.005	0.1	2.8	90	0.83	8.08	18.0
51	0.01	0.1	2.8	70	1.63	8.08	35.4
52	0.01	0.1	2.8	75	1.68	8.08	36.5
53	0.01	0.1	2.8	80	1.65	8.08	36.5
54	0.01	0.1	2.8	85	0.95	8.08	20.6
55	0.01	0.1	2.8	90	0.88	8.08	19.1

Table A-4

Permeability Effects on Apparent Viscosity

Flow Velocity = 2.8 ft/D

Quality (%)	Apparent Viscosity μ_a (cp)			Average μ_a (cp)
	Sand Pack Permeability (d)			
	5.16	7.18	8.55	
70	56.6	58.6	-	57.6
75	-	60.4	53.1	56.8
80	65.9	-	62.5	64.2
85	-	75.4	62.1	68.6
90	70.6	-	64.1	67.4

Table A-5

Surfactant Concentration Effects on Apparent Viscosity

Flow Velocity = 2.8 ft/D

Quality (%)	Apparent Viscosity μ_a (cp)					Average μ_a (cp)	Standard Deviation
	Surfactant Concentration (wt%)						
	0.005	0.01	0.05**	0.15	0.3		
70	21.9	35.4	57.6	56.5	57.8 [#]	57.4	± 1.1 (5) ⁺
75	21.3	36.5	56.8	58.7	60.0	58.1	± 3.4 (4) ⁺
80	19.5	36.5	64.2	60.0	60.8	62.3	± 2.6 (4) ⁺
85	20.6	20.6	68.6	63.7	65.2	66.6	± 6.0 (4) ⁺
90	18.0	19.1	67.4	65.6	62.9	65.8	± 3.4 (4) ⁺

* average of 0.05, 0.15, 0.3 wgt % data

** average values from Table A-4

average of experiments 37 and 42

+ number of data points used in average

Table A-6

Flow Velocity Effects on Apparent Viscosity

Concentration = 0.05 wt%

Quality = 90%

Flow Velocity (ft/D)	Apparent Viscosity (cp)
2.8	67.4
5.8	59.9
14.0	56.1
22.4	39.1*
28.0	28.8

* Quality = 86%

Table A-7

Flow History Effects on Apparent Viscosity

Flow Velocity = 2.8 ft/D

Quality (%)	Apparent Viscosity (cp)	
	No Flow History* ⁺	Flow History**
70	57.4 ±1.1	77.4
75	58.1 ±3.4	-
80	62.3 ±2.6	88.4
85	66.6 ±6.0	-
90	65.8 ±3.4	95.0
95	-	92.1

* flow velocity always 2.8 ft/d

** previous flow velocity of 28.0 ft/d

+ average data from Table A-5

Table A-8

Surface Tension of Suntech IV

Concentration (wt%)	Surface Tension (dynes/cm)	Observation
0.0	72.7	no foam
0.000005	34.4	no foam
0.00005	32.1	no foam
0.0005	35.1	no foam
0.005	32.0	weak foam
0.01	32.1	foam
0.05	34.4	foam
0.15	32.1	stable foam
0.3	31.9	stable foam
0.5	31.3	stable foam

FOAMS IN POROUS MEDIA

A LITERATURE SURVEY

By
S. S. Marsden

TABLE OF CONTENTS

	<u>Page</u>
ACKNOWLEDGEMENT	ii
INTRODUCTION	1
PIONEER WORK	1
THE EARLY 1960'S	2
THE LATTER 1960'S	4
THE EARLY 1970'S	9
THE LATTER 1970'S	14
THE 1980'S	15
REFERENCES	23

1. INTRODUCTION

In 1978 a literature search on selective blocking of fluid flow in porous media was done by Professor S.S. Marsden and two of his graduate students, Tom Elson and Kern Guppy. This was presented as SUPRI Report No. TR-3 entitled "Literature Preview of the Selected Blockage of Fluids in Thermal Recovery Projects."

Since then a lot of research on foam in porous media has been done on the SUPRI project and a great deal of new information has appeared in the literature. Therefore we believed that a new, up-to-date search should be done on foam alone, one which would be helpful to our students and perhaps of interest to others. This has been based on references which were known to the author and supplemented by those in the MS Research Report of Bret Beckner and the drafts of the PhD dissertations of Syed Mahmood and Fred Wang. However, the interpretation and presentation of the material is the sole responsibility of the author.

For various reasons, almost every literature search misses some papers, patents, theses, dissertations, government reports, etc. If the readers of this search know of any such publications, the author would like to hear about them. If the readers find any errors or disagree with the views expressed, the author would also appreciate learning about these.

As can be seen, this is a chronological survey showing the development of foam flow, blockage and use in porous media, starting with laboratory studies and eventually getting into field tests and demonstrations. It is arbitrarily divided into five-year time periods.

2. PIONEER WORK

It is difficult to establish from information in the open literature as to which of two laboratories started this foam research. The first publication of any direct importance was a patent awarded to Bond and Holbrook (1958) but the author of this report was able to observe the essentially complete work of Fried in late 1956. Unfortunately, Fried's original report had an unusually long gestation time in the review process and was not actually published until 1961 in greatly abbreviated form.

Bond and Holbrook (1958) suggested that foam could be generated in an oil reservoir by consecutive injection of aqueous surfactant solution and gas. They considered foam as a displacing medium for oil which would be less mobile than air and therefore have a more favorable mobility ratio relative to oil. It was claimed that sweep efficiency for both miscible and immiscible gas drives would thereby be increased.

Fried's report included theoretical and laboratory work on the flow of foam in both tubes and porous media. This was all relative to what he called a *foam drive*, secondary oil-recovery process. For this, foam would be generated by bubbling a gas, such as air, N_2 or CH_4 , through a surfactant solution and then used to displace oil from a porous medium. In his laboratory work on unconsolidated porous media, the oil recovery, particularly for viscous oil, was much better than that obtained on the same or similar sand packs by gas drive, water flooding or surfactant solution flooding.

Besides oil displacement tests, Fried made a number of interesting measurements on the physical properties of foam. Apparent viscosity was measured in both rotational and tube-type viscometers; and while the treatment of the experimental data leaves a great deal to be desired by current standards, the highly viscous nature of the foam was apparent. He was the first to

measure the streaming potential or electrokinetic nature of foam, and he found that this could lead to complete fluid blockage unless it was suppressed with electrolyte in the foamer solution. Unfortunately, Fried left the U.S. Bureau of Mines at about the time the work was reported and it was not continued by others there.

3. THE EARLY 1960'S

To substantiate the patent of Bond and Holbrook, Bernard carried out experimental work on the generation of foam in porous media and reported this in early 1963. He used an unconsolidated sand having a range of grain sizes giving a permeability of about 6 darcies ($6 \times 10^{-12} m^2$). Surfactant solution was either present prior to injection or injected as a batch just before initiation of gas drive. Either water or a blend of refined oils or both were the original fluids.

Because theory did not exist to predict what foaming agents would be best, a purely empirical approach was used. Preliminary screening was done in equipment similar to that used to evaluate surfactants for removal of liquids from gas wells. As was expected, the commercial foamers worked best when only water was the liquid, and worse when oil was the only liquid, with the performance being intermediate when both were present. Unfortunately, the foamers were only identified by letters and not their chemical formulas.

Various flooding tests were carried out with different combinations of initially saturating and displacing fluids as well as different surfactants. The results of these did not always agree with those of the screening tests as far as the surfactants were concerned. Bernard concluded that the best surfactants would be those that would form foam in both the oil and the water within porous media during immiscible displacement. For miscible displacement with the LPG-gas process, foamers that worked best in water alone were to be preferred.

In an MS thesis Bennett (1963) described laboratory experimental work on the use of foam generated within porous media to displace water in an aquifer in which natural gas storage was going to be initiated. He felt that a gas buffer between the injected surfactant solution and the connate brine increased displacement efficiency, the lack of which may have led to interaction between the electrolyte of the brine and the surfactant itself. In a continuation of this work, Kolb (1964) started with his consolidated porous medium completely saturated with a surfactant solution and reported that liquid recovery increased with surfactant slug size and concentration. Foamability of the surfactant was of primary importance while foam stability and static surface tension were secondary. His results indicated that ultimate gas storage volume in an aquifer could be increased by injecting surfactant solution before gas injection started. In parallel work done by Deming (1964) at the same institution, he reiterated the latter points and also reported that an increase of the surface elasticity of the surfactant solution led to a decrease in the displacement efficiency of the solution.

In the last of this series of theses, Iden (1965) noted that similar efficiency of displacement could be brought about by a small volume of a highly effective surfactant solution or a large volume of a less effective one. He also found that foam stability became an important factor when flow rate was slow.

In 1963 a patent was awarded which dealt with foam generated within the reservoir. Beeson found that the injection of a surfactant followed by a gas-driven solvent bank led to EOR. Although he attributed this to a change from a water-wet to an oil-wet state, it is likely that foam generation made a more significant contribution than did any wettability change.

At the end of 1963 Emery patented a modification of the *in situ* combustion process wherein a surfactant is to be injected in the water bank preceding the combustion zone. He claimed this would lower the oil-water interfacial tension and thereby increase the efficiency of oil displacement by the water bank. While this is probably true, a more important effect (which he did not mention) would be the formation of foam with the N_2 remaining from the injected air after the O_2 had been consumed. From what we have learned later on (c.f. below), this would selectively decrease the permeability of the more permeable strata relative to the less permeable and hence improve the vertical profile of the fluid front.

A very extensive laboratory study was carried out by Bernard and Holm (1964) on the effect of foam on permeability of porous media to gas. Both consolidated and unconsolidated ones ranging from 100 to 146,000 md (0.1 to $146 \times 10^{-12} m^2$) had gas permeabilities less than 1% of the specific permeability when foam was present. The decrease was found to be much greater for loose sands than tight ones, which suggested the use as a selective plugging medium for high permeability channels in various oil displacement processes.

The adverse effect of oil on many foaming agents was reported again but it was noted that some were still effective even in the presence of oil. Continuous injection of foams helped to maintain the foam when oil was present. Permeability reduction increased with foam concentration, but concentrations as low as 0.01% were still effective.

Stable foams in porous media over long periods of time could be obtained if foam solution was added periodically. The stability increased as the specific permeability of the porous media decreased.

In a complementary paper to the one discussed above to water, Bernard *et al.* (1965) described the effect of foam on the aqueous permeability of porous media having trapped gas saturation. Interestingly enough, they found that the aqueous permeability at a given saturation was the same whether or not foam was present. In effect, foam decreases the permeability to water by causing a higher trapped gas saturation to be reached than when foam is absent. Increasing the foam concentration increases the trapped gas concentration even further.

Two other interesting observations were reported here. Foam was found to persist in porous media even after 10 to 25 pore volumes of surfactant-free water was passed through the porous media. In at least two cases it was also found to persist at temperatures up to $140^\circ F$ ($60^\circ C$) for as much as ten days.

The use of externally generated aqueous foam to displace oil from unconsolidated and consolidated sands was also patented by Craig and Lummus (1965). In the preferred form of their invention, they recommended that 0.1 to 10% pore volume of an oil-miscible solvent such as LPG be injected first and that this be followed by gas (natural gas, N_2 , H_2 , CO_2 and CO) equal in volume to 50 to 100% of the solvent. Next, at least 20% pore volume of externally generated foam is injected and this may in turn be driven by water. They claimed that more oil was recovered by externally generated foam than that generated within the core.

The selective blocking of gas flow by foam led to another proposed application by Holbrook and Bernard (1965). They suggested that preferably an oleic or possibly an aqueous solution of surfactant be injected into a formation producing at a high GOR. When the production is resumed, the flowing gas generates foam in the gas-producing strata and impedes further gas flow. They also proposed that use of aqueous surfactant solutions in this manner would cut down coning when natural gas was stored in aquifers.

Although a good deal of experimental work had been done in the flow of foam in porous media by the mid-1960's, the interpretation was based on external measurements of such parameters as pressure drop and flow rate with little or no direct knowledge of what was going on within the pores. As had been done in much earlier work on oil and water flow in porous media, we undertook some microscopic studies of foam flow in thin gas cells packed with glass beads. These were published in an obscure report by Sharma (1965) and will be summarized only briefly here.

He found that the size and extent of the bubbles depended mainly upon the type and concentration of the surfactant as well as the foam quality. With one surfactant at low concentration (0.1% Aerosol MA), small bubbles moved through certain channels at low pressure differentials but at higher pressure differentials, a body of foam made up of bubbles of about the same size moved as a foam bank. Bubble size decreased with an increase in surfactant concentration and this was often manifest in membrane-like foam at low concentrations and small bubble foam at higher ones. Bubble size for another surfactant (Adfoam) also increased with quality.

Foams produced from a generator made up of unconsolidated sand was uniform in size when viewed in a thin empty cell but became heterogeneous when flowing through a packed cell. Some small bubbles became immobile by adhering to glass bead surfaces as if the latter had become oil-wet.

Foam displaced oil in a thin, packed bead cell at low rates in a piston-like manner; but at higher rates there was significant fingering, and at still higher rates foam bubbles became dispersed in the oil itself. With foam breakthrough a frothy emulsion was first produced followed by foam alone. Hence the displacement mechanism and sequence is far more complex than is usually visualized.

4. THE LATTER 1960'S

After reviewing earlier work on foam flow, stability and persistency in porous media, Bond and Bernard (1966) presented results on the effect of sand wettability on foam flow. Their data was difficult to interpret. One problem may have been that the silicones usually used to make the sand surfaces oil-wet are some of the best foam breakers known to man and so the systems which were intended to be oil-wet were simply foam-breaking systems. In other experiments they noted the general relationships between bubble size, pore size, pressure gradients and foamer concentration but no numerical results were presented.

Two studies on foam flow in short, unconsolidated porous media were published in 1966, the first by Marsden and Khan and the second by Abernathy and Eerligh. In both cases externally generated foam of a range of qualities was injected, flow rate and pressure drop measured and liquid saturation determined within the porous medium by electrical conductivity. Marsden and Khan also measured the apparent viscosity, μ_a , of the foam with a modified Fann VG meter and a high shear rate instrument (based on the vibrating reed method) known as the Bendix Ultraviscoson. For the former μ_a decreased with increasing shear rate but usually fell within the range of 50 to 500 cp (50 to 500 mPa · s), and at a given shear rate it increased almost linearly with quality. For the latter instrument, kinematic μ_a was independent of quality but absolute μ_a increased with quality from about 3 to 8 cp (3 to 8 mPa · s).

From the flow rate and pressure drop data, it is possible to calculate an effective permeability-apparent viscosity ratio, k_d/μ_a . This decreased almost linearly with quality for high permeability porous media, but the rate of decrease was less for tighter ones. An attempt

was made to normalize the data for several porous media by calculating a relative permeability to apparent viscosity ratio, k_r/μ_a and plotting this against quality; while this brought the data closer together, it was not entirely successful. The k_r/μ_a ratio increased with surfactant concentration and with liquid saturation in the porous media. Estimates for μ_a of foam in these porous media ranged from 30 to 100 cp.

Abernathy and Eerligh (1966) carried out a number of measurements on externally generated foam made with five different surfactants at three different concentrations. This flowed through four short porous media in series which were packed with graded Ottawa sand having mesh sizes from 20/30 for the first to 80 for the fourth. These porous media were separated by optical cells fitted with a light source and detector for measuring attenuation by scattering at the liquid-gas interfaces. Pressure drop across each porous medium could be measured as well as electrical conductivity. Flow rate was determined by the time required to fill a horizontal burette and quality by its weight empty and filled. Bubble size was measured with an especially constructed thin cell viewed under a microscope.

With two exceptions traced to equipment malfunction, they found a decrease in foam mobility with increase in foam quality. For qualities below 80%, bubble size as indicated by transmitted light did not change appreciably; but above this, bubble size increased with quality. The magnitude depended on the surfactant, but the rate of increase was about the same for all. As measured by the same instrumentation, bubble size decreased with increasing surfactant concentration. With one exception, these foams showed an almost exponential increase in mobility with decrease in bubble size. There was a drastic increase in mobility when the bubble size became smaller than the pore opening estimated from capillary pressure data.

While some authors recommended that preformed foam be injected from the well into the reservoir rock and others thought that the constituents should be injected so that the foam could be generated *in-situ*, Hardy and McArthur (1966) patented still a third method which they felt was superior because it produced the foam out in the reservoir away from the injection wells. To accomplish this, an aqueous solution of both the foaming agent and a soluble gas were to be injected into the formation at a pressure above the bubble point. When the gas came out of solution at the lower pressures out in the reservoir, foam was generated. This method had the advantage that it allowed a low viscosity solution to be pumped under high pressure gradients near the well while the higher viscosity foam was subjected to lower pressure gradients, and hence lower shear stress out away from the well. In one modification of their invention, they suggested using LPG as the solvent.

A common method of storing natural gas in geographical areas close to markets is to inject the gas in underground porous rock formations such as either aquifers or else abandoned oil or gas fields. Many times these have leaks through fractures in the cap-rock or through improperly abandoned or completed wells. Injection of aqueous foam solutions in porous formations overlying the cap-rock was recommended as a remedy for this by O'Brien (1967). Any leaking gas would, of course, generate foam *in situ* and hence impede or block the flow of additional gas. Improved performance was claimed if a viscosity increasing agent was added to the foam solution and if it was previously saturated with CO_2 . A list of suitable commercial foaming agents giving both their trade names and their approximate chemical names was also included in this patent.

Various workers received patents in 1967 which dealt either directly or indirectly with foam generation in reservoirs. Santourian (1967) described the injection of hot aqueous solutions of gas followed by flood waters containing such thickening agents as CMC, CEC, Dextran or Polyox. The latter have some surface activity and so foam may well have been produced and made a significant contribution to the process. O'Brien and Sayre (1967),

Zwicky (1967), and Rai and Bernard (1967) as well as others have mentioned the possibility of wettability changes brought about by the foaming agents, but could not even agree on the direction of change of wettability. The latter authors claimed that successive banks of foam made with anionic and cationic agents produced more oil than either alone, but thought this might also be due to the formation of different kinds of emulsions (O/W or W/O).

The first patent on use of foam in the CO_2 injection was awarded to Bernard and Holm (1967). It also included use of ethane and propane. A long list of suitable surfactants was also included in the patent.

The physical properties of foam and their applications in petroleum operations were reviewed for the Seventh World Petroleum Congress by Marsden *et al.* (1967). Some of the experimental results of Abernathy and Eerligh (1966) on the flow of foam through porous media were included in this paper.

Because of the extremely efficient blocking action of foam in porous media, Bond and Bernard (1967) were concerned that formation of foam in the porous rock adjacent to an injection well would prevent further injection of fluids if foam generation took place too quickly. Therefore, they patented the injection of a water buffer following the surfactant solution and preceding the gas injection to prevent this. They also included in their patent the injection of a sequence of many slugs of surfactant solution, water and gas throughout the project.

Another patent on use of foam in underground storage of natural gas was awarded to Bernard (1967). Besides reiterating the claims of O'Brien's (noted above), it is suggested that an envelope of foam formed from carbonated foamer solution increased the gas storage space in an aquifer by confining the gas within a limited space. He also recommended the use of brine instead of fresh water in preparing the foamer solution to prevent blockage from clay swelling.

While it does not apply directly to foam flow in porous media, the work of Raza and Marsden (1967) on foam flow in small glass tubes (radius 0.25 to 1.5 mm) does have some bearing on this subject. The bubble sizes were much smaller than the tube sizes and so these authors assumed the foam was a continuum and treated their data in terms of a power law fluid. At low shear rates, the flow behavior index was unity and so the foam behaved like a Newtonian fluid. The apparent viscosities* increased with foam quality and cover the range from 15 cp to 266 poise (15×10^{-3} to 26.6 Pa·s).

At higher shear rates these foams had flow behavior indices ranging from about 0.3 to 0.5 and hence they behaved like pseudoplastic fluids. Thus the foam went from a laminar type flow to a semi-plug-like type of flow, the extent of which increased with both foam quality and tube radius.

This paper also includes results on measurement of the streaming potential of foam in both tubes and unconsolidated porous media. An equation was derived which related this to the pressure drop, the tube dimensions, the zeta potential and the dielectric constant, as well as the consistency index, flow behavior index and density of the foam.

*The term *apparent* is used here because there was an unexplained effect of tube radius on the results. This may have been due to foam slippage at or near the tube wall. Unfortunately, a correction was not made for this.

The displacement of Newtonian fluids of different viscosities by foam in Hele-Shaw models was studied by Moser (1967). He used aerosol shaving foam injected by a small syringe pump, varied injection flow rate, measured injection pressure and traced the displacement front. In checking the equipment with viscous oils displacing water, he found the pressure buildups with swept-out area similar to those for foam displacing water, although in most of his runs foam displaced glycerin. Sweep efficiency was less in the lower permeability models as was foam apparent viscosity. Sweep efficiency was higher at lower mobility of the displaced fluid compared to a Newtonian fluid of the same viscosity. Pressure difference from the beginning of displacement to foam breakthrough was essentially independent of injection rate.

During oil production from gas-cap reservoirs, the gas tends to migrate downwards and come into the wells. Ferrell *et al.* (1968) recommended the injection of a foaming agent at or near the gas-oil contact to form foam with the gas. Mixing is achieved either by pumping a liquid into the oil zone and then forcing the foamer into the gas zone or else by producing from the oil zone and allowing the gas cap to expand. It was also claimed that this approach minimized encroachment of oil or flooding media into the gas cap during secondary recovery operations.

To cut down water coning Heuer (1968) recommended the injection of a foamer solution at or near the water-oil contact and then following this with gas to generate a foam barrier when the well is again on production. Limited laboratory work showed that foam did cut down gas flow while still allowing oil flow but the same was not demonstrated for water and oil flow. One field demonstrated a dramatic but temporary four-day decrease in GOR but then gas came in again strongly.

In a very important basic patent containing little experimental justification, Needham (1968) taught that foam made with steam as the gaseous phase be injected into a reservoir to get a better injection profile than with steam alone. When the steam condensed and the foam collapsed, the flow of hot liquids back into the well would not be impeded by the presence of a gaseous phase.

Up to this point in time, different theories had been developed to explain the flow of foam in porous media. Some held that foam could be treated as an almost homogeneous fluid flowing through essentially all of the pore system, while others believed that the gas and the foamer solution would move independently and flow through separate and different pore channels. Holm (1968) reported the results of a series of experiments which supported the latter viewpoint for flow under reservoir conditions. He felt that even with externally generated foam, the gas and liquid separated within the porous medium and then reformed as foam. The liquid moves through the porous medium in the form of the bubble films while the gas moves by breaking and reforming bubbles. The low liquid flow rate corresponds to the low liquid saturations in a foam-bearing porous medium and effective permeability may be calculated by Darcy's law. The gas flow rate deviates from that calculated by Darcy's law modified for more than one fluid present.

As we see it, the crux of the difference in the two viewpoints is that the several investigators are talking about different things but using the term *foam* to describe them. Holm says that, "...the foam bubbles (are) large (>0.1 mm)," but most consolidated reservoir rocks have pore diameters which are smaller than this by at least an order of magnitude. Hence these *bubbles* must have extended over and through at least several pores and his explanation appears to be reasonable for such large bubbles. Other work indicates that large bubbles are present both in higher quality, drier foams or when low concentrations of surfactants are used. But for lower quality, wetter foams or those made with higher concentrations of foaming agent,

smaller bubbles would be produced and these could well flow through porous medias as an essentially homogeneous fluid. This is illustrated in the works described earlier by Marsden *et al.* (1967).

The flow properties of foam in porous media also interested workers in the USSR. Evgenev and Turnier (1969) carried out experiments on both unconsolidated sands. ($3.1 d$ or $3.1 \times 10^{-12} m^2$) in large glass tubes (3.7 cm diameter x 60 cm long) and in flat cells containing large glass beads (2 mm diameter). They observed a threshold pressure and so described the foam as being a Bingham plastic. But they also found this threshold pressure dependent on the length of time the foam had been at rest in the porous medium and so they also described it as being thixotropic. In addition, cessation of flow took place at some finite pressure gradient smaller than the threshold gradient and hence there was a gradient smaller than the threshold gradient and hence there was a hysteresis loop which caused them to describe the foam as being a "pseudosolid." Some problems may have arisen in the terminology because of the difficulties of translation of the paper to English.

In enriched gas drives, more of the injected gas often goes into the more permeable zones than is economically desirable. To cut down on this, Leach (1969) recommended that the gas be preceded by an aqueous solution of an oil-sensitive foaming agent. The enriched gas thus forms a foam which diverts gas into the low permeability zones. After a matter of some weeks, the foam would break because of its sensitivity to oil and this would allow a high injection of dry gas to drive the enriched gas through the formation.

The rheological work of Raza and Marsden (1967) describing the flow of foam through glass tubes was extended to ones of smaller diameter by David and Marsden (1969). In analyzing the data, corrections were made here for the very significant effects of fluid slippage at the tube wall and for the semi compressible nature of the foam. The uncorrected apparent viscosities changed with foam quality, but the corrected ones were independent of foam quality. However, the corrected apparent viscosities still increased with tube diameter, which is not to be expected.

The corrected apparent viscosities decreased, as before, with increasing shear stress, still indicating that the foam behaved like a pseudoplastic fluid, but one with a very low gel strength. The latter, as measured with a Stormer viscometer, increased slowly with quality, but were still an order of magnitude too small to affect the pseudoplastic flow behavior.

The bubble size frequency distribution was found to be asymmetrical, resembling a χ^2 distribution but it approached a normal distribution at high foam quality. The arithmetic mean bubble diameter was found to be proportional to quality. As expected, the bubble size changed with time with the larger ones growing and the smaller ones shrinking.

The need for temporary diverting agents in fracturing and acidizing jobs prompted the work described by Smith *et al.* (1969). They did laboratory work on two packed columns of different permeabilities (having a ratio of 20:1) mounted in parallel. Injection of foamer solution was followed by injection of N_2 in a series of repeated treatments. This method of selective blocking worked better than others in a fractured dolomite with high vertical permeability. They claimed the method could be used in wells with temperatures up to $250^\circ F$ ($121^\circ C$).

5. THE EARLY 1970'S

To increase the degree of plugging and the life of the foam, Raza (1970) felt the foaming solution should be divided into several smaller batches which would be injected alternatively with smaller batches of inert gas. To avoid plugging of the formation near the well, batches of spacer fluid such as water or brine could be injected between the gas and the foamer solution.

In early 1970 two papers appeared on the use of foam as a gas blocking agent with particular reference to underground storage of natural gas. In the first, Albrecht and Marsden (1970) described laboratory experiments on the flow of foam in unconsolidated sands and sandstones. They found that steady gas or foam flow could be established at some injection pressure p_b and then the pressure decreased until flow ceased at some blocking pressure p_b . When flow is again established at a second, higher p_i , blocking can again occur at another p_b that will usually be greater than the first p_i . The blocking pressure depends on the foamer and its concentration as well as its saturation and the kind of porous medium. Gas blockage appeared to be greater in unconsolidated porous media than in consolidated ones.

In the second of the two papers Bernard and Holm (1970) described laboratory work on a model gas storage reservoir. They found that foam was 99% successful in reducing leakage from the sandstone model. The amount of foaming agent required to seal a leak depended on the adsorption-desorption properties of the agent on the rock surface. Certain modified anionic esters of relatively low molecular weight were found to be superior to most nonionics. Methods of applying the foaming agent in the field are recommended in the paper.

Vertical leaking of fluids past cement jobs going through tar sands apparently occurs when heated fluids are pumped down the casing or tubing. Elkins (1970) suggested that a foamer solution be injected around the casing with a permanent gas (unless the leaking fluid was gas) to form a foam and thus eliminate the leakage.

In late 1970 Bernard was awarded what looks like a very general patent on the use of foam drive for oil recovery. Either foam or the ingredients of foam are to be injected to form a foam bank which is then to be driven toward the production wells by a combination of gaseous and aqueous liquid drive fluids. The latter should be in the ratio of 5 to 15 volumes of gas (reservoir temperature and pressure) per volume of liquid, i.e., the proportions that would give a relatively dry foam. A list of suitable, commercially available foaming agents is included here.

According to Dauben and Raza (1970), the stability of foam in earth formations against the adverse effects of oil and elevated temperatures was increased by dissolving water-soluble film-forming polymers in the foamer solutions. Polyvinyl alcohols and polyvinyl pyrrolidones worked well. Stability of the foams could be increased further by adding film plasticizers such as glycerin.

Up to the end of 1970 practically nothing had been published on field work with foam in porous media other than brief mention of short tests in several patents. At this time Holm (1970) described their use in injection tests in the Siggins field, a small shallow one in Illinois. Foamer solutions and compressed air were injected simultaneously and alternately in one well and production observed in five offset production wells. Concentration of foamer solution started at 0.1% and then was increased to 0.5% and eventually to 1%. The foam reduced the mobility of both water and gas to less than 50% of their original values. A more uniform

injection profile was observed and severe channeling to one production well was stopped. When air and 1% slugs of foaming agent were injected alternately, the mobility of the air was reduced significantly.

Ugolev *et al.* (1970) found that foamed acid penetrated low pressure carbonate reservoirs more uniformly and more deeply than did regular acid and thus gave better jobs. The air-to-acid ratio was in the range of 1:1 to 5:1 and hence relatively wet foams were being used. He reported that in one region of the USSR, 434 acid foam jobs had been performed starting in 1956 and that these had led to the production of an additional 135,000 tons of oil. This would have to be a very low cost method of stimulation to make it worthwhile.

A number of tests were carried out by Fujii (1970) on comparing foam drive with water drive in a series of cores having permeabilities ranging from about 30 to about 10,000 md (3×10^{-5} to $10 \times 10^{-12} m^2$). On the average, oil recoveries were about 12% higher with foam drive. The ratio of foam drive to water drive recovery generally decreased as permeability increased.

The results of an extensive series of laboratory tests on foam in porous media were reported by Raza in 1969 and published at the end of 1970. He found that the quality of the foam depended on the type of the foaming agent, its concentration in the solution, the physical properties of the porous medium, the pressure level, and the composition and saturation of fluids present. The nature of the foam depended on the type of foaming agent and its concentration in the foaming solution. He felt that the flow behavior of foam in porous media could neither be described in terms of its high apparent viscosity nor in terms of relative permeability concepts, but he came up with no alternative explanation.

He found that the flow of gas could be restricted for indefinitely long periods of time, that of water for shorter periods of time until the foam decays, and that of hydrocarbons only temporarily. He felt that foam could be used to combat coning, to improve sweep efficiency in heterogeneous reservoirs and to improve displacement efficiency in gas injection processes.

The flow of gas through porous media containing aqueous solutions of surfactant was studied by Nahid (1971). Using tracer studies (CH_4 and He), he found that a portion of the gas phase was immobile while the remainder flowed with the forming and breaking of surfactant solution films. The presence of surfactants decreased gas permeability significantly and increased liquid recovery at gas breakthrough. An increase in pressure level and surfactant concentration led to a decrease in gas permeability, which is inconsistent with the results of Abernathy and Eerligh (1966), who used Ottawa sand packs while he used a Berea core. Limited studies on gas-oil systems containing certain surface active silicones and fluorocarbons indicated behavior similar to that for gas-water systems.

His experimental results were in agreement with a combination of two proposed flow mechanisms. One was that channel flow did develop during steady-state conditions and the second was that gas flows intermittently with the making and breaking of film interfaces. Experiments with gas tracers indicated that about one-third of the gas was trapped at least for a while but not permanently. This work, together with that of others summarized earlier, suggests that foam flow in porous media is probably more complex than we realize.

The flow of foam through etched-glass micromodels saturated with detergent solution has been described by Mast (1972). These models had thin "pore spaces" somewhat like those of intergranular porous media. Mast found that the proportion of gas and liquid that was moved through these models as foam depended on the stability of the foam and on the porous

medium. With unstable foam the transport of gas and liquid occurs primarily by breaking and regeneration of the foam structures in small pores between larger ones. No liquid channels were observed but some liquid was transported via the Plateau borders.

When the foam is stable, the liquid and gas are transported mainly as foam. Flow through portions of the porous medium can be temporarily blocked by the foam. Foam drainage has a strong effect on foam stability.

In the use of a micellar slug for enhanced oil recovery, a mobility buffer such as a polymer solution must be interspaced between the slug itself and the water which is finally injected. This mobility buffer is necessary in order to avoid viscous fingering into and then destruction of the micellar slug. The cost of polymer is a major component in the economics of the entire process.

The viscous nature of aqueous foam together with its relatively low cost and its miscibility with water suggested this as a possible mobility buffer. If it could also be generated from some of the surfactant in the micellar slug, this would simplify its preparation because an inert, insoluble gas could simply be injected following the micellar slug.

Although work along these lines was carried out by Kamal and first reported in 1970, it was not published in the generally accessible literature until late 1973. In the meantime, a patent had been awarded to Earlougher (1972) for essentially this same process.

Kamal and Marsden (1973) reported that micellar slugs could indeed be displaced by foam in unconsolidated porous media. While secondary recovery of oil by either waterflooding or by a miscible slug followed by foam was about the same in his equipment, a tertiary process after waterflooding by the miscible slug-foam combination lead to additional oil recovery. Because less foaming agent than polymer is required, the process appears to have economic advantages.

An extensive study of foam flow in porous media by Minssieux (1974) was preceded by measurements of the rheology and stability of bulk foam. He found that it was impossible to maintain foam flow in unconsolidated sand packs (50 darcies) ($5 \times 10^{-11} m^2$) one meter long, i.e., he got essentially permanent blocking, but that he could do so in shorter sand packs at even somewhat lower pressure gradients.

X-ray absorption studies on 80 cm long sand packs showed that beyond the first 10 cm or so the liquid saturation in the core is essentially constant at 35% to 45% for foams having qualities ranging from 51% to 96% at injection conditions. He believed that this eliminated the concept that foam advanced as a single fluid in a porous medium. But another interpretation is that a high immobile liquid saturation exists in the porous medium while foam continues to flow as such.

He calculated the viscosity of foam flowing in porous media for qualities ranging from about 50% to about 96% and found that they decreased from about 4 cp ($4 mPa \cdot s$) to less than 1 cp ($1 mPa \cdot s$) at the highest qualities. Not only was the direction of the change of viscosity with quality the opposite of that which he and others found for bulk foam, but it was lower by two orders of magnitude. Clearly there is a major discrepancy here.

Foam drive of oil in a porous medium led first to gas breakthrough (from partial degradation of the foam), then to production of connate water bank, next to production of an oil-in-water emulsion and finally to foam breakthrough. The latter may still contain emulsified oil,

particularly if anionic foamers are used. He found that the overall improvement in recovery by foam drive was not appreciable compared to waterflooding, but it was significant compared to gas drive.

Various abstracts and data bases indicate that considerable work has been done in the USSR on the use of foam in petroleum engineering operations. Abstracts indicated that a good deal is repetitive of that done elsewhere, and also because the field applications have been in unfamiliar areas, there has been little interest in translating it. Two short papers in English translation are those by Evgenev and Turnier (1969) and Evgenev (1974), the first of which has already been noted. In the second paper Evgenev gave data indicating a thixotropic, yield-pseudoplastic behavior although his terminology was different. This study was apparently in connection with subsurface natural gas storage.

6. THE LATTER 1970'S

The use of a foaming agent with injected steam in field application was described by Fitch and Minter (1976). Additional oil beyond that expected from steam alone was apparently recovered at an economical cost. In an addendum to the paper, they mentioned encapsulating the foaming agent in a viscous gel to delay foam formation until the material was well out in the reservoir.

A number of aqueous foams made with anionic and nonionic surfactants were prepared by Kanda and Schechter (1976) and such properties as foaming ability, foam stability and bulk viscosity studied along with several solution properties (surface tension, surface viscosity and wettability). Porous media containing the surfactant solutions were then injected with N_2 gas to generate foam *insitu*. Breakthrough time increased with surface tension and surface viscosity but while displacement efficiency increased with surface viscosity, it decreased with surface tension. Permeability to gas was sensitive to wettability of the system. The presence of salt did not significantly change the results but oil adversely affected the performance.

In another academic study, Aizad and Okandan (1977) described experimental results from the injection of foam into unconsolidated porous media. They believed that their foam flowed as a body and not as the separate components. It behaved like a pseudoplastic fluid with a flow behavior index of about 0.1 for foams made with one surfactant and 0.3 for those made with another. Apparent viscosity, however, did increase with quality. They found that both foams displaced oil from a porous medium better than did water, but also that less of a high quality foam would displace the same amount of oil than would a lower quality foam. Displacement by the latter is, however, faster than by the former.

While Elson and Marsden (1978) were mainly concerned with screening surfactants for extended use at elevated temperatures, they also reported some observations on flow blockage at temperatures only slightly over the boiling point of water. Relative to water saturated porous media, gas flow rate was much less with surfactant solution saturated ones. While the gas flow rate would increase with time, it could be decreased even further than before by injection of more surfactant solution.

In a very extensive patent based on both laboratory work and field tests, Dilgren *et al.* (1978) described the importance of including both noncondensable gas and also an electrolyte (e.g., NaCl) in their steam-foam recipe. Their idea seemed to be to impede steam and oil flow in high permeability-producing channels so they would expand in thickness and thereby produce more oil.

In still another patent Dilgren and Owens (1978) eliminated the steam as such and suggested instead the injection of a hot foam made of aqueous solution, noncondensable gas and surfactant. This process would be used for a less viscous oil than those in reservoirs being produced with steam injection.

The earlier observations of the experimental conditions under which foam would not flow in porous media by Albrecht and Marsden (1970), Kanda and Schechter (1976), and Minssieux (1974) prompted purely theoretical work of Slattery (1979). He found that there was a critical value of the surface tension above which foam cannot be displaced by a given pressure gradient. He concluded that the maximum displacement efficiency occurs when the surface tension was just below this critical value. Also, the displacement efficiency was increased by increasing the surface viscosity as well as the viscosity of the solution itself. These predictions agreed with the published observations of others cited above.

7. THE 1980'S

For the effective application of foam in field tests, the surfactants used must be thermally stable over an extended period of time. This has been tested by Owete *et al.* (1980), who used as the criterion for success not only the chemical stability but also the decrease of gas mobility in porous media containing surfactant, water and displacing gas, relative to those containing only water and displacing gas. At temperatures of 350° to 400° (177° to 205°C) two commercial surfactants -- Suntech IV and Thermofoam BWD -- performed well, while two more were satisfactory, and five additional ones unsatisfactory.

Production by gravity override by foam generated in a two-dimensional, vertical sandpack was observed by Chiang *et al.* (1980). They simulated steam injection by using N_2 gas at ambient temperatures and observed both the displacement front, which could be seen through the clear wall of the model, and breakthrough time. Both liquid recovery and breakthrough time increased when the pack was saturated with surfactant solution instead of just water. Also gravity override was decreased significantly. *In situ* foaming increased with surfactant concentration up to CMC (critical micelle concentration). In one case isobutanol had a favorable affect on a lower molecular weight surfactant (Suntech IV) and an adverse effect on a higher molecular weight one (Suntech IX). In a sandpack initially saturated with a white mineral oil and irreducible water, with a surfactant slug injected prior to N_2 oil recovery was doubled.

Yet another method of generating foam out in the reservoir was patented by Richardson *et al.* in 1980. They listed a number of reactants which would by a change of pH of the system generate N_2 and hence foam in an aqueous solution of surfactant.

For the first twenty years of its use in petroleum engineering, foam was mainly studied as a selective blocking agent for steam used in thermal recovery projects and for underground natural gas storage reservoirs. It was proposed as a blocking agent for liquids in porous media (particularly in patents), but most workers recognized that the liquid would still flow through the foam lamellae. Originally, it was thought that it would be an effective displacing medium for oil because adsorption both on the mineral and oil droplet surfaces as well as dissolution in the oleic phase ruled this out.

With the growing interest in the late 1970's, after much earlier work on the use of carbonated water in floods, attention was focused on using foam as a way of overcoming the major obstacle to CO_2 use on a oil being displaced. The first paper of any significance was that of Bernard *et al.*, which was submitted in mid-1979 and published a year later. Because

the critical temperature of CO_2 is below that of most petroleum reservoirs ($31^\circ C$), there was a temptation to call it a very dense fluid and its dispersions in water an emulsion, but we shall use the terms "vapor" and "foam" here. A good deal of what is said here can therefore be applied to emulsion flow in porous media and vice versa.

Because CO_2 is chemically more reactive in many situations than is steam or hot water as well as being acidic in nature, surfactants had to be selected carefully for their compatibility as well as their effectiveness and long-term stability. While members of all three major surfactant classes were effective, a commercial sulfate ester known as Alipal CD-128 was found to be superior. Its solutions, however, were highly susceptible to acid-promoted hydrolysis, but the products of this decomposition were probably effective in themselves. Its solutions together with CO_2 led to greater mobility reduction in the higher permeability zones just as was the case with foam. A low molecular weight ethoxylated sulfate of unspecified composition was found to have the best combination of chemical stability, low adsorption and high mobility reduction at reservoir conditions, as well as being a good "emulsifier" for CO_2 and water. Permeability reductions would be removed by the passage of several pore volumes of water through the system and hence were not permanent. As was the case with the early work on the use of foam in steam projects, the descriptions were general in nature and no real rheological data was given here.

While some of the chemical conditions for CO_2 injection are more restrictive than for steam injection, the temperatures are generally much lower. Thus different surfactants are needed to produce stable foams and so Bernard and Holm (1980) patented the use of alkyl polyethylene oxide sulfates which are effective under the conditions of low pH, high salinity and relatively high Ca^{++} concentrations. The ratio of ethylene oxide groups to carbon atoms in the alkyl group suggested these surfactants might be better emulsifiers than foamers.

The first results of a field test using a surfactant "encapsulated" in a polymer gel for injection in a steam drive was presented by Eson and Fitch (1981). These preliminary results in the heavy oil, North Kern Front Field of California, were economically promising. At about the same time, the first annual report on this DOE-supported project was also published by Eson *et al.* (1981). In the following year, another progress report was made by Eson *et al.* (1982) with details given in a paper by Eson and O'Nesky (1982).

In connection with the field test just mentioned, laboratory work was carried out elsewhere to learn more about the flow of foam and gas-surfactant solutions in porous media. Some by Owete *et al.* (1982) were on micromodels made of highly regular, uniform channels etched glass plates between uniformly spaced islands. Air-displacing surfactant solution produced bubbles which often extended over several pore spaces. Even in spite of the uniformity of the system, some liquid and some gas was immobilized in the system. Air mobility in this highly artificial system was decreased by a factor of two over that where no surfactant was present.

Laboratory work on some of the expected problems for a field test were reported by Al Khafaji *et al.* (1980). They found that $CaCl_2$ at concentrations of 0.5% and greater and NaCl at concentrations of 2% and greater produced significant degradation of a particular foamer (Suntech IV). They also found there was phase-partitioning into the oil phase but only small adsorption on a quartz sand. The steam mobility was reduced significantly in the presence of surfactant solutions and also the average steam saturation in the saturated steam zone increased as the steam zone grew.

In a paper screening surfactants for use in generating foam in steam injection projects, Dilgren *et al.* (1982) found two necessary ingredients beyond those already recognized. One was the presence of a small amount of a permanent gas such as N_2 in the steam so that there would not be a complete collapse of the foam when the steam condensed. The other was the presence of at least a small amount of NaCl (several percent) which was necessary for the dodecylbenzene sodium sulfonates and the $C_{16} - C_{18}$ alpha olefin sodium sulfonates they studied. They found that the latter yield what they called stronger foams than the former. After laboratory tests in Ottawa sand packs, they used the foamers in a pilot test described later and found both the predicted increased pressure at the injection wells and increased oil production rate.

More laboratory results plus those from field tests were published by Doscher and Hammerschaimb (1982) and then presented in a more detailed report the following year. Details of the laboratory procedures and the results of the tests are given in the paper. Besides the minor effects of KCl and Ca^{++} on foam volume, there was a major effect of crude oil improved the performances of some surfactants, particularly at somewhat elevated temperatures. Tests in sandpacks eliminated most remaining foamers. Corrosion inhibitors had an adverse effect on surfactants. As had Dilgren *et al.* (1982), they found that the presence of a noncondensable gas in the steam was essential. Final laboratory testing in a 16-ft (4.9 m) sandpack indicated that Thermophoam BW-D (Farbest) should be field tested. This was done in five heavy oil fields of California over a period of two years and enhanced recovery found. They believed that besides the increased volumetric conformance expected, there was additional oil recovery from emulsification, lowered interfacial tensions and entrainment of oil droplets in the steam and hot water phase.

Commercial foaming agents are often mixtures of different chemical species of various sorts. Some have simply different hydrocarbon chain lengths resulting from a petrochemical synthesis process or from the occurrence of mixtures in nature and more often than not this enhances their performance. Others have different functional groups [such as those mentioned above in the work of Dellinger *et al.* (1984)] and the combination is better than the sum of the parts. To evaluate the effect of chain length alone, Sharma *et al.* (1982) studied the foaming behavior and other surface chemical properties of mixtures of $C_{12}H_{25}SO_4Na$ and the even C-atom alcohols from C_8 to C_{16} . They found that both breakthrough time and fluid displacement efficiency in sand packs and Berea sandstone were at a maximum when both the alcohol chain length and that of the Na alkyl sulfate were the same. Also at this condition there was a minimum in the surface tension and bubble size, but a maximum in surface viscosity and bubble stability as well as fluid displacement efficiency and breakthrough time.

In later study along these lines, Sharma and Shah (1983) showed that there was a maximum in oil recovery at air-foam breakthrough, at steam-foam breakthrough and at surfactant breakthrough when the alkyl sulfate and alcohol had the same chain lengths. They also reported that for a system made up of $0.005 M NaC_{12}SO_4$ and $0.00005 M C_{12}OH$, the bubble size increased much more rapidly at $80^\circ C$ than at $20^\circ C$.

In a paper that was more like a research proposal than a finished piece of work, Heller *et al.* (1982) discussed the expected performance of a high-pressure CO_2 -in-water "foam" which, because of the low compressibility and high density of CO_2 under these reservoir conditions, behaved more like an emulsion than a foam. For best performance they suggested the aqueous phase content be as low as possible, which would correspond to a high-quality foam, and that the mobility of this "foam" be adjustable to be about that of an oil bank which was expected to be formed.

In work indirectly related to that described here, Blair *et al.* (1982) described how the injection of thin film spreading agents (TFSA) with cyclic steam injection lead to increased oil production. While these are certainly surface active, no mention was made of foam here and in related papers and patents by these authors.

In a progress report on a US DOE-sponsored project for finding suitable surfactants for CO_2 mobility control, Patton *et al.* (1983a) found ethoxylated adducts of C_8 to C_{14} linear alcohols and low molecular weight co-polymers of ethylene oxide and propylene oxide were the most promising. These withstood degradation for two weeks at $125^\circ F$ ($52^\circ C$) but sulfated esters of ethoxylated C_9 - C_{16} linear alcohols did not.

The flow behavior of CO_2 -water foams in capillary tubes of different lengths and diameters was described by Patton *et al.* (1983b). As expected, they could be described by the power law relationship and behaved like pseudoplastic fluids. Apparent viscosities of 10 to 100 cp (10 to 100 $mPa \cdot s$) were reported but unfortunately no K and n values were given. Unlike the much earlier work of Raza and Marsden (1967) and David and Marsden (1969), they did not feel that they had fluid slippage in the capillary tubes. A graph of apparent viscosity vs. quality increased rapidly and went through a maximum at about 95% quality, as would be expected.

While several authors had described over the years the rheological properties of foam, as measured in capillary tubes and concentric cylinder instruments, none gave the elegant theoretical treatment of the subject as did Hirasaki and Lawson (1985). They emphasized the importance of foam texture in determining the nature of the foam flow. Most of their work dealt with the flow of bubbles having radii close to those of the tubes and so foam could not be considered here as a continuum and treated as a fluid. When the bubbles were large compared to the tube radius, the apparent viscosity varied to the 2.5 power and to the 2.0 power when the bubbles were small compared to the tube radius. For uniform-sized foams, the apparent viscosity varied with the -2.0 power of bubble radius small relative to tube radius and the -3.0 power when well explain the differences in results between different laboratories and resolve the different viewpoints on foam vs gas-surfactant solution flow in porous media.

In the final report on a US DOE-sponsored project on mobility control of CO_2 by Heller and Taber (1983), they described results not only for CO_2 -foams but also on polymers dissolved in CO_2 . For the former, they screened more than 60 commercially available surfactants for their suitability but also for their adsorption on reservoir rock samples. For the polymer studies they did not have much success. This report contains a great deal of information which should be studied carefully by new workers in the field. Some were presented in a more accessible source the following year by Heller (1984). Here, he specifically mentioned that the most promising surfactants for CO_2 foams were anionic sulfonate surfactants. He also dwelt on the use of WAG (Water-Alternated-with-Gas) as a means of introducing the components into the reservoir.

The results of extensive field tests carried out on a DOE-sponsored project were presented in a detailed report by Bowman (1983). These were preceded by laboratory work first on surfactant screening and then on steam displacements with surfactants in large porous media. The former included both a mixing test developed by Chevron and also a modification of the refluxing method described by Elson and Marsden (1978). Again the importance of noncondensable gas as well as corrosion inhibitors were recognized along with the desirability of partial rather than complete blocking of steam in highly permeable zones. The five field tests in the Midway-Sunset, Cat Canyon and San Ardo Fields of California either led to production of incremental oil or else lead to other positive benefits.

Another report on a field test described by Eson and O'Nesky (1982) was presented by Brigham *et al.* (1984). They reported no operational problems when injecting surfactant solution and nitrogen gas with steam in the Kern River Field. Tracer studies, injecting profiles, temperatures at the producing wells, logging and well tests all indicated at least qualitatively that steam was effectively diverted toward previously unswept areas. A production response was observed after injection of each slug of surfactant solution.

The necessity of having inert gas such as N_2 along with the steam was reiterated by Duerksen (1984). He also emphasized that the foaming agent must be one that would regenerate foam at flow rates far from the injection well. He found that foamability varied indirectly with temperature and directly with N_2 concentration. He screened 50 commercial and experimental surfactants and found four commercial ones which were particularly good. These were alpha olefin sulfonates which were relatively insensitive to foam liquid volume fraction, had good thermal stability (as did most of the sulfonates) but were somewhat affected by brine. One of his company's proprietary sulfonates was then selected for the field tests described later on.

Unlike most workers studying use of foam for mobility control, Hu *et al.* (1984) felt that it was more profitable to study foam flow in capillary tubes than in sand packs. They recognized that the relative size of bubbles and tubes are important as had others, but a good deal of their work was on flowing lamellae. As the title of their paper indicated, they used alpha-olefin sulfonates for most of their work.

It is well known that mixtures or combinations of more than one surfactant will often be more effective than a single, chemically pure species because while some are more effective in foam generation others are more effective in stabilization. Dellinger *et al.* (1984) carried out screening tests on a large number of surfactants and their combinations and found that both amine oxides and amides improved stability for many anionic surfactants. They recognized, however, that because of chromatographic separation of surfactant mixtures during flow and displacements in porous media, such synergistic effects observed outside porous media are an illusion.

Foams made of CO_2 were studied by Wang (1984) who reported that their stability increased with increasing pressure and decreased with increasing temperature. Their foams deteriorated rapidly when they came in contact with SACROC and Rock Creek crude oils, two candidates for field in use. He found that while his foams improved oil recovery only slightly and that too high a surfactant concentration could generate a rigid foam and lead to lower recovery.

The results of many field tests using thin-film spread agents with steam injection were reported recently by Blair *et al.* (1984). While it is not believed that these act as foaming agents, they are certainly surfactants that are effective in EOR, probably by affecting rock wettability and possibly the properties of the oil-hot water interface. In any event, they reported that 4700 times the volume of oil was recovered as chemical used.

Two very successful field tests based on the laboratory work of Duerksen (1984) described earlier were presented by Ploeg and Duerksen the next year. They found that their proprietary sulfonate both increased oil recovery by steam injection significantly and did so economically. To get proper mixing of the sulfonate and N_2 , they used a "static in-line mixer," which has almost no pressure drop across it. They felt that sulfonate slug injection was an acceptable alternative to continuous injection but were unable to optimize both the amount and frequency of the sulfonate injection. Nor were they able to determine the amount of the non-condensable gas (N_2) to be injected by the results of these tests. Sulfonate concentrations of

Task 29 - INTEVEP shall provide DOE with information from research and screening tests performed by INTEVEP, leading to a field test on steam with additives in Venezuela. The Project Managers shall consult with one another concerning screening tests and exchange information on screening tests previously obtained, to avoid unnecessary duplication of research efforts.

DETERMINATION OF STEAM - WATER RELATIVE PERMEABILITIES
FROM EXPERIMENTALLY OBSERVED PRESSURE PROFILES

Task 29 under the present Annex IV Agreement, calls for INTEVEP to supply DOE with information on research performed leading to a field test on steam with additives in Venezuela.

Venezuela's latest experience on the use of additives with steam is a field test performed in cyclic steam injection wells in the Bolivar Coast. Details of the field test were presented on the SPE Enhanced Oil Recovery Symposium (SPE/DOE paper 14905) held at Tulsa, Oklahoma on April, 1986. At present, INTEVEP's research effort has been addressed to evaluate the influence of the additives on the performance of the field test.

Hereafter follows a summarizing report containing the description of a mathematical model used to simulate steam-water steady state flow through porous media. This model has been used to interpret experimental data in order to evaluate the influence of a surfactant on the steam-water relative permeability curves.

DETERMINATION OF STEAM - WATER RELATIVE PERMEABILITIES
FROM EXPERIMENTALLY OBSERVED PRESSURE PROFILES

(Task 29 of Annex IV of the Implementing Agreement)

Prepared by:

José Luis Ziritt and Freddy Paz

INTEVEP

and

María Elena Barboza and Armando Monsalve

Escuela de Ingeniería Química

Universidad de Los Andes

Los Teques, Venezuela

July 1986

CONTENTS

	Page
SUMMARY	29-5
LIST OF ILLUSTRATIONS	29-6
LIST OF TABLES	29-8
NOMENCLATURE	29-9
INTRODUCTION	29-11
MATHEMATICAL FLOW MODEL	29-14
SIMULATION ALGORITHM	29-18
THEORETICAL SIMULATIONS	29-20
EXPERIMENTAL APPARATUS AND PROCEDURES	29-21
EXPERIMENTAL RESULTS & ESTIMATION OF RELATIVE PERMEABILITIES	29-22
CONCLUSIONS	29-24
REFERENCES	29-25
ILLUSTRATIONS AND TABLES	29-28
APPENDIX A. CORRELATIONS	29-44

SUMMARY

A steam-water steady state flow numerical simulator in one dimensional porous media was used in order to estimate relative permeability curves that describe the flow process. The estimated curves were obtained by trial and error, matching the simulator results with the experimental pressure profiles for the flow in sand packs.

The simulator is based on a mathematical model which considers simultaneous flow of the two phases under steady state conditions and local thermodynamic equilibrium. Heat losses in the direction normal to the flow, as well as the effect of capillary forces are taken into account.

The method was proven to be an adequate tool to generate relative permeability information from experimental data on pressure drops along the porous medium, total mass flow rate, enthalpy at the system inlet and temperature differences between core and surroundings.

The computer simulator was also used to analyze the importance of capillarity during the flow process under a wide range of flow conditions and system parameters, providing qualitative information that can be used to properly design experimental work.

LIST OF ILLUSTRATIONS

	Page
Fig. 1. Steam/water relative permeability curves (2).	29-28
Fig. 2. Steam/water relative permeability curves (20).	29-28
Fig. 3. Steam/water relative permeability curves (5).	29-29
Fig. 4. Steam/water relative permeability curves (5).	29-29
Fig. 5. Steam/water relative permeability curves (5).	29-30
Fig. 6. Simulated saturation profiles.	29-30
Fig. 7. Simulated saturation profiles.	29-31
Fig. 8. Simulated pressure profiles.	29-31
Fig. 9. Simulated saturation profiles.	29-32
Fig. 10. Simulated pressure profiles.	29-32
Fig. 11. Simulated saturation profiles.	29-33
Fig. 12. Simulated pressure profiles.	29-33
Fig. 13. Experimental setup.	29-34
Fig. 14. Fitted steam-water relative permeability curves.	29-34
Fig. 15. Experimental & calculated pressure profiles for the 300 psia steam flow tests.	29-35
Fig. 16. Experimental & calculated pressure profiles for the 200 psia steam flow tests.	29-35
Fig. 17. Experimental and calculated pressure profiles for the 100 psia steam flow tests.	29-36
Fig. 18. Pressure profiles calculated with different relative permeability curves.	29-36
Fig. 19. Calculated saturation profiles for the 306.5 psia steam flow test.	29-37
Fig. 20. Calculated saturation profiles for the 193.2 psia steam flow test.	29-37

	Page
Fig. 21. Calculated saturation profiles for the 117.1 psia steam flow test.	29-38
Fig. 22. Steam/water relative permeability curves in presence of surfactant.	29-38
Fig. 23. Pressure profiles with and without surfactant.	29-39
Fig. 24. Calculated saturation profiles in the presence of surfactant.	29-39

LIST OF TABLES

	Page
Table 1. Results of the 300 psia steam flow tests.	29-40
Table 2. Results of the 200 psia steam flow tests.	29-41
Table 3. Results of the 100 psia steam flow tests.	29-42
Table 4. Results of the steam-surfactant flow tests.	29-43

NOMENCLATURE

- A_c = superficial area, m^2
 A_t = heat transfer Area, m^2
 e = emissivity coefficient, dimensionless
 h = specific enthalpy, Kj/kg
 h_c = convective heat transfer coefficient, $1 \times 10^{-4} \left(\frac{\Delta T}{2r}\right)^{1/4}$, $Kw/m^2 \cdot ^\circ K$
 K = absolute permeability, m^2
 K_{ss} = stainless steel thermal conductivity, $Kw/M \cdot ^\circ K$
 k_e = effective permeability, m^2
 k_r = relative permeability, dimensionless
 \dot{M}_o = total mass flow rate, Kg/s
 P = pressure, Pa
 Q_p = total rate of heat loss, Kw
 R = universal gas constant, $8.134 \text{ KPa} \cdot m^3 / Kg \text{ mole} \cdot ^\circ K$
 r = radius, m
 S = saturations, dimensionless
 T = absolute temperature, $^\circ K$
 t = time, s
 V = specific volume, m^3 / Kg
 v = velocity, m^3 / s
 z = z-direction, m

SUBSCRIPTS

c = capillary
e = external
i = internal
j = component index
L = liquid water (water)
o = total
out= at the outlet
r = residual
s = matrix (sand)
surf=at the surface
V = water vapor (steam)

GREEK

ϕ = porosity
 λ = mobility, (K.kr/M) m²/Pa.s
 μ = dynamic viscosity, Pa.s
 ρ = density, Kg/m³
 σ = $5,6699 \times 10^{-5}$ Kw/m²°K

1. INTRODUCTION

During the last years a considerably amount of work has been done to improve the efficiency of oil recovery methods. Since steamflooding is one of the most efficient ones, very important efforts have been made in order to develop new technologies to reduce the negative effects of gravity override and steam channeling, which affect the efficiency of steamflood projects.

The simultaneous injection of additives and wet steam appears to be an encouraging approach to achieve steam mobility control by developing a foam blockage in the zones of high steam flow ^{6.8.9.10.18.22.23}. Even though the formation of foam fronts and the reduction of steam mobility have been experimentally observed in the laboratory, not many advances have been made in the understanding of the mechanism of the blocking process.

Previous studies on steam-additives injection have concentrated in two areas. First, some authors have looked at the reduction of steam injectivity by observing the process behavior after addition of surfactant during steady state flow conditions. The results have been expressed in terms of the permeability reduction factor, (PRF), which is the ratio of the pressure drop with steam flow alone, to the pressure drop with steam flow in the presence of surfactant. The PRF is a convenient parameter to test the relative efficiency of additives as mobility control agents, but it gives no information on fundamental physical aspects and it is not very useful for design purposes. The second area of study has been the vertical sweep efficiency, which some investigators have been looking at in two-dimensional physical models. In this case, the obtained information has been reported in terms of increased oil recovery, and/or in terms of the modification of the steam front advance pattern, during unsteady state conditions, which some researchers have been able to monitor. Again, this information by itself is not very useful for design purposes but can be included in theories or models for the description of the steam-additive process.

The needed information to properly describe the foam blocking process should probably be concerned with fundamental aspects such as the rheological behavior of the created foam or the modification of the relative permeability curves in the presence of surfactant. To the authors knowledge, there is no reported data on the rheology of steam foams and recent studies on relative permeabilities are unfortunately very scattered and contradictory^{2,5,13,14,15,20}.

If the channel flow concept is assumed to be valid to describe vapor-liquid flow, that is, if the liquid and its vapor move through their own separate network of interconnecting channels, then, the conductivity of a porous medium to each phase can be expressed by the effective permeability of the medium, as defined by Darcy's law⁷. In theory, any standard method can be used to measure the effective permeabilities of simultaneous vapor-liquid flow. Nevertheless, most methods require the measurement of the flow rates of each phase as well as the saturations inside the porous medium^{16,17}, and in the case of steam, measuring flow rates becomes the problem of measuring steam quality, which has been the bottleneck of this kind of work, specially for the flows involved in laboratory flooding tests. Furthermore, saturations in flowing steam systems are also troublesome to measure. Most difficulties in measuring these variables are associated to heat exchange between the flowing steam, the porous medium and the surroundings. The effect of heat transfer on the flow behavior has been pinpointed by previous investigations and it has been demonstrated that the flow pattern inside the porous media is a function of the heat losses to the surroundings¹⁵.

These experimental difficulties are probably the main reason for the apparent differences in the reported relative permeability curves of steam-water systems, as shown in Figures 1 through 5. Obviously, if the steam-water relative permeability curves are not well defined, it would be hard to make any solid conclusion about the effect of the presence of a surfactant.

In order to partially avoid the above difficulties we can use a different

approach, which consists in combining easy-to-get experimental data with computer simulation techniques based on general models for the flow process. Using the conservation equations for mass and energy, it is possible to write a general model for the simultaneous flow of vapor and liquid, provided that the flow channel concept is applicable to the system. The validity of the model depends on the availability of proper relative permeability relationships. A trial and error technique can then be used to match the mathematical simulation results with the experimental data. The fitting parameters will be the relative permeability relationships, and the testing criteria will be the difference between calculated and observed pressure profiles. This method reduces the experimental task to monitoring pressures along the flow system, eliminating the need of measuring individual phase flow rates and saturations inside the porous media.

If the same technique is applied to data obtained in the presence of surfactant, then some insight on the additive effect on the relative permeabilities can be obtained.

2. MATHEMATICAL FLOW MODEL

The continuity equation for two-phase flow of liquid and vapor through an horizontal porous media, can be written as:

$$\frac{\partial}{\partial t} [\phi (\rho_L S_L + \rho_V S_V)] + \nabla \cdot [\rho_L \bar{v}_L + \rho_V \bar{v}_V] = 0 \quad (1)$$

If the system operates under steady state conditions and the flow is one dimensional, then equation (1) reduces to:

$$\frac{d}{dz} [\rho_L \bar{v}_L + \rho_V \bar{v}_V] = 0 \quad (2)$$

which, in an integrated form is:

$$\rho_L v_L + \rho_V v_V = \frac{\dot{M}_o}{A} \quad (3)$$

The velocities in this equation are given by Darcy's law as:

$$v_j = - \left(\frac{k_{ej}}{\mu_j} \right) \frac{dP_j}{dz} \quad (4)$$

where the effective permeabilities are defined as:

$$k_{ej} = K k_{rj} \quad (5)$$

The introduction of equations (5) and (4) into (3), in order to eliminate the velocities and effective permeabilities, results in the following expression which relates the pressure gradients in each phase:

$$- \frac{\rho_L K k_{rL}}{\mu_L} \frac{dP_L}{dz} - \frac{\rho_V K k_{rV}}{\mu_V} \frac{dP_V}{dz} = \frac{\dot{M}_o}{A} \quad (6)$$

For this system, an energy balance under the assumption of negligible heat conduction in the direction of flow is:

$$\frac{\partial}{\partial t} [\phi(\rho_L S_L h_L + \rho_V S_V h_V) + (1-\phi)\rho_S h_S] + \nabla \cdot [\rho_L \bar{v}_L h_L + \rho_V \bar{v}_V h_V] - \nabla \left(\frac{Q\rho}{A_t} \right) = 0 \quad (7)$$

where heat loss from the core to the surrounding environment is given by the following expression, which describes the heat flow by conduction through the core holder, and radiation and convection from its surface:

$$\frac{Q\rho}{A_t} = K_{ss} (T_i - T_{surf}) / \ln(r_e/r_i) = e\sigma (T_{surf}^4 - T_e^4) + h_c (T_{surf} - T_e) \quad (8)$$

With the assumption of steady state conditions and one dimensional flow, then equation (7) can be written as:

$$\frac{d}{dz} (\rho_L v_L h_L + \rho_V v_V h_V) - \frac{d}{dz} \left(\frac{Q\rho}{A_t} \right) = 0 \quad (9)$$

In an integrated form and after introducing Darcy's velocities, the previous equation becomes:

$$- \frac{\rho_L K k_{rL} h_L}{\mu_L} \frac{dP_L}{dz} - \frac{\rho_V K k_{rV} h_V}{\mu_V} \frac{dP_V}{dz} - \frac{Q\rho}{A_t} = \frac{\dot{M}_o h_o}{A} \quad (10)$$

The pressures in each phase are related to each other through the capillary pressure:

$$P_C = P_V - P_L \quad (11)$$

as well as to the vapor pressure and temperature of the system through Kelvin's equation²¹,

$$\ln \left(\frac{P_o}{P_v} \right) = \left(\frac{P_o - P_L}{\rho_L / RT} \right) \quad (12)$$

The mathematical model becomes totally defined by introducing proper expressions for the pressure-temperature equilibrium relationship, the density, enthalpy and viscosity of each phase, the relative permeabilities and capillary pressure vs. saturation relationships, and the definition of saturations:

$$P_o = P_o(T) \quad (13)$$

$$\rho_L = \rho_L(P_L, T) \quad (14)$$

$$\rho_v = \rho_v(P_v, T) \quad (15)$$

$$h_L = h_L(P_L, T) \quad (16)$$

$$h_v = h_v(P_v, T) \quad (17)$$

$$\mu_L = \mu_L(P_L, T) \quad (18)$$

$$\mu_v = \mu_v(P_v, T) \quad (19)$$

$$k_{rL} = k_{rL}(S_L) \quad (20)$$

$$k_{rV} = k_{rV}(S_L) \quad (21)$$

$$P_C = P_C(S_L) \quad (22)$$

$$S_L + S_v = 1 \quad (23)$$

The integration boundary conditions for equations (6) and (10) can be established by taking into account the continuity of the pressure at the outlet of the porous medium, and by fixing the flow condition at the inlet or at the outlet of the system. Pressure continuity is achieved only when the non-wetting phase saturation at the outlet of the porous medium is equal to the residual value, which means that there is a very large saturation gradient at the outlet of the system (and the capillary pressure approaches zero)¹⁹. Thus, the boundary conditions can be expressed as:

$$S_L = 1 - S_{vr} \quad \text{at } z = L \quad (24)$$

and

$$P_L = P_v = P_{out} \quad \text{at } z = L \quad (25)$$

The integration of equations (6) and (10) can be performed by any suitable numerical technique after some algebraic manipulation to separate the dependent variables. In fact, if dP_v/dz is eliminated by direct substitution of (6) into (10), an explicit equation for the liquid pressure gradient is obtained as:

$$\frac{dP_L}{dz} = - \frac{\dot{M}_o}{\rho_L \lambda_L} \cdot \frac{A_t}{A_c^2} \left[\frac{(h_v - h_o)(A_c/A_t) - (Q/\rho_c A_c^2) / (\dot{M}_o A_t^2)}{h_v - h_L} \right] \quad (26)$$

3. SIMULATION ALGORITHM

The previous mathematical model was solved by the following procedure, given the dimensions of the porous medium, the total mass flow rate and enthalpy of the injected steam, the outlet pressure and the proper relationships for equations (13) to (22):

a. The equilibrium temperature and relative permeabilities are calculated from the given relationships and the known boundary conditions at the outlet.

b. The properties of the fluids are calculated from the supplied correlations and assuming the same pressure for both phases (zero capillary pressure) for the initial step.

c. The derivative of the liquid phase pressure with respect to position in the porous medium is calculated from equation (26).

d. The derivative of the vapor phase pressure with respect to position is calculated from equation (6).

e. The two pressure gradients are integrated numerically, using a fourth order Runge-Kutta technique, to obtain the values of the pressures at a new position inside the porous medium.

f. The capillary pressure at the new position is obtained from the capillary pressure definition (11).

g. The Kelvin equation (12) and the equilibrium relationship (13) are simultaneously solved to obtain the new vapor pressure and temperature.

h. The saturations and permeabilities are then calculated at the new position.

i. The calculation procedure is repeated from step b until the inlet of the system is reached.

Appendix A presents the set of correlations used for the vapor pressure vs. temperature relationship, the densities, enthalpies and viscosities of each phase, and the capillary pressure vs. saturation relationship.

4. THEORETICAL SIMULATIONS

In order to test the suitability of the computer model, several runs were made in order to predict the pressure profiles and saturations along an hypothetical porous medium. For this purpose, two previously reported sets of relative permeability curves were used, which are included in Appendix A. All of the simulations were performed keeping constant the following parameters:

Core length:	30.0 cm
Core diameter:	3.8 cm
Porosity:	0.35
Inlet steam quality:	0.80
Mean temperature difference between the core and the surroundings:	5 °F

Figures 6 through 12 present typical saturation and pressure profiles obtained by simulation under different flow rates, pressure levels and absolute permeabilities.

These results indicate that, for typical dimensions and characteristics of cores used in the laboratory, capillary forces are important and should not be neglected during the analysis of experimental data. As previously observed for gas-liquid systems, the importance of capillarity is reflected in a very sharp increase of wetting phase saturation towards the outlet of the system. The relative magnitude of this non-homogeneous saturation profile is reduced by increasing the total flow rate, (Figures 7 and 9), by reducing the absolute working pressure, (Figures 7 and 11), or by reducing the absolute permeability (Figures 6 and 9).

5. EXPERIMENTAL APPARATUS AND PROCEDURES

The experimental arrangement shown in Figure 13 was used to obtain pressure profiles during the steady state flow of wet steam water through unconsolidated sand packs. ATICA sand, (92% quartzs, 4% AL_2O_3 and 4% Fe_2O_3) was packed by vibration into a 30 cm long, 3.8 cm internal diameter stainless steel core holder, given a 0.34 porosity sand pack with an absolute permeability of 4 darcies. The experimental procedure consisted of first saturating the porous media with water and then heating the whole system to a temperature of about the boiling point of water at a pre-established outlet pressure. Superheated steam was then generated by circulating water through a generator (20 °C superheating) and allowed it to flow into the sand pack simultaneously with a stream of liquid water at a flow rate enough to obtain 80% quality saturated steam. The flow through the cell was monitored by reading pressure and temperature at the inlet, outlet and at three points through the porous medium. The total flow rates were carefully measured at the inlet and outlet of the system. The experimental data finally obtained and used to feed the simulator, corresponded to the values gathered once the steady state condition was achieved, as indicated by constancy of the measured variables.

6. EXPERIMENTAL RESULTS AND ESTIMATION OF RELATIVE PERMEABILITIES

The obtained experimental pressure profiles are presented in Tables 1 through 3. Starting with a polynomial which represented Martin's relative permeability curves, the simulator was used to obtain by trial and error the coefficients of third order polynomials for permeability versus liquid saturation, which gave, in the average, the calculated pressure profiles closest to the experimental ones. The obtained equations were the following:

$$K_{rL} = 0.489285 - 3.98495 S_L + 8.955563 S_L^2 - 2.967175 S_L^3 \quad (27)$$

$$K_{rV} = 2.50995 - 0.35611 S_L - 11.2325 S_L^2 + 8.678125 S_L^3 \quad (28)$$

In Figure 14 we present these equations for the saturation range predicted by the simulations. The fitted experimental pressure profiles are presented in Figures 15 to 17 and, for comparison, Figure 18 shows the pressure profiles that are predicted by using the permeability relationships reported by Martin and Council. This last figure indicates that none of these two permeability relationships represent the flow characteristics of the studied system while the obtained empirical correlations give a suitable representation of the experimentally observed pressures.

The saturation profiles for some of the experiments, calculated using the above polynomials, are presented in Figures 19 to 21. We can observe that capillary end effects are important in all cases.

To verify the sensitivity of the method to changes in the relative permeability curves arising from the presence of additives, an experimental run was made using 80% quality steam with an ionic commercial surfactant (0.5% w of the liquid phase). The experimental data is presented in Table 4.

Following the same procedure as before, the relative permeability equations for the system were found to be:

$$K_{rL} = -0.38303 - 2.35624 S_L - 4.80944 S_L^2 + 3.32352 S_L^3 \quad (29)$$

$$K_{rV} = 0.27199 - 0.39845 S_L + 0.12498 S_L^2 \quad (30)$$

These relationships are graphically presented in Figure 22 and comparing with Figure 14, it is noticed that the presence of the surfactant drastically reduces the relative permeability to the vapor phase and shifts the liquid permeability curve toward higher saturation values. Figure 23 shows the corresponding pressure profiles when the surfactant material is added to the system, while Figure 24 presents the calculated saturation profiles. An important reduction in the capillary end effect is observed (very uniform saturation profile).

7. CONCLUSIONS

The computer simulator implemented in this work properly describes the qualitative aspects of the wet steam flow process in a porous medium, as indicated from the expected behavior of pressure profiles and saturations under typical conditions. The hypothetical simulations using relative permeability data from the literature have shown that the capillary end effect is more important at lower flow rates. This is the result of an increase in the relative importance of capillary forces with respect to viscous forces, as velocity is reduced. Finally, the reduction in importance of capillarity, as the total pressure of the system is lowered, was also verified by the simulator.

Furthermore, the computer model was used to generate relative permeability curves that properly represented wet steam flow conditions in porous media. The technique was tested for steam flow in the presence and absence of surfactant, and we verified previously reported observations about reduction of both phases relative permeabilities when a surfactant is present.

REFERENCES

- 1) ARAUJO, H.: "Effect of Steam Quality on Flow Through a Porous Media and Oil Recovery". M.A. Thesis. Pennsylvania State Univ., (1968).
- 2) ARIHARA, N.: "A Study of Non-Isothermal Single and Two-Phase Flow Through Consolidated Sandstones". PhD Thesis, Stanford University, (1974).
- 3) CHOU, J.C.S. and ROWE, A.M.: "Entalphies of Aqueous Sodium Chloride Solutions". Desalination 6: 105-115, (1969).
- 4) COLLINS, R.E.: "Flow of Fluids Through Porous Materials". The Petroleum Publishing Co., (1976).
- 5) COUNSIL, J.R.: "Steam-Water Relative Permeability". PhD Thesis, Stanford University, (1979).
- 6) DILGREN, R.E., HIRASAKI, G.D., HILL, H.J., and WHITTEN, D.G.: "Steam-Channel-Expanding Steam Foam Drive". U.S. Patent 4,086,964, (1978).
- 7) DULLIEN, F.A.L.: "Porous Media. Fluid Transport and Pore Structure". Academic Press, (1979).
- 8) ELSON, T., MARSDEN, S.S. and GUPPY, K.: "Literature Review of the Selective Blockage of Fluids in Thermal Recovery Projects". Supri-TR-3, Stanford University Petroleum Reseach Institute, Stanford, California, (1977).
- 9) ESON, R.L. and FITCHI, J.P.: "North Kern Front Field Steam Drive with Ancillary Materials". SPE/DOE Paper 9778, (1981).
- 10) FERRER J.C., COLINA, J.U. y D'ORAZIO, F.: "Factibilidad de Procesos No Convencionales para el Recobro Adicional de Petróleo". VI Jornadas

Técnicas de Petróleo. Instituto de Investigaciones Petroleras de LUZ. Maracaibo, (1979).

- 11) FRIED, A.N.: "The Foam-Drive Process for Increasing the Recovery of Oil", USBM Dept. of Investigations, Report 5866, (1961).
- 12) JUZA, J. and MARES, R.: "Equation of State for Saturated and Superheated Steam". In Proceedings 9th Intern. Conf. on the Properties of Steam. Ed. by J. Straub and K. Scheffler. Pergamon Press, Elmsford: 91-97, (1980).
- 13) MARTIN, J.C.: "Analysis of Internal Steam Drive in Geothermal Reservoirs". JPT XXVII: 1493-1499, (1975).
- 14) MONSALVE, A.: "Gas-Liquid and Vapor-Liquid Flow in Porous Media in the Presence of Surfactant". PhD Dissertation, University of Texas at Austin, (1985).
- 15) MONSALVE, A., SCHECHTER, R.S. and WADE, W.H.: "Relative Permeabilities of Surfactant/Steam/Water Systems". SPE Paper 12261, (1984).
- 16) MORSE, R.A., TERWILLIGER, P.L., and YUSTER, S.T.: "Relative Permeability Measurements on Small Core Samples". Oil & Gas J. 109: 109-125, (1947).
- 17) OSOBA, J.S. et al: "Laboratory Measurement of Relative Permeability" Pet. Trans. 192: 47-56, (1951).
- 18) RANCEL, C. and ZIRITT, J.L.: "Literature Survey on Foaming Agents for Enhanced Oil Recovery". DOE/BC-84/6/SP: 12A1-12A91, (1984).
- 19) RICHARDSON, J.G. et al: "Laboratory Determination of Relative Permeability". Pet. Trans. AIME 195: 187-196, (1952).
- 20) TRIMBLE, A.E., and MENZIE, D.E.: "Steam Mobility in Porous Media". SPE

Paper 5571, (1975).

- 21) UDELL, K.S.: "The Thermodynamics of Evaporation and Condensation in Porous Media". SPE Paper 10779, (1982).
- 22) ZIRITT, J.L. y PAZ, F.: "Inyección de Vapor con Aditivos. Prueba Piloto en el Campo Pirital". INTEVEP, S.A., (1985).
- 23) ZIRITT, J.L., PAZ, F. y RANCEL, C.: "Inyección de Vapor con Agentes Espumantes", I SIREMCRU, Maracaibo, (1985).

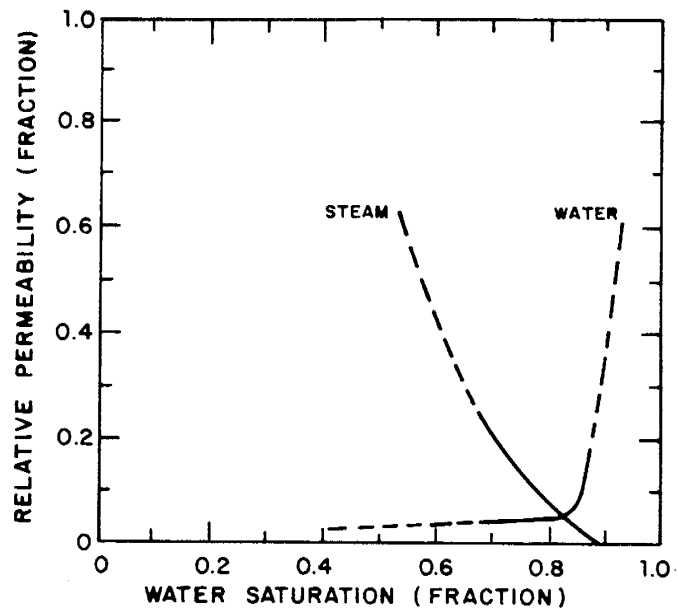


Fig. 1 STEAM/WATER RELATIVE PERMEABILITY CURVES²

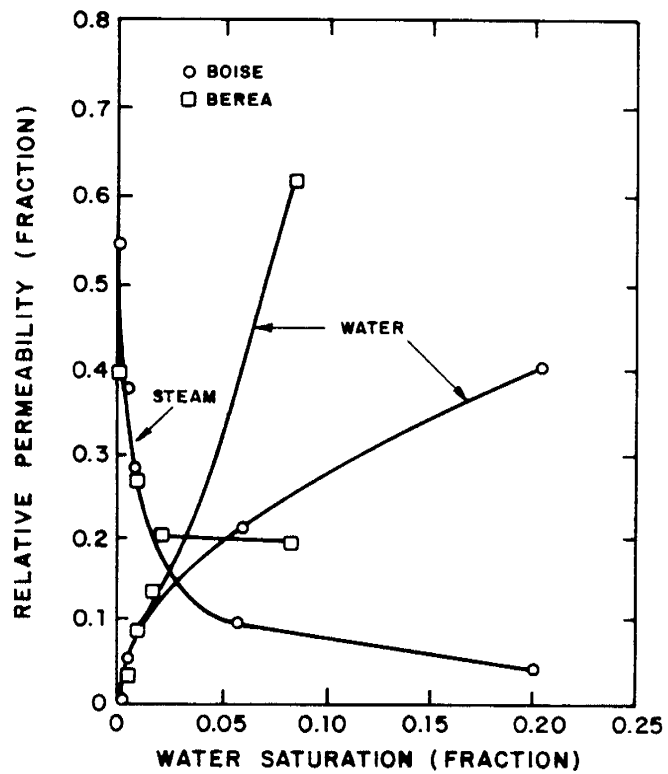


Fig. 2 STEAM/WATER RELATIVE PERMEABILITY CURVES²⁰

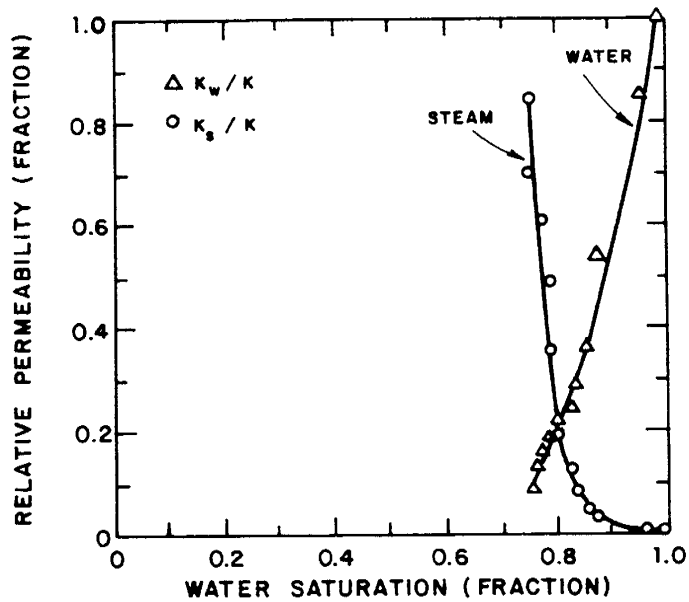


Fig. 3 STEAM/WATER RELATIVE PERMEABILITY CURVES⁵

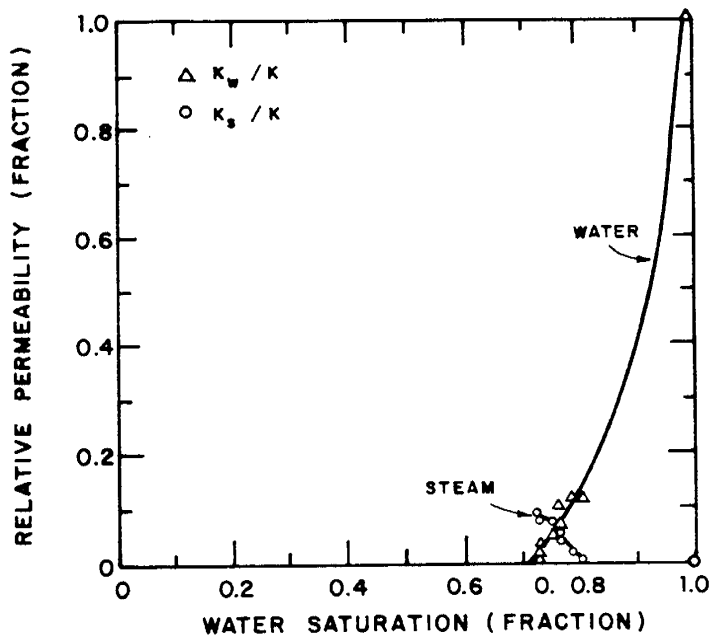


Fig. 4 STEAM/WATER RELATIVE PERMEABILITY CURVES⁵

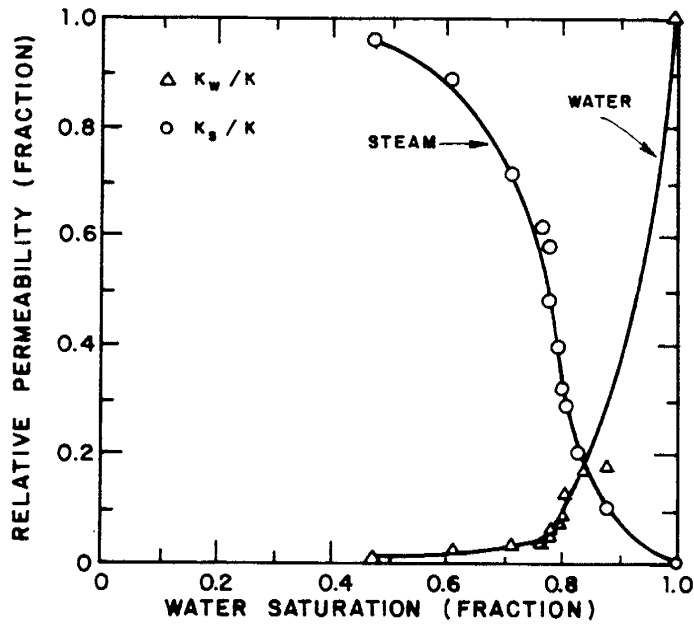


Fig. 5 STEAM/WATER RELATIVE PERMEABILITY CURVES⁵

POUT = 50 psia $\beta = 20\%$
 Mo = 1 gr/min K = 0.5 D

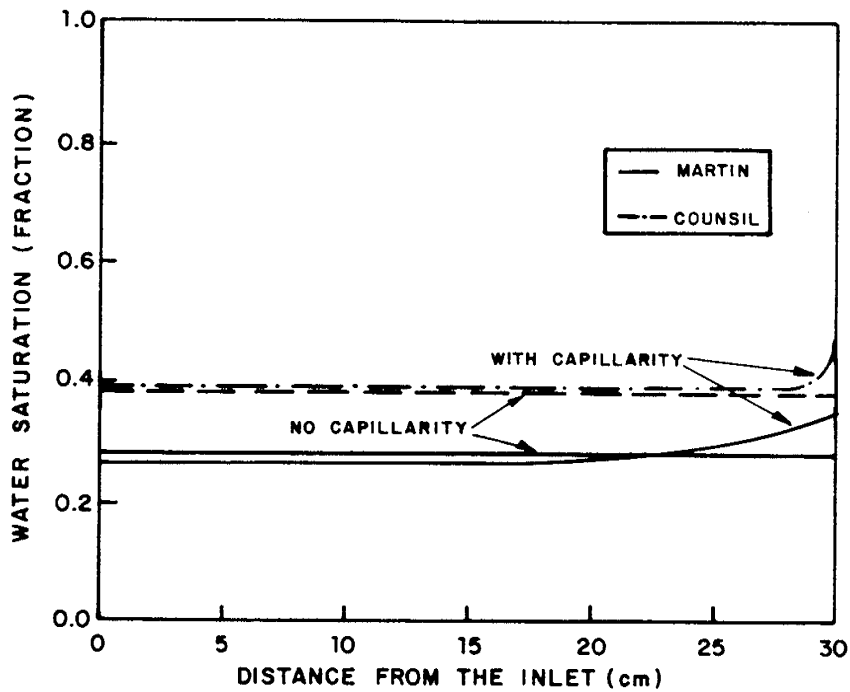


Fig. 6 SIMULATED SATURATION PROFILES

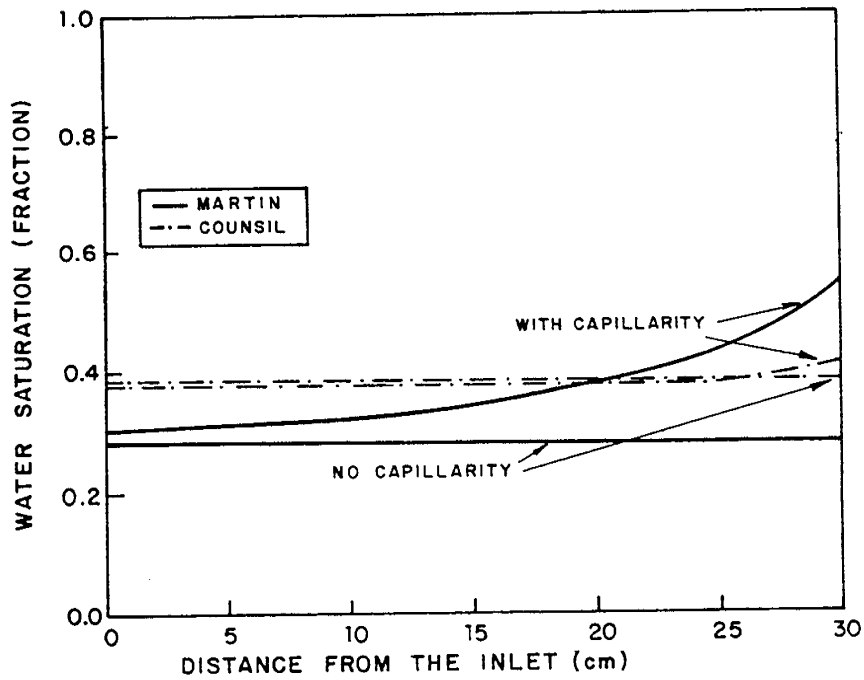


Fig. 7 SIMULATED SATURATION PROFILES

POUT = 50 psia $\phi = 35\%$
 Mo = 2 gr/min K = 4D

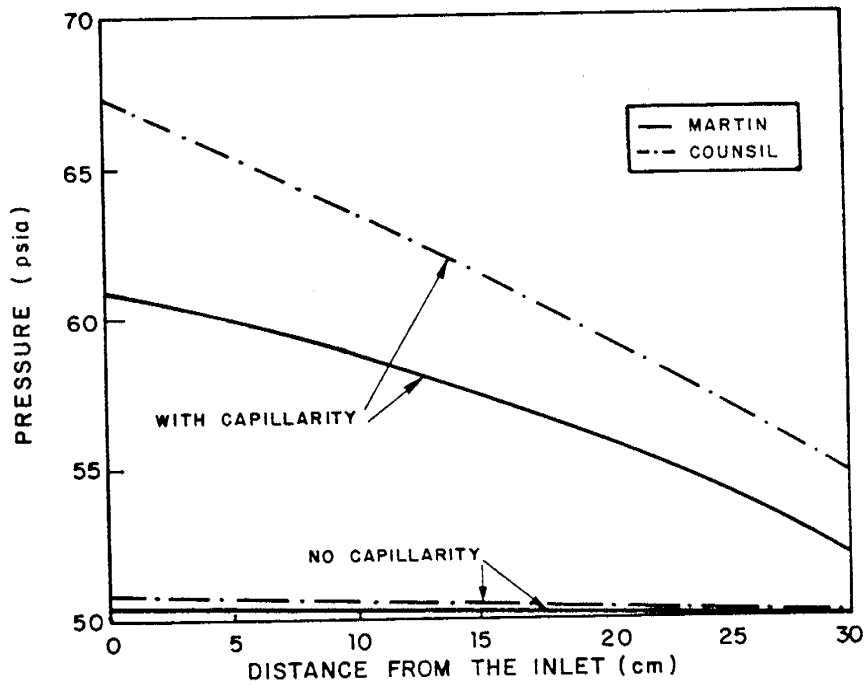


Fig. 8 SIMULATED PRESSURE PROFILES

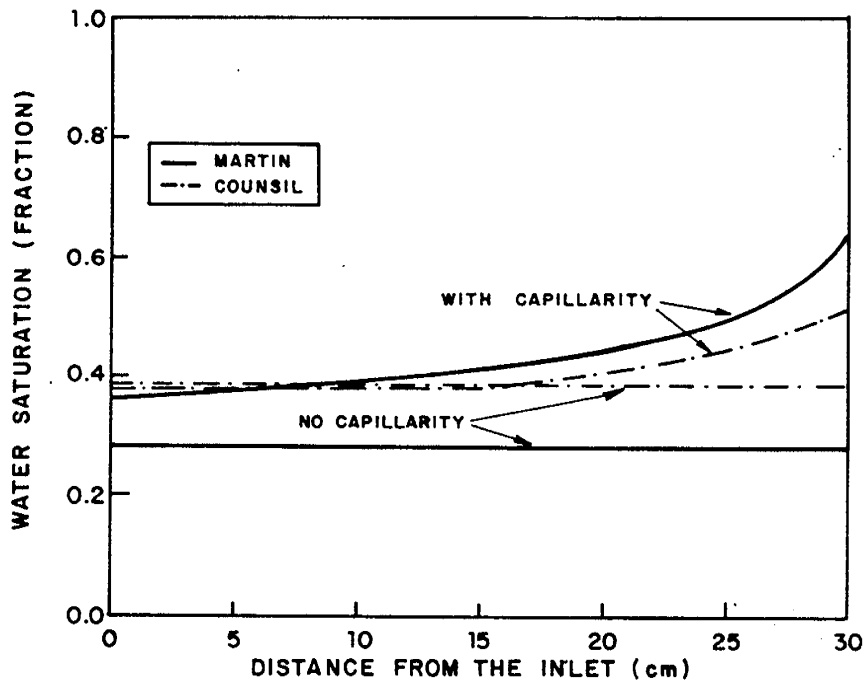


Fig. 9 SIMULATED SATURATION PROFILES

$P_{OUT} = 50 \text{ psia}$ $\phi = 35\%$
 $M_o = 1 \text{ gr/min}$ $K = 40$

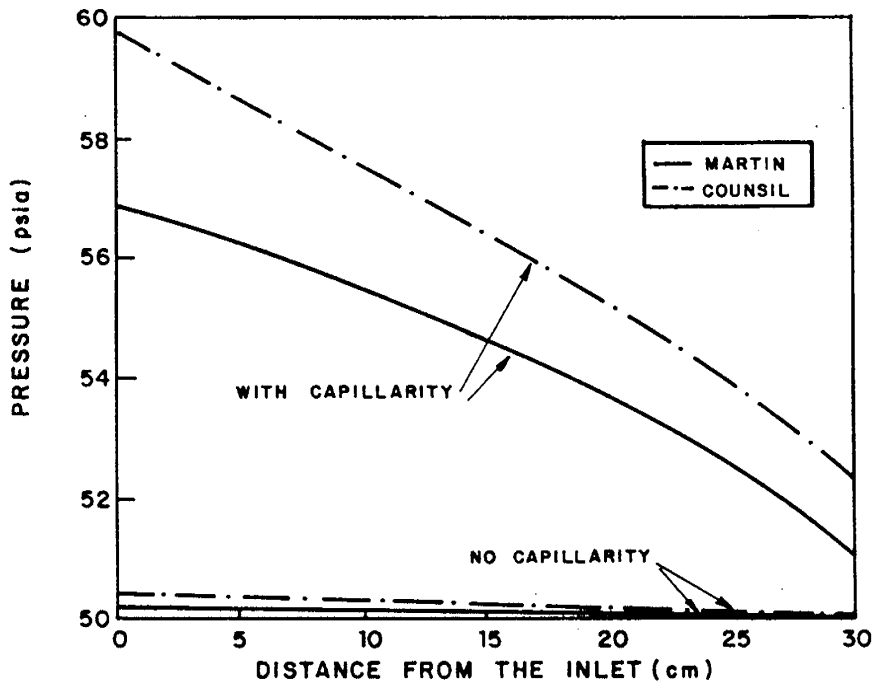


Fig. 10 SIMULATED PRESSURE PROFILES

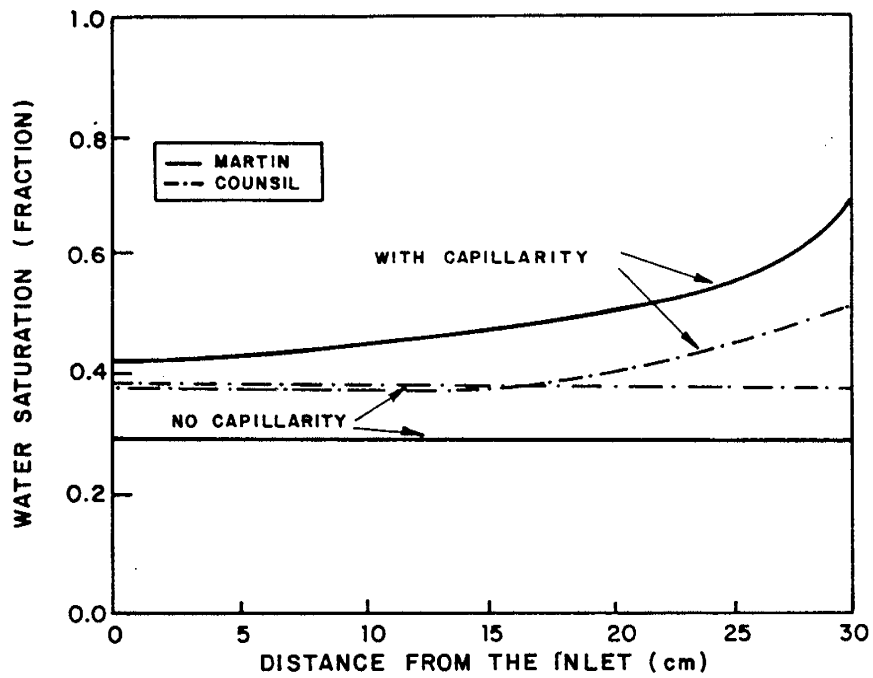


Fig. 11 SIMULATED SATURATION PROFILES

POUT = 100 psia $\phi = 35\%$
 Mo = 2 gr/min K = 40

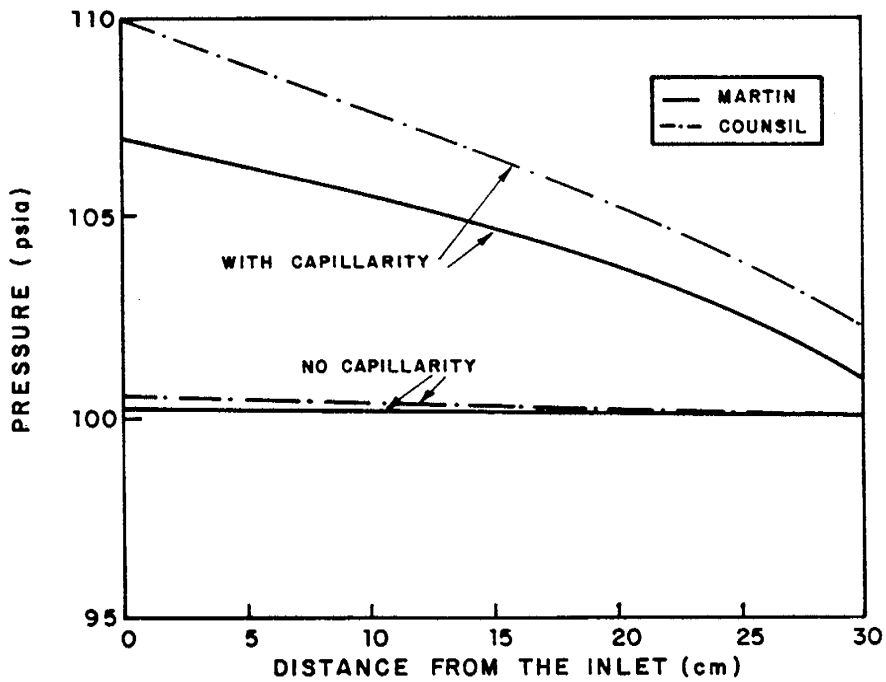


Fig. 12 SIMULATED PRESSURE PROFILES

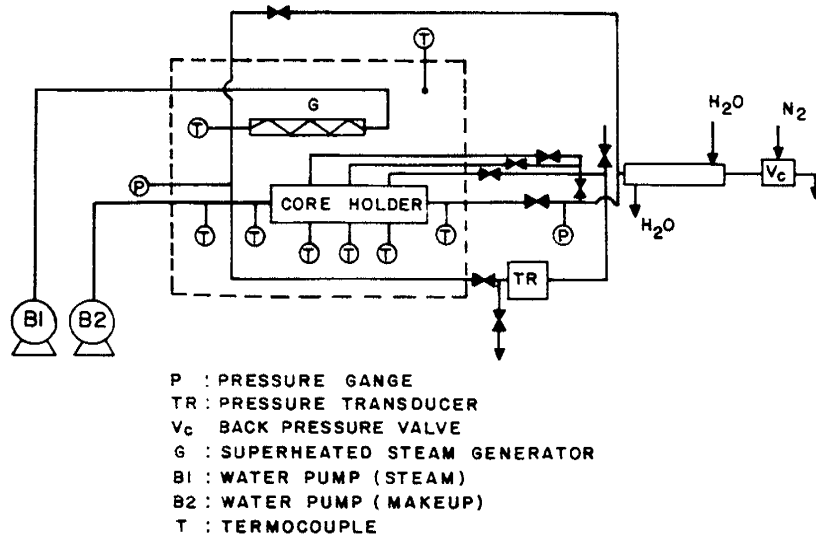


Fig. 13 EXPERIMENTAL SETUP

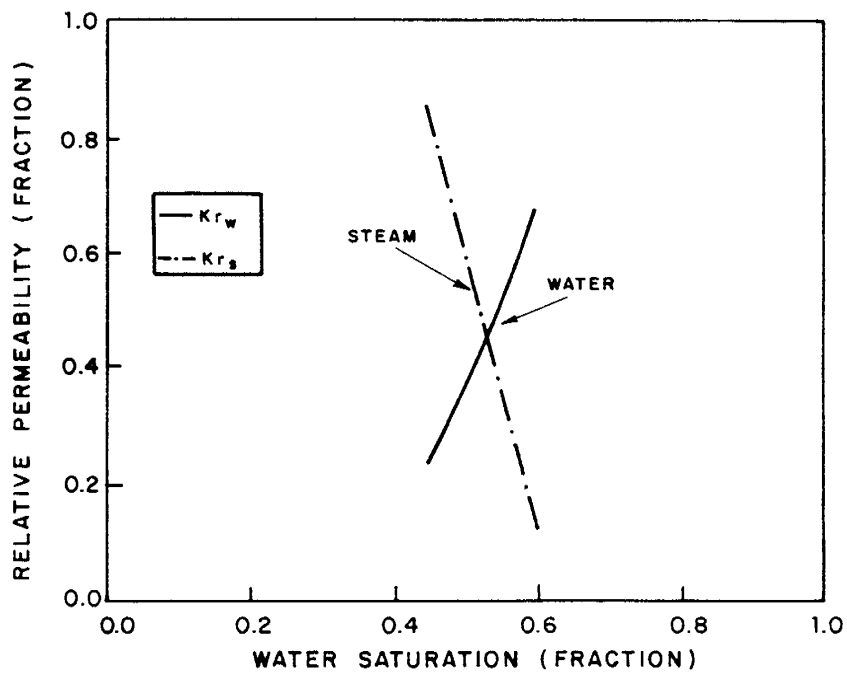


Fig. 14 FITTED STEAM/WATER RELATIVE PERMEABILITY CURVES

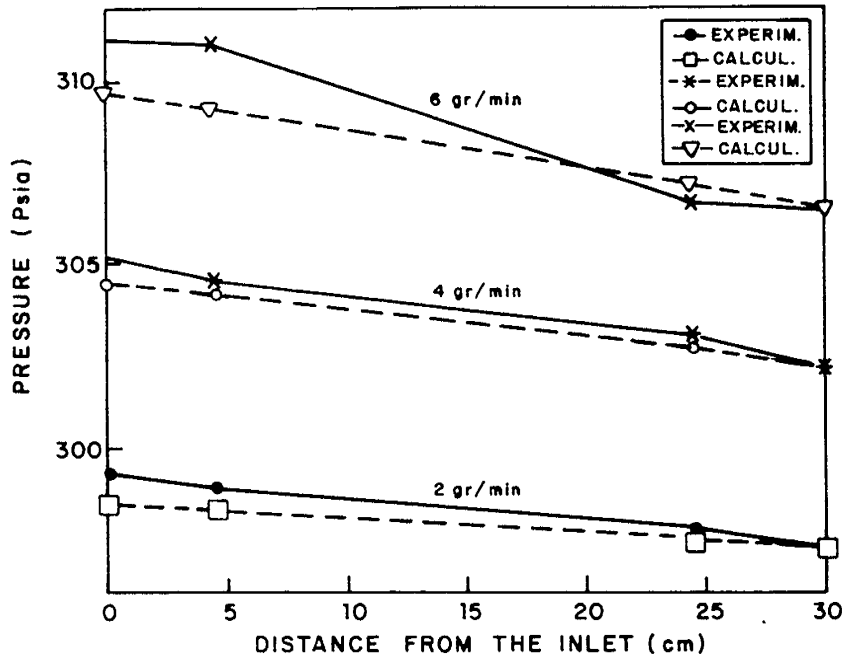


Fig. 15 EXPERIMENTAL AND CALCULATED PRESSURE PROFILES FOR THE 300 psia TESTS.

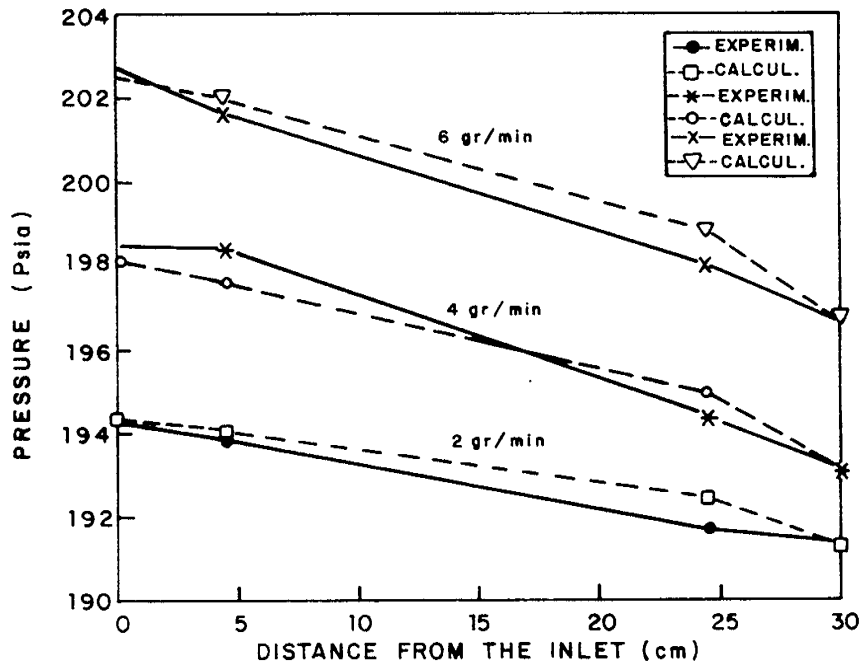


Fig. 16 EXPERIMENTAL AND CALCULATED PRESSURE PROFILES FOR THE 200 psia TESTS.

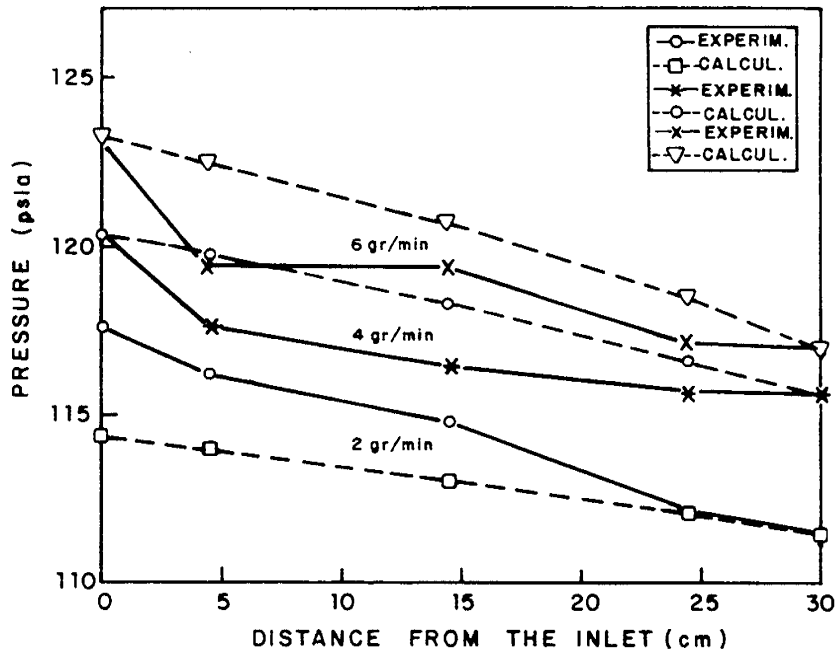


Fig. 17 EXPERIMENTAL AND CALCULATED PRESSURE PROFILE FOR THE 100 psia TESTS.

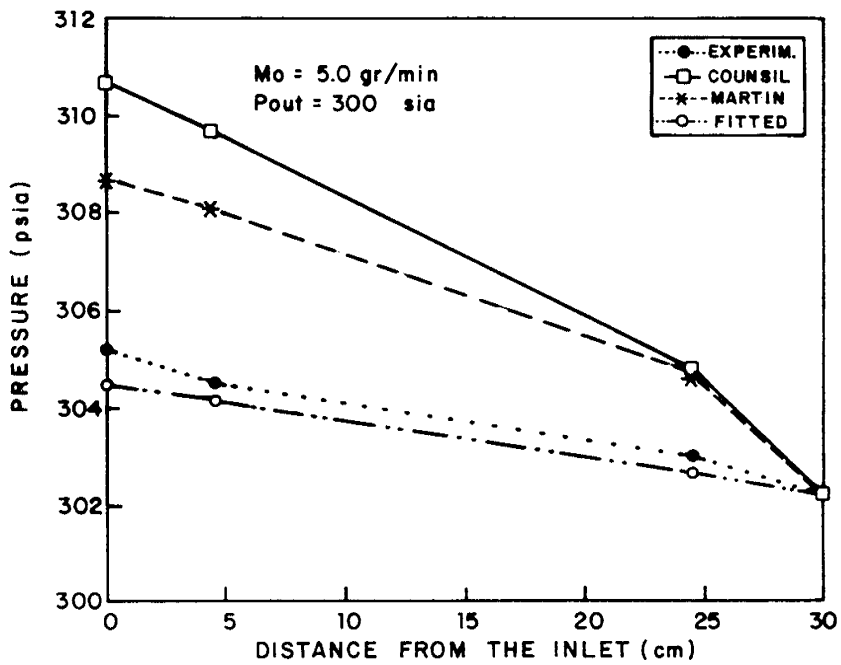


Fig. 18 PRESSURE PROFILES CALCULATED WITH DIFFERENT RELATIVE PERMEABILITY CURVES

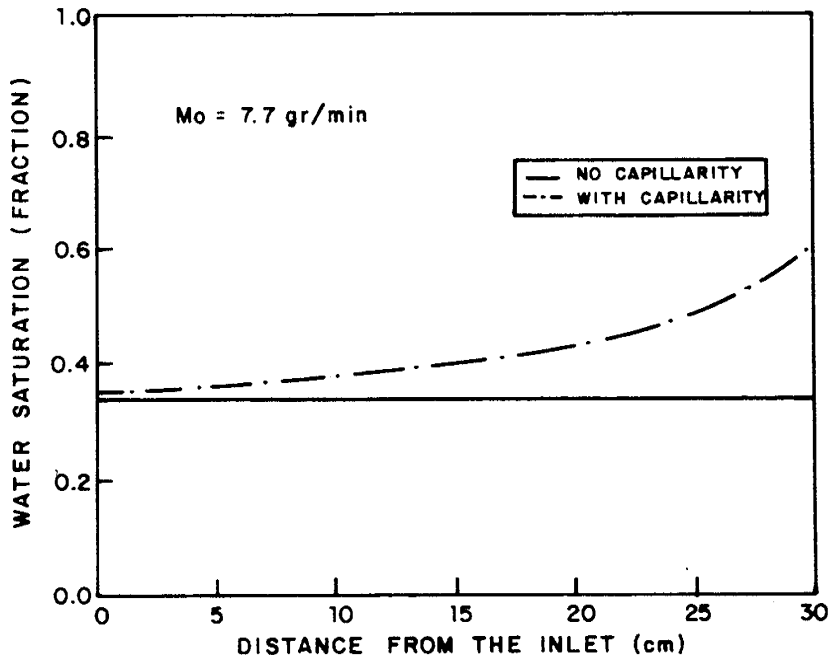


Fig. 19 CALCULATED SATURATION PROFILE FOR THE 306.5 psia TESTS.

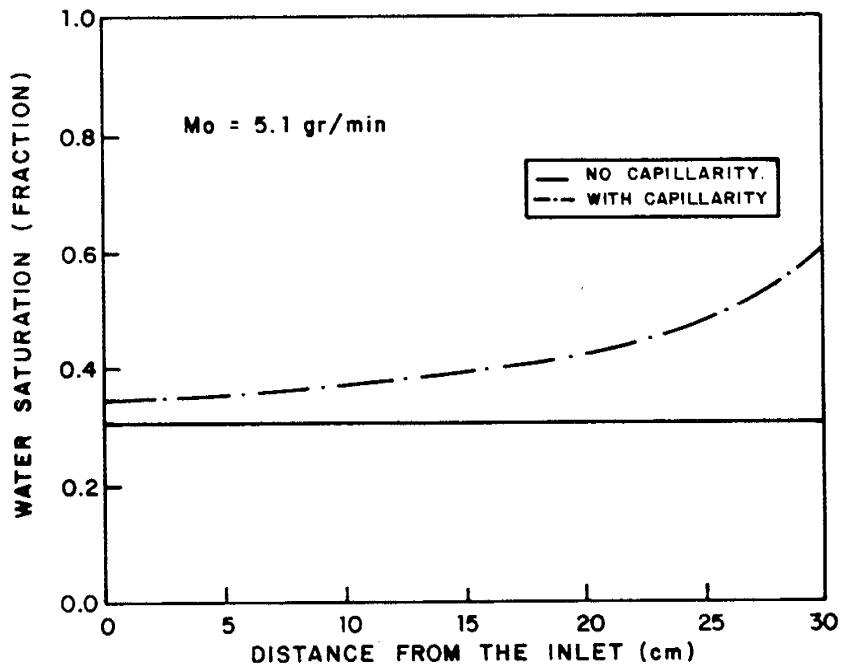


Fig. 20 CALCULATED SATURATION PROFILES FOR THE 193.2 psia TESTS.

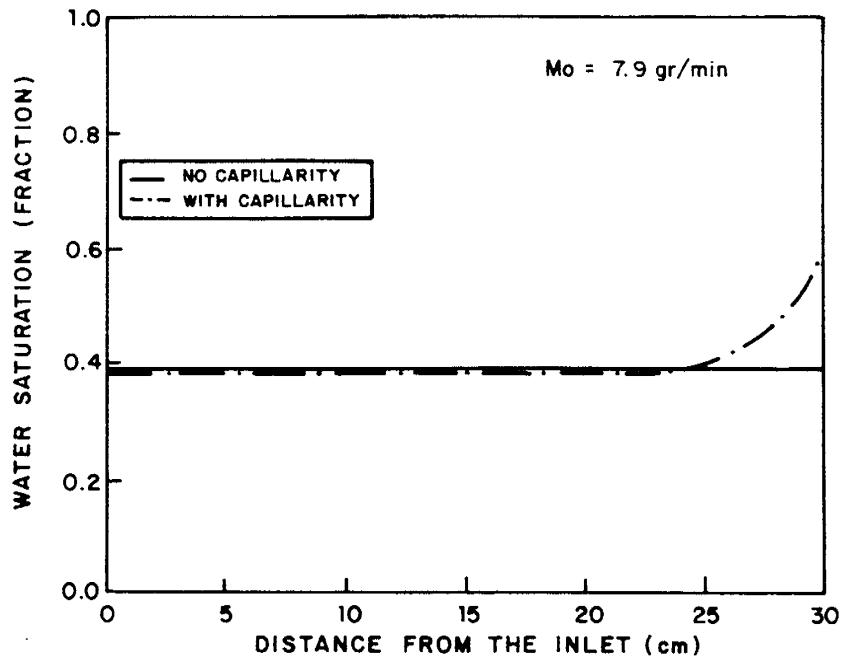


Fig. 21 CALCULATED SATURATION PROFILES FOR THE 117.1 psia TEST

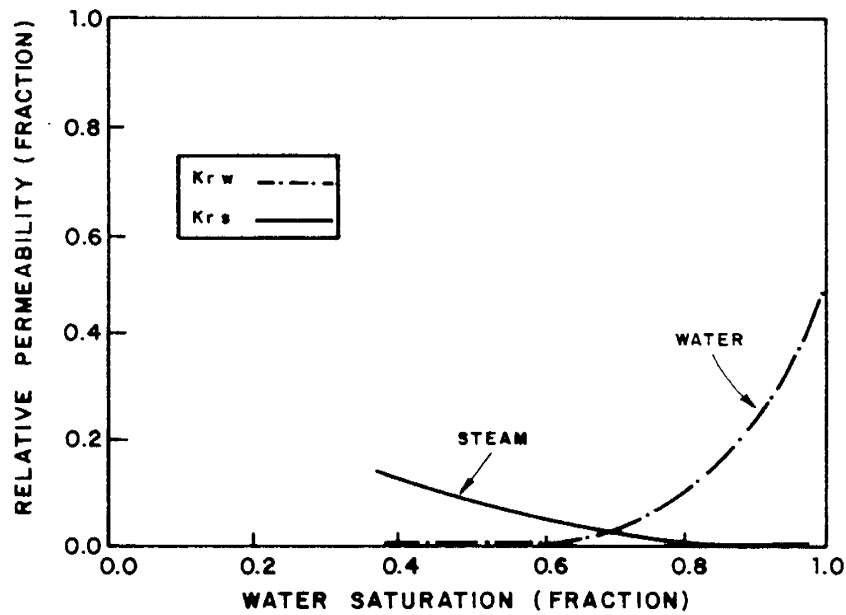


Fig. 22 STEAM/WATER RELATIVE PERMEABILITY CURVES IN PRESENCE OF SURFACTANT.

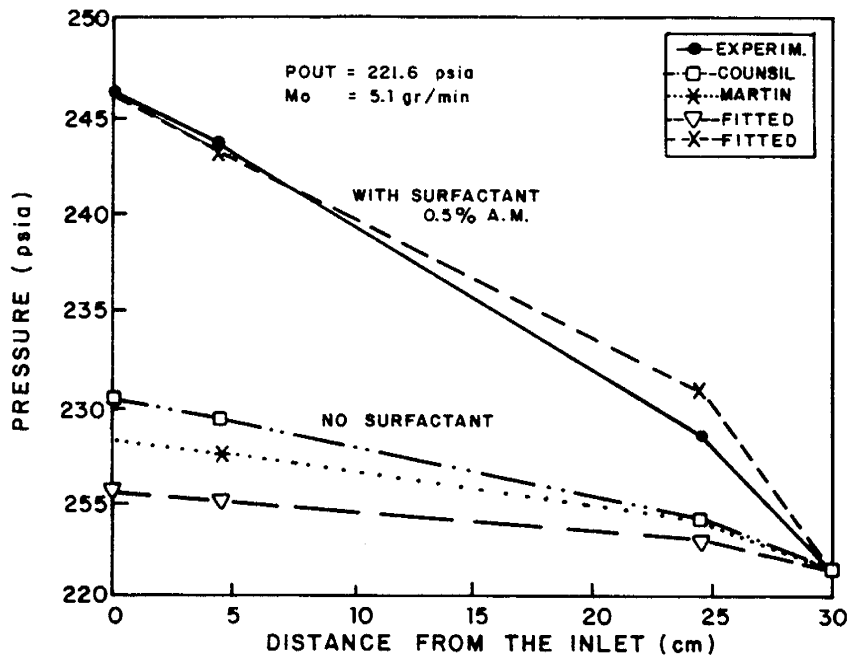


Fig. 23 PRESSURE PROFILES WITH AND WITHOUT SURFACTANT.

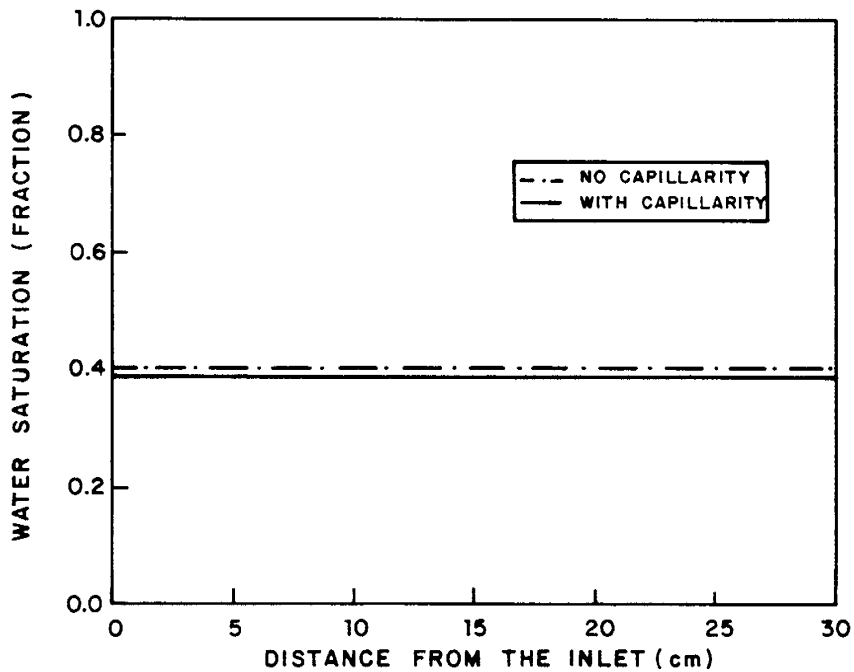


Fig. 24 CALCULATED SATURATION PROFILE IN THE PRESENCE OF SURFACTANT.

TABLE 1. Results of the 300 psia steam flow tests.

Mass Flow Rate (g/min)	Position (cm)	P _{Exp} (psia)	P _{Counsil} (psia)	P _{Martin} (psia)	P _{Calcul} (psia)
2	0.0	299.32	302.29	301.41	298.44
	4.5	298.94	301.72	301.02	298.27
	24.5	297.77	298.81	298.89	297.45
	30.0	297.22	297.22	297.22	297.22
4	0.0	305.22	310.69	308.72	304.48
	4.5	304.53	309.70	308.08	304.18
	24.5	303.04	304.79	304.69	302.70
	30.0	302.24	302.24	302.24	302.24
6	0.0	311.24	318.41	315.08	309.72
	4.5	311.02	316.92	314.21	309.28
	24.5	306.74	309.94	309.67	307.15
	30.0	306.46	306.46	306.46	306.46

TABLE 2. Results of the 200 psia steam flow tests.

Mass Flow Rate (g/min)	Position (cm)	P _{Exp} (psia)	P _{Council} (psia)	P _{Martin} (psia)	P _{Calcul} (psia)
2	0.0	194.21	197.27	196.17	194.30
	4.5	193.90	196.62	195.73	194.05
	24.5	191.76	193.23	193.26	192.49
	30.0	191.41	191.40	191.40	191.40
4	0.0	198.44	204.45	201.53	198.08
	4.5	198.40	203.07	200.71	197.61
	24.5	194.42	196.56	196.35	195.00
	30.0	193.22	193.22	193.22	193.22
6	0.0	202.74	211.05	206.82	202.52
	4.5	202.66	209.25	205.80	201.95
	24.5	298.07	200.87	200.51	198.83
	30.0	196.72	196.71	196.71	196.71

TABLE 3. Results of the 100 psia steam flow tests.

Mass Flow Rate (g/min)	Position (cm)	P _{Exp} (psia)	P _{Counsil} (psia)	P _{Martin} (psia)	P _{Calcul} (psia)
2	0.0	117.62	121.64	119.12	114.35
	4.5	116.22	120.44	119.39	113.98
	14.5	114.82	117.76	116.60	113.10
	24.5	112.22	114.60	114.42	112.12
	30.0	111.52	111.52	111.52	111.52
4	0.0	120.47	132.36	127.18	120.35
	4.5	117.62	130.26	126.02	119.75
	14.5	116.43	125.48	123.25	118.31
	24.5	115.77	120.44	120.00	116.68
	30.0	115.62	115.62	115.62	115.62
6	0.0	123.385	139.67	132.03	123.38
	4.5	119.530	136.82	130.48	122.58
	14.5	119.330	130.25	126.88	120.69
	24.5	117.143	123.34	122.72	118.51
	30.0	117.055	117.05	117.05	117.05

TABLE 4. Results of the steam-surfactant flow test.

Mass Flow Rate (g/min)	Position (cm)	P _{Exp} (psia)	P _{Counsil} (psia)	P _{Martin} (psia)	P _{Calcul} (psia)	P _{w/surf.} (psia)
2	0.0	239.85	242.45	241.42	239.58	251.14
	4.5	238.99	241.84	240.98	239.32	249.53
	24.5	237.18	238.53	238.57	237.83	242.27
	30.0	236.75	236.75	236.75	236.75	236.75
4	0.0	246.12	230.38	228.30	225.58	246.10
	4.5	243.60	229.34	227.65	225.19	243.35
	24.5	228.79	224.24	224.12	223.04	230.88
	30.0	221.56	221.56	221.56	221.56	221.56

APPENDIX A. CORRELATIONS

A.1 Liquid water properties³

A.1.1. Water density

The density of water can be calculated as the inverse of the specific/volume, and this is given by the expression:

$$V_L = 10^{-3} (A - BP - CP^2) \quad V_L = 10^{-3} (A - BP - CP^2)$$

where P is the pressure in psi and A, B and C are temperature dependent coefficients defined as follows:

$$A = A_1 - A_2T + A_3T^2 - (A_4/T) + (A_5/T^2)$$

$$B = -B_1 + B_2T - B_3T^2 + (B_4/T) - (B_5/T^2)$$

$$C = C_1 + C_2T$$

and the constant parameters are:

$$A_1 = 5.916365$$

$$B_1 = 0.52049144 \times 10^2$$

$$A_2 = 1.0357941 \times 10^{-2}$$

$$B_2 = 0.10482101 \times 10^{-4}$$

$$A_3 = 9.2700482 \times 10^{-6}$$

$$B_3 = 0.83285321 \times 10^{-8}$$

$$A_4 = 1.1275221 \times 10^3$$

$$B_4 = 1.1702939$$

$$A_5 = 1.006741 \times 10^5$$

$$B_5 = 1.0227831 \times 10^2$$

$$C_1 = 0.11854697 \times 10^{-7}$$

$$C_2 = 0.65991434 \times 10^{-10}$$

A.1.2 Water enthalpy

The enthalpy of water is given by:

$$h_L = (0.166807 \times 10^{-3} T^2 + 0.930556 T - 24.5765) / 4.03031 \times 10^{-4}$$

where h_L is in Joules/kg and T in °F.

A.1.3 Water viscosity

The viscosity of water is obtained through the empirical equation:

$$\mu = (0.182143 \times 10^{-4} \times T^2 - 6.5464 \times 10^{-3} + 0.7555) \times 10^{-3}$$

with T in °C and the viscosity in N/(seg m²).

A.2 Properties of the vapor phase ¹²

A.2.1 Steam density

Steam density is obtained as the inverse of the specific volume given by the equation:

$$V_V = ((R T_C T_R / P_R) + 10^{-3}\alpha) / P_R$$

where:

V_V = Specific volume (m³/kg)

R = Universal gas constant

T_C = Critical Temperature (°K)

T_R = Reduced Temperature

P_R = Pseudoreduce Pressure (x 10⁵ pascals).

$$\alpha = B_T + 2 \times C_T \times P_R + 5 \times D_T \times P_R^4 + 15 \times E_T \times P_R^{14}$$

and B_T , C_T , P_T y E_T being temperature dependent coefficients given by the following expressions:

$$B_T = B_1 T_R + B_2 + (B_3/T_R) + (B_4/T_R^2) + (B_5/T_R^5) + (B_6/T_R^6)$$

$$C_T = C_1 T_R + C_2 + (C_3/T_R) + (C_4/T_R^2) + (C_5/T_R^{10})$$

$$D_T = D_1 + (D_2/T_R) + (D_3/T_R^2) + (D_4/T_R^{15}) + (D_5/T_R^{25}) + (D_6/T_R^{45})$$

$$E_T = (E_1/T_R^{70}) + (E_2/T_R^{75})$$

where:

$$\begin{array}{ll} B_1 = 4.1538 & C_1 = 5.6304 \\ B_2 = -12.497 & C_2 = -28.236 \\ B_3 = 37.681 & C_3 = 47.442 \\ B_4 = -73.427 & C_4 = -26.684 \\ B_5 = 5.2756 & C_5 = -2.5064 \\ B_6 = -5.914 & \end{array}$$

$$\begin{array}{ll} D_1 = 0.52193 \times 10^{-2} & E_1 = 0.2136 \times 10^{-4} \\ D_2 = -0.12163 \times 10^{-1} & E_2 = -0.30436 \times 10^{-4} \\ D_3 = 0.93878 \times 10^{-2} & \\ D_4 = 0.026 & \\ D_5 = -0.14692 & \\ D_6 = -0.28834 \times 10^{-3} & \end{array}$$

A.2.2 Steam enthalpy

The enthalpy of steam, in Joules/kg, is obtained from the following correlation:

$$h_V = -R T_C A T_1 T_R^2 + C P_R \alpha$$

with

$$\alpha = BT_D + P_R CTD - DTD P_R^4 + ETD P_R^{14}$$

Where AT_1 , BT_D , CTD , DTD y ETD are also temperature dependent coefficients¹⁴.

A.2.3 Steam viscosity

Steam viscosity was calculated using the following equation¹:

$$\mu_V = E_T + \rho_V (3470 + 5.90 T)$$

where

ρ_V is the steam density in m^3/kg ,

T is the temperature in $^\circ\text{K}$, and

$$E_T = -6.5634 + 0.267 T + 2.55 \times 10^{-4} T^2 - 1.3303 \times 10^{-7} T^3 \\ - 2.2475 \times 10^{-11} T^4 + 1.8488 \times 10^{-14} T^5$$

A.3 Steam-water equilibrium relationship

The following equation was used to determine the equilibrium temperature of wet steam³:

$$\ln(P_0) = A - (B/T) - C \ln(T) + D T$$

where:

$$A = 71.024449$$

$$B = 7381.6477$$

$$C = 9.0993037$$

$$D = 0.0070831558$$

A.4 Capillary pressure

The following expression has been used to calculate capillary pressure assuming that the steam-water system behaves like an air-water system¹⁴

$$\log (P_C / 6894.76) = (2.14763 - 4.19084 S_L + 2.04415 S_L^2)$$

with pressure in psi.

A.5 Steam-water relative permeability curves

The following two sets of steam-water relative permeability curves, as given by Martin¹³ and Counsil⁵, have been used for the simulations.

A.5.1 Martin's relative permeability curves

The curves in Figure A.1 have been fitted by Monsalve¹⁴ to the following expressions:

$$k_{rL} = 0.195714 - 1.59398 S_L + 3.582225 S_L^2 - 1.18687 S_L^3$$

$$k_{rV} = 1.00398 - 0.142444 S_L - 4.49301 S_L^2 + 3.47125 S_L^3$$

for

$$0.28 < S_L < 0.95$$

A.5.2 Counsil's relative permeability curves

The curves in Figure A.2 have also been fitted by Monsalve¹⁴ to the following equations:

$$k_{rL} = -1.06675 + 6.56214 S_L - 13.3943 S_L^2 + 9.2559 S_L^3$$

$$k_{rV} = 0.757482 - 1.10969 S_L + 0.348068 S_L^2$$

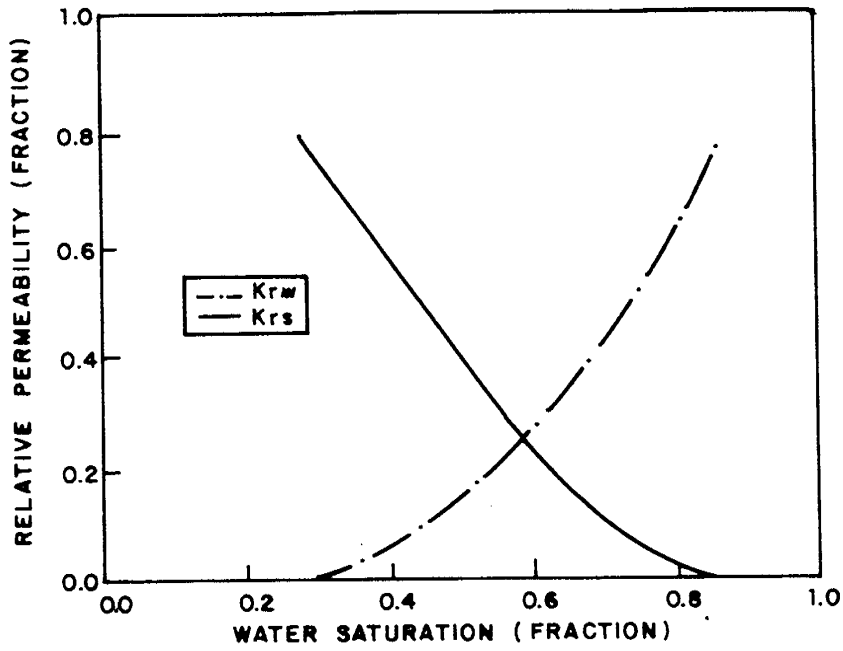


Fig. A1 MARTIN'S STEAM/WATER RELATIVE PERMEABILITY CURVES¹³

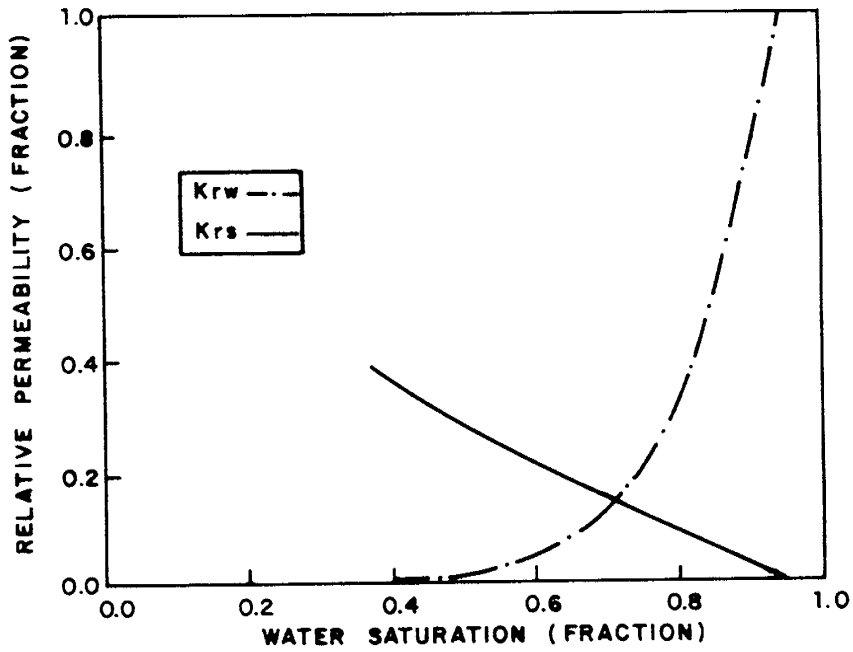


Fig. A2 COUNCIL'S STEAM/WATER RELATIVE PERMEABILITY CURVES⁵

Task 30 - DOE shall provide INTEVEP with information from laboratories studies conducted by Sandia on the injection of combustion gases with steam as a thermal recovery method. The project will determine the possible effects of non-condensable gases, such as nitrogen, and potentially soluble carbon dioxide on oil recovery.

THERMAL EOR PROCESS RESEARCH AND DEVELOPMENT

Daniel P. Aeschliman
Donald L. Markwell

Sandia National Laboratories
Albuquerque, New Mexico

INTRODUCTION

One particularly critical aspect of EOR technology is process control. Production rates, injection rates, and the location and number of wells can be used to control the migration of fluids in the reservoir and thereby influence the amount of oil ultimately recovered. Moreover, monitoring the geometry of fluid migration patterns and inferring the shape and velocity of the constitutive zones of an EOR process is central to process control and is, therefore, essential to optimize production.

A variety of instrumentation techniques have been applied to the problem of monitoring EOR processes.¹ These include tracer techniques,² pressure interference,³ and transient analysis,⁴ passive,⁵ and active⁶ seismics and the electromagnetic techniques, geotomography,⁷ and controlled-source audio magnetotellurics (CSAMT).⁸ In contrast to geotomography which requires two or more wells to accommodate a crosshole survey, CSAMT is a pure surface technique. As such, resource depth and overburden electrical properties are important parameters relating to technique applicability. The CSAMT technique has been described in Task 27.

As a practical matter for EOR front mapping by CSAMT or other electromagnetic techniques, it is essential to know the resistivity variations associated with the EOR process in order to interpret the field data quantitatively. A fundamental assumption is that significant changes in reservoir electrical properties, resistivity in particular, of the reservoir occur as a result of the EOR process. In this context, "significant" is generally regarded to be at least a factor of two, and preferably an order of magnitude or more. CSAMT demonstration field

data^{8,9} suggest substantial resistivity contrasts; however, a subsurface resistivity contrast map prior to steam injection was not obtained, so it is not possible to draw quantitative conclusions from those data. An important observation of that study was that the spatial resolution appears to be substantially better than expected based on plane-wave theory; consequently, resistivity contrasts may not need to be quite as large as is generally believed.

Therefore it is important to understand what changes occur and how those changes relate to the constitutive zones of the process. One approach to gaining the understanding involves laboratory studies using combustion and steam tubes. Combustion tube experiments have shown a two-decade change in resistivity as the combustion front traverses the core material.¹⁰ Current research at Sandia National Laboratories includes physical simulations of EOR processes using the Petroleum Extraction Simulation Laboratory (PESL).

To date three experiments have been performed in PESL that relate to thermal EOR process-dependent reservoir electrical properties. The first was conducted in December of 1984 and represented a demonstration of most of the PESL subsystems. Low-pressure (100 psig) steam of undetermined quality was used to displace heavy (13 degree API) crude from an uncharacterized sandpack (core pressure measurement capability was not available at that time.) Results of the first test were summarized briefly.¹¹ In general, the conclusions from that effort were discouraging in that observed electrical conductance variations in the simulated core were only 25% or so; if true, such low contrasts would not be sufficient to support application of CSAMT in the field.

Subsequent to the 1984 test substantial staff personnel changes resulted in the facility being idled for nearly a year, at which time the decision was made to restaff, to implement certain needed facility modifications, and to resume experimentation. Since then, a number of important changes have been made to PESL, and two tests have been

conducted. The first of these was a steam displacement of brine, performed December 11-12, 1986. The second, conducted February 18-19, 1987, was a steam displacement of heavy oil and brine, and was designed to simulate, as closely as possible, heavy oil recovery using steam drive in a California heavy oil reservoir. Specifically, the test simulated a steam flood in the Tulare "D" sand at a depth of about 700 ft (210 m) in the South Belridge field, under development by Shell California Production Inc. near Bakersfield.

PESL DESCRIPTION

PESL is designed to allow a variety of EOR process simulations for realistic reservoir conditions and process parameters. Pressures up to 1180 psig and external wall temperatures of up to 662°F are permissible simultaneously. In principle, core temperatures in excess of 1500°F are allowable so long as external temperature limitations are observed. However, instrumentation internal to the coreholder is limited to sustained temperatures of 600°F and below.

Although the design of PESL is directed primarily at thermal EOR processes (steam injection, with or without additives, and in situ combustion) other process simulations are feasible (chemical and immiscible gas flooding, for example). Current interest centers on the determination of reservoir fluid electrical properties, electrical resistivity in particular, during steam injection as a function of process variables and reservoir characteristics.

As shown by Leslie¹² complete physical scaling of thermal EOR processes in PESL is not feasible, since thermal and fluid mechanical scaling laws cannot be satisfied simultaneously except at low pressure.¹³ The electrical properties of fluid electrolytes are strong functions of temperature, primarily through the dependence of ion mobility on viscosity; hence, we have chosen to reproduce the thermal and fluid environment at the expense of physical scaling. Our objective is

to determine the relative change in electrical resistivity of simulated reservoir fluids that occurs as a result of the recovery process. To the extent that the simulation provides a realistic representation of an actual reservoir undergoing an equivalent EOR process, such data should provide essential information for the interpretation of CSAMT (or any other electrical measurement system, Surface Electric Potential (SEP)), process front mapping data from the field.

A generalized PESL system schematic is shown in Figure 1. The various subsystems are described below.

Coreholder/Core/Pressure Vessel

The coreholder is a 4.00-in ID x 72-in. long x .042-in. wall Inconel 600 cylinder. Pressure and thermocouple ports are provided as shown in Figure 2. Inconel flanges and metal O-rings provide isolation of the coreholder from the pressure vessel.

The core consists of unconsolidated 80-100 mesh Ottawa sand. The core is a sandpack assembled vertically, outlet end up, with the coreholder removed from the pressure vessel and with the impedance grid structure and core thermocouples in place. A sintered metal filter, with 16 holes for the impedance grid leads, is used to prevent sand production.

A total of 12 two-piece cylindrical bandheaters, each 5 in long and rated at 1500 w at 240 vac, are strapped to the coreholder at 6-in intervals. The bandheaters are wired to independent variable transformers to compensate for radial heat loss as the thermal front progresses axially through the core.

The ASME-code pressure vessel (p.v.) is 10.5 in ID x 81.0 in long, excluding flanges, with a wall thickness of 1.125 in. The p.v. is mounted on a swiveled yoke to permit operation at any dip angle with respect to horizontal. The coreholder is bolted to the p.v. flange at

the inlet end; the p.v. flange is provided with 12 NPT ports for fluid and electrical feedthroughs. In addition, the p.v. inlet flange is provided with temperature-controlled heat tapes and insulated to allow preheating, so as to minimize heat loss from steam during the early phases of steam injection.

Steam Generator

A high-pressure (6000 psi MAWP) resistance-heated stainless steel autoclave was adapted for steam generation. The maximum steam generation rate is about 2 l/hr CWE, a limit imposed by the input power rating. Average input power for steady operation at a given mass flow is maintained by means of a temperature controller which senses the heating element temperature. Water is injected using a high-pressure, medium-capacity (3000 psi, 6 l/hr) positive displacement pump.

Saturated or slightly superheated steam from the generator is further heated to a desired degree of superheat (typically 40°F) by temperature-controlled heat tapes on the generator outlet line. Saturated steam of a given quality is produced by injecting cold water at a rate dependent on the mass flow and observed degree of superheat using a low-capacity, high-pressure (0.5 l/hr, 6000 psi) positive displacement pump. (Additives such as foaming agents or other chemicals could be introduced downstream of the cold water injection point.) All steam lines are insulated with 1 to 2 inches of high-density fiberglass pipe insulation.

Flow Control

The flow control and distribution system consists of stainless steel tubing and Swagelok fittings throughout, with insulation on all lines subject to high-temperatures. Valves subject to steam use metal-to-metal stainless steel seats. System pressure is controlled via a precision backpressure regulator at the effluent drain. A water-cooled concentric-tube heat exchanger immediately upstream of the regulator is used to remove residual heat in the effluent during steam displacement, and acts

as a total calorimeter for evaluating the steam quality when used in the core bypass mode.

The steam generation system is stable within a few percent with only minor, infrequent adjustment over indefinite periods when there is minimal core pressure drop. During steam injection into a core saturated with viscous heavy oil, however, most of the system pressure drop can be expected to occur within the core, and to be a maximum at the start of steam injection and decrease in time as oil is heated and displaced by steam. Although this problem was anticipated, we had underestimated the difficulty in maintaining stable system operation during oil displacement.

Instrumentation

Temperatures are determined using Type K ungrounded .062-in. OD stainless steel sheath thermocouples: 12 along the core centerline, 12 at the core perimeter, and 12 at the coreholder surface, all at 6.0-in intervals, and seven other system locations.

Pressures are determined using Validyne variable-reluctance transducers. The absolute pressures measured are the steam inlet and coreholder outlet pressures, core pressure at pressure taps 1 and 6, the coreholder confining pressure (i.e., the pressure in the p.v./coreholder annulus), and ambient pressure. Differential pressures are measured between each adjacent pair of coreholder pressure taps located on 1-ft center.

The core fluid electrical conductance was determined as a function of frequency for each grid pair. Excitation frequencies vary from 5-5000 Hz, and span the approximate range of values for field applications. The grid and grid support structure consist of eight electrically-independent grid pairs on 9-in. (22.9 cm) centers. The grids are fabricated from gold-plated nickel shim stock, bonded to .040-in. thick alumina supports, and separated by 0.50-in. thick ceramic insulators. The system is assembled as a complete unit using a

triangular arrangement of 4-40 threaded rods. This provides a strong, light-weight assembly that simplifies installation into the coreholder and ensures that the grids remain parallel and correctly positioned during core fabrication and subsequent operations.

Data Acquisition and Control System

The data acquisition and control system consists of a computer, multiprogrammer, multiprogrammer interface, variable-frequency impedance analyzer, scanners, and autoranging digital voltmeter. The computer controls the function of all other components via software, stores data, and writes permanent records on floppy disc and on paper. The program allows for a substantial amount of operator control via keyboard interrupts. The multiprogrammer and interface act as an intelligent switchbox to relay data and logic instructions between the computer and the other peripherals. The impedance analyzer determines the real and imaginary parts of the complex impedance (resistance and reactance, respectively) for each grid circuit individually for the program-selected frequencies. Short and open calibrations are used to compensate for lead and contact resistance, and for stray capacitance and inductance. The scanners direct analog temperature and pressure signals to the digital voltmeter and return digitized data in a program-controlled cycle. The digital voltmeter has a resolution of 1 microvolt and an absolute accuracy of 10 microvolts or better, depending on range.

CORE CHARACTERIZATION

Average core porosity was determined to be 36%, based on the ratio of volume of water injected during core fabrication to the total coreholder volume. Using Darcy's law, the differential pressure, and the volume flow rate, the absolute permeability k was determined to be 14-18 darcies as a function of position (averaged over 1-ft intervals, the pressure tap spacing) in a series of steady flow experiments. Some of these involved displacements of deionized water by brine, or vice versa. Consistent

with this apparent high degree of uniformity are the data of Figure 3 which shows time of displacement front passage (as evidenced by a sharp change in resistivity) vs impedance grid position. A summary of the measured core properties and the properties of the Tulare "D" sands as reported by Hite¹⁴ is presented along with other relevant test and system parameters in Table I. The most significant difference is in the permeability, which averages 16 darcies in the sandpack and 2-3 darcies in the field.

A concern in using confined cores is the possibility of high-permeability paths at the interface between core and coreholder. A series of steady flow experiments with varying confining pressures showed no statistically significant effect of confining pressure on core permeability. This suggests to us that the coreholder is probably in a state of slight tensile hoop stress, a favorable condition for maintaining core uniformity.

TEST DESCRIPTIONS

Brine Displacement Test

This test was performed to exercise all facility subsystems under test conditions and to gain operational experience over expected test times (10- 20 hrs) prior to saturating the core with oil.

The core was saturated with brine (1.5 wt% NaCl in deionized water). Brine injection was continued until the conductance as measured at each grid pair was constant; brine quantity injected was in excess of 2 pore volumes. The pressure vessel flange was preheated to approximately 400°F to minimize heat loss from the steam. Steam at a pressure of 250 psia and quality of 70% was injected at 1.0 liter/hr. Except for bandheater no. 1, which was activated at the start of steam injection, the bandheaters were energized as the steam front passed the adjacent downstream centerline thermocouple.

Examination of the core temperature vs time data indicates that the core centerline temperature increases somewhat more rapidly than does the temperature at the wall, with saturated steam reaching the center 6-20 min ahead. For the average steam front velocity observed, 0.3 cm/min, this represents a difference of 2 to 6 cm in axial distance. We suspect that the discrepancies are related to bandheater operation, both in time of actuation and power level.

The fluid conductance in Siemens (reciprocal ohms) is shown as a function of time for the seven grid pairs in Figure 4. The overall electrical response at each station is similar, a response interpreted as follows. As an example, consider grid pair 3, located 22 in. from the inlet. Initially, the conductance is essentially steady as brine at nearly constant temperature and velocity flows through the grids. This is denoted as Region A in Figure 4. Due to thermal conduction and convection the temperature ahead of the brine/condensation interface starts to increase, Region B. The temperature rise increases the ion mobility, which is reflected in an increased conductance at constant ion concentration. The decrease in conductance in region C is ascribed to steam condensate mixing with brine ahead of the steam front; presumably the decrease would be sharper were it not partially compensated by the effect of increasing temperature as the steam front approaches. The period of again nearly constant conductance, denoted by D, is the condensate zone; for a constant steam front velocity and condensation rate, its length is proportional to axial distance along the core (i.e., to cumulative condensate volume.) The conductance increase denoted as Region E reflects the rising condensate temperature as the steam front approaches. As the steam front passes through the grids, condensate is replaced by vapor and the conductance rapidly decreases (Region F). The rate of change of conductance during steamfront passage is a function of the grid separation, steam front velocity and geometry (planarity, tilt), and quality variations behind the front. The time for the conductance to decrease to half value is about 10 minutes, of which 5 minutes can be ascribed to steam front transit time between grids and the remainder to the other effects noted.

Approximately 10 hrs into the run, at which time the steam front had traversed 75% of the core, a sudden and complete loss of bandheater power occurred and we could no longer compensate for core heat loss. As a result the steam front stagnated, and the test was aborted.

Oil/Brine Displacement Test

The core was prepared by first flushing the core extensively with deionized water followed by saturation with 1.5 wt% brine. The core was preheated to approximately 150°F to improve injectivity and then saturated with heavy oil. The oil was a dewatered sample of 13.9 API crude supplied by Shell California Production, Inc. An autoclave incorporating a gas-driven piston and provided with temperature-controlled heat tapes was used to inject oil preheated to 150°F. Injection rate was monitored via observed piston displacement, and was typically 20 ml/min. Oil injection was from the top (core inlet) to provide a stable displacement of brine. Injection was continued until the produced oil was totally water-free. A volume-balance at that point yielded an oil saturation of 83%. The "D" sand oil saturation averages 65%.

Pressure data were obtained throughout the injection procedure. These data were used to derive the apparent viscosity. The agreement with data provided by Hite¹⁴ is excellent. The core conductance before and after oil saturation and the brine saturation were then used to determine the wettability state of the sand based on the Archie saturation equation.¹⁵ The exponent n was 1.6, leading to the conclusion that the sand was fully water wet.

Again the pressure vessel flange was preheated to a temperature near 400°F prior to steam injection. The core was preheated to about 150°F in order to improve steam injectivity. Steam injection rate was 1 l/hr at a nominal pressure of 250 psia and quality of 70%, as before. The effluent was periodically sampled and centrifuged to obtain oil cut. All effluent was collected.

Core temperature data as a function of time were similar to the brine displacement results. Average steam front velocity was approximately 0.25 cm/min, with more variation than before. The effects of uncertainties in bandheater actuation and power level were again apparent in the wall temperature data.

The conductance vs time data are presented in Figure 5. Although somewhat noisier, and with one exception, the data are qualitatively similar to the results seen for steam displacing brine alone. The exception is that the conductance at each grid station steadily decreased with time after the start of steam injection, although the overall change was about the same. Again the overall conductance variations are several orders of magnitude, more or less equally divided between the effects of condensate and vapor.

Gross production exhibited large oscillations. The oscillations correlated with core inlet-to-outlet pressure drop fluctuations, which proved impossible to eliminate through manual control of the backpressure regulator. The oil cut exhibited a rapid decline from 1.0 at start of steam injection to a value averaging about 0.3, substantially less than a numerical simulator prediction of about 0.75.¹⁶ It is noted, however, that the test and numerical simulation differed in several respects, the most notable being that preheating of the core was not included in the model, and the system pressure history in the test and in the model did not match. There is also some indication, as evidenced by the steady decrease in conductance following the start of steam injection noted above, that condensate was percolating downward through the sandpack. This issue is important and requires further study to satisfactorily resolve; such an effect was not predicted by the simulator.

At 23:00, again 10 hrs into the test, an electrical short internal to the pressure vessel resulted in a complete bypass of the variable transformer for bandheater no. 2. The instantaneous power increase from 25 to 1500 w resulted in a rapid overheating of the core to 800°F. At the time of the failure, the steam front had traversed 60% of the core.

The effect of superheated (dry) vapor on conductance after the bandheater failure is very pronounced, an additional 3-order of magnitude decrease to near open-circuit calibration levels.

CONCLUSIONS

For both the brine and oil/brine displacement tests, the net change in conductance is seen to be 2-2.5 orders of magnitude, 1-1.5 decades due to the displacement of brine by condensate, and another order of magnitude due to the displacement of condensate by steam vapor. The contribution due to brine displacement will vary with salt concentration; the value of 15000 ppm (1.5%) is typical, but may be lower or higher depending on the particular reservoir. The effect of condensate displacement by vapor should be much less dependent on the assumed connate water characteristics. It thus seems very likely that process-driven resistivity contrasts will exceed an order of magnitude in actual steamflooded reservoirs. We therefore conclude that these results support the viability of remote surface-based electromagnetic (or electric potential) diagnostics for steam front mapping of reservoirs undergoing steam flooding if other requirements are met. These include the absence of highly conductive or very thick strata overlying the target reservoir, and the availability of appropriate numerical models for the inversion of field data. It is worthy of note, however, that as stated by Bartel⁹ even the raw data can provide a meaningful indication of resistivity contrast location.

These initial tests have demonstrated that we can successfully measure core fluid electrical properties in the laboratory at conditions representative of real reservoirs. Much valuable data was obtained despite the fact that both tests were ultimately aborted. Because these properties are intrinsic, data should be relevant to the field even though the experiments are not physically scaled.

REFERENCES

1. Leighton, A. J. and J. R. Wayland, "Techniques for Mapping and Diagnosing EOR Processes," J. Pet. Tech., February 1987, p. 129.
2. D'Hooge, J. A., C. Q. Sheely, and B. J. Williams, "Interwell Tracers--An Effective Reservoir Evaluation Tool: West Sumatra Field Results," J. Pet. Tech., May, 1981.
3. Earlougher, R. C., Jr., Advances in Well Test Analysis, SPE Monograph, Vol. 5, 1977.
4. Benson, S. M., and G. Bodrarrson, "A Pressure Transient Method for Front Tracking," SPE 12130, Presented at 58th Annual SPE Meeting, San Francisco, CA, October, 1983.
5. Nyland, E., and M. B. Dusseault, "Fireflood Microseismic Monitoring: Results and Potential for Process Control," Pet. Soc. CIM, No. 82-33-39, 1982.
6. Britton, M. W., W. L. Martin, R. J. Leibrecht, and R. A. Harmon, "Street-Ranch Pilot Test of Fracture Assisted Steamflood Technology," J. Pet. Tech., March, 1983.
7. Dines, K. A., and R. J. Lytle, "Computerized Geophysical Tomography," IEEE Proceedings, v. 67, July, 1979.
8. Wayland, J. R., D. O. Lee, and T. J. Cabe, "CSAMT Mapping of a Utah Tar Sand Steamflood," J. Pet. Tech., March 1987, p. 345.
9. Bartel, L.C., "Modeling and Analysis for the CSAMT Geophysical Technique Results to Map Oil Recovery Processes," SPE 11192, 57th Annual Meeting, New Orleans, Sept., 1982.

10. Lee, D.O., and J.R. Wayland, "Measurement of Formation Resistivity Changes Induced by In Situ Combustion," SPE 11051, 57th Annual Meeting, New Orleans, Sept., 1982.
11. Progress Review No. 44, Contracts of Field Projects and Supporting Research on Enhanced Oil Recovery, Bartlesville Project Office, U.S. Department of Energy, Sept., 1986.
12. Leslie, I.H., "Flow Scaling Laws for PESL," Final Report, Sandia Contract 1-4-23216, Dec., 1986.
13. Stegemeier, G.L., D.D. Laumbach, and C.W. Volek, "Representing Steam Processes with Vacuum Models," J. Soc. Pet. Eng., April, 1981, 249-258.
14. Hite, R.H., Shell California Production Co., Inc., Private Communication, 1986.
15. Archie, G.E., "The Electrical Resistivity Log as an Aid in Determining Some Reservoir Characteristics," Trans. AIME, 1942, 54-62.
16. Meldau, R.F., Dolphin Petroleum Consultants, "Memorandum: Prediction of PESL Steamflood," Private Communication, Dec., 1986.

Table I. Heavy Oil Displacement Test Parameters

Reservoir Matrix			Oil	
Lab	Tulare "D" Sand			
Unconsol. Ottawa sand, 80-100 mesh (.006-.007-in) d \approx .0065 in)	Unconsol. sand (.002-.020 in.) d \approx .007 in.)		API gravity	13.9
			Viscosity (95°F)	850 cp
			Viscosity (150°F)	125 cp
			Residual emulsion breakers present (Ref. 15)	
Porosity, ϕ .35-.37 ($\phi = .36$)	.35			
Permeability k 14-18 darcies (k = 16 darcies)	2-3 darcies			
Initial Oil Saturation S_{oi} .83	.65			
Initial Water Saturation, S_{wi} .17	.35			
Connate Water Salinity 15000 ppm	~15000 ppm			
Connate water pH 7	7 (?)			
Wettability 100% water wet	100% water wet			
			Steam	
			Lab	Tulare "D" Sand
			Pressure 250 psia	250-400 psia
			Quality = .70	.75-.80 (generator)
				.60-.65 (bottomhole)
			Flow Rate = 0.2 pv/hr	-
			pH = 7	11.5-12.0

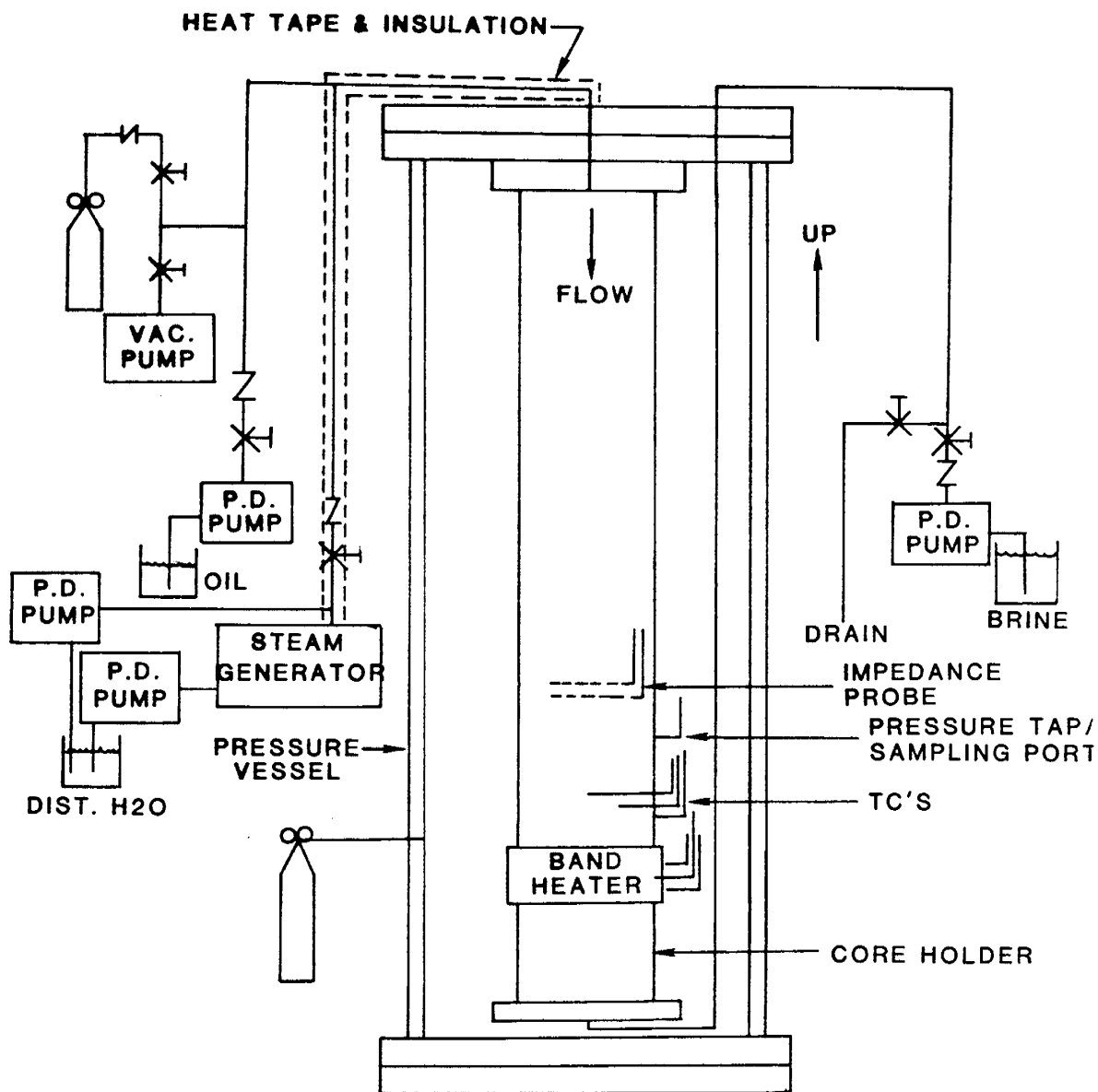


Figure 2. Schematic of PESL and flow systems.

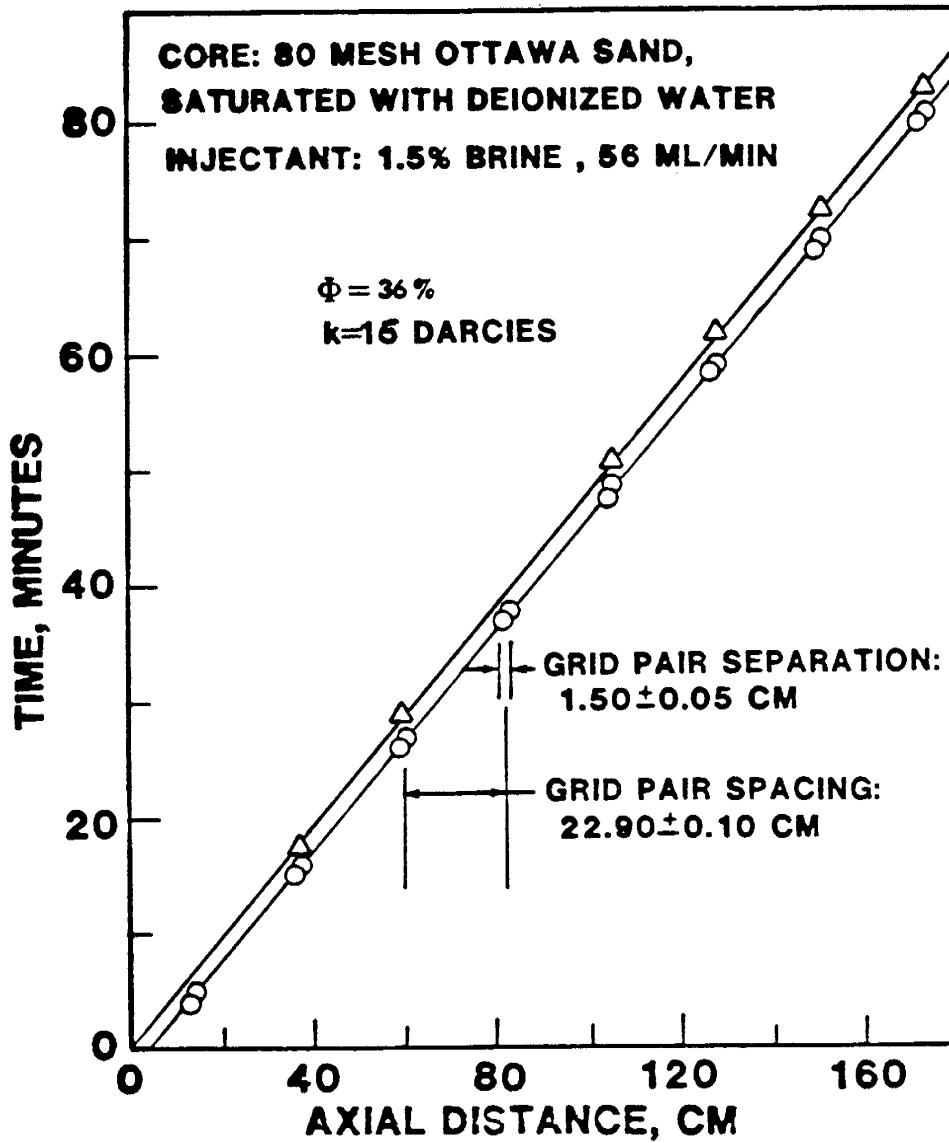


Figure 3. Time of observed grid-to-coreholder resistance decrease as a function of grid position for stable injection of brine into deionized water.

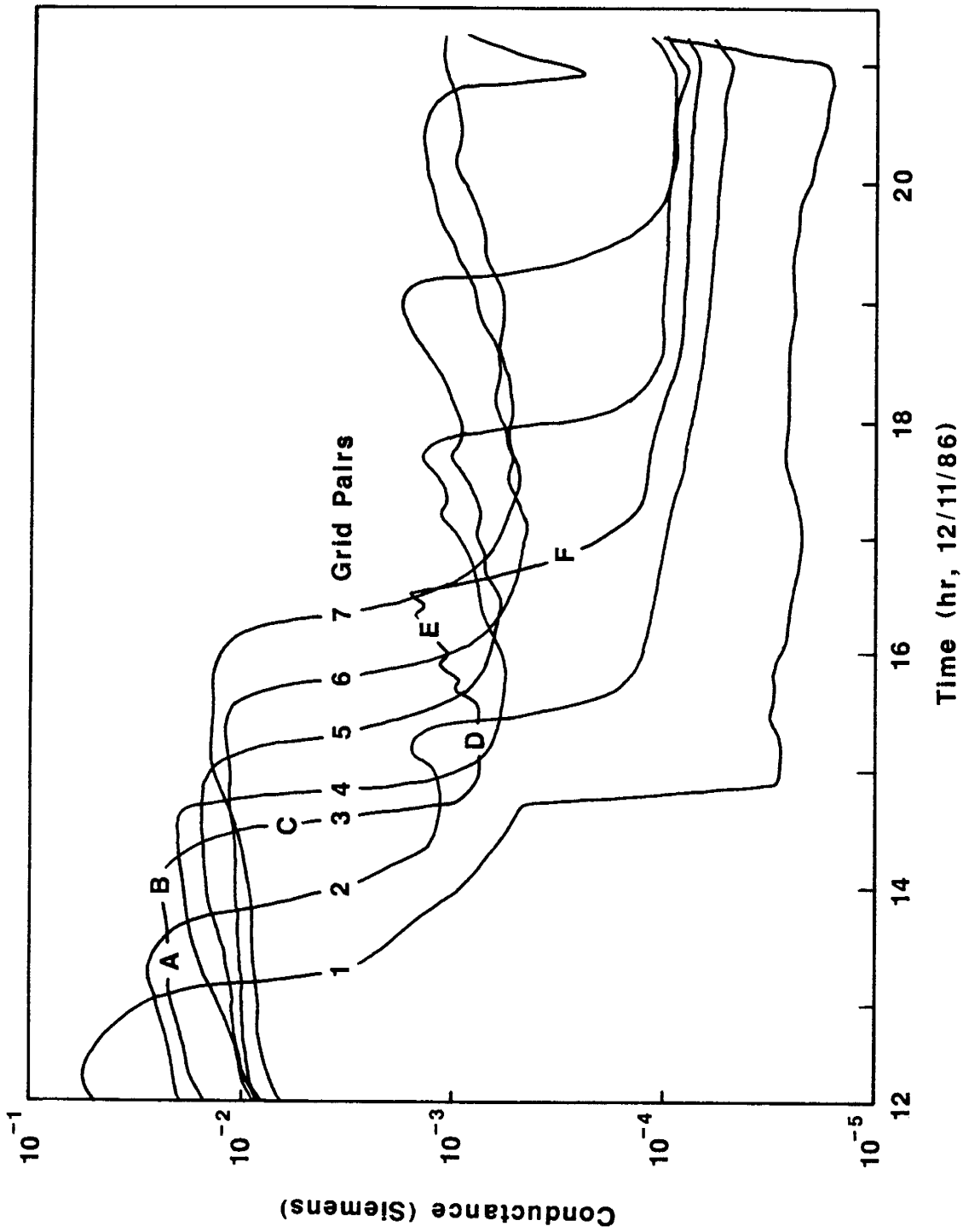


Figure 4. Conductance vs. time at different grid stations for steam displacement of brine.

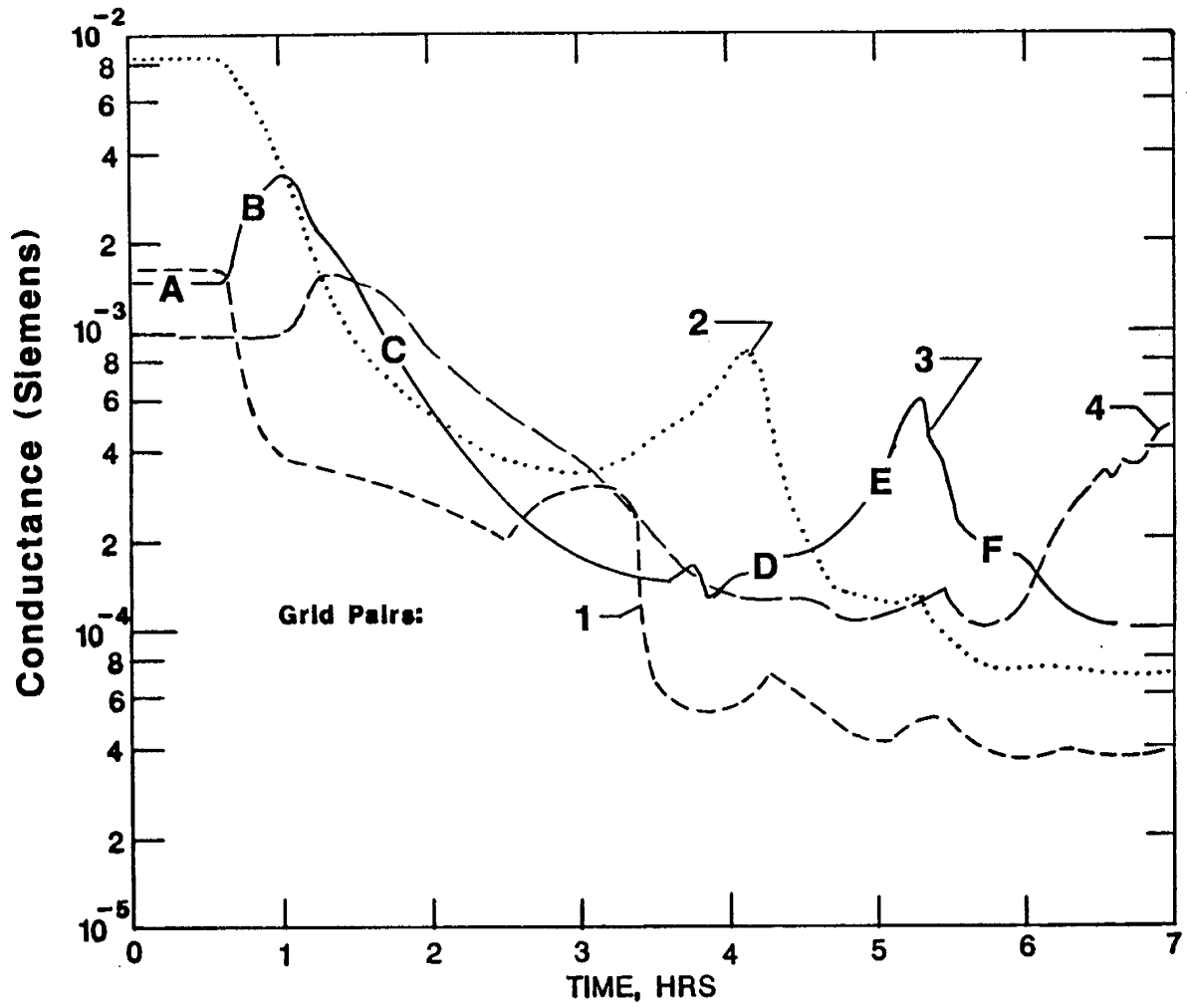


Figure 5. Conductance vs time at selected grid stations for steam displacement of heavy oil.

Task 31 - INTEVEP will provide DOE with information from laboratory studies on the injection of carbon dioxide as a potential oil viscosity reduction agent.

RESEARCH PROGRAM ON HEAVY OIL RECOVERY BY CO₂

(Task 31 of Annex IV of the Implementing Agreement)

Prepared by:

Thays M. de Pedroza

Elena Escobar

Orlando Rivas

INTEVEP, S.A.

Los Teques, Edo. Miranda

Venezuela

March 1986

SUMMARY

This report summarizes the results of an experimental program to evaluate heavy oil recovery by CO₂ injection. A 10° API oil from the Venezuelan Boscan field was selected for the study. Thermodynamic and rheological studies were performed for CO₂/heavy oil systems. Displacement experiments inside the porous medium, were also performed at reservoir conditions.

Results indicate that the flow behavior of the fluids is Newtonian and that CO₂ solubility produces a high swelling of the crude and appreciably reduces the viscosity and interfacial tension of the oil. Continuous CO₂ displacement in porous media showed rapid CO₂ channelling while CO₂ water alternating gas schemes gave higher displacement efficiencies.

CONTENTS

	Page
SUMMARY	31-3
CONTENTS	31-4
LIST OF FIGURES	31-5
LIST OF TABLES	31-6
1. INTRODUCTION	31-7
2. RHEOLOGICAL STUDIES	31-8
3. PROPERTIES OF CO ₂ /STOCK TANK CRUDE MIXTURES AT RESERVOIR TEMPERATURE	31-9
3.1 CO ₂ Solubility	31-9
3.2 Density-swelling factor	31-10
3.3 Viscosity reduction	31-10
3.4 Interfacial tension	31-10
	31-11
4. PROPERTIES OF CO ₂ /RECOMBINED CRUDE MIXTURES	31-12
4.1 Phase behavior	31-12
4.2 Physical Properties	31-12
	31-13
4.3 Discussion on the properties of CO ₂ /Boscan crude mixtures	31-13
5. DISPLACEMENT EXPERIMENTS	31-14
5.1 Experimental procedure	31-14
	31-14
5.2 Results	31-15
	31-16
6. CONCLUSIONS	31-17
	31-17
FIGURES	31-18
TABLES	31-24

LIST OF FIGURES

	Page
Fig. 1. Solubility of CO ₂ in Boscan Crude	31-18
Fig. 2. Swelling Factor vs. CO ₂ Solubility in Boscan Crude	31-19
Fig. 3. Viscosity of CO ₂ /Boscan Stock Tank Crude Mixture. Reservoir Temperature: 177 °F.	31-20
Fig. 4. Viscosity reduction vs. CO ₂ solubility in Boscan Crude	31-21
Fig. 5. Interfacial tension vs. CO ₂ saturation pressure in Boscan Crude. Reservoir temperature: 177 °F.	31-22

LIST OF TABLES

	Page
Table 1. Reservoir and fluids properties. Boscan field	31-23
Table 2. Boscan crude distillation Data	31-24
Table 3. Properties of CO ₂ /Boscan Stock Tank Crude Mixtures Reservoir Temperature: 177 °F	31-25
Table 4. Properties of CO ₂ /Boscan recombined Crude Mixtures at 177 °F	31-26
Table 5. Properties of CO ₂ /Boscan Recobined Crude Mixtures at 150°F and 2000 psi	31-27
Table 6. Displacement Tests Conditions	31-28
Table 7. Displacement Tests Results	31-29
Table 8. Displacement Tests Results	31-30

1. INTRODUCTION

This report presents the results obtained from an experimental research program carried out to evaluate the effectiveness of CO₂ injection to recover heavy oil.

The research program was divided in two phases:

- A - Rheological and Thermodynamic Studies for CO₂/heavy crude systems outside the porous medium.
- B - Dynamic studies inside the porous medium to evaluate the efficiency of heavy crude displacements by CO₂ and to determine the more effective injection strategy.

To perform these studies we selected a 10° API crude from the Venezuelan Boscan field. The reservoir and fluids properties of this field are given in Tables 1 and 2.

2. RHEOLOGICAL STUDIES

The main objective of this activity was to examine the flow behavior of CO₂/BOSCAN crude mixtures. The following systems were studied:

- a) Stock tank crude saturated with CO₂ at 177 °F and pressures from 500 to 3000 psi.
- b) Recombined crude with solution gas G.O.R. = 100 Scf/bbl saturated with CO₂ at 177 °F and 2000 psi.
- c) Recombined crude with solution gas G.O.R. = 80 Scf/bbl saturated with CO₂ at 177 °F and 2000 psi.
- d) Recombined crude with solution gas G.O.R. = 80 Scf/bbl saturated with CO₂ at 150 °F and 2000 psi.
- e) Recombined crude with solution gas G.O.R. = 60 Scf/bbl saturated with CO₂ at 177 °F and 2000 psi.

These five mixtures were introduced in a cell and forced to flow in a capillary tube at constant flow rate. The pressure drop between both ends of the tubing was measured under steady state conditions. Flow rates were varied from 15 to 750 cm³/hr, when the pressure drop reached the maximum value allowed by the differential pressure gage. (73 psi).

The viscosity results for all of the systems at different flow rates remained constant indicating newtonian flow behavior. These results are given in Tables 3, 4 and 5, and Figure 4.

3 PROPERTIES OF CO₂/STOCK TANK CRUDE MIXTURES AT RESERVOIR TEMPERATURE.

3.1. CO₂ Solubility

The thermodynamic and PVT properties of CO₂/ BOSCAN stock tank crude mixtures were measured at pressures between 500 and 3000 psi at reservoir temperature. This range was chosen because the reservoir pressure when put in production was 3450 psi and it has so far declined to 2000 psi.

Before starting any quantitative determination, the two phase fluid was observed in a high pressure sapphire cell which allowed complete visibility of the system under consideration. First, the oil was introduced in this cell, and it was then saturated with CO₂ in the above pressure range. Only "normal" two-phase liquid-vapour equilibria took place while decompressing the CO₂/crude mixture from 3000 to 500 psi.

Analysis of the gaseous phase in equilibrium with the liquid phase showed that it was almost pure CO₂. This means that no noticeable stripping of hydrocarbons occurred in this pressure range. Neither two liquid phases nor a solid asphaltenic phase were observed in our experiments.

CO₂ solubility in stock tank crude were then measured and the results expressed in terms of Gas-Oil Ratio as defined by the relation:

$$\text{G.O.R. (CO}_2\text{)} = \frac{\text{CO}_2 \text{ Volume at } 60^\circ\text{F, } 760 \text{ mmHg}}{\text{stock tank crude volume at } 60^\circ\text{F, } P_a}$$

where P_a is the atmospheric pressure.

The data are given in Table 3 and shown in Fig. 1. The reproducibility of these values is considered to be within $\pm 3\%$.

3.2. Density-swelling factor

The density of the crude oil and that of the CO₂ saturated oil were measured as functions of pressure. The Swelling Factor was then computed by the expression:

$$S.F. = \frac{\text{Volume of CO}_2 \text{ saturated crude at T,P}}{\text{Volume of crude at T,P}}$$

This relation gives directly the swelling of the oil at reservoir conditions due to CO₂ dissolution. All the results are presented in Table 3 and shown in Fig. 2; the reproducibility of the density data is within ± 0.002 g/cm³.

3.3. Viscosity reduction

The viscosity of the crude oil as a function of pressure was first determined and then the same data were obtained for CO₂/oil mixtures. The Viscosity Reduction effect was calculated by the following equation

$$V.R. = \frac{\text{Viscosity of crude at T,P.}}{\text{Viscosity of CO}_2 \text{ saturated crude at T,P.}}$$

This parameter is also directly related to the effect of CO₂ dissolution on the oil viscosity at reservoir conditions. The experimental results are also given in Table 3 and shown in Figures 3 and 4. The reproducibility of viscosity data is considered to be within $\pm 10\%$

3.4. Interfacial tension

Since decreasing interfacial tension may be an important mechanism to improve displacement efficiency, in this work we measured interfacial tension of Boscan crude oil saturated with CO₂ at reservoir temperature and

pressures between 1500 and 3000 psi.

The experimental measurements were based on:

- either taking a photograph of a hanging drop of the liquid phase in equilibrium with the surrounding gas phase, and then using correlations between the characteristic dimensions of this drop and the interfacial tension value under the operating conditions.
- or counting the number of drops in a certain time interval. These drops are displaced by means of a small pump having a very stable flow rate. Which allows us to determine volume of one drop. The interfacial tension is then computed through appropriate correlations.

The first method can be used only if the hanging drops have a symmetrical shape around the vertical axis. Otherwise, the second procedure is to be used. For the mixtures considered here, the hanging drop technique did not give reliable results while the drop counting method lead to consistent data. The interfacial tension values thus obtained are given in Table 3 and shown in Fig. 5, their reproducibility being within ± 0.55 dyne/cm.

4 PROPERTIES OF CO₂/RECOMBINED CRUDE MIXTURES

4.1 Phase behavior

As in the previous case, before starting any quantitative determination, we observed the phase behavior of the fluids under consideration in a high pressure sapphire cell. Recombined oil was introduced in this cell at a pressure above its bubble point, and then it was further saturated with CO₂.

In all cases in the specified range (G.O.R.: 60 to 100 scf/bbl and T: 150°F and 177°F), it was noticed that at pressures higher than 3000 psi we had a CO₂ rich liquid phase in equilibrium with a hydrocarbon-rich liquid phase. However, in the 500 to 3000 psi pressure range only "normal" two phase liquid-vapour equilibria took place while depleting the CO₂/recombined crude mixture.

Analysis of the gaseous phase in equilibrium with the liquid phase showed that it contained light hydrocarbons, essentially methane. This indicates that stripping of these components from the oil occurred under the influence of CO₂.

4.2 Physical Properties

PVT properties, viscosities and interfacial tensions of recombined crude oils and recombined crude/CO₂ mixtures were determined at the reservoir temperature (177°F) and at the well head temperature (150 F). At the 177°F temperature we carried out experiments with 100 GOR, 80 GOR and 60 GOR recombined oils and at pressures from 1500 psi to 3000 psi. At the 150°F temperature we only did experiments with the 80 GOR oil at a 2000 psi pressure.

In each case we first determined the bubble point pressure of the recombined oil to then measure its density and viscosity at the higher pressures. Next, we saturated the oil with CO₂ at each one of the pressures and then we determined the properties of the resulting recombined oil/CO₂ mixtures. CO₂ solubility was obtained by flashing the CO₂ saturated oil to standard conditions (15°C, 147 psi) and measuring and analysing the gas phase.

Resulting data are shown in Figures 1 to 5 and in Tables 4 and 5.

4.3. Discussion on the properties of CO₂/Boscan crude mixtures

Figure 1 shows that CO₂ gas oil ratio in the oil increases with pressure and decreases with temperature as expected. At constant temperature and pressure, CO₂ solubility is enhanced by decreasing the solution gas G.O.R. of the oil.

Figure 2 and 4 indicates the Swelling Factor and the viscosity reduction correlates very well with CO₂ solubility independently of oil G.O.R. and temperature within the limits given above. In these Figures we can notice that swelling effects can be as high as 20% while the viscosity reduction can reach a value of about 30, both for the CO₂ solubility associated with the highest pressure studied in this work.

In Figure 5 we show the interfacial tension as a function of the CO₂ saturation pressure. We can see that CO₂ dissolution decreases the interfacial tension up to three times at the highest pressure.

5. DISPLACEMENT EXPERIMENTS

In this phase of the study we performed a series of five tests at reservoir temperature (177°F), with the objective of evaluating the efficiency of displacing Boscan Crude with CO₂ and with water alternating CO₂ injection schemes. These tests were carried out in two horizontal one dimensional tubes packed with reservoir sand. The characteristics of the tests are presented in Table 6.

5.1 Experimental procedure

In all of the tests we used a basic displacement system which consisted of an injection pump, storage cells, sand pack holders, temperature and pressure regulation systems and a system to control injection rate.

We simulated the reservoir fluids and porous medium in our experiments by using a sample of 10° API Boscan Crude which was dehydrated and recombined with the formation gas at 2000 psi and 178°F, to give a gas oil ratio of 80 scf/bbl. The formation and injection water were prepared to contain 7000 ppm TDS and a pH of 7.5. and reservoir sand, prepared according to preliminary granulometric analyses, was used as sand pack.

In Test N° 1 we injected CO₂ continuously at 3000 psi while in the other tests we use water alternating CO₂ injection schemes at 2500 psi injection pressure. The first WAG scheme studied in this work was with a 1.3 CO₂/water injection ratio since results obtained in another investigation with a similar crude, showed it to be the optimum injection scheme (Reinose, J. y Osorio, O., "Recuperación de crudo de la Faja Petrolífera del Orinoco por inyección de CO₂ y agua", U.D.O., Noviembre 1979). The other tests were carried out to confirm these results by varying CO₂/water ratios, CO₂ slug sizes and porous media characteristics.

The general procedure that we followed in our experiments consisted of the following steps:

- . Saturation of the sandpack with water and determination of pore volume (PV), porosity and permeability.
- . Displacement of water with oil until we obtained irreducible water saturation and resaturization of the core from 2000 psi up to the injection pressure of the test.
- . Injection of CO₂ (or CO₂/water) until the effluent had a gas/oil ratio over 10 Mscf/bbl or a water/oil ratio over 0.85.
- . Depressurization until the pressure reached a previously defined blowdown pressure.

5.2 Results

The results obtained in Tests 1 and 2 (shorter sand pack) are presented in Table 7. We can observe that in the case of continuous injection, CO₂ breakthrough is quite rapid indicating channelling of CO₂ due to the large differences in the viscosities of the fluids. During the WAG injection test

there was no indication of CO₂ breakthrough as a free phase. This result confirms laboratory and field experiences, which had shown the effectiveness of this method to control CO₂ channelling. It is observed that after injecting 2 PV the CO₂ requirements in the case of alternating injection are lower than those of continuous injection while the total oil recovery is much larger in the alternating case.

The results obtained with the longer sand pack (Test 3,4 and 5) are given in Table 8, results of Test 2 are also included for comparison. Test N° 4 could not be completed due to operational difficulties which developed after injecting 0.67 PV of CO₂. However, results obtained up to this stage are presented. Recoveries and CO₂ requirements with the longer tube test are better than those corresponding to the shorter one. This may be that the length/ diameter ratio of the longer tube is more favorable for displacements at our experimental conditions.

The results given in Table 8 show that the highest recovery, at 0.6 PV injected, is obtained with the 1.1 ratio. CO₂ requirements, however, are twice in this case than in the 1.3 ratio experiment. Total recovery for the three tests could not be compared since the 1:3 WAG experiment was stopped after we have injected 0.67 PV. Nevertheless, the results suggest that the best WAG process, in terms of oil recovery vs CO₂ requirements, is the 1.3 injection scheme. This confirms the results of Reinise and Osorio.

Taken into account the high gravity of the oil studied, we conclude that the oil recoveries obtained in our laboratory experiments are high enough to suggest the CO₂ water alternating gas injection process may be potentially useful for displacing heavy oils.

6. CONCLUSIONS

This report presents a substantial amount of experimental data which were collected in order to help with the correlation, interpretation and prediction of the thermodynamic and transport properties of CO₂/ heavy crude mixtures, both outside and inside porous media.

Rheological studies showed that for the mixtures compositions and pressure conditions studied in this work the CO₂/oil system behaves as a Newtonian fluid. Qualitative phase behavior experiments of CO₂/Boscan crude mixtures at reservoir temperature showed that only normal two phase liquid vapour equilibria existed in the pressure range studied.

The experimental data measured here show CO₂ solubility in the oil produces a high oil swelling and reduces appreciably the viscosity and interfacial tension of the crude.

Displacement of Boscan crude oil with CO₂ is characterized by rapid channelling of CO₂ due to large differences in their viscosities. The efficiency of the displacement process, however, can be improved notably by using a CO₂ WAG scheme. The results obtained here seem to indicate that injecting in a 1:3 CO₂/H₂O volumen ratio is the more efficient way to use the CO₂.

F I G U R E S



FIG. 1 SOLUBILITY OF CO₂ IN BOSCAN CRUDE

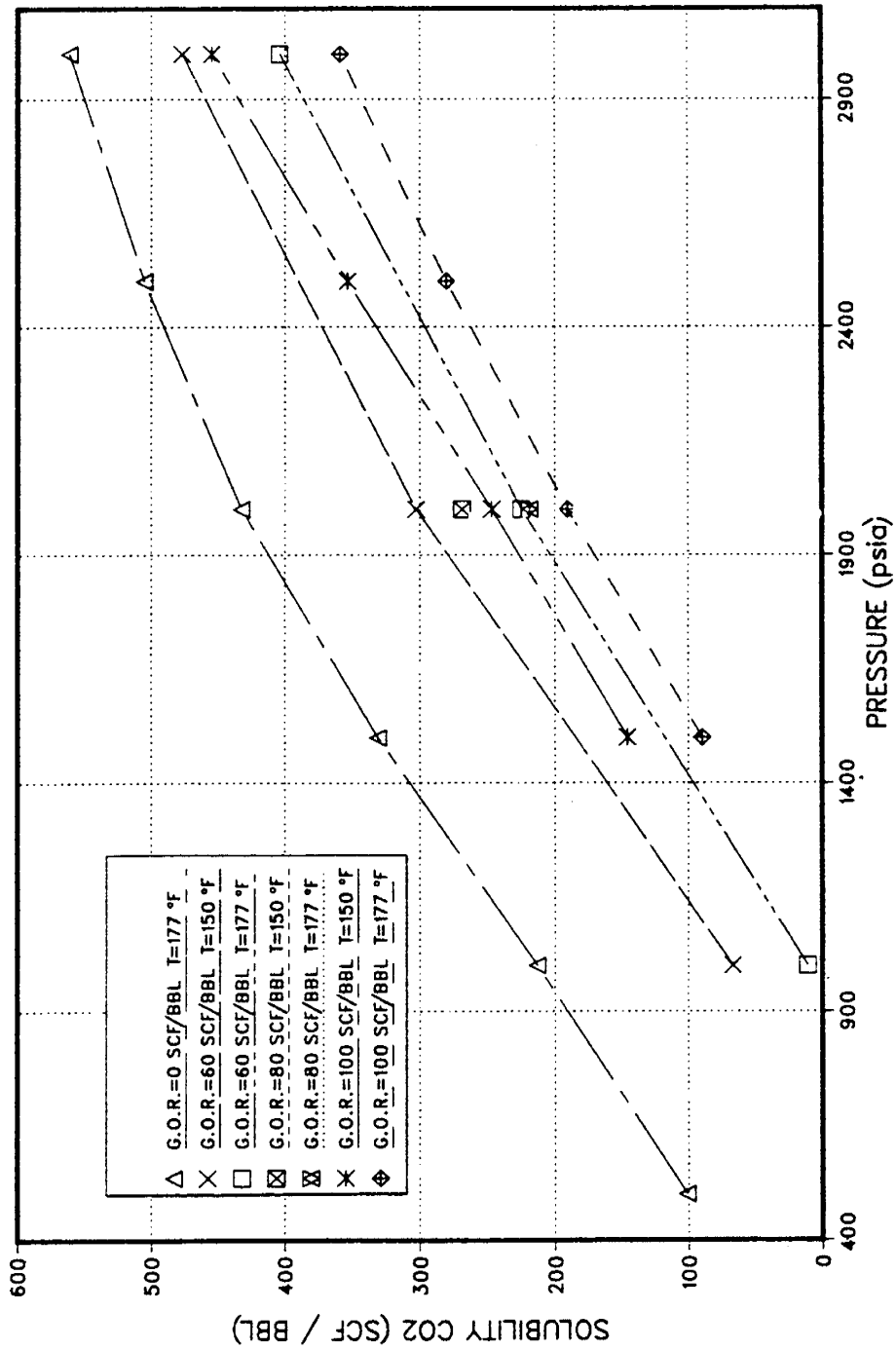




FIG. 2 SWELLING FACTOR VS CO2 SOLUBILITY IN BOSCAN CRUDE

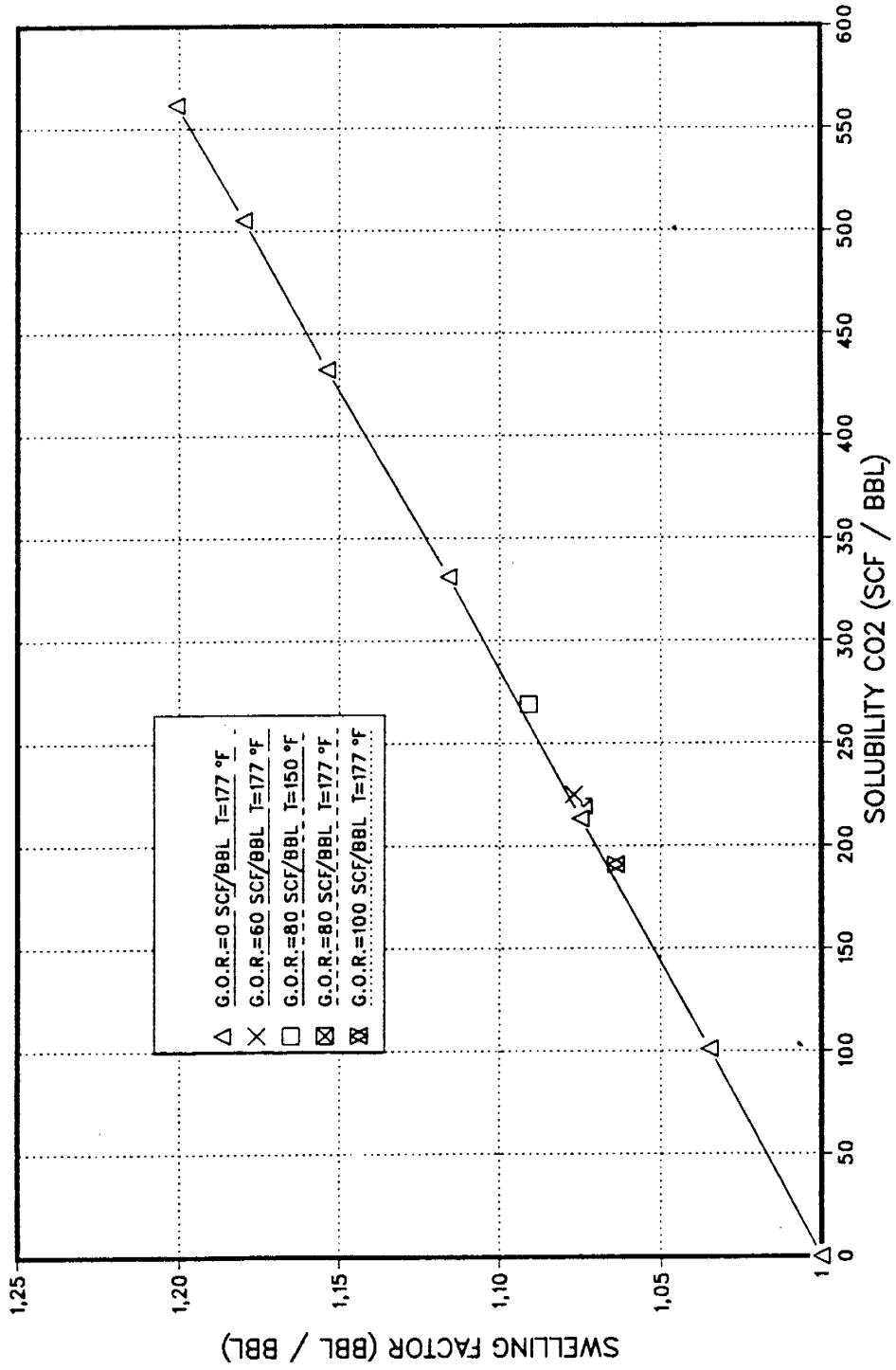
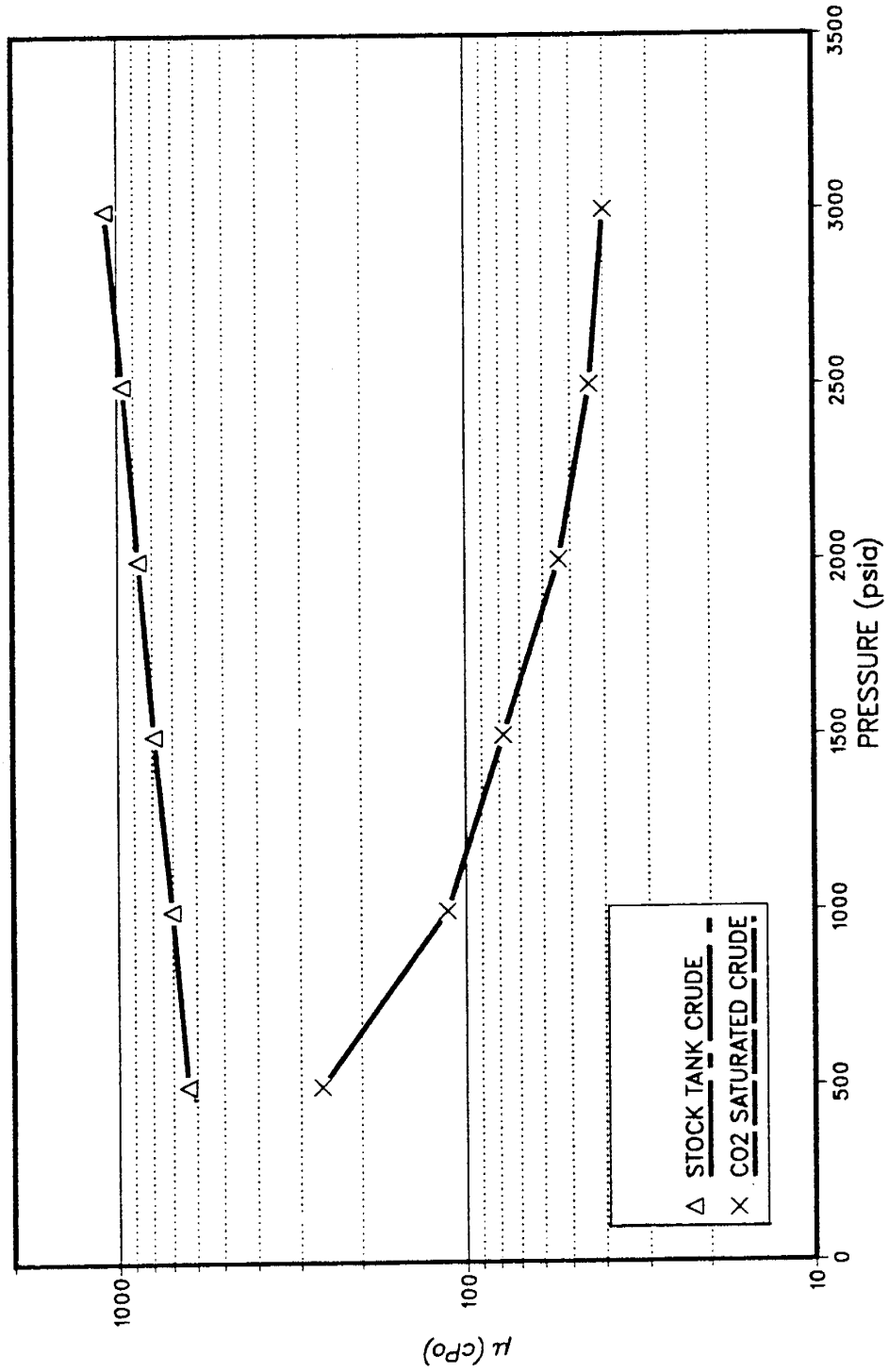




FIG. 3 VISCOSITY OF CO₂/BOSCAN STOCK TANK CRUDE MIXTURES
RESERVOIR TEMPERATURE: 177 °F



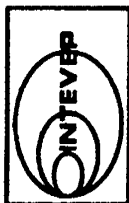
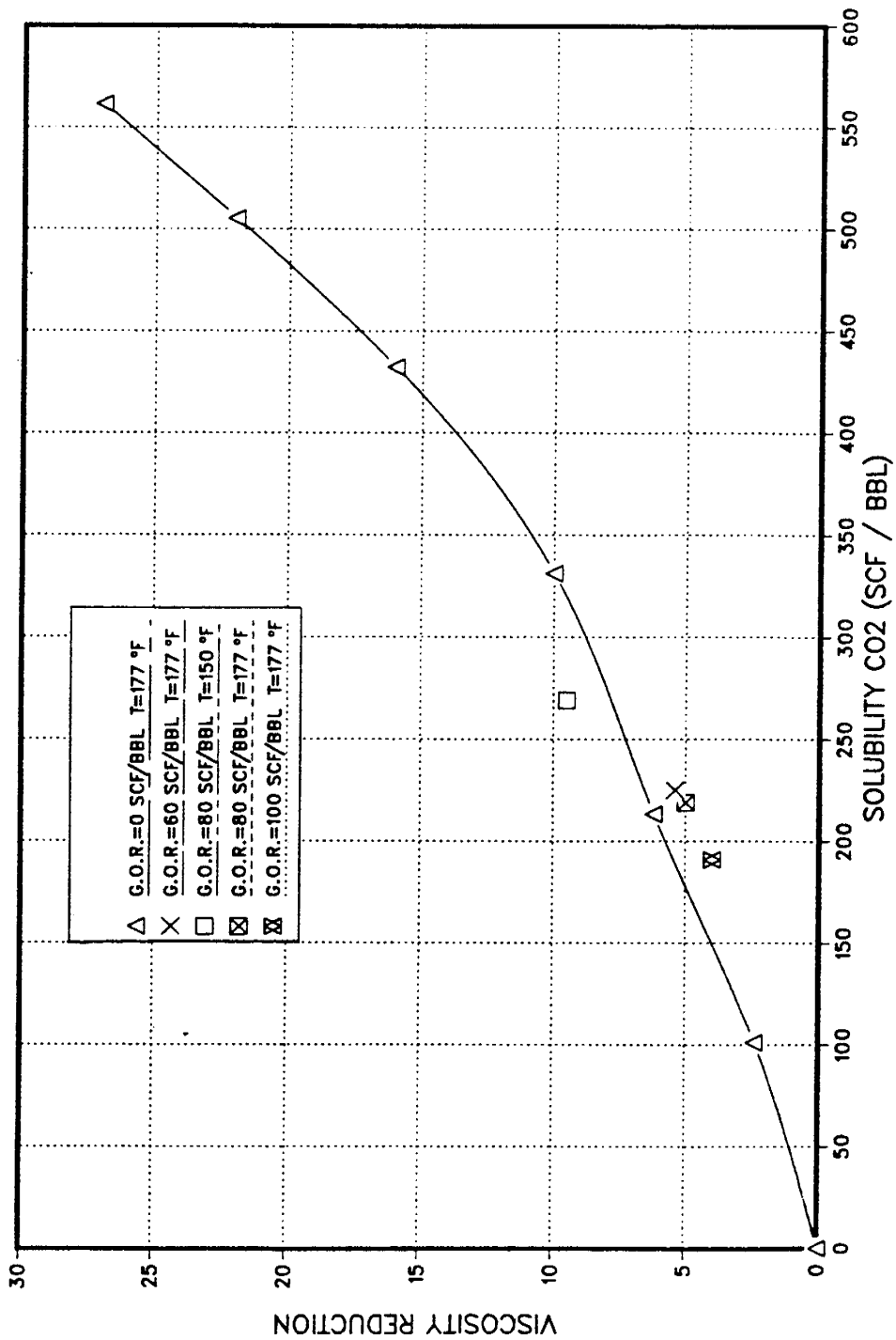


FIG. 4 VISCOSITY REDUCTION VS CO2 SOLUBILITY IN BOSCAN CRUDE



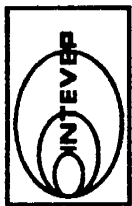
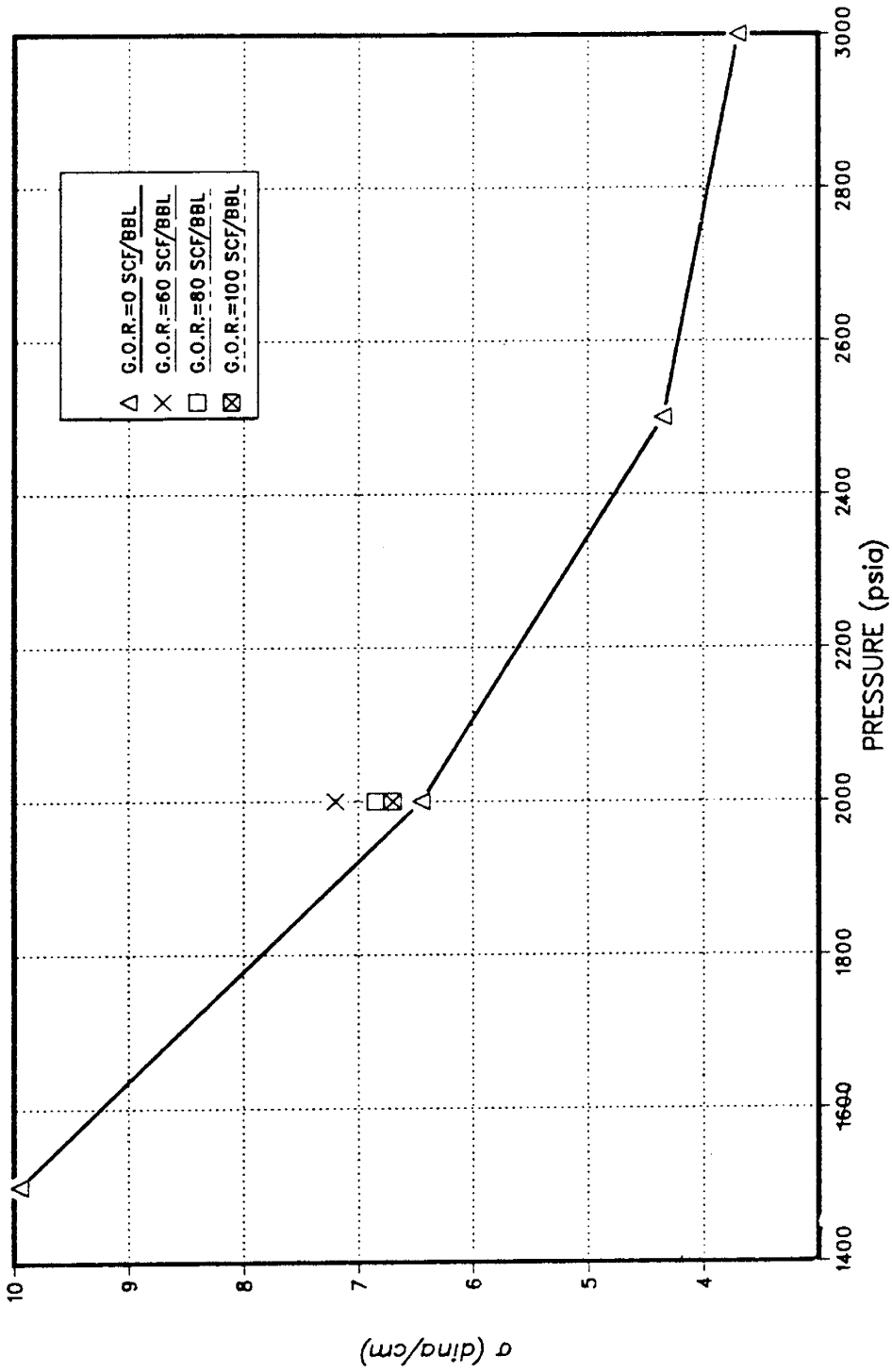


FIG. 5 INTERFACIAL TENSION VS CO₂ SATURATION PRESSURE IN BOSCAN CRUDE. RESERVOIR TEMPERATURE: 177 °F



T A B L E S

TABLE 1

Reservoir and Fluids Properties

Boscan field

Initial pressure (psia)	3,450
Temperature (°F)	177
Porosity (%)	24-26
Permeability (md)	500-700
Depth (ft)	8,000
API Gravity	10.2
Initial solubility ratio (SCF/Bbl)	108
Stock tank crude Molar mass (g/mol)	656

TABLE 2

Boscan Crude Distillation Data

Fraction	Temperature Interval (°C)	Volume %	Mol. Weight (g/mol)
1	44-200	6.36	128
2	200-310	10.57	223
3	310-400	11.03	290
Residue	400	72.04	801

4	400-575	21.60	410
Residue	575	50.44	-

5	400-635	37.80	500
Residue	635	34.24	-

TABLE 3

P.V.T Properties of CO₂/Boscan Stock Tank Crude Mixtures
Reservoir Temperature: 177 °F

Pressure	(psi)	500	1,000	1,500	2,000	2,500	3,000
GOR (CO ₂)	(scf/bbl)	101	213	331	432	505	561
Crude Density	(g/cm ³)	0.972	0.974	0.976	0.978	0.980	0.982
Mixture Density	(g/cm ³)	0.970	0.970	0.970	0.970	0.970	0.970
Swelling factor		1.035	1.075	1.116	1.154	1.180	1.201
Crude Viscosity	(cp)	635	703	790	874	965	1,084
Mixture Viscosity	(cp)	260	113	78	54	44	40
Viscosity reduction		2.4	6.2	10	16	22	27
Interfacial tension	(dyne/cm)	-	-	9.95	6.45	4.85	3.70

TABLE 4

Properties of CO₂/Boscan recombined crude mixtures at 177 °F

Solution Gas GOR = 100 (scf/bbl) Bubble Pressure (psi) = 1,116					Sol. Gas GOR = 80 (scf/bbl) Bubble Pressure = 895 (psi)		Sol. Gas GOR = 60 (scf/bbl) Bubble Pressure = 841 (psi)		
Pressure (psi)	1500	2000	2500	3000	2000	1000	2000	3000	
Property									
Crude Density (g) cm ³	0.953	0.956	0.957	0.958	0.963	--	0.967	--	
Crude Viscosity (cp)	290	300	330	360	430	--	452	--	
CO ₂ GOR (scf/bbl)	90	191	281	359	219	11	225	404	
Mixture Density (g/cm)	--	0.955	--	--	0.961	--	0.964	--	
Mixture Viscosity (cp)	--	75	--	--	86	--	84	--	
Swelling factor	--	4	--	--	5	--	5.4	--	
Viscosity Reduction	--	6.70	--	--	6.85	--	7.2	--	
Interfac. Tension (dyne/cm)									

TABLE 5

Properties of CO₂/Boscan Recombined Crude Mixtures at 150°F
and 2000 psi

Solution gas GOR (scf/bbl)	100	80	60
Bubble pressure (psi)	1,001	812	711
GOR-CO ₂ (scf/bbl)	247	270	303
Density crude (g/cm ³)	-	0.967	-
Density mixture (g/cm ³)	-	0.965	-
Swelling factor	-	1.091	-
Viscosity crude (cp)	-	1,315	-
Viscosity mixture (cp)	-	139	-
Viscosity reduction	-	9.5	-

TABLE 6

Displacement Tests Conditions

Test number	<u>1</u>	<u>2</u>	<u>3</u>	<u>4</u>	<u>5</u>
Model Properties:					
Length (ft)	3.08	3.08	6.92	6.92	6.92
Internal diameter (in)	2	2	1.18	1.18	1.18
PV (cm ³)	714.50	733.00	559.00	557.37	555.74
So (%)	73.8	70.0	82.0	93.3	91.9
∅ (%)	37.5	38.5	38.0	37.9	37.8
K (mD)	112	172	7,500	7,500	7,500
Injection pressure (psi)	3,000	2,500	2,500	2,500	2,500
Production pressure (psi)	2,600	2,200	2,300	2,300	2,300
Injection rate (cm ³ /h)	NM	NM	12.0	12.0	12.0
CO ₂ :H ₂ O injection ratio	*	1:3	1:2	1:3	1:1
CO ₂ slug size** (% PV)	-	1.05	1.84	1.38	2.76
Blowdown pressure (psi)	800	14.7	14.7	14.7	14.7

NM: Not measured

*: Continuous CO₂ injection

** : Average value

PV: Porous volume

TABLE 7
Displacement Tests Results

Test number		<u>1</u>	<u>2</u>
CO ₂ injected at breakthrough	(PV fraction)	0.47	not observed
Recovery at breakthrough	(% OOIP)	15.50	-
CO ₂ requirement at breakthrough	(Mscf/bbl)	6,232	-
Recovery after 2 PV injected	(% OOIP)	17.30	23.8
CO ₂ requirement after 2 PV injected	(Mscf/bbl)	23,892	3,836
Displacement oil recovery	(% OOIP)	17.90	38.30
Blowdown oil recovery	(% OOIP)	10.00	6.00
Total oil recovery	(% OOIP)	27.90	44.30
Total CO ₂ + H ₂ O injected	(PV fraction)	2.63	4.4
Total CO ₂ requirement	(Mscf/bbl)	30,198	5,257

PV: porous volume

TABLE 8

Displacement Tests Results

Test number	<u>2</u>	<u>3</u>	<u>4</u>	<u>5</u>
CO ₂ -H ₂ O injection ratio	1:3	1:2	1:3	1:1
CO ₂ + H ₂ O injected at breakthrough (PV fraction)	n.o.	0.98	n.o.	0.84
Recovery at breakthrough (% OOIP)	-	42.24	-	43.59
CO ₂ requirement at breakthrough (Mscf/bbl)	-	1,201	-	1,296
Recovery after 0.6 PV injected (% OOIP)	6.50	33.19	34.58	37.49
CO ₂ requirement after 0.6 PV injected (Mscf/bbl)	4,472	1,251	702	1,401
Displacement oil recovery (% OOIP)	38.30	42.51	38.48	49.14
Blowdown oil recovery (% OOIP)	6.00	2.28	4.80	4.27
Total recovery (% OOIP)	44.30	44.79	43.28	53.41
Total CO ₂ + H ₂ O injected (PV fraction)	4.40	1.06	0.67	1.04
Total CO ₂ requirement (Mscf/bbl)	5,257	1,488	599	1,385

PV: porous volume

n.o.: not observed

